

Olga Alexandra Rosero Vlasova

Diffuse reflectance spectroscopy
for estimation of soil organic
matter and texture in burned and
abandoned cropland areas

Departamento
Geografía y Ordenación del Territorio

Director/es
Montorio Llovería, Raquel
Pérez Caballero, Fernando

<http://zaguan.unizar.es/collection/Tesis>



Reconocimiento – NoComercial – SinObraDerivada (by-nc-nd): No se permite un uso comercial de la obra original ni la generación de obras derivadas.

© Universidad de Zaragoza
Servicio de Publicaciones

ISSN 2254-7606



Universidad
Zaragoza

Tesis Doctoral

DIFFUSE REFLECTANCE SPECTROSCOPY FOR
ESTIMATION OF SOIL ORGANIC MATTER AND
TEXTURE IN BURNED AND ABANDONED
CROPLAND AREAS

Autor

Olga Alexandra Rosero Vlasova

Director/es

Montorio Llovería, Raquel
Pérez Caballero, Fernando

UNIVERSIDAD DE ZARAGOZA
Geografía y Ordenación del Territorio

2019

OLGA A. ROSERO VLASOVA

**DIFFUSE REFLECTANCE SPECTROSCOPY
FOR ESTIMATION OF SOIL ORGANIC
MATTER AND TEXTURE IN BURNED AND
ABANDONED CROPLAND AREAS**



Directores:

Fernando Pérez Cabello
Raquel Montorio Llovería



Universidad Zaragoza

Departamento de Geografía y Ordenación del Territorio

Foto portada: Foto de 2013 en el Municipio de Encinacorba (Región de Aragón- España), área afectada por incendio forestal en 2003.

Tesis Doctoral

DIFFUSE REFLECTANCE SPECTROSCOPY
FOR ESTIMATION OF SOIL ORGANIC
MATTER AND TEXTURE IN BURNED AND
ABANDONED CROPLAND AREAS

Autora:

Olga Alexandra Rosero Vlasova

Directores:

Dr. Fernando Pérez Cabello

Dra. Raquel Montorio Llovería

UNIVERSIDAD DE ZARAGOZA

Departamento de Geografía y Ordenación del Territorio

2019

La autora de esta tesis recibió financiación como becaria del Programa Convocatoria Abierta 2012 Fase 1 del SENESCYT (Ecuador) hasta enero 2017. Para la continuación y finalización de esta tesis además contó con el apoyo financiero de la Universidad de Zaragoza en conjunto con Santander Universidades de una de las “Ayudas de Movilidad para Latinoamericanos – Estudios de Doctorado | 2017-2018.

Dedicado a mis padres.

Agradecimientos

Quiero agradecer a todas aquellas personas que me ayudaron a iniciar y culminar mi programa de doctorado, las cuales han sido muchas a lo largo de la investigación.

Gracias a mis directores, el Dr. Fernando Pérez-Cabello y Dra. Raquel Montorio Llovería por la ayuda y paciencia durante el desarrollo del trabajo, sus aportaciones y guía han permitido llegar a la meta propuesta. Además de estar siempre dispuestos ayudarme en aquellos trámites administrativos que al ser una estudiante extranjera fueron muchos.

Mi agradecimiento al Grupo de Investigación GEOFOREST que me acogió desde el primer momento, me brindó un espacio de trabajo y me permitió realizar todos los experimentos en el laboratorio de espectro-radiometría con flexibilidad de horario y acceso a los equipos.

Agradezco a la Dra. Maite Echeverría que siempre me trató de la mejor manera cuando solicitaba su ayuda en cuestiones administrativas especialmente aquellas relacionadas con asistencia a eventos científicos.

Gracias a la Dra. Estela Nadal-Romero por su colaboración en la investigación. Aprecio mucho su tiempo dedicado a las revisiones y acertadas aportaciones, pero sobre todo su trato amable y cercano.

A mi amiga de toda la vida Giss por ayudarme a sobrellevar las complicaciones de salud y cuidarme en el momento preciso que iniciaba mi investigación, sin ti todo hubiera sido más complicado.

A mi querida amiga Gina, el universo te puso en mi camino para inyectarme positivismo y ánimo de seguir adelante y llegar al final de la meta.

A todos los becarios del Departamento y del Laboratorio de Espectro-Radiometría y Teledetección Ambiental por esos cafés, conversas y agradable ambiente de trabajo.

Haciendo uso de la posibilidad que ofrece la Universidad de Zaragoza, esta tesis doctoral se presenta como un compendio de artículos, siéndola estudiante de doctorado **Olga Alexandra Rosero Vlasova** la principal autora de todos ellos:

1. **Rosero-Vlasova, O. A.**, Pérez-Cabello, F., Llovería, R. M., & Vlassova, L. (2016). Assessment of laboratory VIS-NIR-SWIR setups with different spectroscopy accessories for characterisation of soils from wildfire burns. *Biosystems Engineering*, 152, 51-67. <https://doi.org/10.1016/j.biosystemseng.2016.06.011>

Status: published

JCR® Impact factor (2016): 2.044

2. **Rosero-Vlasova, O.**, Rosero Tufiño, P., & Vlassova, L. (2017). Espectroscopia VIS-NIR aplicada para predicción del contenido de materia orgánica en los suelos bajo sistema de cultivo roza-y-quema. In P. Domínguez, J. Morán, O. Rea, I. Parra, & L. Corzo (Eds.), *Memoria Científica del III Congreso Internacional de Ingeniería, Ambiental, Forestal y Ecoturismo* (pp. 16-28). Guayaquil, Ecuador: Editorial CIDE Centro de Investigación y Desarrollo Ecuador. Retrieved from: https://docs.wixstatic.com/ugd/54b18d_130e402800d74b4aa0fb8a45301d1cb8.pdf

Status: published

JCR® Impact factor: N/A

3. **Rosero-Vlasova, O. A.**, Vlassova, L., Pérez-Cabello, F., Montorio, R., & Nadal-Romero, E. (2019). Soil organic matter and texture estimation from visible-near infrared-shortwave infrared spectra in areas of land cover changes using correlated component regression. *Land Degradation & Development*, 30(5), 544-560. <https://doi.org/10.1002/ldr.3250>

Status: published

JCR® Impact factor (2018): 4.275

4. Rosero-Vlasova, O. A., Vlassova, L., Pérez-Cabello, F., Montorio, R., & Nadal-Romero, E. (2018). Modeling soil organic matter and texture from satellite data in areas affected by wildfires and cropland abandonment in Aragón, Northern Spain. *Journal of Applied Remote Sensing*, 12(4), 042803. <https://doi.org/10.1117/1.JRS.12.042803>

Status: published

JCR® Impact factor (2018): 1.344

5. **Rosero-Vlasova, O.**, Alves, D. B., Vlassova, L., Pérez-Cabello, F., & Montorio, R. (2017). Modeling soil organic matter (SOM) from satellite data using VIS-NIR-SWIR spectroscopy and PLS regression with step-down variable selection algorithm: case study of Campos Amazonicos National Park savanna enclave, Brazil. *Remote Sensing for Agriculture, Ecosystems, and Hydrology XIX* (Vol. 10421, p. 104210V). International Society for Optics and Photonics. <https://doi.org/10.1117/12.2278701>

Status: published

JCR® Impact factor: N/A

Making use of the possibility offered by the University of Zaragoza, this thesis is presented as compendium of scientific articles, being the Ph.D. student **Olga Alexandra Rosero Vlasova** the author responsible for all of them:

1. **Rosero-Vlasova, O. A.**, Pérez-Cabello, F., Llovería, R. M., & Vlassova, L. (2016). Assessment of laboratory VIS-NIR-SWIR setups with different spectroscopy accessories for characterisation of soils from wildfire burns. *Biosystems Engineering*, 152, 51-67. <https://doi.org/10.1016/j.biosystemseng.2016.06.011>

Status: published

JCR® Impact factor (2016): 2.044

2. **Rosero-Vlasova, O.**, Rosero Tufiño, P., & Vlassova, L. (2017). Espectroscopia VIS-NIR aplicada para predicción del contenido de materia orgánica en los suelos bajo sistema de cultivo roza-y-quema. In P. Domínguez, J. Morán, O. Rea, I. Parra, & L. Corzo (Eds.), *Memoria Científica del III Congreso Internacional de Ingeniería, Ambiental, Forestal y Ecoturismo* (pp. 16-28). Guayaquil, Ecuador: Editorial CIDE Centro de Investigación y Desarrollo Ecuador. Retrieved from: https://docs.wixstatic.com/ugd/54b18d_130e402800d74b4aa0fb8a45301d1cb8.pdf

Status: published

JCR® Impact factor: N/A

3. **Rosero-Vlasova, O. A.**, Vlassova, L., Pérez-Cabello, F., Montorio, R., & Nadal-Romero, E. (2019). Soil organic matter and texture estimation from visible-near infrared-shortwave infrared spectra in areas of land cover changes using correlated component regression. *Land Degradation & Development*, 30(5), 544-560. <https://doi.org/10.1002/ldr.3250>

Status: published

JCR® Impact factor (2018): 4.275

4. Rosero-Vlasova, O. A., Vlassova, L., Pérez-Cabello, F., Montorio, R., & Nadal-Romero, E. (2018). Modeling soil organic matter and texture from satellite data in areas affected by wildfires and cropland abandonment in Aragón, Northern Spain. *Journal of Applied Remote Sensing*, 12(4), 042803. <https://doi.org/10.1117/1.JRS.12.042803>

Status: published

JCR® Impact factor (2018): 1.344

5. **Rosero-Vlasova, O.**, Alves, D. B., Vlassova, L., Pérez-Cabello, F., & Montorio, R. (2017). Modeling soil organic matter (SOM) from satellite data using VIS-NIR-SWIR spectroscopy and PLS regression with step-down variable selection algorithm: case study of Campos Amazonicos National Park savanna enclave, Brazil. *Remote Sensing for Agriculture, Ecosystems, and Hydrology XIX* (Vol. 10421, p. 104210V). International Society for Optics and Photonics. <https://doi.org/10.1117/12.2278701>

Status: published

JCR® Impact factor: N/A

Resumen

La protección y conservación de los suelos es vital para el logro de las metas formuladas en la Agenda para el desarrollo Sostenible de Naciones Unidas 2030 (Nations, 2015). Los objetivos más importantes incluyen el de procurar lograr un mundo con efecto neutro en la degradación del suelo y conseguir la seguridad alimentaria.

La evaluación del estado actual del suelo y apreciación de los efectos de las actividades de gestión son imposibles de realizar sin un regular monitoreo, especialmente en áreas con perturbaciones naturales y antropogénicas, tales como la regiones del Mediterráneo en Europa y Amazonía en América del Sur.

En este contexto, el objetivo principal de la presente investigación consiste en establecer una metodología operativa en base de las opciones existentes más idóneas para la estimación del contenido de materia orgánica (CMO) y textura de suelos y aplicarla en diferentes áreas que experimentan cambios en la cobertura y el uso de suelo que incluyen (i) áreas afectados por los incendios forestales, (ii) áreas de agricultura bajo sistema de cultivo de roza-y-quema, y (iii) campos agrícolas abandonados.

En la primera fase de investigación se compararon montajes experimentales de laboratorio de detección próxima utilizados en la espectroscopia de suelos que incluyen diferentes accesorios: la esfera integradora, lampa de iluminación halógena ASD y la sonda de contacto óptica. Aunque se obtuvieron resultados similares con los tres diseños experimentales utilizados, los modelos estadísticos basados en los espectros medidos por la configuración experimental que incluía una lámpara halógena como fuente de iluminación, han demostrado la mejor capacidad de predicción con el coeficiente de determinación ~10% más alto que modelos basados en los datos generados por las otras dos configuraciones. La utilidad de esta configuración y el procedimiento de mediciones espectrales establecido para obtención de los espectros estables de suelos fueron posteriormente comprobada en las mediciones espectrales de las muestras de suelos en áreas de cultivos bajo sistema de roza-y-quema en la región costera del Ecuador, donde los residuos de biomasa son quemados al final de cada ciclo de producción.

La siguiente fase de investigación consistió en utilizar los espectros de suelos de las diferentes áreas de estudio (áreas de incendios forestales en España y Brasil, áreas de

quemadas agrícolas en Ecuador, y área con campos de cultivo abandonados en el noroeste de España) para calibración de modelos predictivos de materia orgánica y textura utilizando varios métodos estadísticos multivariantes: (i) regresión parcial por mínimos cuadrados usando todas las bandas de reflectancia disponibles como predictores (PLSR-full), (ii) regresión parcial por mínimos cuadrados usando como predictores las bandas seleccionadas con la prueba de incertidumbre de Martens (PLSR-MUT) y (iii) regresión de las componentes correlacionadas y el algoritmo iterativo para la selección de los predictores (CCR-SD).

El método CCR-SD por primera vez aplicado en la espectroscopia de suelos en esta investigación mostró los mejores resultados generando los modelos de mejor ajuste utilizando limitado número de predictores; en la estimación simultánea de CMO, arcilla, limo y arena estos modelos obtuvieron coeficientes de determinación R^2 en el rango de 0.80–0.86 y 0.70–0.87 en las etapas de calibración y validación, respectivamente.

Finalmente, los espectros de alta resolución generados durante las mediciones espectrales de suelos en el laboratorio fueron re-muestreados para explorar la posibilidad de estimación del CMO y textura de suelos a partir de las imágenes de los tres satélites de última generación (Landsat-8, Sentinel-2, and EnMAP). Los resultados son altamente prometedores para todos los satélites, mostrando los modelos para CMO basados en las bandas de EnMap la precisión más alta ($R^2 \sim 0.90$).

Abstract

Soil protection and conservation is vital for achievement sustainability goals formulated in the United Nations 2030 Agenda for Sustainable Development (United Nations, 2015). Among the most important targets are those related to achievement of food security and a land degradation-neutral world.

It is impossible to evaluate the present status of soils and assess/measure the effect of the management activities without regular soil monitoring, particularly in areas of natural and anthropogenic disturbances, such as Mediterranean in Europe and Amazon in South America.

In this context, the main objective of the present research is to establish the viable methodology for estimation of organic matter and texture of fire-affected soils from spectral data and test it on data from different areas of land use/land cover change: (i) soils from the areas affected by wildfire burns and slash-and-burn agriculture; and (ii) soils from areas of cropland abandonment.

The study began with comparison of laboratory setups which included different spectroscopy accessories (the external integrating sphere, halogen lamp ASD and the optical contact probe) used to obtain VIS-NIR-SWIR spectra of soils from wildfire burns. Although similar results were obtained with all the setups, the best quality predictions of soil organic matter (SOM) resulted from spectra generated with the setup using halogen lamp as illumination source. Statistical models based on the spectra measured by the experimental configuration that included a halogen lamp as the light source have demonstrated the best prediction capability with the determination coefficient ~10% higher than models based on the data generated by the other two configurations. The viability of modeling methodology was then successfully confirmed in modeling of SOM of soils affected by anthropogenic fire in slash-and-burn crop cultivation system on the Ecuadorian coast.

In the next stage of the research, different modeling algorithms were applied for estimation of SOM and soil texture using soil spectra from the different study areas (forest fire areas in Spain and Brazil, agricultural burn areas in Ecuador, and area with abandoned fields in northwestern Spain), which include the partial least square regression using all available reflectance bands as predictors PLSR-full, partial least

square regression using the bands selected with the Martens uncertainty test as predictors PLSR-MUT and correlated component regression CCR. Spectral measurements were performed using previously determined laboratory setup. The correlated components regression (CCR) with step-down variable selection algorithm applied in soil spectroscopy outperformed other tested methods and allowed generation of well-fit models with a limited number of predictors.

The CCR-SD method for the first time applied in soil spectroscopy in this investigation showed the best results generating the best fit models using limited number of predictors; in the simultaneous estimation of SOM, clay, silt and sand these models obtained R^2 determination coefficients in the range of 0.80-0.86 and 0.70-0.87 in the calibration and validation stages, respectively.

Finally, high-resolution laboratory reflectance spectra of fire-affected soils from the forest burns in northeastern Spain and savanna enclave in central Brazil were up-scaled to explore the possibility of modelling SOM and soil texture from data generated by the three last generation satellites (Landsat-8, Sentinel-2, and EnMAP). The highly promising results were obtained for all the satellites; being the SOM models based on simulated EnMAP bands the most accurate ($R^2 \sim 0.90$).

Table of contents

Resumen

Abstract

1. Background, objectives and structure	1
2. Soil organic matter and texture estimation from VIS-NIR-SWIR spectra.....	5
2.1. Soils and soil monitoring	5
2.2. Visible and Near-Infrared soil spectroscopy	6
2.3. Spectral properties of soils.....	10
2.3.1. Soil organic matter	12
2.3.2. Soil texture.....	13
2.4. Soil properties estimation from VIS-NIR-SWIR spectra	15
2.5. Integration of soil spectroscopy with other data sources and methods.....	16
3. Study area and soil sampling	18
3.1. Aragón, Spain	18
3.2. Campos Amazônicos National Park, Brazil	21
3.3. Mocache, Ecuador	22
4. Methodology	24
4.1. Spectral measurements	25
4.1.1. Experimental setup IS (external integrating sphere)	26
4.1.2. Experimental setup L (illuminator lamp and pistol grip)	28
4.1.3. Experimental setup CP (contact probe).....	29
4.1.4. Statistics used for spectra comparison.....	30
4.2. Simulation of satellite spectral bands	30
4.3. Multivariate statistical modeling of SOM and soil texture fractions.....	31
4.3.1. Partial Least Square Regression (PLSR).....	33
4.3.2. Step-Down predictors selection Algorithm	33
4.3.3. Correlated Components Regression	34
4.3.4. Assessment of model performance.....	35
5. Comparison of laboratory setups used to obtain laboratory VIS-NIR-SWIR spectra of soils	37
6. Estimation of SOM content in areas of slash-and-burn agriculture from VIS-NIR-SWIR spectra.....	55

7. Testing algorithms applied in multivariate statistical modeling of SOM and texture fractions of fire-affected soils	69
8. Modeling soil organic matter and texture from satellite data.	87
8.1. Case study of Aragón, Northern Spain	87
8.2. Case study of Campos Amazônicos National Park savanna enclave, Brazil.	103
9. Conclusions and future research	111
10. Conclusiones y trabajos futuros	114
Appendix A	132

1. Background, objectives and structure

Soil is a loose surface layer of the earth surface consisting of mixture of weathered rocks and organic material necessary for plants growth (Nortcliff et al., 2006; Troeh & Thompson, 2005). Soil regulates the environment and ensures food security. Changes in land cover and land use, such as wildfires, deforestation, desertification and urbanization, negatively affect soil properties and can trigger erosion processes leading to environmental degradation.

Wildfires have long been a natural disturbance factor relevant for evolution of some ecosystems. However, at present, due to human activities and climate change, the number and intensity of fires are experiencing continuous increase (Pausas et al., 2004). Fire effects on soils are multiple, the degree of changes in soil properties depending on fire severity and frequency (Lentile et al., 2006; Mataix-Solera, Cerda, Arcenegui, Jordan, & Zavala, 2011). The first and most obvious effect is the loss of soil organic matter and, as a consequence, decrease in soil fertility (Certini, 2005). Consumption of vegetation and above surface biomass alters energy and water cycles, and modifies surface runoff and infiltration. In clayey soils fire-related loss of organic matter is often related to the increase of soil hydrophobicity, i.e. water repellence, which is the cause of greatly accelerated soil erosion and loss (Úbeda & Outeiro, 2009).

On the other hand, fire-related changes in soil properties may also result from controlled anthropogenic fires regularly applied for burning of residual biomass as part of traditional slash-and-burn (swiddening/shifting) agriculture still widely used in small-scale farming of developing countries of Asia, Africa and South America (Hauser and Norgrove, 2013). Positive effects of low intensity fires include soil fertilization with organic ash, elimination of weeds, reduced risk of plant parasites and diseases (Jordan, 1989; Kato, Kato, Denich, & Vlek, 1999). During centuries, long time between rotation cycles in subsistence agriculture of indigenous peoples together with low population density ensured sustainability of the system (Sponsel, 2013). However, at present demographic pressure and market orientation of the economy lead to decrease of time periods between burns (Lawrence, Radel, Tully, Schmook, & Schneider, 2010), and as a consequence, lowering of soil fertility due to nutrients volatilization (Mackensen et al., 1996), soil erosion and reduction of agricultural yields in areas of shifting agriculture (Sommer et al., 2004; Comte et al., 2012).

While fire, provoked by natural or human-related factor has long been affecting ecosystems in the studied areas, the spread of cropland abandonment in the Mediterranean is a more recent driver of land cover changes related to the soil conditions in the region (Nadal-Romero, Cammeraat, Pérez-Cardiel, & Lasanta, 2016). Massive migration of population to urban areas and abandonment of the cultivated fields in the last decades are the processes taking place throughout extensive mountainous areas in Mediterranean. Ecosystem evolution of the abandoned areas follows different paths and various management strategies aimed to soil restoration and improvement are often applied (Lasanta, Nadal-Romero, & Arnáez, 2015). There is no doubt, that cropland abandonment can affect soil properties, although no clear pattern has been observed (Nadal-Romero et al., 2016).

Maintaining of soil conditions is a key condition for sustainability (Lal & Stewart, 2010; Pimentel, 2006). The United Nations 2030 Agenda for Sustainable Development (United Nations, 2015) in one of the Sustainable development goals (SDGs) calls for action to achieve a land degradation-neutral world.

Regular soil monitoring is necessary to get better understanding of soil/ecosystem evolution and assess the effectiveness of the mitigation strategies (Tóth, Hermann, da Silva, & Montanarella, 2018), especially in areas of natural and anthropogenic disturbances, such as Mediterranean (Merino, Moreno, Navarro, & Gallardo, 2016). Soil status can be evaluated through a set of soil attributes/indicators, which usually include soil organic matter (SOM) and texture.

Traditionally estimation of soil properties has been based on data generated by soil surveys involving extensive fieldwork and a series of laboratory analysis often referred to as “wet chemistry”. These conventional methods demand great investment of time and effort, which motivated the search for alternatives.

Extensive research during last decades has shown that SOM and texture are spectrally active properties and can be estimated with spectral sensing methods, such as visible (VIS)-near infrared (NIR)-shortwave infrared (SWIR) spectroscopy, combined with multivariate statistical modelling. The technique allowing quick and undestructive

testing requires minimum sample preparation and could offer time and cost-effective alternative (Demattê et al., 2016).

Spectral measurements can be performed in laboratory and in-situ. Laboratory conditions ensure stable observation geometry, and environment, which should be accounted for when working in the field (Schaepman & Dangel, 2000; Viscarra-Rossel, Walvoort, McBratney, Janik, & Skjemstad, 2006). Yet, some issues as, for example, the impact of laboratory instrumentation and procedures, the feasibility of models up- and downscaling (Viscarra-Rossel et al., 2016), as well as conditions determining model transferability from one study area to the other (Ben-Dor, Ong, & Lau, 2015; Guerrero, Viscarra-Rossel, & Mouazen, 2010; Stevens et al., 2008), still need to be clarified.

Because high variability in proportion of soil constituents has a great impact on their spectra (Ben-Dor & Demattê, 2016), soil properties cannot be estimated directly from the spectral curves. Thus, the variables of interest are quantified using methods of multivariate statistics. The most often used models are those resulting from linear regression, especially very popular partial least squares regression (PLSR) (Mouazen, Kuang, De-Baerdemaeker, & Ramon, 2010; Vasques, Demattê, Viscarra-Rossel, Ramírez-López, & Terra, 2014; Viscarra-Rossel, McGlynn, & McBratney, 2006). However, lately reports present examples when PLSR models are outperformed by data mining techniques and tools, which include neural networks (Mouazen, et al., 2010), support vector machines (Viscarra-Rossel & Behrens, 2010), and artificial intelligence algorithms (Gholizadeh, Borůvka, Saberioon, & Vašát, 2016).

Continuous evaluation of new modelling approaches is being performed, as well as the scope of VIS–NIR–SWIR soil spectroscopy use in scenarios of particular interest (e.g., Gholizadeh, Saberioon, Carmon, Boruvka, & Ben-Dor, 2018; Ogen, Neumann, Chabrilat, Goldshleger, & Ben-Dor, 2018; Ostovari et al., 2018; Terra, Demattê, & Viscarra-Rossel, 2018; Viscarra-Rossel & Brus, 2018).

In this context, the main objective of this study is to estimate organic matter and texture of fire-affected and cropland abandoned soils from spectral data at different scales, i.e. determine and test the viable/operational methodology for this purpose. The main objective was approached through the work on several specific objectives:

1. Compare laboratory setups including different commercially available spectroscopy accessories used to obtain VIS-NIR-SWIR spectra soils from areas of landcover change (affected by fire and cropland abandonment) (article in *Biosystems Engineering*, 152);
2. Apply VIS-NIR-SWIR laboratory spectroscopy to estimate SOM and texture of soils from in erosion-prone areas of wildfire burns, slash-and-burn agriculture and cropland abandonment in three different study areas (articles in *Land Degradation & Development*, 30(5), and *Scientific Report of the III International Congress of Engineering, Environmental, Forestry and Ecotourism* (pp. 16-28));
3. Assess the performance of different algorithms applied in modelling of SOM and texture fractions of burned soils (article *Land Degradation & Development*, 30(5)).
4. Explore the potential of the three last generation satellites (Landsat-8, Sentinel-2, and EnMAP) to estimate SOM content and texture of soils affected by fire and cropland abandonment (articles *Journal of Applied Remote Sensing*, 12(4), 042803, and *Remote Sensing for Agriculture, Ecosystems, and Hydrology XIX* (Vol. 10421, p. 104210V)).

The structure of thesis contains ten chapters. Chapter 1 describes the scientific context of research and formulates its objectives. It is followed by the theoretic rationale for the VIS-NIR-SWIR soil spectroscopy and review of the up-to-date advances (Chapter 2); description of the study area (Chapter 3), data and tools used in the study (Chapter 4). General view of research methodology is presented in Chapter 4, while details of research performed when working on each of the objectives are presented in Chapters 5-8, each of the chapters being the original version of the published articles. The main findings and further research opportunities arising from this work are summarized in the final chapters in English (Chapter 9) and Spanish (Chapter 10). They are followed by sections containing References for Chapters 1-4 and Appendices, specifying contribution of the PhD student to the published papers and documents certifying that the five presented articles are authorized for the exclusive use in this thesis.

2. Soil organic matter and texture estimation from VIS-NIR-SWIR spectra

2.1. Soils and soil monitoring

Soil is the loose mixture of organic and inorganic components on the earth surface allowing vegetation development. It is a main support for food production. Soils are also relevant in climate change issues (Lal, 2004). Land use change processes, which include deforestation, biomass burning, and urbanization are important contributors to carbon (C) emission into the atmosphere. On the other hand, soils can act as carbon sinks retaining stable soil organic and inorganic carbon components. This capacity varies depending on soil type (Ingram & Fernandes, 2001).

While our food security depends on soils, human activities together with natural processes promote soil and land degradation. Among these processes are natural and anthropogenic fires. Consumption of organic matter alters the structure of burned soils reducing their permeability; increased surface runoff accelerates soil erosion leading to its deterioration and loss (Cerdà & Robichaud, 2009; DeBano & Neary, 2005; Pérez-Cabello, Echeverria, Ibarra, & De la Riva, 2009).

Different management strategies have been developed and applied worldwide to maintain/improve soil quality, prevent soil degradation and mitigate the effects of soil disturbances. To evaluate their success, it is necessary to establish, register, and compare indicators of soil status (Montanarella & Panagos, 2018). There is a consensus among the experts (Bünemann et al., 2018) that a minimum set should consist of soil chemical, physical and biological attributes/indicators.

The minimum set of properties for soil quality assessment usually includes SOM and texture (Bünemann et al., 2018). SOM, which is one of the main sources of soil carbon and plant nutrients, determines soil fertility and plays an important role in both water cycle (infiltration and runoff) (Tóth et al., 2018). On the other hand, land productivity is directly impacted by soil erosion (Troeh & Thompson, 2005), with texture being one of the basic indicators of soil erodibility (Goldman, Bursztynsky, & Jackson, 1986) and other hydraulic properties (Tóth et al., 2018).

Assessment of soil properties is usually performed through application of methods specific for corresponding scientific discipline. Thus, physical soil properties are quantified using procedures common to physics; chemical properties uses methods applied in chemistry and biological properties are estimated with methods developed in biology (Demattê et al., 2016). Traditional methods are destructive and resource-intensive; the test results are not readily available. Moreover, there is often inconsistency between approaches applied in different soil surveys (Sánchez et al., 2009) making difficult comparison and integration of the results (Louis et al., 2014).

2.2. Visible and Near-Infrared soil spectroscopy

Known limitations of conventional soil analysis motivated the search for alternatives, arising spectral sensing methods as one of the time and cost-effective solutions (Demattê et al., 2016) It has been demonstrated that information on soil characteristics can be obtained from spectral regions which include the ultraviolet (UV: 200–380 nm), visible (VIS: 350–700), near-infrared (NIR:700–1000 nm), shortwave infrared (SWIR: 1000–2500 nm),and mid-infrared (MIR: 2500–25000 nm) shown in Fig. 1. Even though soil spectra present a greater number of spectral features in the MIR range, VIS– NIR– SWIR spectroscopy is more often used due to the ease of application and lower cost of the equipment.

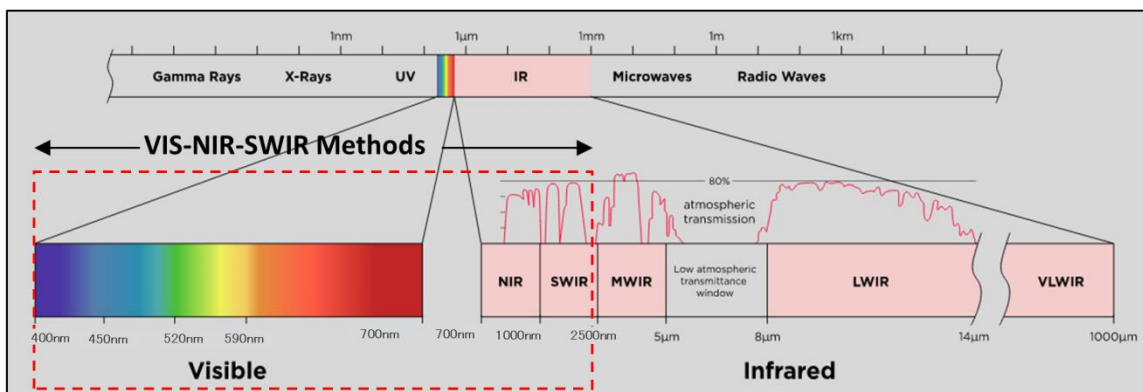


Figure 1. Electromagnetic spectrum with wavelength ranges indicating spectral regions. Modified after original (<https://www.infinitioptics.com/technology/multi-sensor>).

When electromagnetic waves come into contact with a material, they are transmitted, reflected, and/or absorbed, as evident from the following expression based on the law of conservation of energy:

$$\rho + \alpha + \tau = 1 \quad (1),$$

where ρ - reflectance, α - absorptance, and τ – transmittance.

Since soil is an opaque material, the energy is not transmitted, but either absorbed or reflected. The absorption-reflection proportion is wavelength dependent and varies from one type of material to another.

The reflectance factor (ρ) (Eq. 2) spectrum is the result of collecting values at every spectral band (λ) from the ratio of the radiant flux (B) actually reflected by a target surface (e.g. soil) to that of a perfectly diffuse surface under the same geometry of illumination and observation (Fig.2) (Schaepman-Strub, Schaepman, Painter, Dangel, & Martonchik, 2006). "Perfectly diffuse" (Fig. 4) means a Lambertian surface with $\rho(\lambda)=1$ (Spectralon® reference panel).

$$\rho(\lambda) = \frac{B(\lambda)}{C(\lambda)} \quad (2)$$

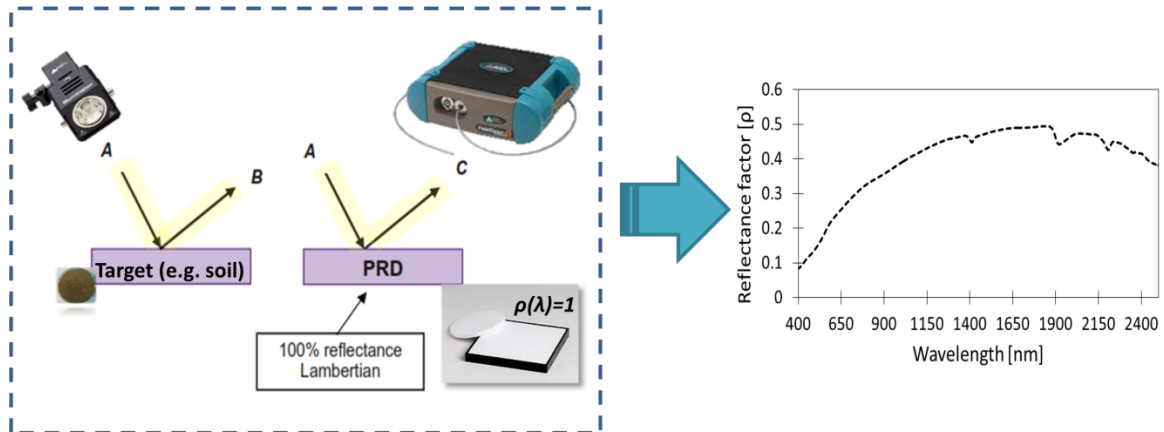


Figure 2. Acquisition of reflectance factor spectrum: A= irradiance; B is target radiance; C is radiance of the reference panel; ρ -reflectance factor and PRD is Perfectly Reflecting Diffuser

The amount of reflected energy can be registered by the sensors and obtained spectra used for information extraction allowing materials differentiation and characterization (Fig. 3).

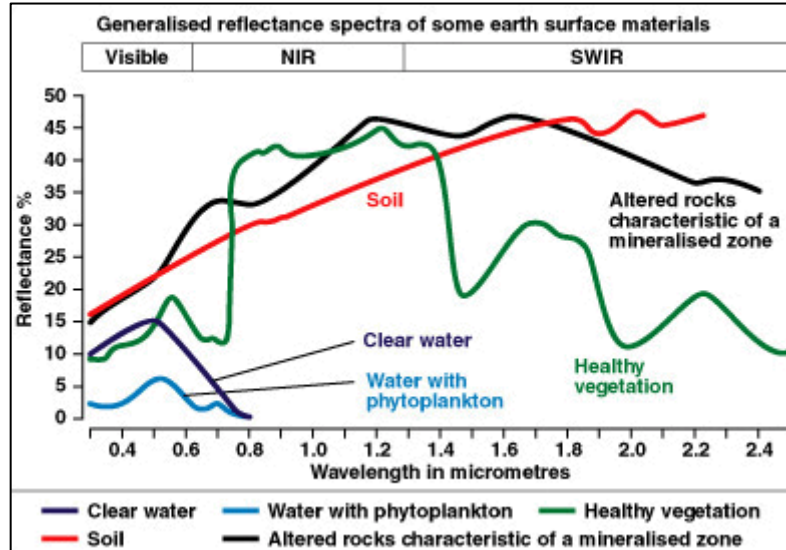


Figure 3. Typical spectra of materials usually found on Earth’s surface. (Source: https://www.usna.edu/Users/oceano/pguth/md_help/html/ref_spectra.htm)

When radiomagnetic radiation strikes the matter, it triggers the processes of electronic or vibrational transition. Electronic processes involve transition of the electrons from one level to another in atoms/ions of soil constituents with the consequent charge transfer; whereas vibrational processes result from the excitation and vibration of anion groups and molecules (e.g. H₂O, CO₂) in the crystal structure of soil minerals (Hunt & Salisbury, 1971). The effects of electronic transitions are evident mainly in VIS-NIR-SWIR spectral regions (Fig. 5), while the vibrational processes mostly impact the MIR spectral range.

Two types of reflectance are observed: specular reflectance and diffuse reflectance (Fig. 4). For specular reflectance, the angle of reflection is equal to the angle of incidence (Fig. 4a); at all other angles, only diffuse reflectance (Fig. 4b) is observed. Because VIS-NIR-SWIR soil spectroscopy measures only diffuse reflectance, it is often referred to as diffuse reflectance spectroscopy (DRS) (Torrent & Barrón, 2008). It is also sometimes called “Proximal sensing” (Viscarra-Rossel, Adamchuk, Sudduth, McKenzie, & Lobsey, 2011).

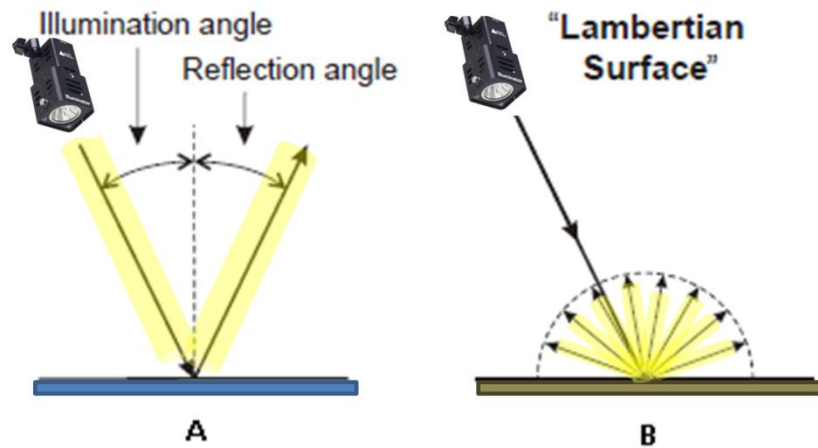


Figure 4. Types of reflectance: A- specular and B – diffuse (modified after (Lillesand, Kiefer, & Chipman, 2014))

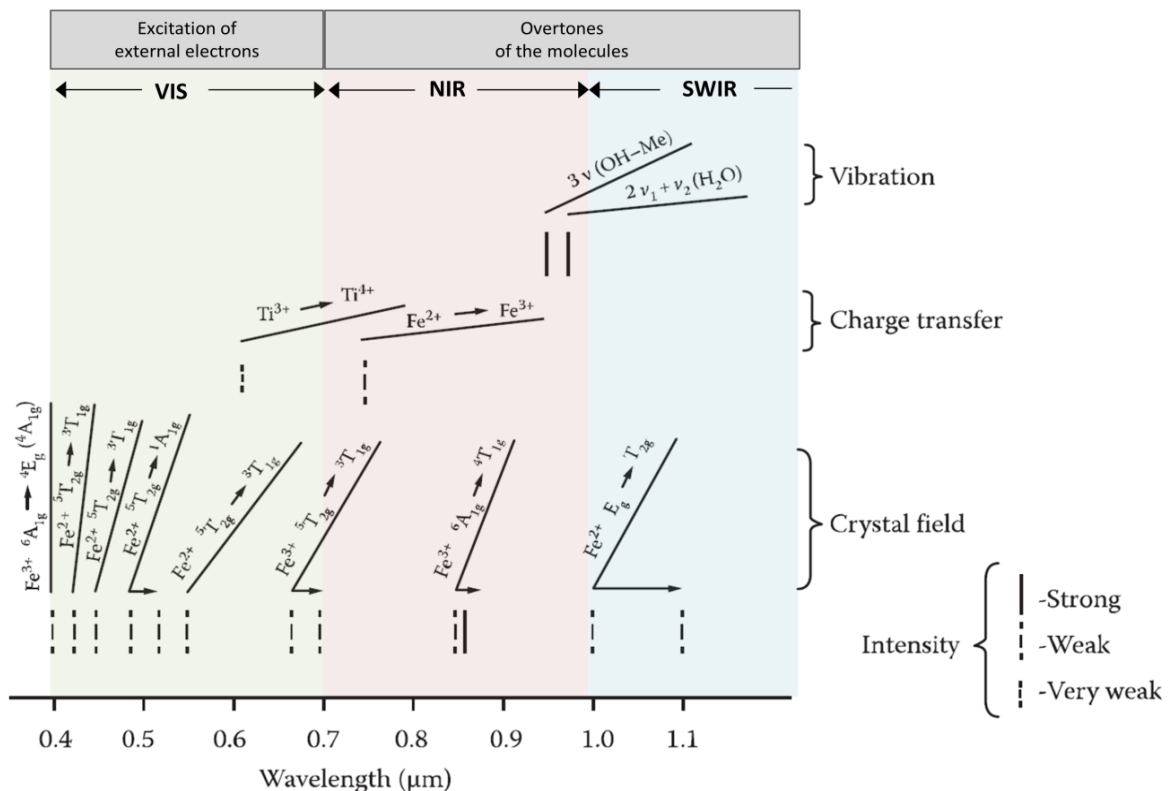
Proximal sensing is an integral part of remote sensing, which is defined as “acquisition of information about an object by detecting its reflected or emitted energy without being in direct physical contact with it” (Elachi & Van-Zyl, 2006; Jensen, 2009). While the term Remote Sensing can be applied to energy detection by sensors located on any platform (ground, air-borne, satellite, etc.) and in any type of environment (field, laboratory, etc.), “Proximal Sensing” is used only for sensors registering the signal from a short distance (Viscarra-Rossel et al., 2011). Spectral measurements are performed with spectroradiometers which register energy coming from natural (sunlight) or built-in (spectral probe) sources of illumination. Soil preparation for laboratory measurements consists of spreading sieved and air-dried samples into plastic or glass containers (petri dishes). Laboratory conditions provide the opportunity to control illumination conditions and observation geometry, which results in high-resolution spectra characterized by high signal-to-noise ratio. Various properties can be estimated simultaneously and results are immediately available.

Field measurements use illumination from the sun or a probe with a built-in light source. In-situ acquisition of soil spectra is more complicated because additional factors, such as atmosphere and moisture content, should be taken into account. Under natural illumination contribution of specular and diffuse components of reflectance is comparable, and the proportion of each one depends on atmospheric conditions, topography and soil “surface state” properties (Escadafal, 1989), i.e. particle size,

structure and surface roughness. When working in the field, it is possible to scan not only the surface layer, but also under surface horizons of the undisturbed soils.

2.3. Spectral properties of soils

It has been demonstrated that some chemical and physical properties of soils are related to soil spectral properties. The components of soil mixture that absorb incident radiation in discrete energy levels and whose reflectance spectra reveal chemical (Fig. 5) and physical attributes (Fig. 6) are called chromophores (Ben-Dor et al., 1999; Dematte et al., 2002). Spectral behavior of soils was first described by (Condit, 1970) and (Baumgardner, Silva, Biehl, & Stoner, 1986) who identified several spectral shape patterns typical for soils (three and five, respectively). More detailed methodology of using spectral reflectance curves for differentiation of soils, based on curve shape, reflectance intensity and absorption features, was developed by (Demattê, 2002). Essential edaphic components, such as organic matter, clay minerals and iron oxides present characteristic absorption features caused by electronic transitions in the VIS and by overtones and combination modes of functional groups in the NIR and SWIR spectral regions (Hill, Udelhoven, Vohland, & Stevens, 2010; Stenberg, Viscarra-Rossel, Mouazen, & Wetterlind, 2010).



Continue below...

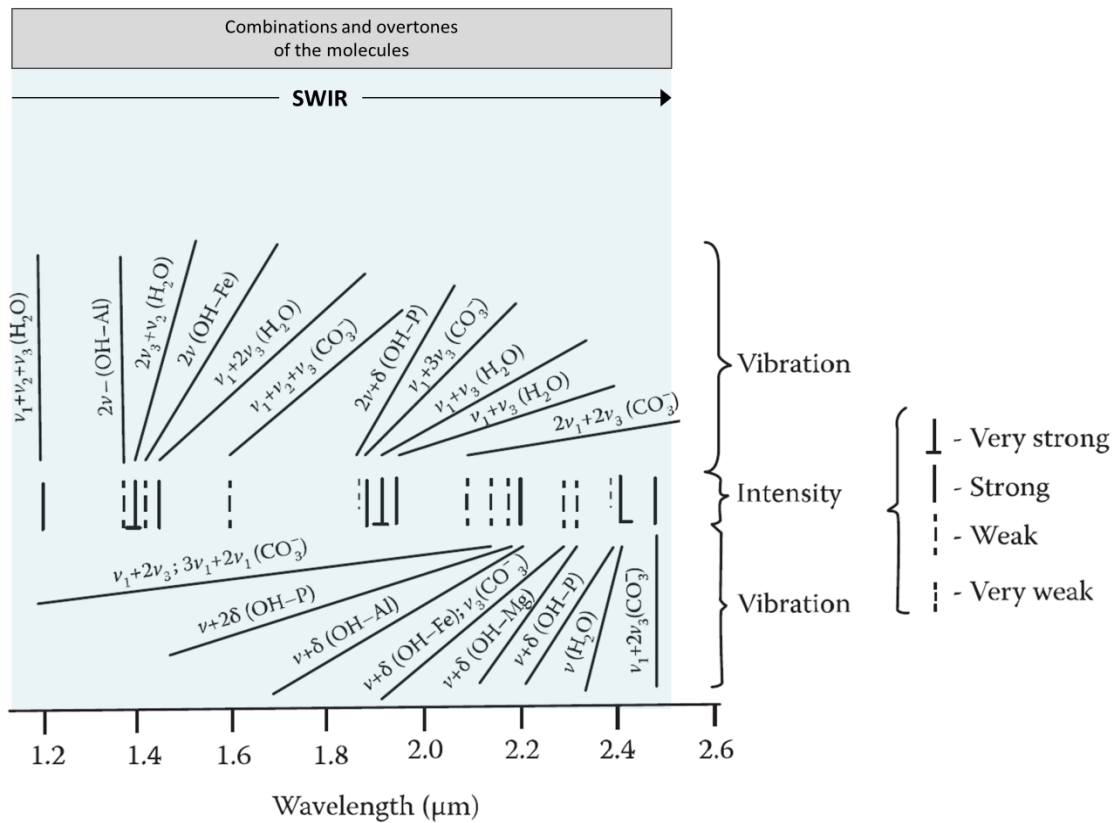


Figure 5. The spectral active groups and mechanisms of the chemical soil chromophores. The wavelength range and feature intensity are given for each possible group (Ben-Dor et al. 1999, modified)

Because soils are mixtures of organic and inorganic particles with highly variable proportions of each substance and particle size, their spectra present overlaps of spectral features corresponding to specific soil constituents (Ben-Dor & Demattê, 2016), Spectral response is also strongly influenced by water content, with the strongest absorption bands near 1400 and 1900 nm, and with weaker bands in other parts of the spectra (Liu et al., 2003). The mineral part of soils, which represents in general 50% of its volume (Schulze, 2002), has strong distinct characteristics in the VIS-NIR-SWIR region in reflectance intensity, curve shape and absorption features (Fig. 6) (Hunt, 1977). Particle size is also distinguishable in soil spectra (Curcio, Ciruolo, D'Asaro, & Minacapilli, 2013).

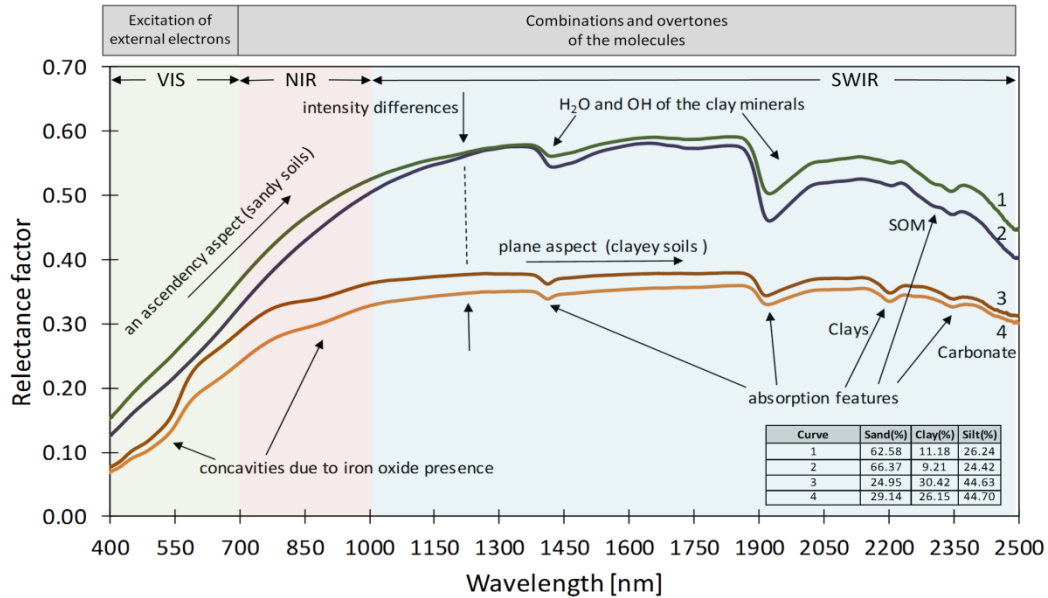


Figure 6. Soil reflectance spectra with indication of typical spectral features and characteristics.

2.3.1. Soil organic matter

Soil organic matter and the composition of the organic components have a strong influence on the soil reflectance; previous works assessing SOM content found a wide spectral range influenced by this property what suggests that OM is an important chromophore across the entire spectral region (Baumgardner et al., 1986; Ben-Dor et al., 1999). When organic matter content exceeds a concentration of $2 \text{ g } 100\text{g}^{-1}$, it causes reflectance to decrease, particularly in the VIS, and can mask absorption bands of other materials. These masking properties become less effective as the organic matter content drops below $2 \text{ g } 100\text{g}^{-1}$ (Baumgardner et al., 1986; Ben-Dor et al., 1999). Different organic constituents affect soil reflectance to a varying degree (Fig. 7).

(Ben-Dor, Inbar, & Chen, 1997) investigated the change of the reflectance spectra of organic matter in the VIS-NIR to SWIR regions (400-2500 nm) during a biological decomposition process and revealed that OH- and C-H_x groups of hygroscopic water, starch, cellulose, and lignin correlate highest with composting time and may be used for estimation of organic matter contents.

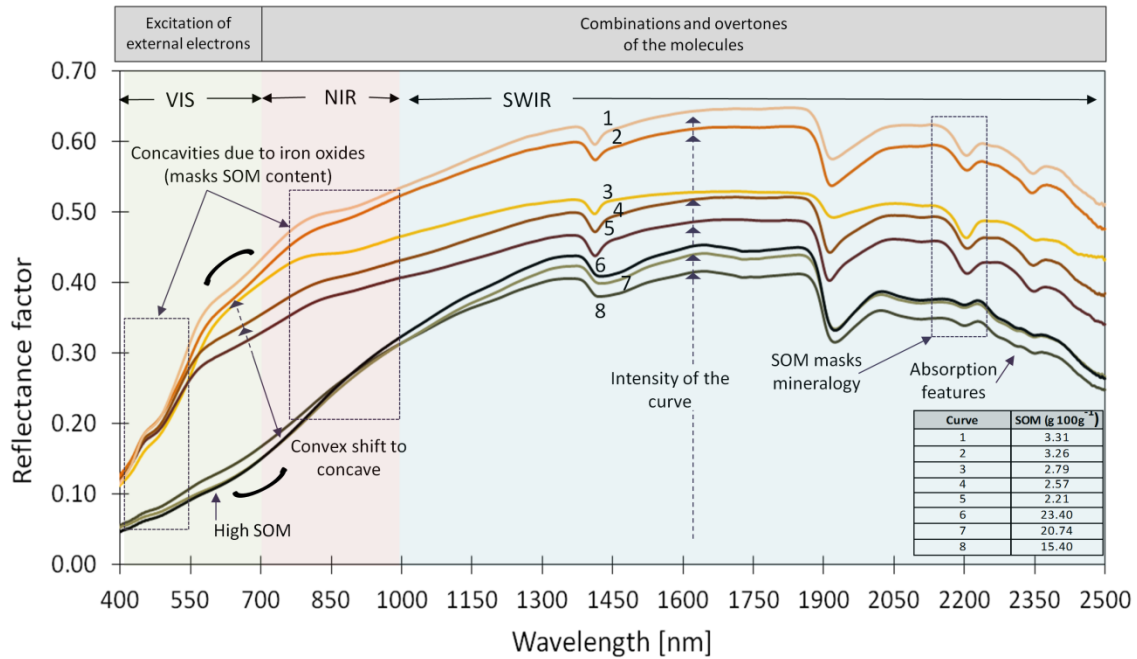


Figure 7. Reflectance spectra of soils with high and low organic matter content and the shape of the curves that change due to SOM.

2.3.2. Soil texture

Reflectance and scattering of light striking soil surface depends not only on soil chemical composition, it is also affected by the size and form of soil particles, e.g. soil texture, determining the angle of light incidence and index of refraction of the surface material, factors governed by Fresnel's law. Fig. 8 illustrates how these factors impact the soil spectrum base height and modify the intensity of absorption features (Ben-Dor, Goldshleger, Benyamini, Agassi, & Blumberg, 2003).

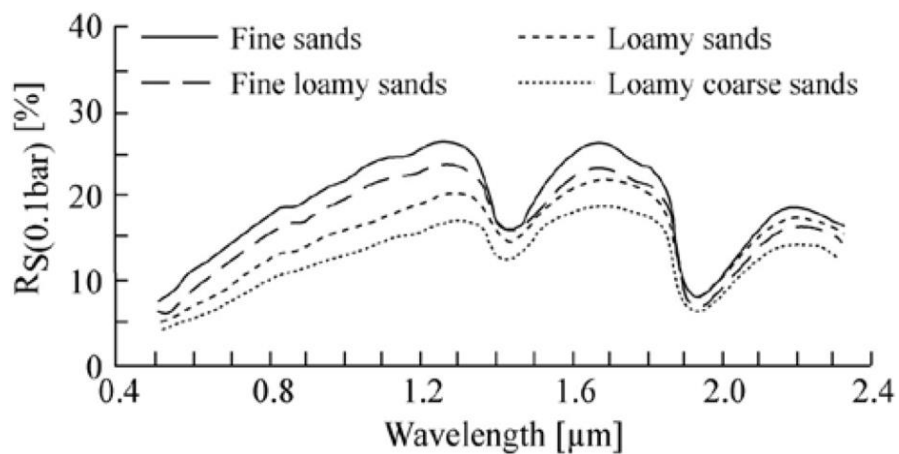


Figure 8. Reflectance spectra of soils with different texture (Baumgardner et al. 1986).

Soil texture is closely related to the mineral composition of soils, mainly to the presence of clay minerals and the quartz content. Thus, it directly influences the soil spectra. The increased proportion of smaller particles often causes higher overall reflectance and decrease in the depth of the absorption features of soil spectra (Baumgardner et al., 1986; Van-der-Meer, 1995). This is especially true for spectral features in SWIR region in the spectra of transparent materials, such as silicates (Hunt & Salisbury, 1971). On the contrary, the spectra of opaque materials show reflectance decrease with the increment of smaller size particles. Some materials, such as iron oxides, show behavior typical for transparent materials in the wavelengths greater than 550nm and reflectances typical for opaque materials in the wavelengths shorter than 550nm (Hunt & Salisbury, 1971).

In soil spectra collected under natural illumination, the effect of size particle can be masked by effect of soil aggregation, which explains why clayey soils with large size aggregates produce spectra characteristic for “rougher” surfaces (Matthias et al., 2000; Stoner & Baumgardner, 1981).

Clay content is one of the soil properties most successfully quantified with spectroscopic methods mainly due to the presence of OH group spectrally active in the VIS-NIR-SWIR region (Ben-Dor et al., 1999). The clay mineral main spectral response (for smectite minerals in particular) is localized within three spectral regions: 1300-1400 nm, 1800-1900 nm, and 2200-2500 nm (Chabrilat et al 2002). For calcium montmorillonite (a common clay mineral in the soil environment) spectral activity is found at 1414 nm and at 2205 nm. The OH absorption features of free water are located at 1455 nm, 1915 nm, and 1980 nm (Fig. 4). These positions can change slightly from one smectite sample to another, depending upon the chemical composition and surface activity.

Sand content can also be predicted using spectroscopic techniques (Soriano-Disla et al., 2014). Sand spectra usually present an absorption peak around 1400 nm related to the -OH stretch vibration of water in crystal lattice of silicates (Bishop, Pieters, & Edwards, 1994; Hunt & Salisbury, 1971; Sørensen, Demler, & Lukin, 2005).

2.4. Soil properties estimation from VIS-NIR-SWIR spectra

Because soil spectra consist of a large number of highly correlated bands and represent overlaps of spectral features characteristic to the constituents, soil variables are not directly calculated from the spectra, and empirical quantitative approaches have been developed to obtain chemical–physical information. Multivariate statistical methods are used to develop calibrations based on reference attribute values of a set of samples representative of the soil variation in the study area. The quality of input data is sometimes improved with spectral pretreatment; commonly used procedures available in various software packages include Savitsky-Golay transform (Savitzky & Golay, 1964), multiplicative scatter correction (Geladi, MacDougall, & Martens, 1985) and the use of first and second derivative spectra (Stenberg & Viscarra-Rossel, 2010). The spectra of representative spectra generated following established protocols and accompanied by reference information, conform spectral libraries, allowing reuse and data sharing.

Modeling methods based on linear models have long proved their efficiency (Mouazen, et al., 2010; Vasques et al., 2014; Viscarra-Rossel et al., 2006). The most frequently used algorithms include multiple linear regression (MLR), principal component analysis (PCA) and partial least squares regression (PLSR) achieving quite good predictions of organic matter/organic carbon, iron oxides, clay minerals, carbonates and water at local (Kuang & Mouazen, 2013; Udelhoven, Emmerling, & Jarmer, 2003) and regional (Stevens, Nocita, Tóth, Montanarella, & van Wesemael, 2013) levels.

The frequent choice of PLSR is explained by its capacity to produce well-fit models from data sets containing a small number of observations characterized by a great number of correlated predictors. Robustness of the models is mainly achieved through reduction of data dimensionality using a set of orthogonal vectors (components) (Wold, Sjöström, & Eriksson, 2001). Still, PLSR models sometimes demonstrate unrealistically high fit due to inclusion of noise variables relevant only for calibration dataset, which is known as overfitting (Babyak, 2004; Esbensen, 2000). One of the recently introduced alternatives is the correlated components regression (CCR) approaching overfitting problem in a different way. It prevents model over fit through application of the

regularisation process, which involves identification of suppressors and elimination of less relevant predictors (Magidson, 2013).

In spite of general success, results of the studies using linear-based methods are quite variable. One of the possible reasons is that complex interactions between soil components affecting their spectra are often non-linear (Ben-Dor, Chabrilat, Demattê, Lyon, & Huete, 2019). Hence, there is a need for more research addressing the issue. Soil scientists analyzing soil spectra lately have been paying much attention to machine learning algorithms, and data mining techniques and tools, such as, for example, artificial neural networks (Mouazen et al., 2010), support vector machines (Viscarra-Rossel & Behrens, 2010), memory-based learning (Hong et al., 2019) and fuzzy rule-based models (Tsakiridis, Theocharis, Ben-Dor, & Zalidis, 2019). In these studies new tested methods have outperformed most common algorithms.

2.5. Integration of soil spectroscopy with other data sources and methods

Multiple studies have demonstrated that inclusion of additional variables characterizing landscape and/or environment; improve the quality of spectroscopic predictions (Demattê et al., 2016; Viscarra-Rossel & Chen, 2011). On the other hand, data generated by proximal soil sensing can serve as support for more precise land cover mapping from images acquired by airborne and satellite sensors (Escribano, Schmid, Chabrilat, Rodríguez-Caballero, & García, 2017).

In this context several approaches can be implemented: laboratory soil spectra can be used for simulation of satellite resolution spectra to assess the feasibility of soil properties estimation in the satellite images (Melendez-Pastor, Navarro-Pedreño, Gómez, & Koch, 2008; Palacios-Orueta, Pinzon, Ustin, & Roberts, 1999; Palacios-Orueta & Ustin, 1998), as well as the benefit of their use as one of the endmembers in spectral mixture analysis (Chabrilat, Goetz, Krosley, & Olsen, 2002); together with other landscape variables soil spectra (not only of a surface, but also subsurface layers) can be one of the inputs for geostatistical modeling of soil spatial patterns in digital soil mapping (Minasny & McBratney, 2016).

Finally, modeling soil properties can involve fusion of proximal and remote sensing data (Grunwald, Vasques, & Rivero, 2015). The creation of meta-models, encompassing

large databases of point soil observations, environmental data and data generated by sensors of different types has also been suggested (Koricheva, Gurevitch, & Mengersen, 2013; Pigott, 2012). The greatest limitation to meta-analysis is the lack of homogeneity in the primary data and the in case of soil spectral libraries, incomparability of data due to the lack of standardization in protocols and instrumentation of spectral measurements (Ge, Thomasson, & Sui, 2011).

3. Study area and soil sampling

The present research used datasets coming from the three different study areas shown in Fig. 9. One of them is located in Europe (Spain), and the other two are situated in Ecuador and Brazil in South America.

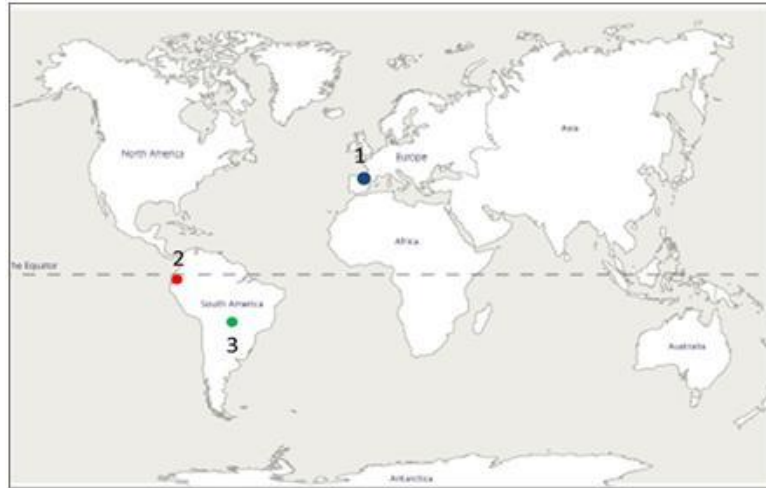


Figure 9. Location of the study sites in Spain (1), Ecuador (2) and Brazil (3).

3.1. Aragón, Spain

Methodological part of research (the first two specific objectives) were developed using soil samples from the wildfire burns and areas of cropland abandonment in Autonomous region of Aragón in northeastern Spain (Fig. 10). The hilly area of approximately $\sim 300\text{km}^2$ at elevations 450-1300 m above sea level is part of pre-Pirinean range. The climate is semiarid with average annual temperature of 12.5 °C, and precipitation around 560 mm unequally distributed throughout the year (peaks in spring and autumn and minimum in summer) (Cuadrat & Vide, 2007). The forest vegetation covering most of the area is dominated by *Pinus halepensis* (Vicente-Serrano, Pérez-Cabello, & Lasanta, 2011) and dense understory with species, such as *Buxus sempervirens*, *Quercus coccifera*, *Juniperus oxycedrus*, *Rosmarinus officinalis* and *Genista scorpius*. The same species can be seen in places where forests are interspersed with brushlands. This area is regularly affected by wildfires, which are mainly responsible for structure and development of Mediterranean forests. Even though these ecosystems have demonstrated high capacity of post-fire auto-regeneration, the increase in frequency and intensity of fires observed in last decades make it necessary to plan

and implement efficient management strategies stimulating natural forest recovery after fires.

Typical soils are coarse and medium-textured Cambisols over calcareous bedrock (Fig. 10), with important amounts of changeable minerals in silt and clay fraction. In some areas Cambisols are interspersed with Regosols and Leptosols (Badía-Villas & del Moral, 2016). Regosols are unconsolidated soils of recent formation whose properties mainly depend on those of underlying parental material. On the other hand, Leptosols are shallow soils of silt and loam texture present a physical (rock) or chemical (highly carbonated substrate) barrier layer immediately below the surface material. These soils thin and stony soils typical for areas of agricultural abandonment (FAO, 2015) are characterized by low water-holding capacity. In semiarid and mountainous Mediterranean environment the property increases surface runoff and exacerbates soil vulnerability to water erosion (Badía, Valero, Gracia, Martí, & Molina, 2007).

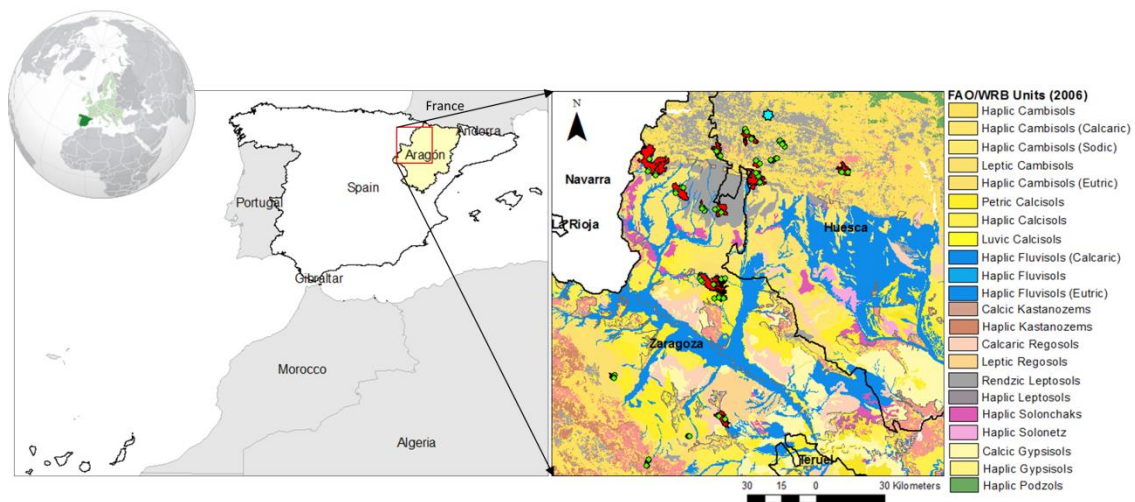


Figure 10. Soils in the Aragón study area. The map uses the color scheme adopted by ISRIC World Soil Information for SoilGrids250m (FAO/WRB 2006). Sampled wildfire burns are shown in red, sampling sites in green dots and cropland abandonment area in light blue dot.

Soil samples from wildfire burns (82) and areas of cropland abandonment (31) were collected in summer of 2013 and 2014 (Fig. 11). The selection of the burns is based on the information from the database of wildfire burns maintained by the Aragón Government (Service for Management of Wildfires and Coordination, Head Office for Forest Management) complemented with cartography created in the frame of the research project “Forest fires and predictive models of ecologic vulnerability to fire:

restoration management activities and application of climate change scenarios” GA-LC-042/2011 (Caixa-DGA). Only the samples obtained from the surface soil layer were used in this research. Analysis of soil organic matter content and the percentage of oxidisable SOM were performed in the Aragón Government Agroenvironmental Laboratory (Food Safety Service of Department for Food and Agricultural Development).



Figure 11. Photos of the 1995 wildfire burn area in Aragón, Spain taken during the 2013 sampling campaign: general view (A) and sampling site (B, C and D).

Other group of surface soil samples was collected from different land covers in the catchment of Araguás, abandoned for agricultural activities in the 1950s (Fig. 12). Parts of the area were later afforested with *Pinus nigra* and *Pinus sylvestris*, while other areas experienced the process of natural succession with *Genista scorpius* and *Buxus sempervirens*. Typical land covers determined based on the analysis of aerial photography, topographic maps, and field survey information are bare soil, permanent pasturelands, secondary succession, afforestation with *Pinus sylvestris* and *Pinus nigra*. For these samples, the loss on ignition method was used to determine SOM; soil texture fractions were determined using a particle analyser (Micromeritics, SediGraph 5100, Nocross, USA).

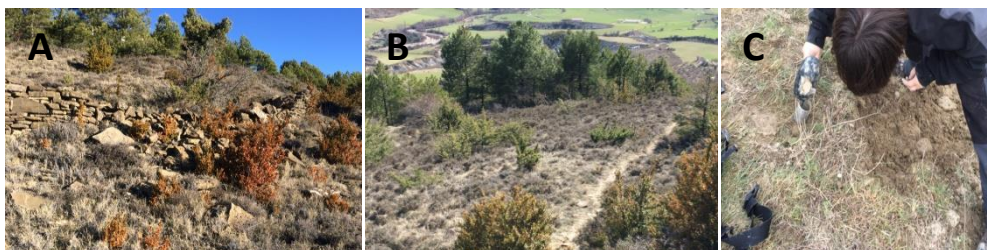


Figure 12. Photos of the cropland abandonment in the catchment of Araguás in Aragón, Spain taken during the 2014 sampling campaign: general view (A, B) and sampling site (C). Source: photos taken by Dr. Nadal-Romero and researchers in 2014.

3.2. Campos Amazônicos National Park, Brazil

The research methodology developed in the main study area in Spain was applied in analysis of soils from the Campos Amazônicos National Park (CANP) in Brazil, area which regularly suffers from wildfire burns. Soil samples were collected in Campos Amazônicos Savanna Enclave (CASE) within CANP (Fig. 13).

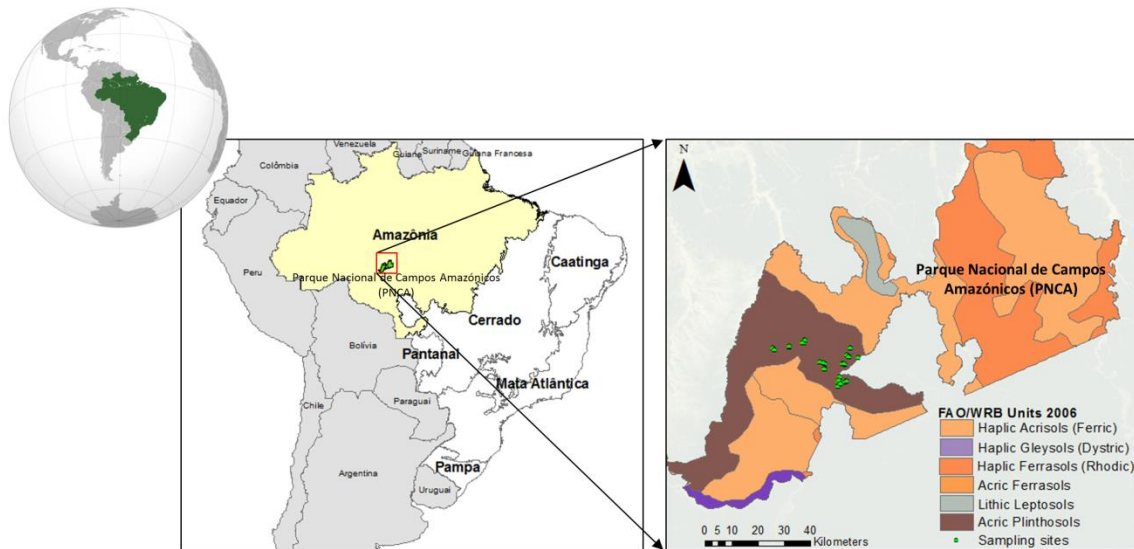


Figure 13. Location of the study area in Campos Amazônicos National Park in Brazil.

The climate of this relatively flat area is characterized by 24°C-28°C mean temperature and more than 2000mm annual rainfall. There are two seasons, wet (November-March) and dry (May-September); April and October usually correspond to the transition between the two seasons (Marengo et al., 2008). The vegetation cover is quite variable, while forested areas are common in the proximity of the streams (riparian vegetation), grasslands, shrubby grasslands and shrubby savanna cover the rest of the area (Oliveira-Filho & Ratter, 2002).

Although various soil types are present in the CANP, the Plinthosols characterized by the presence of plinthite in the B horizon) (Blake et al., 2008) predominate (Fig. 13). Plinthosols are rich in kaolinitic clay mixed with quartz and other components; this mixture is easily hardens or transforms to irregular aggregates when it is repeatedly wetted and dried.

Soil samples were obtained in September 2016 in areas CASE recovering from wildfire burns (Fig. 14). They come from areas of shrubby grassland (15 samples) and riparian (15 samples) vegetation. The standard method of wet combustion was used for determination of SOM values.



Figure 14. Collection of soil samples in CANP Savanna Enclave, Brazil: general view (A) and sampling site in area of riparian vegetation (B, C, D). Source: photos taken by Dr. Borini and researchers of CANP in 2016.

3.3. Mocache, Ecuador

The work on the third specific objective of this research was developed on a farm located in the district of Mocache, province of Los Rios, in Ecuadorian lowlands (Fig. 15). The hilly area at elevations ranging between 80m and 120m above sea level is characterized by tropical climate with mean annual temperature around 25°C and 1800-2000mm of annual precipitation. There are two clearly distinguishable seasons: dry (June – December) and wet (January –May).

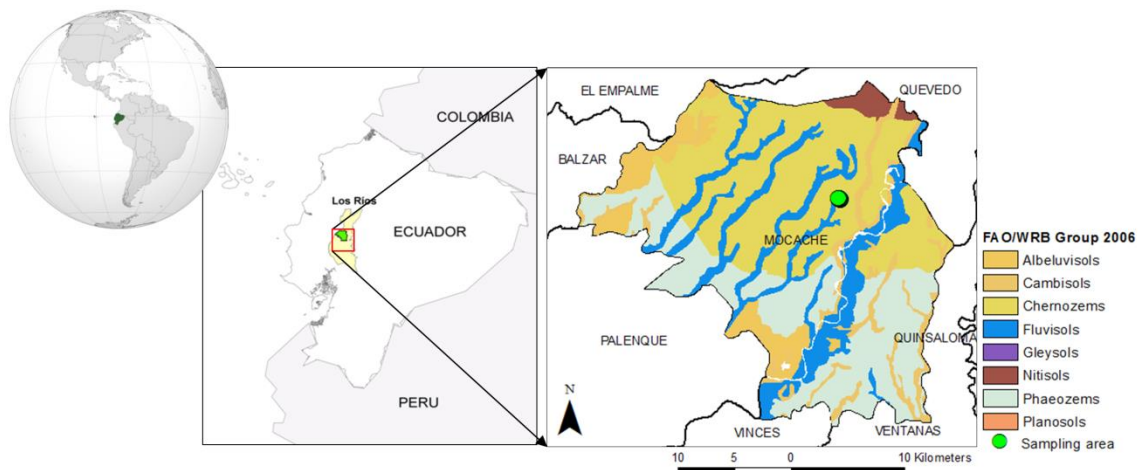


Figure 15. Location of the study area in Mocache district in Ecuador.

The Bella Siria study site is the area of intensive production of maize (*Zea mays*) under the slash-and-burn system (Fig. 16), which requires a minimum investment of

funds and technology. The total of 18 surface-layer samples was collected during the field campaign of September 2015. One of the areas has been experiencing regular controlled burns during 6 years before sampling, while another is the area where the cocoa trees were recently eliminated to use it for growing maize. Both areas were sampled next day after the burning of residual biomass at the end of the crop growing cycle.

Each sample was divided in two parts. One part was analyzed using conventional methods of SOM and texture estimation in the Laboratory of National Institute for Agricultural Research, Quevedo, Ecuador; and the other (approximately 160 g of air-dried soil per sample) was used for spectral measurements in the University of Zaragoza, Zaragoza, Spain.



Figure 16. Photos of fire-affected soils in areas of slash-and-burn agriculture in Mocache district, Ecuador taken during the 2016 sampling campaign : general view (A, B) and sampling sites (C, D, E).

4. Methodology

The research workflow discussed in this chapter is presented in Fig. 17. The following sub-sections give more details on each step.

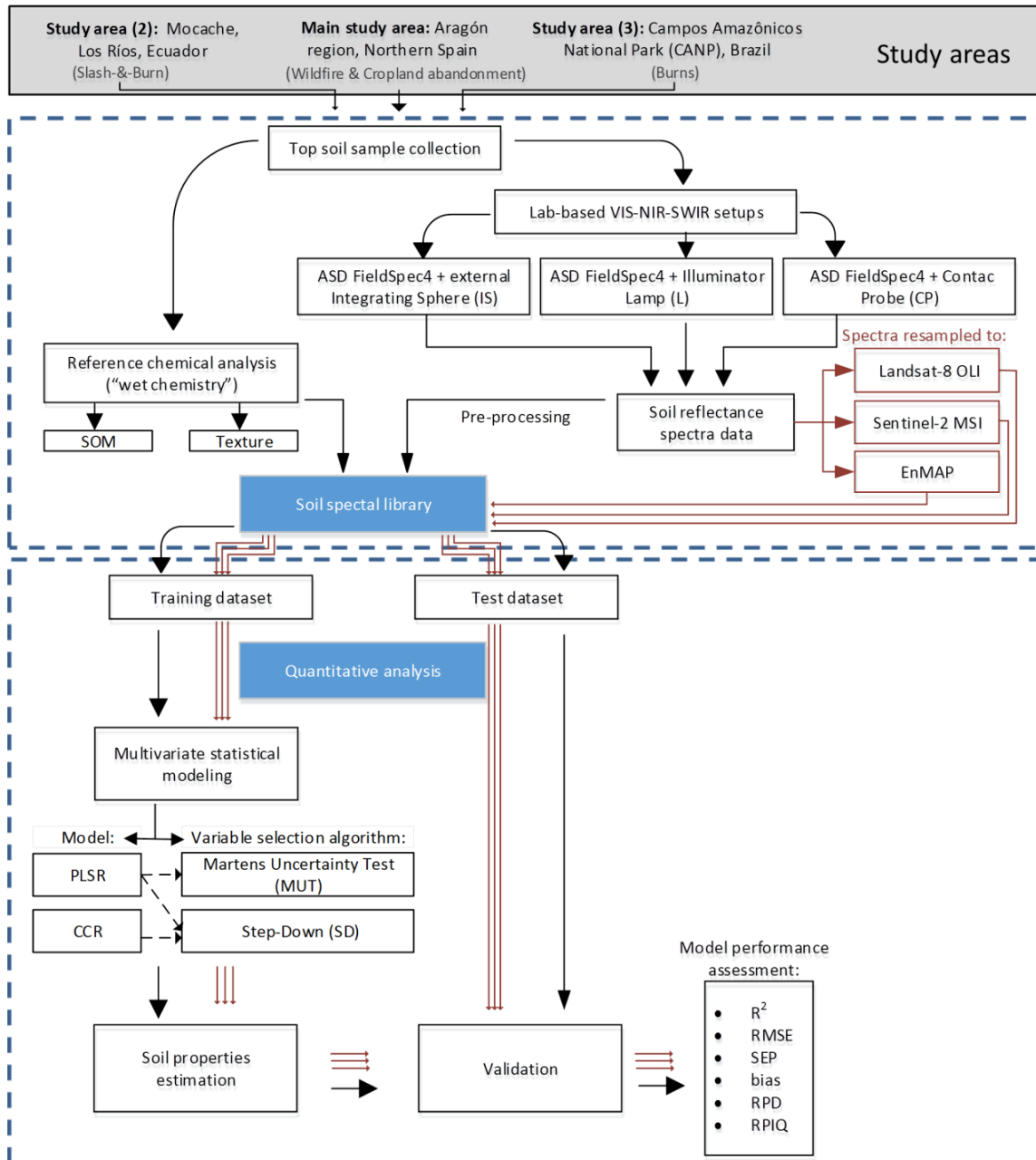


Figure 17. Workflow diagram for the methodology of the thesis.

4.1. Spectral measurements

VIS-NIR-SWIR spectra of soil samples were obtained in the laboratory conditions. Sample preparation consisted in separation of particles smaller than 2mm. The sieved soil was then placed in 90mm-diameter Petri dishes, smoothed to obtain a homogeneous layer of ~15 mm thick weighing approximately 160g, and dried in the oven (24h at 105°C).

Reflectance spectra were obtained with high-resolution Analytical Spectral Device (ASD) FieldSpec®4 spectroradiometer, which incorporates three spectrometers (detectors) for three specific spectral ranges: VISNIR (350-1000 nm), SWIR1 (1001-1800 nm) and SWIR2 (1801-2500 nm). The spectral sampling interval of the instrument is 1.4 nm and 2 nm, and spectral resolution (Full Width at Half Maximum - FWHM) of 3 nm and 10 nm, for VIS-NIR and SWIR spectral regions, respectively (ASD, 2012a). During measurements device software performs correction for baseline electrical signal (dark current) and resampling of the spectra to a 1 nm interval over the whole sensed wave range (Fyfe, 2004). The spectroradiometer uses a fiber optic cable to register the source light reflected by the sample surface, and provides the choice of attachments to be used for different targets and environments different (Fig. 18).

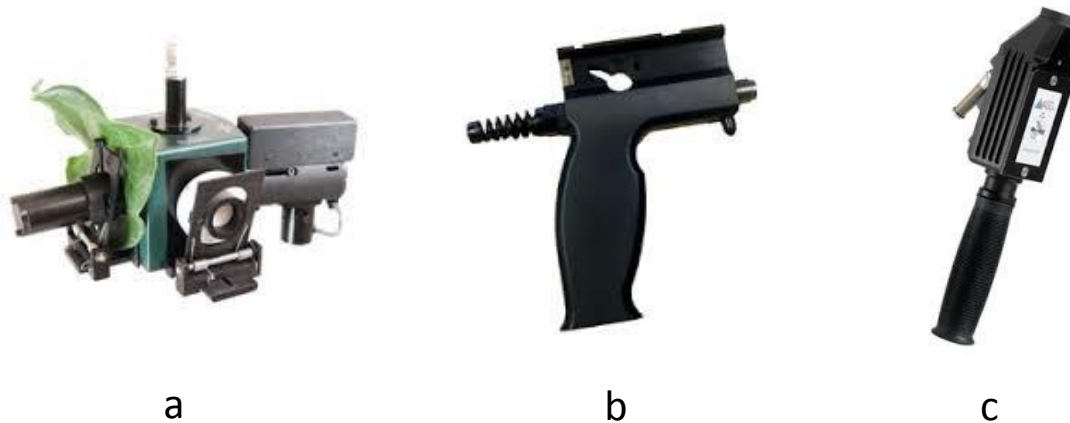


Figure 18. Different attachments to spectroradiometer FieldSpec®4 used in spectral measurements: (a) integrating sphere; (b) pistol grip; and (c) contact probe.

Actually, the radiometer has been measuring reflectance factor, which is the ratio of the radiant flux reflected by the target surface to that reflected by the ideal standard surface (Schaepman-Strub et al., 2006). In fact, when both incoming and reflected

radiances can be approximated as cones, non-imaging spectroradiometers register Biconical Reflectance Factor (BCRF) (Schaepman-Strub et al., 2006), as in case of the present research.

The calibrated Spectralon® polytetrafluoroethylene (PTFE) reference surface from the radiometer manufacturer was used as reference, since it satisfies all the requirements (perfect reflectance over the full wavelength range and environmental resistance).

To determine on the more adequate instrument configuration, the spectra were obtained in dark laboratory with three laboratory setups including different ASD accessories (Fig. 19): (i) the RTS-3ZC external integrating sphere (IS); (ii) Illuminator lamp (L) and pistol grip; and (iii) contact probe (CP). The ASD RS3 software (ASD, 2012a) was configured to average 10 spectra per each sample scan, 25 white reference, and 10 dark current to reduce noise and improve signal-to-noise ratio.

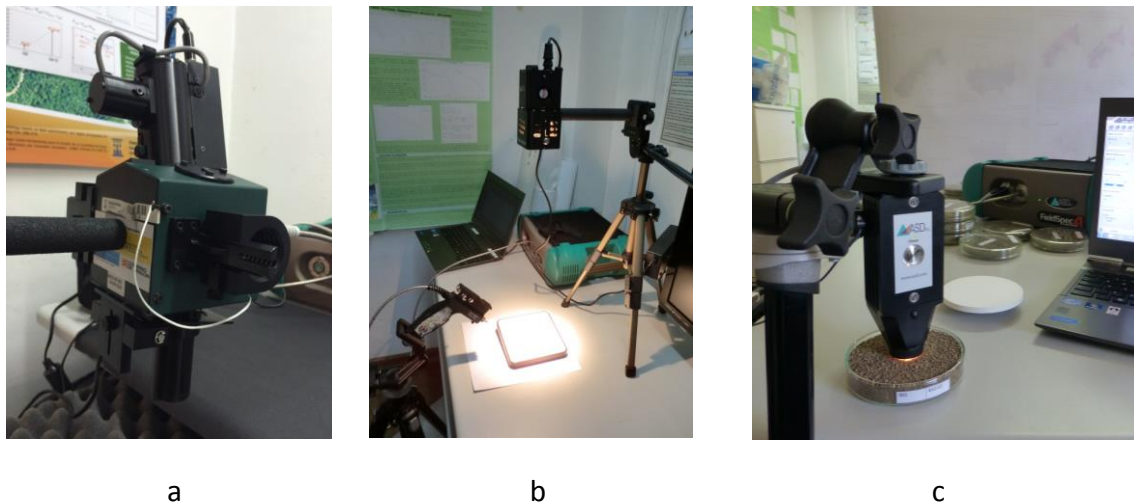


Figure 19. Experimental configurations tested in this study: (a) Setup IS with integrating sphere, (b) Setup L with the ASD Illuminator Lamp and pistol grip; and (c) Setup CP with the ASD contact probe.

4.1.1. Experimental setup IS (external integrating sphere)

The experimental setup with external integrating sphere RTS-3ZC coupled with the ASDFieldSpec®4 spectroradiometer (IS) is shown in Fig. 18a. The word “external” refers to the position of the sample, i.e. external to the sphere. The spherical cavity of the attachment is coated with a white diffuse polymer (PTFE) allowing spatial

integration of radiation reflected by the sample, which ensures the accuracy of the measurements. The internal coating of the sphere is an almost perfect Lambertian reflector over the whole operating spectral range of the spectroradiometer. During the measurement, a sample placed in the holder acts as a part of the sphere wall allowing it to “concentrate” the signal reflected from the sample and distribute it over the internal surface of the sphere. The sensor registers the light reflected by the wall and makes an estimate of the sample reflectance. The sphere provides six ports 13 mm (ports A, D and H), 15 mm (ports C and B) and 19 mm (port E) in diameter, which serve as attachment points for supplied sample holders, a light source assembly, fiber adaptor, light trap, and port plugs. The following expression (Eq. 3) was applied to correct total reflection of the sample $R_T(\lambda)$ for the stray light (ASD, 2008):

$$R_T(\lambda) = \frac{(R_{sample}(\lambda) - DR(\lambda))}{(R_{reference}(\lambda) - DR(\lambda))} R_{ref_cal}(\lambda) \quad (3)$$

where R_{sample} is the measured reflectance of the target; $R_{reference}$ is the measured reflectance of the white reference; and DR is the dark current reading registered when the light trap is located in the place of the target. Although the background radiation DR is often negligible, in this research it was considered in reflectance calculations. The reflectance of calibrated reference standard R_{ref_cal} was estimated from cross-calibration of the two reference surfaces (Miura & Huete, 2009):

$$R_{ref_cal}(\lambda) = \frac{L_{ref_cal}(\lambda)}{L_{RP}(\lambda)} R_{RP}(\lambda) \quad (4)$$

where: L_{ref_cal} is the radiance of the calibrated reference standard provided with the sphere (corrected for background current); L_{RP} is the radiance of calibrated reference panel (corrected for background current); and R_{RP} is the reflectance factor of calibrated reference panel provided with the ASD FieldSpec®4 spectroradiometer.

Although it is recognized that protocols can influence measurement results, no standards exist at the moment. In case of this study, the Petri dish containing soil sample was covered with unglazed black paper (optically flat surface) to prevent soil from entering the integrating sphere and to avoid undesired particle orientations (Torrent & Barrón, 2002). A circle of a size similar to the sample port aperture (18 mm) was cut in the center of the cover, to avoid the contact of soil particles with the external wall of the

sphere. In order to obtain spectral measurements the calibrated reference and soil samples were placed in the adjustable standard holders. A light trap was used to prevent from setup illumination with ambient light. In this setup, light comes from the collimated dual light source with high setting suitable for soils, instead of the low setting more suitable for vegetation targets. The integrating sphere was fixed on a tripod with a mounting rod attached to the port H on the underside of the sphere assembly (Fig. 19a). During the measurements the Petri dish with the soil sample is always maintained in a horizontal position, while the integrating sphere is rotated. Following the manufacturer recommendation, the sample spectrum is the average of 200 measured spectra (ASD, 2008).

Since three scans are necessary to obtain total reflectance of each sample with the above described setup, considerable time is necessary to complete the measurements. On the other hand, long sessions resulted in light intensity degradation due to the battery charge exhaustion. Hence, several 90 minute sessions were necessary to complete the measurements, each lasting about 1 h (16 processed samples per session).

4.1.2. Experimental setup L (illuminator lamp and pistol grip)

In another tested setup the optic fiber extreme is located inside the pistol grip (Fig. 18b). This setup uses an ASD illuminator lamp as a light source turned on 15 minutes before measurements for better stability (ASD, 2012b). Observation geometry was calculated considering various parameters: distance between the sample and the sensor, distance between the sample and the lamp, and angle between the two. The resulting setup configuration, ensuring that the sensor registers the signal from the spot within the petri dish, can be observed in Fig. 20.

The measurement protocol involved regular calibration of the fiber optic through cable direction at the reference panel using the same viewing geometry. The sample spectrum is an average of 50 radiometric measurements.

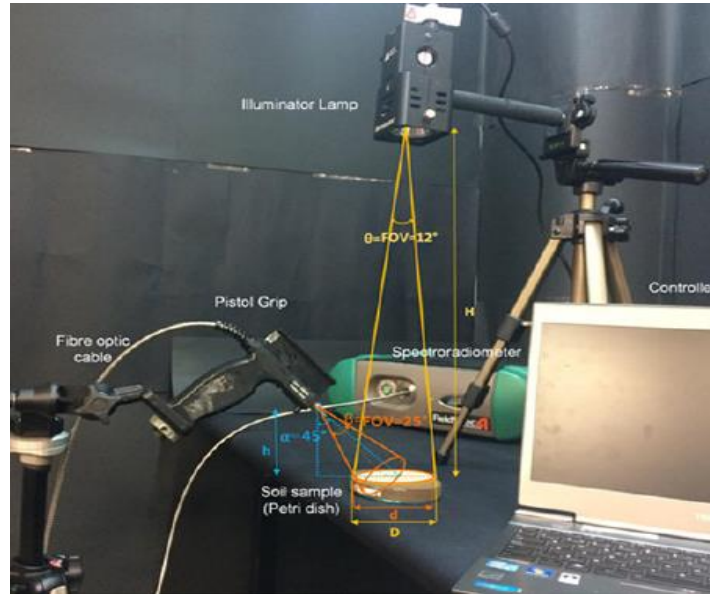


Figure 20. Observation geometry in the setup, which uses an ASD illuminating lamp as a light source, referred to as setup L.

4.1.3. Experimental setup CP (contact probe)

The experimental setup CP shown in Figure 18c uses ASD contact probe with the in-built light source. There are five circles cut in the paper covering the surface of the soil sample in the petri dish. The size of the circles coincides with that of the contact probe window (approximately 20 mm) to isolate the measured area and improve the quality of the obtained data.

The reflectorized halogen lamp inside the probe ensures a fixed 12° angle to the probe body during the measurements and avoids the influence of ambient light sources. The angle between optical fiber of spectroradiometer and contact probe is also fixed at 35° . The sensor, which has the FOV of 1.33cm^2 , registers the signal coming from the spot $\sim 1.1\text{cm}$ in diameter. The resulting spectrum is the average of 5 measurements at random points of soil sample, each being the average of 10 scans, totaling 50 processed spectra. This procedure reduces the risk of shadows and stray light affecting the measurements. Because of the laboratory environment and controlled illumination conditions calibration was performed every 15 min.

4.1.4. Statistics used for spectra comparison

Spectra generated with different setups were tested for differences using BIAS (Eq. 5) and Root-Mean-Square Difference RMSD (Eq.6):

$$BIAS = \frac{1}{N} \sum_{i=1}^N x_i - y_i \quad (5)$$

$$RMSD = \frac{1}{N} \sqrt{\sum_{i=1}^N (x_i - y_i)^2} \quad (6)$$

where: x_i and y_i are reflectance values of the compared spectra, and N is the number of measured samples.

Analysis of variance (one-way ANOVA) was performed to determine whether the differences among spectra from different setups were significant. The test, which relies on F distribution, is applied when estimation of one dependent variable is based on one or more continuous predictors. The test should be applied when: (i) errors are independent and normally distributed; (ii) samples are independent and drawn from populations with equal variances. The null hypothesis assuming that samples are taken from the same population is accepted or rejected based on the F -statistic (the ratio of the variance calculated among the means to the variance within the samples).

4.2. Simulation of satellite spectral bands

Laboratory soil spectra were used to simulate spectra of the three satellites to evaluate feasibility of SOM and texture estimation and monitoring from multispectral (Landsat-8 and Sentinel-2) and hyperspectral (EnMAP) remotely-sensed images (Fig. 21).

The first two are currently operational and are part of the long-term United States (Landsat-8) and European (Sentinel-2) Earth observation programs. Landsat-8 Operational Land Imager (OLI) produces images consisting of nine optical bands (VIS-bands 1 to 4 and 8 (panchromatic); NIR-band 5 and SWIR-bands 6, 7, and 9) at medium spatial resolution (30m pixel size). On the other hand, images taken with multispectral instrument (MSI) sensor on board of Sentinel-2 contain 13 VIS-SWIR bands at spatial resolution ranging between 10m and 60m. It also has better temporal resolution: a 5-day revisit period versus 16 days in case of Landsat. Resampling of ASD spectra to the

corresponding satellite bands was based on spectral response functions available from NASA and ESA for Landsat-8 and Sentinel-2, respectively.

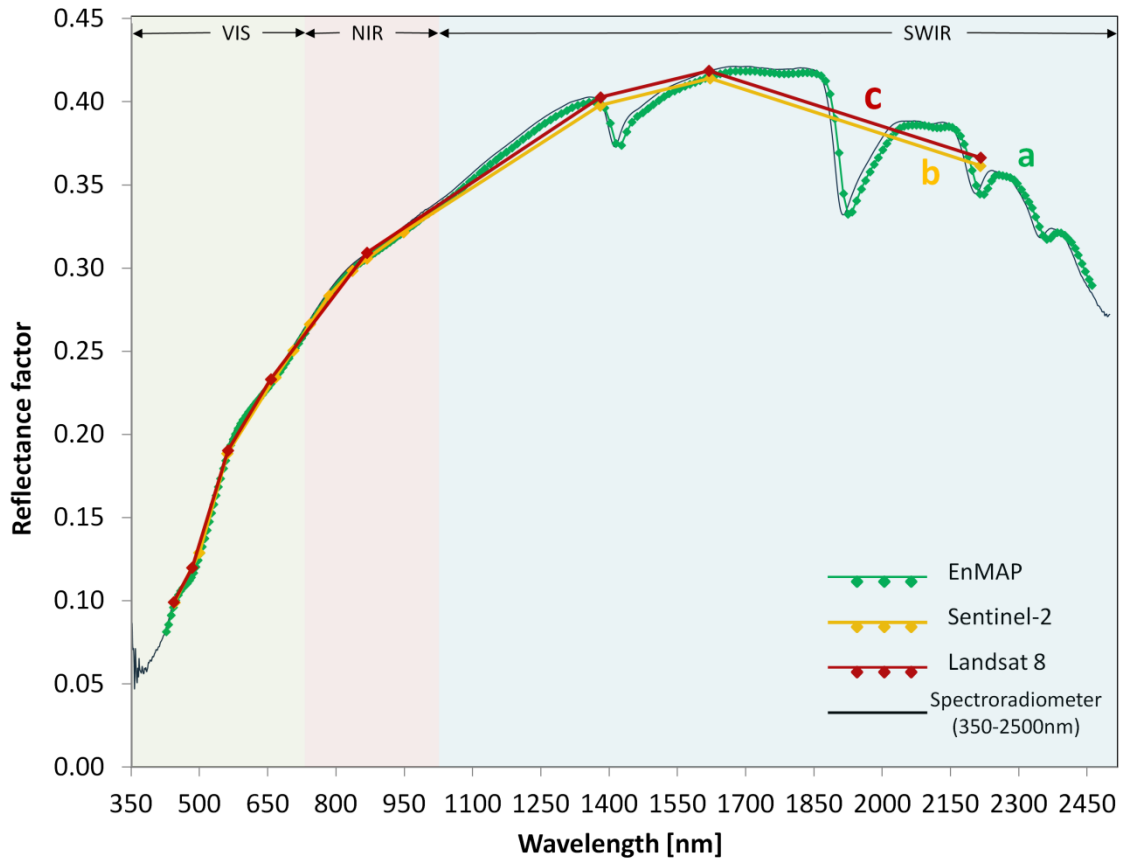


Figure 21. Reflectance spectrum of one of the soil samples resampled to (a) EnMAP), (b) Sentinel-2, and (c) Landsat-8 optical bands.

ASD spectra were also resampled to simulate hyperspectral images from EnMap satellite developed in the frame of the German space program. EnMap toolbox was the source of the spectral response functions for the 244 narrow bands located in the 420-2450 nm spectral range. The sensor sampling interval is 6.5 nm in VIS-NIR and at 10 nm in SWIR at a spatial resolution of 30 m.

The resampling of ASD FieldSpec@4 bands to those of the satellite sensors was accomplished using the ENVI 4.7 (The Environment for Visualizing Images) software.

4.3. Multivariate statistical modeling of SOM and soil texture fractions

Measured spectra were used to develop empirical statistical calibrations for simultaneous predictions of SOM and texture fractions (sand, clay, silt) in collected soil samples. Modeling included both routinely applied and novel approaches. The

following algorithms were compared: (a) a standard partial least squares regression PLSR (Demattê et al., 2016) implemented in The UnscramblerX software (2016; CAMO Software AS, Norway, 2016), version 10.4 (<https://www.camo.com/unscrambler>), which uses the full range of available reflectances (PLSR-full); (b) PLSR with predictors selected by Martens uncertainty test (Martens & Martens, 2000) available in The Unscrambler X software (2016) version 10.4 (PLSR-MUT), (c) PLSR with Step-Down predictors selection Algorithm (Jay Magidson, 2013) (SA-PLSR), and (d) a novel technique of CCR with a step-down variable selection algorithm (CCR-SD) (Magidson, 2010; Magidson, 2013).

The Unscrambler X software (2016; CAMO Software AS, Norway, 2016), version 10.4 (<https://www.camo.com/unscrambler>) was used as modeling environment for PLSR-full and PLSR-MUT procedures, while SA-PLSR and CCR-SD were implemented in XLSTAT Pearson Edition (Addinsoft S.A., New York, NY, USA, 2014), version 2014.5.03 (<http://www.xlstat.com>) software, which is the complement for the Microsoft Office Excel (2010). For each sample, all the soil properties of interest in our study (SOM, clay, silt, and sand) were predicted simultaneously.

Although spectral data are usually pre-processed before modeling to increase signal-to-noise ratio, due to the high stability of obtained spectra it was not considered necessary in this research.

However, the correction of radiometric jumps, present at the wavelengths between detectors (at 1000 and 1800 nm) was performed before further use of the spectra. The following formulas suggested by (Danner, Locherer, Hank, & Richter, 2015) were applied to compensate for the differences using the first detector as the reference value:

$$Corr_val_{1000} = R_{\lambda=1001} - (2 \cdot R_{\lambda=1000} - R_{\lambda=999}) \quad (7)$$

$$Corr_val_{1800} = R_{\lambda=1801} - (2 \cdot R_{\lambda=1800} - R_{\lambda=1799}) \quad (8)$$

where R_{λ} is the reflectance at λ wavelength and $Corr_val_{1000}$ and $Corr_val_{1800}$ are correction values at the spectral splitting points, which are added to the original values and, depending on their algebraic sign, either increase or decrease reflectances in corrected wave range. Besides, the noisy bands at the beginning and at the end of the spectra (<400 nm and >2470 nm) were eliminated.

4.3.1. Partial Least Square Regression (PLSR)

PLSR is routinely applied in soil VIS-NIR-SWIR spectroscopy (Demattê et al., 2016). The method is based on underlying linear model. PLSR is often applied in situations when the number of predictors is much bigger than the number of observations (Wold et al., 2001), which is the case of soil VIS-NIR-SWIR spectroscopy. The method gained great popularity in spectroscopic modeling because of its capability of dealing with a great number of collinear predictors and modeling several response variables (soil properties) simultaneously (Viscarra-Rossel et al., 2006).

PLSR first establishes the relationship between the matrix of predictors' scores (X), referred to as factors, and the matrix of the dependent variables' scores (Y). In the next step the Y -scores are used to predict the values of responses (Tobias, 1995). The algorithm calculates a few factors, i.e. latent variables, which account for most of the variance in the response. It chooses X - and Y -scores that establish the strongest relationship between successive pairs of scores.

Determination of the optimum number of factors/components and selection of the final model is performed through the leave-one-out cross-validation: the model is developed leaving out one of the samples, which is later substituted into the model to evaluate the adjustment; the process is repeated for each sample, and the final model is that showing the best fit (Duckworth, 1998).

4.3.2. Step-Down predictors selection Algorithm

It is recognized that PLSR is prone to overfitting, i.e., including in models predictors relevant only to the calibration dataset (Babyak, 2004). One of the ways to control overfitting is to reduce the number of predictors, leaving out less important, which results in sparser models (Chun & Keleş, 2010). Thus, PLSR was combined with the step-down variable selection algorithm (PLSR-SD). The step-down variable selection algorithm reduces the number of variables without the loss of information through elimination of the less important variables, i.e., those with the lowest (absolute value) coefficient, during cross validation. For each model, this iterative process was configured to run 10 rounds of five-fold cross validation.

The step-down variable selection algorithm reduces the number of variables without the loss of information through elimination of the less important variables, i.e., those with the lowest (absolute value) coefficient; during cross validation (Bennett, 2013). For each model, this iterative process was configured to run 10 rounds of fivefold cross validation.

Because exclusion of the less important (noisy) predictors may improve model accuracy, in the second tested method, PLSR models used only most important variables selected by the Martens uncertainty test (PLSR-MUT), which estimates uncertainty of regression coefficients obtained in leave-one-out cross validation (Martens & Martens, 2000).

4.3.3. Correlated Components Regression

Both CCR and PLSR are capable of dealing with a large number of highly correlated predictors (in this study, the correlation coefficients R^2 are in the range of 0.639–0.999). Multicollinearity of spectral data is approached by means of regularization (the enforcement of model sparsity), consisting in dimension reduction. In CCR-SD, data dimension is reduced through (a) calculation of correlated components and (b) elimination of less relevant predictors from the model with step-down variable selection algorithm, resulting in sparser models (Magidson, 2013).

CCR utilizes $K < P$ correlated components, with each S_K component being an exact linear combination of g predictors ($g = 1, 2, \dots, P$). Predictions for Y in the first (primary) component (\hat{Y}) directly affect the outcome and are obtained from the simple ordinary least squares (OLS) regression of Y on S_1 . Similarly, the second component S_2 is calculated by the simple OLS regression of Y on S_1 and S_2 . The calculation of the remaining components follows the same process. Once the models for all the components are obtained, the final model (Eq. 9) is computed using the expression:

$$\hat{Y} = \alpha^{(K)} + \sum_{g=1}^P \beta_g X_g \quad (9)$$

where α and β are regression coefficients.

Thus, the components are not orthogonal; the second and subsequent components are correlated to the first component and represent the influence of ‘suppressor’ variables (Magidson & Wassmann, 2010). The inclusion of suppressor variables

removes the noise of some irrelevant variables included in the first component, improving the model quality.

At the same time, the method controls overfitting through a reduction in the number of predictors, leaving out the less important predictors. Thus, CCR was combined with a step-down variable selection algorithm, which excludes the least important predictors (Bennett, 2013; Magidson, 2010). This is achieved through M-fold cross-validation. Each round (10 rounds in this study) consists of a series of operations. First, the data are randomly divided into M groups (folds) of equal size (5 groups of $80/5 = 16$ samples each in our study). Next, samples from four groups are used to build the model, while the samples from the fifth group are used for model validation. The process is run for each group (M times). In the next round, the process is repeated with newly randomized M groups. Thus, the quality of the final model is assessed on the out-of-sample fit, ensuring replication of the calibration results on real-life data, which has been a long-time concern related to published models (Nuzzo, 2014). Model assessment based on new out-of-sample cases means that modeling with CCR does not pose requirements to satisfy sampling assumptions, which are the basis of traditional hypothesis testing (Curl, Thompson, & Aspinall, 2015).

4.3.4. Assessment of model performance

Different aspects of model performance were evaluated with a series of statistical indicators described below.

Model fit was assessed through coefficient of determination of calibration (R^2_{cal}), coefficient of determination of cross-validation (R^2_{CV}), coefficient of determination of validation (R^2_v), while model accuracy was assessed by means of the root mean square error of prediction (RMSEP) (Bellon-Maurel & McBratney, 2011). These statistics were calculated according to the following expressions:

$$R^2_{CV} = 1 - \frac{\sum_{i=1}^{n_c} (Y_{i,c} - \hat{Y}_{i,c})^2}{\sum_{i=1}^{n_c} (Y_{i,c} - \bar{Y}_c)^2} \quad (10)$$

$$R^2_v = 1 - \frac{\sum_{i=1}^{n_p} (Y_{i,p} - \hat{Y}_{i,p})^2}{\sum_{i=1}^{n_p} (Y_{i,p} - \bar{Y}_p)^2} \quad (11)$$

$$RMSEP = \sqrt{\frac{\sum_{i=1}^{n_p} (Y_{i,p} - \hat{Y}_{i,p})^2}{n_p}} \quad (12),$$

where: c and p refer to the corresponding calibration and validation datasets; n is the number of samples, Y_i is the observed SOM value for i th sample, $\hat{Y}_{i,c}$ is the predicted SOM value for the i th sample, and \bar{Y} is the mean value of Y_i for all samples. Model predictive capacity was assessed with either residual prediction deviation (RPD) or the ratio of performance to interquartile range (RPIQ), computed according Eq. 13 and 14. (Bellon-Maurel, Fernandez-Ahumada, Palagos, Roger, & McBratney, 2010; Minasny & McBratney, 2013) explained that the use of RPD is justified only with normally distributed datasets recommending application of RPIQ, instead. Hence, at different stages of research we used one of these indicators or another.

$$RPD = \frac{\sqrt{\frac{\sum_{i=1}^{n_p} (Y_{i,p} - \bar{Y}_p)^2}{n_p - 1}}}{RMSEP} \quad (13)$$

It is generally considered (Gomez, Viscarra-Rossel, & McBratney, 2008; Gras, Barthès, Mahaut, & Trupin, 2014) that model has good predictive capacity when its RPD is above 2.0, satisfactory when its RPD between 1.4 and 2.0, and poor when RPD below 1.4 (Gomez et al., 2008; Gras et al., 2014).

$$RPIQ = \frac{Q_3 - Q_1}{RMSEP} \quad (14)$$

RPIQ is based on inter-quartile distances (IQ = $Q_3 - Q_1$), where Q_1 represents the lowest 25% of the samples and Q_3 is the value below which 75% of the samples can be found. RPIQ is the ratio of IQ to the RMSEP. Its use is preferable to that of RPD when working with datasets characterized by skewed distributions and a large number of low values. Finally, Akaike information criterion (AIC) computed according Eq. (15) was used to assess the parsimony of the developed models (Akaike, 1973).

$$AIC = n \ln RMSEP + 2f \quad (15)$$

here n is the number of samples and f is the number of predictors. Smaller AIC values denote more efficient, i.e. sparser, models.

5. Comparison of laboratory setups used to obtain laboratory VIS-NIR-SWIR spectra of soils

This chapter reproduces the text of the following article:

Title:

Assessment of laboratory VIS-NIR-SWIR setups with different spectroscopy accessories for characterization of soils from wildfire burns

Authors:

Olga A. Rosero Vlasova

Fernando Pérez-Cabello

Raquel Montorio Llovería

Lidia Vlassova



Available online at www.sciencedirect.com

ScienceDirect

journal homepage: www.elsevier.com/locate/issn/15375110



Special Issue: Proximal Soil Sensing

Research Paper

Assessment of laboratory VIS-NIR-SWIR setups with different spectroscopy accessories for characterisation of soils from wildfire burns



Olga A. Rosero-Vlasova ^{a,*}, Fernando Pérez-Cabello ^a,
Raquel Montorio Llovería ^a, Lidia Vlassova ^{a,b}

^a Department of Geography and Land Management, GEOFOREST Group, IUCA, University of Zaragoza, Spain

^b Department of Environmental Sciences, Technical State University of Quevedo, Ecuador

ARTICLE INFO

Article history:

Published online 18 July 2016

Keywords:

Illuminator lamp
Contact probe
Integrating sphere
Soil reflectance spectra
SOM
Wildfire burns

Thousands of hectares of Mediterranean forests are burned every year. Fires affect all the landscape components. They trigger erosion processes, which can have catastrophic consequences. Thus, detection and post-fire monitoring of soil properties is of great importance. Changes in soil caused by the fire can be detected by proximal soil sensing. In this context, the study evaluates the applicability of laboratory experimental setups for spectral analysis of burnt soils. Three setups of Analytical Spectral Device (ASD) Field-Spec[®]4 spectroradiometer with different spectroscopy accessories (external integrating sphere, illuminator lamp and contact probe) were used for measurement of reflectance spectra and evaluation of soil organic matter (SOM) in 82 soil samples from wildfire burns in Aragon, Northern Spain. No statistically significant differences were detected between values obtained by different setups. Lower reflectances registered with integrating sphere are probably due to the fact that the internal cavity of the device is not perfectly spherical because of the existence of multiple port windows. Measurements with Illuminator lamp and contact probe were more stable and corresponding calibration models for SOM built using partial least square regression combined with step-down variable selection algorithm (SA-PLSR) demonstrated acceptable predictive ability ($0.75 \leq R^2_v \leq 0.81$; $2.00 \leq RPD \leq 2.55$). The coefficients are ~10% higher than those obtained with the integrating sphere. The study demonstrated feasibility of using Visible – Near InfraRed – Short Wave InfraRed (VIS-NIR-SWIR) spectroscopy for monitoring post-fire evolution of burnt soils and showed that the choice of the appropriate accessory (e.g., Illuminator lamp) improves the reliability of SOM estimations.

© 2016 IAGRE. Published by Elsevier Ltd. All rights reserved.

* Corresponding author.

E-mail address: oarosero@unizar.es (O.A. Rosero-Vlasova).

<http://dx.doi.org/10.1016/j.biosystemseng.2016.06.011>

1537-5110/© 2016 IAGRE. Published by Elsevier Ltd. All rights reserved.

1. Introduction

Fire is a major disturbance of Mediterranean forests. Although wildfires do not affect mineral composition of soils, they cause considerable changes in soil organic constituents and modify soil physical properties (Mataix Solera, 1999; Neary, Ryan, & DeBano, 2005). Consumption of organic matter alters the structure of burned soils decreasing erosion resistance and soil permeability. In high-intensity fires, in which the consumption of organic matter is greater, aggregation levels decrease, leading to soil loss (Badía & Martí, 2003; Cerdà, 1999). Together with the loss of organic matter and destruction of aggregates, the loss of protection against rain provokes changes in the quantity and size of pores (Giovannini & Lucchesi, 1997). The splash effect mobilises the fine particles of the soil, which clog the pores, reducing soil aeration and infiltration ability (Cerdà & Robichaud, 2009). Finally, fire is often related to soil water repellency. Volatilisation of organic compounds and their subsequent condensation around the soil aggregates generates a coating that reduces infiltration and increases surface runoff (Cerdà & Robichaud, 2009; DeBano, 2000).

Changes in soil caused by the fire are related to changes in soil spectral properties, which can be detected by proximal soil sensing in VIS-NIR-SWIR (Visible at 400–700 nm, Near-Infrared at 700–1300 nm, and Short-Wave-Infrared at 1300–2500 nm, respectively) regions of electromagnetic spectrum (Lugassi, Ben-Dor, & Eshel, 2014; Montorio et al., 2006; Vergnoux et al., 2009).

This technique has been used to detect soil properties relevant for engineering (Chabrilat, Goetz, Olsen, & Krosley, 2001; Kariuki, Van Der Meer, & Siderius, 2003; Waruru, Shepherd, Ndegwa, Kamoni, & Sila, 2014), industry (Goetz, Curtiss, & Shiley, 2009), agriculture (Dematté, Campos, Alves, Fiorio, & Nanni, 2004; Genot et al., 2011; Stevens et al., 2008), ecology (Foley et al., 1998), and environmental studies related to soil erosion (Cañasveras, Barrón, Del Campillo, Torrent, & Gómez, 2010), soil salinity (Farifteh, Van der Meer, Van der Meijde, & Atzberger, 2008), soil contamination (Cheng, Shi, & Zhu, 2007; Gholizadeh et al., 2015; Kooistra, Wehrens, Leuven, & Buydens, 2001), and composition, i.e. content of organic matter (He, Huang, García, Hernández, & Song, 2007; Kuang & Mouazen, 2013), and nutrients. Detailed reviews of fundamentals and applications of soil spectroscopy have been made by Ben-Dor, Irons, and Epema (1999), Viscarra-Rossel; Walvoort, McBratney, Janik, Skjemstad (2006) and Stenberg, Viscarra-Rossel, Mouazen, and Wetterlind (2010).

Spectral behaviour of soils was first described by Condit (1970) and Baumgardner, Silva, Biehl, and Stoner (1985) who identified several spectral shape patterns typical for soils (three and five, respectively). More detailed methodology of using spectral reflectance curves for differentiation of soils, based on curve shape, reflectance intensity and absorption features, was developed by Dematté (2002). Essential edaphic components, such as organic matter, clay minerals and iron oxides present characteristic absorption features caused by electronic transitions in the VIS and by overtones and combination modes of functional groups in the NIR and SWIR spectral regions (Hill, Udelhoven, Vohland, & Stevens, 2010;

Stenberg et al., 2010). Spectral response is also strongly influenced by water content, with the strongest absorption bands near 1400 and 1900 nm, and with weaker bands in other parts of the spectra (Liu et al., 2003). The mineral part of soils, which represents in general 50% of its volume (Schulze, 2002), has strong distinct characteristics in the VIS-NIR-SWIR region in reflectance intensity, curve shape and absorption features (Hunt, 1977). Particle size is also distinguishable in soil spectra (Curcio, Ciraolo, D'Asaro, & Minacapilli, 2013).

According to the review by Viscarra-Rossel et al. (2006), soil organic matter (SOM) and clay content, as well as some constituents of soil minerals, e.g. Fe and Ca, can be successfully predicted from VIS-NIR-SWIR spectra. These are the characteristics usually altered by wildfires (Lugassi et al., 2014). Thus, techniques involving generation and analysis of soil spectra could contribute to characterisation and quantification of wildfire effect on soil properties. Compared to traditional methods of analysis VIS-NIR-SWIR spectroscopy is: (1) non-destructive, (2) flexible: measurements can be performed either in the field or in the laboratory; (3) several properties can be estimated from one spectrum (Viscarra-Rossel et al., 2006).

Soil reflectance is composed of regular (specular) and diffuse (non-directional) reflectance (Torrent & Barrón, 2008). In field measurements, which are usually performed on large areas, the contribution of both of these components is comparable, and the proportion of each one depends on atmospheric conditions, topography and soil "surface state" properties (Escadafal, 1989), which include particle size, structure and surface roughness. By contrast, in laboratory conditions when a spectroradiometer measures soil reflectance of a small spot of a sieved sample composed of small size particles, diffuse reflectance dominates (Torrent & Barrón, 2008).

Even though spectral measurements in controlled conditions overcome the problems related to unstable illumination and other environmental conditions (Schaeppman & Dangel, 2000; Viscarra-Rossel et al., 2006), there are still some issues that have not been fully clarified including those related to the applicability of the spectral library created for one area to predicting properties of soils in a different area (Guerrero et al., 2015; Stevens et al., 2008); limitations related to models up- and downscaling (Viscarra-Rossel et al., 2016); and the transferability of models obtained with different laboratory equipment and standards (Ben-Dor, Ong, & Lau, 2015). Previous research shows that the quality of predictions of soil properties from their spectra greatly depends on instrumentation used for measurements (Castro-Esau, Sanchez-Azofeifa, & Rivard, 2006; Ge, Morgan, Grunwald, Brown, & Sarkhot, 2011), sample preparation (Brunet, Barthès, Chotte, & Feller, 2007; Stenberg et al., 2010); and applied protocol (Ben-Dor et al., 2015; Knadel, Stenberg, Deng, Thomsen, & Greve, 2013). While the impact of different spectroradiometers on the quality of predictive models has been explored in several studies (Ben-Dor et al., 2015; Castro-Esau et al., 2006; Knadel et al., 2013), to the best of our knowledge there are no studies quantifying the effect of the spectroscopy accessories provided by the equipment manufacturers. The use of accessories is quite common in VIS-NIR-SWIR spectroscopy. Thus, integrating sphere has been used for collecting spectra of

minerals (Torrent & Barrón, 2003) and vegetation (Merzlyak, Chivkunova, Melø, & Naqvi, 2002; Yáñez-Rausell, Schaeppman, Clevers, & Malenovsky, 2014); contact probe has been employed for obtaining spectra of soil (Brown, Shepherd, Walsh, Mays, & Reinsch, 2006) and snow (Painter, Molotch, Cassidy, Flanner, & Steffen, 2007); and halogen lamp has been applied by Kooistra et al. (2003) in the study of sediment properties and soil contamination by Gholizadeh et al. (2015). Incorporation of spectroscopy accessories creates setups with different illumination conditions and observation geometry, which could affect measurement results (Ben-Dor, Pimstein, & Notesco, 2010).

Unlike rocks and minerals, soil spectra lack spectral features clearly attributable to its constituents, and it is often necessary to take into account the overall shape and reflectance levels of different spectral regions (Ben-Dor et al., 2015; Viscarra-Rossel & Behrens, 2010). Thus, even slight variations in sample preparation, instrument configuration and measurement protocols can affect the quality of models relating spectral and edaphic properties. However, up to now little attention has been paid to estimating the effect different accessories can have on collected soil spectra and resulting predictive models. It is worth mentioning that comparative studies by Knadel et al. (2013) and Ben-Dor et al. (2015) tested setups which included attachments, but the impact attributable to the use of specific accessory was not estimated. Moreover, Ben-Dor et al. (2015) noted that performance of the

accessory used (contact probe) was more critical than that of the spectroradiometer for the stability of reflectance measurements.

In this context, the objectives of this study are: (1) to compare VIS-NIR-SWIR spectra of forest soils from wildfire burns obtained by three laboratory setups which include different commercially available spectroscopy accessories; and (2) to evaluate the impact of between-setups differences in reflectances on predictive ability of statistical models, for example, for SOM. Our working hypothesis is that incorporation of the attachment in the setup affects both spectral measurements and the quality of modelling of soil properties altered by wildfires.

2. Materials and methods

2.1. Study area and soil sampling

Soil samples were collected in the region of Aragón (Northern Spain; geographical coordinates 41° - 42° N 0° 10'- 1° 30'W) (Fig. 1 and Table 1) between March and April 2013. The hilly area at elevations ranging from 450 to 1300 m above sea level is part of the pre-Pyrenean range. Typical Mediterranean climate is characterised by average annual temperature of 12.5° C, and precipitation of around 560 mm with maxima in spring and autumn and minimum in summer (Cuadrat & Vide, 2007). This

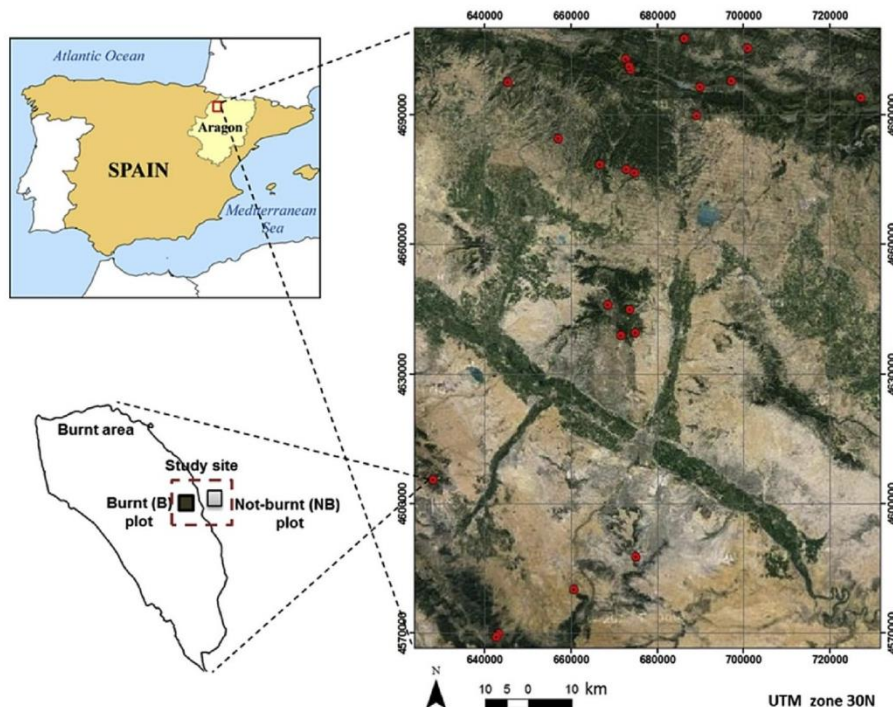


Fig. 1 – Location of the sampled burns (shown on the map as red points). Schematic drawing on the left shows location of burnt (B) and not-burnt (NB) plots on one of the study sites. (For interpretation of the references to colour in this figure legend, the reader is referred to the web version of this article.)

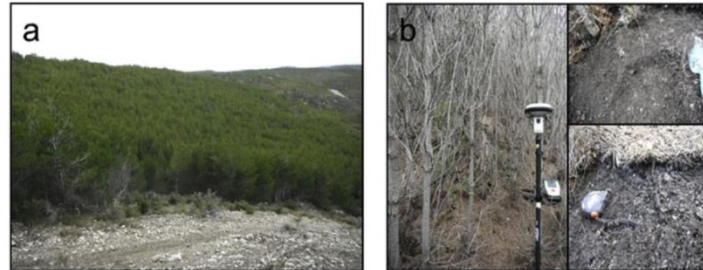


Fig. 2 – A typical view of the study area and one of the sampling points.

Table 1 – Data on sampled burns.

Municipality	Fire date	Burnt area	Number of samples
		[ha]	
Las Peñas de Riglos	31/07/1975	1279	2
	05/08/1985	735	4
	12/08/1990	200	2
Loarre	26/08/1981	147	2
	01/08/2001	3278	4
Nueno	31/07/1986	1706	6
Bailo	21/08/1994	1814	6
Caldearenas	19/08/1986	420	8
Luna	25/07/1978	1809	4
	12/05/1979	472	4
	08/07/1979	759	4
Zuera	23/06/1995	2491	4
	25/07/2006	39	2
	05/08/2008	2514	4
	30/07/1983	2536	4
Asín	16/07/1994	8078	6
Sos del Rey Católico	28/07/1994	431	4
Épila	01/08/2001	49	4
Villanueva de Huerva	29/07/2003	278	2
Encinacorba	02/08/2005	82	2
	29/07/2009	1706	4

is an area of repeated wildfires (Schmuck et al., 2012). The compact forest mass is dominated by *Pinus halepensis* (Vicente-Serrano, Pérez-Cabello, & Lasanta, 2011). Dense understory includes typical Mediterranean species, such as *Buxus sempervirens*, *Quercus coccifera*, *Juniperus oxycedrus*, *Rosmarinus officinalis* and *Genista scorpius*. In more degraded zones, forests are interspersed with brushlands consisting of species common

to the forest understory. Typical soils are coarse and medium textured Cambisols over calcareous bedrock. In some areas Cambisols are interspersed with regosols and leptosols (Badía-Villas & del Moral, 2016).

Several wildfire burns, which occurred between 1975 and 2009, were identified for sampling in an area of 308.23 km² (Fig. 1 and Table 1). Samples were obtained from the upper soil layer (0–10 cm) of burnt (B) and not-burnt (NB) plots which were established on each test site (Fig. 1); the burnt plot was located within the fire-affected area; the corresponding not-burnt plot was situated in an area with similar environmental conditions not affected by the fire and close to the burnt plot on each site (Fig. 2). The total of 82 samples (41 pairs of B-NB samples) was used for analysis. SOM content was assessed by conventional methods in the Aragon Government Agroenvironmental Laboratory (Food Safety Service of Department for Food and Agricultural Development). The percentage of oxidisable SOM was estimated using UV–visible spectrophotometry.

2.2. Laboratory spectral measurements

Soil collected in the field was first sieved to separate the fine fraction (particle size <2 mm). This was spread in optical-glass Petri dishes 90 mm in diameter and pressed to form a layer ~15 mm thick. The samples obtained (~160g) with a smooth and homogeneous surface (Fig. 3) were dried in the laboratory oven for 24 h at 105 °C. Details about additional steps in sample manipulation specific to protocols followed with different setups are described in Sections 2.2.1–2.2.3.

Analytical Spectral Device (ASD) FieldSpec[®]4 spectroradiometer with three spectrometers (detectors), each dedicated

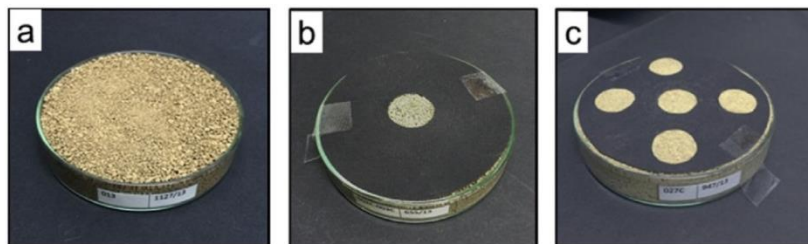


Fig. 3 – Samples prepared for measurements using Illuminator Lamp (a), integrating sphere (b) and contact probe (c).

to a specific spectral range, was used to obtain soil spectra. The instrument is designed to register the signal in the VIS-NIR (350–1000 nm) and two SWIR regions (1001–1800 nm and 1801–2500 nm) with spectral sampling interval of 1.4 nm and 2 nm, and spectral resolution (Full Width at Half Maximum – FWHM) of 3 nm and 10 nm, respectively (ASDa, 2012). The signal received by the sensors is corrected for baseline electrical signal (dark current) and resampled to a 1 nm interval over the whole sensed wave range by the device software (Fyfe, 2004). The spectroradiometer collects light passively by means of a fibre optic cable. Depending on the nature of the target and measurement environment, different accessories can be attached.

The measurements estimating reflectance factor are usually referred to as reflectance. It is defined as the ratio of radiant flux actually reflected by the target surface to that reflected by the ideal standard surface in the same observation geometry (Schaepman-Strub, Schaepman, Painter, Dangel, & Martonchik, 2006). Actually, when measurements are realised in controlled illumination conditions, the non-imaging spectroradiometer registers Biconical Reflectance Factor (BCRF), since in this case both incoming and reflected radiances can be approximated as cones (Schaepman-Strub et al., 2006).

The reference surface should have perfect reflectance over the full wavelength range and be resistant to environmental contamination. Calibrated Spectralon® references from polytetrafluoroethylene (PTFE) provided by the manufacturer satisfy all the requirements and were used to convert measured radiances into reflectance values. Measurements were performed in a dark laboratory under controlled illumination conditions using three setups with different ASD accessories (Fig. 4): (i) the RTS-3ZC external integrating sphere (IS); (ii) Illuminator lamp (L) and pistol grip; and (iii) contact probe (CP). Sample preparation and measurement protocols were similar for three setups. Before scanning, the ASD RS³ software (ASDa, 2012) was configured to average 10 spectra per each sample scan, 25 white reference, and 10 dark current to reduce noise and improve signal-to-noise ratio.

2.2.1. Experimental setup IS (external integrating sphere)

Figures 4a and 5 show the experimental setup IS, which uses external integrating sphere RTS-3ZC coupled with the ASD FieldSpec[®]4 spectroradiometer. The word “external” in the name of the accessory is due to the fact that the position of the sample is external to the sphere. The main part of the accessory is a spherical cavity 7.62 cm in diameter coated with a white diffuse polymer (PTFE). This standard optical material allows spatial integration of radiation reflected by the sample ensuring the accuracy of the measurements. The internal coating of the sphere is characterised by an almost perfect Lambertian reflectance over the wavelengths in the 350–2500 nm range coinciding with the operating spectral range of the attached spectroradiometer. During the measurement, a sample placed in the holder acts as a part of the sphere wall allowing it to “concentrate” the signal reflected from the sample and distribute it over the internal surface of the sphere. The sensor registers the light reflected by the wall and makes an estimate of the sample reflectance. It is evident from Fig. 6 that the sample is outside of the detector Field Of View (FOV).

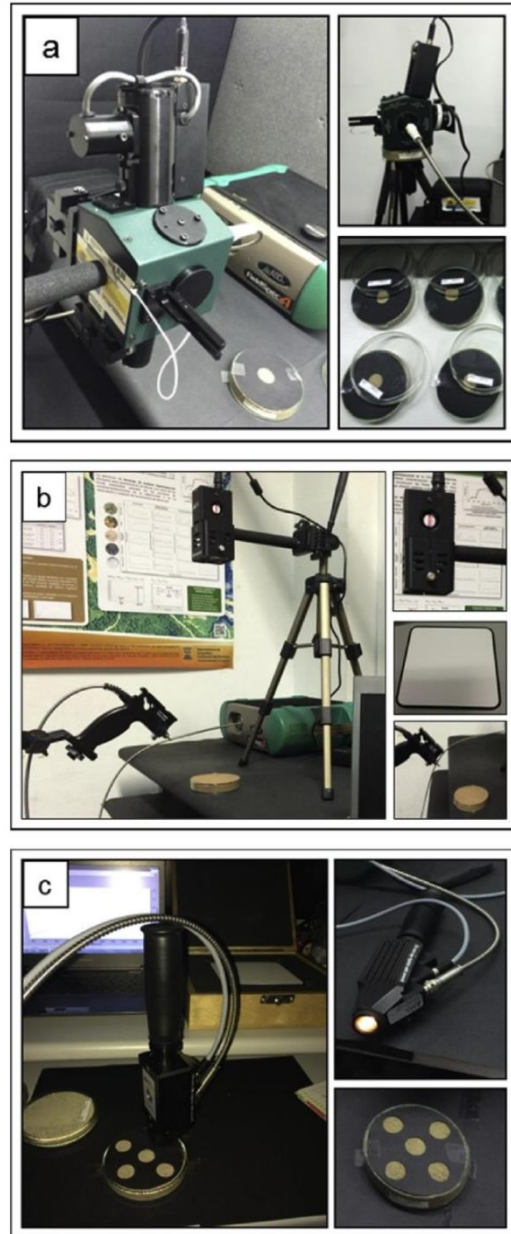


Fig. 4 – Experimental configurations: (a) Setup IS with integrating sphere, (b) Setup L with the ASD Illuminator Lamp + pistol grip, and (c) Setup CP with the ASD contact probe.

The sphere provides six ports 13 mm (ports A, D and H), 15 mm (ports C and B) and 19 mm (port E) in diameter, which serve as attachment points for supplied sample holders, a light source assembly, fibre adaptor, light trap, and port plugs. To obtain the total surface reflection of a soil sample, the

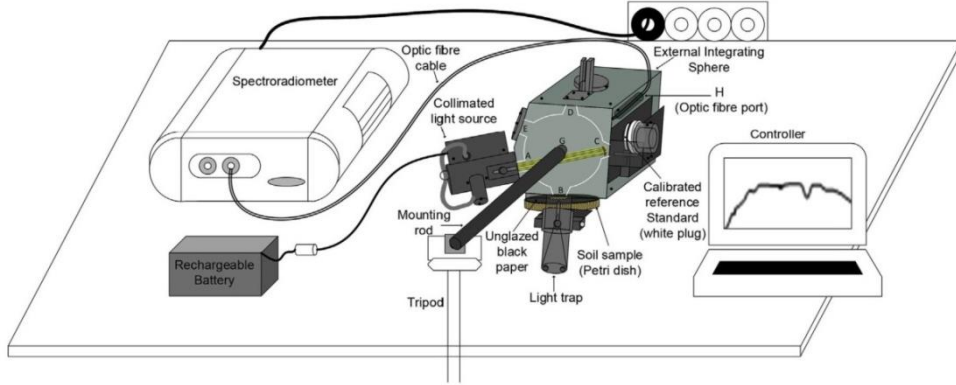


Fig. 5 – Setup IS (Integrating Sphere): diagram and observation geometry configuration.

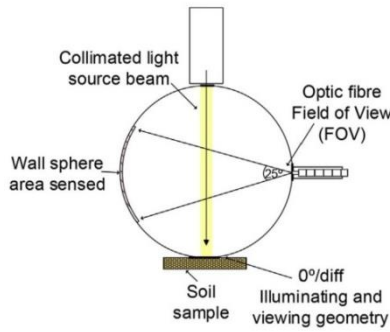


Fig. 6 – Side view of the sphere (modified from Manual of ASD Integrating Sphere).

study applied port configuration recommended by manufacturer (Table 2).

Total reflectance of the sample $R_T(\lambda)$ (Eq. (1)) measured by the sphere and corrected for the stray light was calculated using the expression (ASD, 2008):

$$R_T(\lambda) = \frac{(R_{sample}(\lambda) - DR(\lambda))}{(R_{reference}(\lambda) - DR(\lambda))} R_{ref_cal}(\lambda) \quad (1)$$

where $R_{sample}(\lambda)$ is the measurement of the sample (configuration specified in Fig. 7b); $R_{reference}(\lambda)$ is the measurement of the reference material (configuration specified in Fig. 7c); and $DR(\lambda)$ is the dark reading or the stray light estimate resulting from the measurement taken with the light trap placed instead of the

holder with the sample (configuration specified in Fig. 7a). $DR(\lambda)$ is the background radiation that the source may contribute to the baseline signal; most of the time it is negligible and can be ignored, but it was taken into account in our calculations.

$R_{ref_cal}(\lambda)$ (Eq. (2)) is the reflectance of calibrated reference standard obtained from cross-calibration of the two reference surfaces according to Miura and Huete (2009):

$$R_{ref_cal}(\lambda) = \frac{L_{ref_cal}(\lambda)}{L_{RP}(\lambda)} R_{RP}(\lambda) \quad (2)$$

where: $L_{ref_cal}(\lambda)$ is the radiance of the calibrated reference standard provided with the sphere (with the dark current subtracted); $L_{RP}(\lambda)$ is the radiance of calibrated reference panel (with the dark current subtracted); and $R_{RP}(\lambda)$ is the reflectance factor of calibrated reference panel provided with the ASD FieldSpec[®]4 spectroradiometer.

No standard protocol exists for sample preparation when working with an integrating sphere. In our experiment, a previously prepared soil sample in the petri dish was covered with unglazed black paper (optically flat surface) to prevent soil from entering the integrating sphere and to avoid undesired particle orientations (Torrent & Barrón, 2002). A central circle 18 mm in diameter (similar to that of the sample port aperture) was cut in the black paper cover to prevent direct contact of soil particles with the external wall of the sphere (Fig. 7b). In order to obtain spectral measurements the calibrated reference and soil samples were placed in the adjustable standard holders. The configuration used a light trap to prevent ambient light illuminating the back sides of ports “B” or “C” (Fig. 7) (ASD, 2008). In this setup, illumination is provided by a collimated dual light source with high setting suitable for soils rather than low setting recommended for samples of vegetation. The integrating sphere was fixed on a tripod with a mounting rod attached to the port H on the underside of the sphere assembly (Fig. 5). During the measurements the Petri dish with the soil sample is attached to port B or C (Fig. 7c and b, respectively) always in a horizontal position, while the integrating sphere is rotated so that the port with the attached sample is directed downwards. Sample spectrum obtained using this setup is the average of 20 scans; taking into account spectrum average configuration, the

Table 2 – RTS-3ZC integrating sphere port configurations for reflectance measurements (ASD, 2008).

Quantity	Reflectance measurement port configuration				
	Port A	Port B	Port C	Port D	Port E
DR	LS	WR	LT	P	P
R_{sample}	LS	WR	SS + LT	P	P
$R_{reference}$	LS	SS + LT	WR	P	P

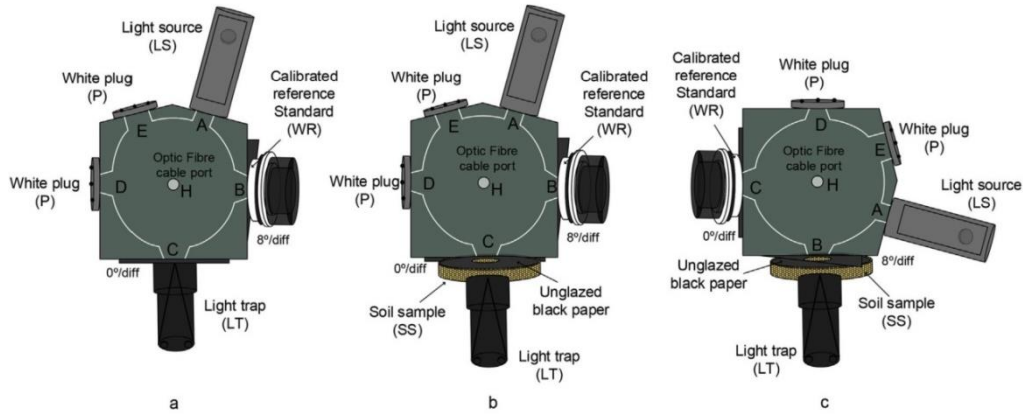


Fig. 7 – Configurations for measurement of (a) dark reading (stray light) DR, (b) soil sample reflectance R_{sample} , and (c) reference reflectance $R_{reference}$.

spectrum represents the total of 200 collected spectra per sample, as recommended by the manufacturer.

The above description of the measurement procedure makes it clear that three scans are necessary to calculate total reflectance of each sample. The time involved in multiple measurements and degradation of light intensity caused by the diminishing battery charge prevented working sessions being longer than 90 min. Hence, 5 sessions were necessary to complete the measurements, each lasting about 1 h with an average of 16 processed samples per session.

2.2.2. Experimental setup L (illuminator lamp and pistol grip)

The experimental setup L shown in Fig. 4b employs ASD Illuminator halogen lamp as a light source. The lamp was warmed for about 15 min before taking measurements (ASDb, 2012). To ensure that the soil surface spot is not too small for the sensor FOV and achieve optimal illumination of the

sample, observation geometry was previously calculated taking into account (i) distance between the target and the sensor, (ii) distance between the target and the source of illumination, and (iii) the angle between the two.

Calculation of the area detected by the sensor was based on the Illuminator lamp documentation. It resulted in the following configuration (Fig. 8): (1) Illuminator Lamp (lamp beam angle $\theta = 12^\circ$) attached to the tripod vertically above the soil sample ($H = 42$ cm) generating a lighted spot 8.82 cm in diameter (D); (2) pistol grip attached to another tripod at a height of $h = 7.5$ cm ($FOV_{BareFiber} \beta = 25^\circ$, Diameter SPOT $d = 6.99$ cm) and an angle $\alpha = 45^\circ$ relative to vertical axis.

In this configuration, the sensor registers the signal from the spot, which covers the area within the petri dish, and the measurement procedure does not involve sample manipulation. The sample spectrum is an average of 50 radiometric measurements. During the working session, the fibre optic

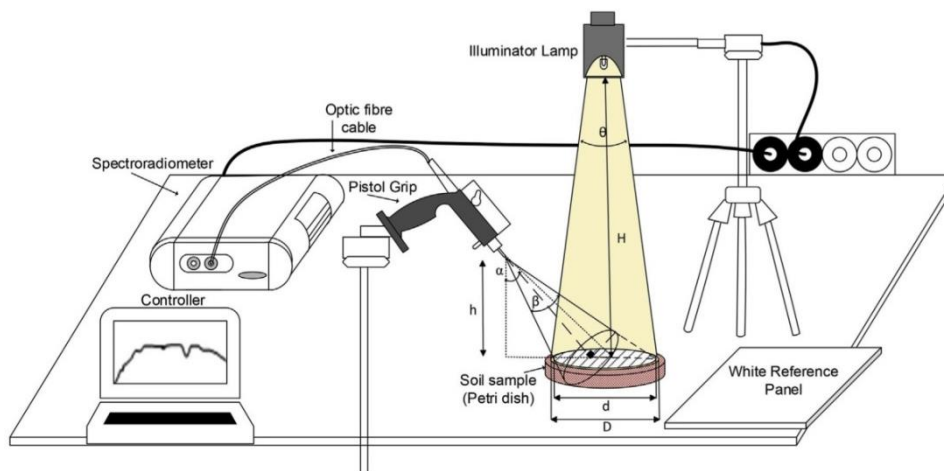


Fig. 8 – Setup 2 (Illuminator lamp and pistol grip): diagram and observation geometry configuration.

cable was regularly directed at the Spectralon reference panel with the same viewing geometry. Since the measurements were realised in the laboratory under controlled illumination conditions, it was not necessary to perform calibrations before each scan.

2.2.3. Experimental setup CP (contact probe)

In the experimental setup CP (Fig. 4c), samples contained in the petri dish are covered with unglazed black paper with 5 apertures (Fig. 3c) of the size equal to that of internal window of the contact probe ($d_{\text{PROBE}} \approx 20$ mm) so that during the measurement the rubber edge of the contact probe window touches the paper cover zone around the cut circle to isolate the measured area from the surroundings.

In this configuration illumination is delivered to the sample by the contact probe internal light source composed of a reflectorised halogen lamp aligned at 12° to the probe body, ensuring illumination at a fixed angle without the influence of ambient light. The optical cable of the spectroradiometer is attached to the contact probe at a fixed measurement angle of 35° (Fig. 9). The sensed spot has a diameter (d_{probe}) of ~ 1.1 cm with a FOV of 1.33 cm². The spectrum provided by the spectroradiometer results from 5 measurements recorded as the

average of 10 readings, which totals 50 processed spectra. Spectra are acquired at five random points of the soil sample (Fig. 10) and then averaged. This procedure minimises the risk of shadows and errors associated with stray light. Since measurements were realised in the laboratory under controlled illumination conditions, calibration was performed once every 15 min.

2.3. Statistical analysis

2.3.1. Statistical analysis of measured spectra

Analysis of measured reflectance spectra was based on wavebands with the highest information on edaphic properties, as suggested by Dematté and Terra (2014). The importance of these bands for detection of organic matter, clay minerals, and iron and aluminium oxides has been reported in earlier research (Ben-Dor, Heller, & Chudnovsky, 2008; Melendez-Pastor, Navarro-Pedreño, Gómez, & Koch, 2008). The analysed bands include 5 bands in VIS (440 nm, 530 nm, 550 nm, 650 nm, 700 nm), 7 bands in NIR (845 nm, 850 nm, 870 nm, 901 nm, 931 nm, 951 nm, 1051 nm) and 8 bands in SWIR (1302 nm, 1401 nm, 1903 nm, 2201 nm, 2263 nm, 2300 nm, 2352 nm and 2430 nm) spectral regions. No spectral pre-processing of raw

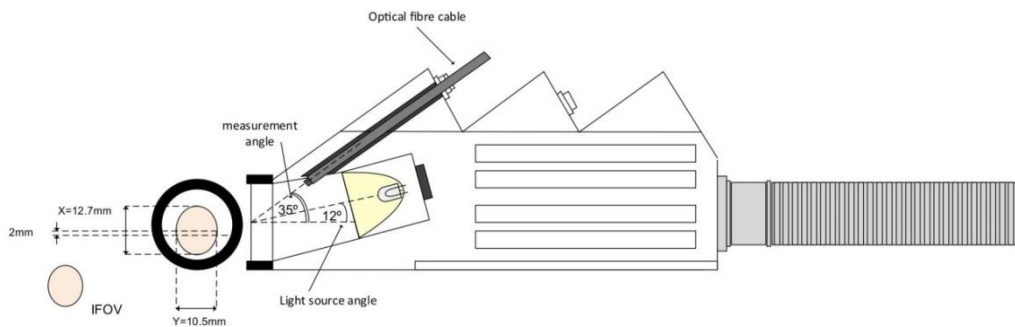


Fig. 9 – Illumination and measurement angles of contact probe (modified from ASD, 2008).

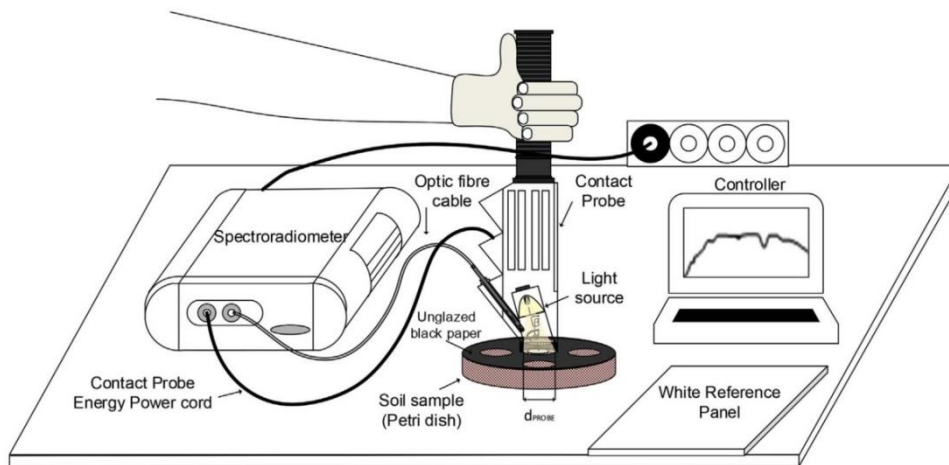


Fig. 10 – Experimental setup CP (contact probe): diagram and observation geometry configuration.

spectra, sometimes used to reduce uncertainty (Vasques, Grunwald, & Sickman, 2008), was applied.

BIAS (Eq. (3)) and Root-Mean-Square Difference RMSD (Eq. (4)) were applied to estimate differences between reflectance values obtained using tested setups:

$$\text{BIAS} = \frac{1}{N} \sum_{i=1}^N x_i - y_i \quad (3)$$

$$\text{RMSD} = \frac{1}{N} \sqrt{\sum_{i=1}^N (x_i - y_i)^2} \quad (4)$$

where: x_i and y_i are values of the compared setups, and N is the number of measured samples.

Analysis of variance (one-way ANOVA) was applied to test significance of the observed differences. The technique uses F distribution to test if means of three or more groups are different. It is applied when continuous variables are used as predictors of one dependent variable (that is why it is called one-way ANOVA). The null hypothesis says that samples are taken from the same population; it is accepted or rejected based on the F -statistic (the ratio of the variance calculated among the means to the variance within the samples). To be considered reliable, some assumptions should be satisfied: (1) errors are independent and normally distributed; (2) samples are independent and drawn from populations with equal variances.

2.3.2. Multivariate models for SOM prediction

Partial-Least-Square Regression (PLSR) approach (Tenenhaus, 1998; Wold, Sjöström, & Eriksson, 2001) with Step-Down predictors selection Algorithm (Magidson, 2013) (SA-PLSR) implemented in XLSTAT software (Addinsoft S.A., 2014) was applied for calibration and validation of a predictive model for SOM, one of the most relevant properties for soil post-fire evolution.

PLSR is routinely applied in soil VIS-NIR-SWIR spectroscopy (e.g. Kooistra et al., 2003; Viscarra-Rossel et al., 2006) because of its capacity to deal with a great number of predictors successfully solving the problem of multicollinearity

(Vasques et al., 2008; Wold et al., 2001). The method combines the characteristics of principal component analysis and multiple linear regression; based on predictors, it computes a set of orthogonal vectors, which explain most of the variance in the dependent variable(s), referred to as latent variables (Martens & Naes, 1989). The number of latent variables (components) and the final model are defined by cross-validation (leave-one-out approach) (Duckworth, 1998). A series of regression models are computed, each time leaving out one of the samples; the model is then used to predict the value for the omitted sample. PLSR models tend sometimes to overfit the data (Beebe, Pell, & Seasholtz, 1998; Christy & Kvalheim, 2007; Wold et al., 2001), i.e. they may include explanatory variables relevant only to the training set (noise) showing considerably lower predictive capacity when analysing independently acquired data. In order to overcome this problem, the study applies the step-down algorithm (Magidson, 2013) to exclude the least important predictors. Ten-fold cross-validation was used to determine the number of components and predictors, in each run excluding the predictor with the smallest (absolute value) standardised coefficient. The modelling was performed on 81 samples; one outlier was removed based on the PLSR results.

To ensure the robustness of multivariate models, calibration was repeated ten times on a random 61 samples (~75% of the dataset), each time leaving out 20 samples for validation.

2.3.3. Statistics estimating performance of calibration and validation models

The performance of calibration and validation models was evaluated using the following indicators: the determination coefficient of cross-validation (R^2_{CV}), the determination coefficient of validation set (R^2_V), the root-mean-square error of cross-validation (RMSECV), the root-mean-square error of prediction (RMSEP), the standard error of prediction corrected by bias (SEP_c) (Bellon-Maurel, Fernandez-Ahumada, Palagos, Roger, & McBratney, 2010) and the residual prediction deviation (RPD) (Chang, Laird, Mausbach, & Hurburgh, 2001;

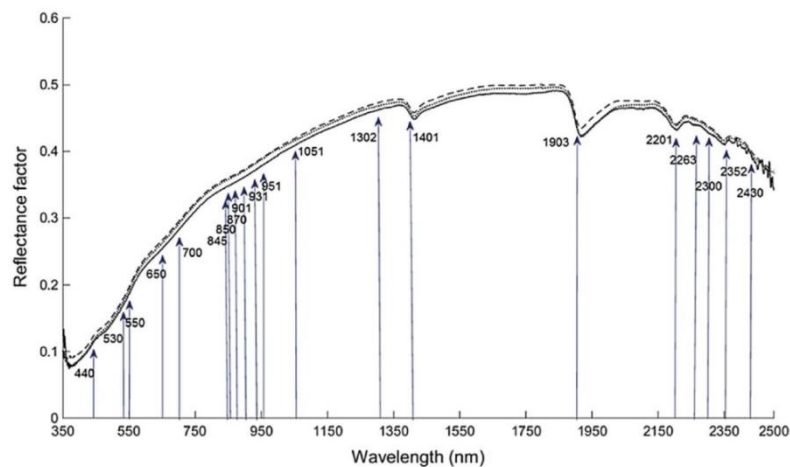


Fig. 11 – Mean spectral curves obtained by Setup IS (solid line), Setup L (dotted line), and Setup CP (dashed line).

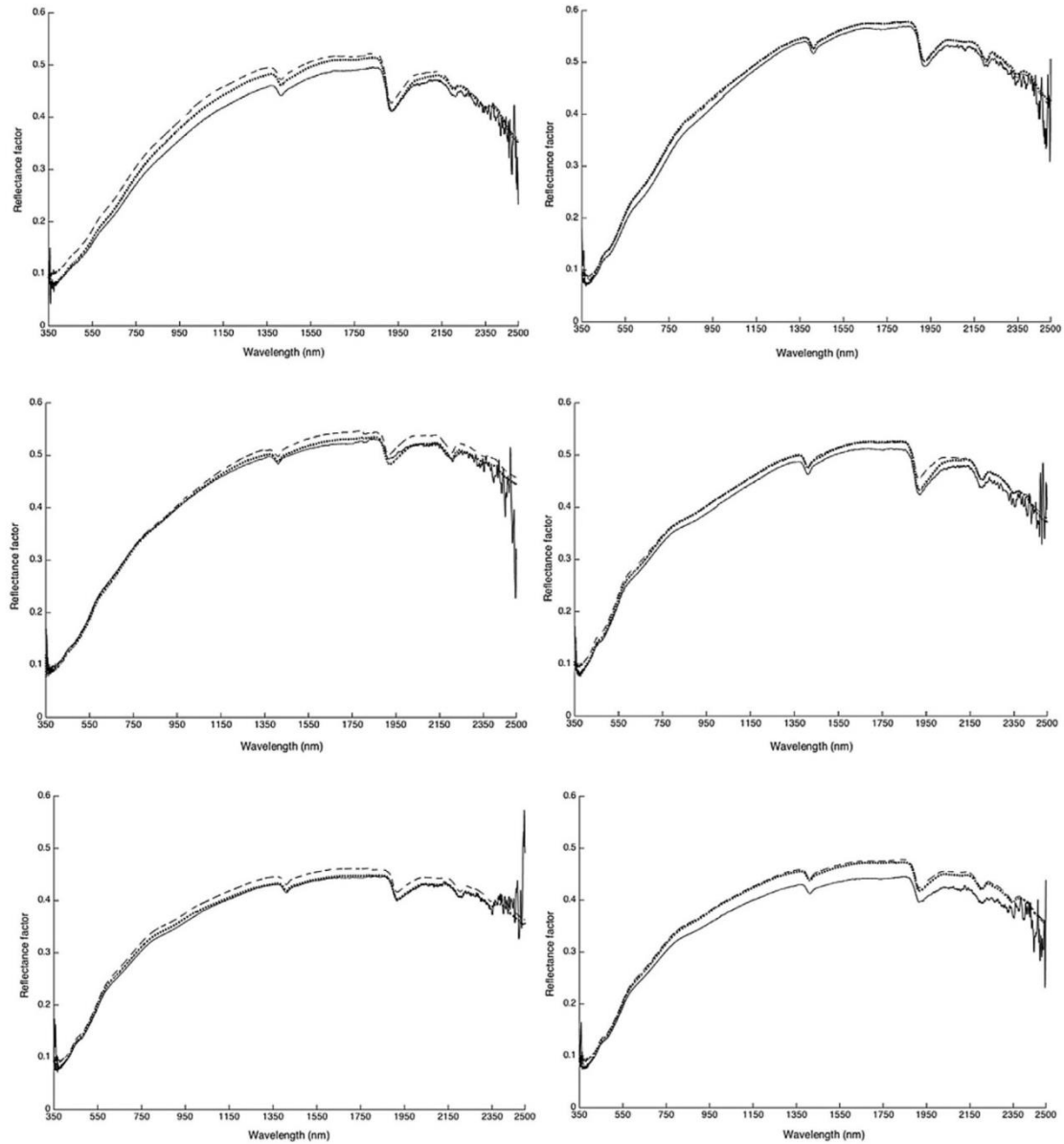


Fig. 12 – Spectral curves of selected soil samples obtained by Setup IS (solid line), Setup L (dotted line), and Setup CP (dashed line).

Williams, Williams, & Norris, 1987). Coefficient of variation (CV), calculated as the ratio of the standard deviation to the mean, was used to assess the stability of the measurements.

R_{CV}^2 (Eq. (5)) and R_V^2 (Eq. (6)) were used to assess goodness-of-fit of obtained models. According to Terra, Dematté, and Viscarra-Rossel (2015), a value for $R^2 > 0.75$ indicates accurate models for quantitative soil prediction, whereas a value for R^2 between 0.50 and 0.75 reveals fair models that can be

improved and calibration models having R^2 lower than 0.50 are considered unreliable. R_{CV}^2 and R_V^2 were calculated according to the following equations:

$$R_{CV}^2 = 1 - \frac{\sum_{i=1}^{n_c} (Y_{i,c} - \hat{Y}_{i,c})^2}{\sum_{i=1}^{n_c} (Y_{i,c} - \bar{Y}_c)^2} \quad (5)$$

Table 3 – Descriptive statistics of soil reflectance values obtained using different experimental setups (for 82 samples).

Selected bands (nm)	Setup	Mean	SD ^a	Min	Max
440	IS	0.112	0.034	0.060	0.266
	L	0.115	0.034	0.059	0.267
	CP	0.122	0.032	0.071	0.241
530	IS	0.168	0.052	0.088	0.357
	L	0.173	0.052	0.091	0.358
	CP	0.179	0.047	0.098	0.325
550	IS	0.186	0.057	0.094	0.376
	L	0.193	0.057	0.103	0.379
	CP	0.198	0.051	0.111	0.346
650	IS	0.254	0.066	0.120	0.452
	L	0.263	0.065	0.142	0.441
	CP	0.268	0.058	0.154	0.421
700	IS	0.283	0.069	0.137	0.481
	L	0.291	0.067	0.162	0.470
	CP	0.296	0.061	0.174	0.446
845	IS	0.347	0.074	0.188	0.558
	L	0.357	0.071	0.211	0.538
	CP	0.360	0.066	0.216	0.502
850	IS	0.348	0.074	0.190	0.560
	L	0.358	0.071	0.212	0.539
	CP	0.362	0.066	0.216	0.503
870	IS	0.353	0.074	0.197	0.565
	L	0.363	0.071	0.214	0.543
	CP	0.367	0.066	0.218	0.508
901	IS	0.362	0.073	0.207	0.575
	L	0.372	0.071	0.218	0.550
	CP	0.375	0.066	0.222	0.521
931	IS	0.372	0.073	0.218	0.583
	L	0.382	0.071	0.223	0.558
	CP	0.385	0.067	0.227	0.534
951	IS	0.379	0.073	0.224	0.590
	L	0.388	0.071	0.227	0.563
	CP	0.391	0.067	0.230	0.542
1051	IS	0.409	0.074	0.257	0.617
	L	0.417	0.071	0.242	0.582
	CP	0.421	0.068	0.245	0.571
1302	IS	0.462	0.082	0.297	0.669
	L	0.468	0.079	0.262	0.628
	CP	0.474	0.077	0.264	0.623
1401	IS	0.455	0.082	0.291	0.641
	L	0.460	0.079	0.253	0.617
	CP	0.466	0.077	0.254	0.609
1903	IS	0.439	0.081	0.277	0.622
	L	0.438	0.078	0.243	0.603
	CP	0.449	0.077	0.244	0.603
2201	IS	0.434	0.081	0.272	0.615
	L	0.439	0.078	0.238	0.593
	CP	0.443	0.076	0.236	0.584
2263	IS	0.439	0.081	0.275	0.625
	L	0.447	0.079	0.243	0.611
	CP	0.450	0.076	0.242	0.594
2300	IS	0.428	0.079	0.270	0.612
	L	0.436	0.077	0.238	0.599
	CP	0.440	0.074	0.237	0.583
2352	IS	0.410	0.078	0.241	0.584
	L	0.417	0.075	0.224	0.569
	CP	0.420	0.072	0.224	0.558
2430	IS	0.398	0.080	0.241	0.594
	L	0.397	0.074	0.213	0.552
	CP	0.402	0.072	0.212	0.545

^a SD – Standard Deviation.

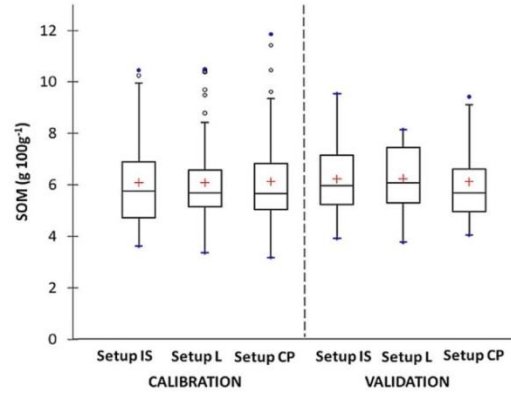


Fig. 13 – Box-whisker plots showing SOM distribution in datasets used for calibration and validation (from 10 runs). The bottom and top of the box represent the 25th and 75th percentile, respectively. The cross inside the box shows the mean. The band near the middle of the box is the median. The ends of the whiskers represent the 5th and the 95th percentile. Solid dots correspond to maximum and minimum values; hollow dots represent outliers.

$$R^2_v = 1 - \frac{\sum_{i=1}^{n_p} (Y_{i,p} - \hat{Y}_{i,p})^2}{\sum_{i=1}^{n_p} (Y_{i,p} - \bar{Y})^2} \quad (6)$$

where: c and p refer to the corresponding calibration and validation datasets; n is the number of samples, Y_i is the observed SOM value for i th sample, $\hat{Y}_{i,c}$ is the predicted SOM value for the i th sample, and \bar{Y} is the mean value of Y_i for all samples.

RMSECV (Eq. (7)) and RMSEP (Eq. (8)) were used to reflect the inaccuracy of the spectroscopic models and were calculated according to the following expressions:

$$\text{RMSECV} = \sqrt{\frac{\sum_{i=1}^{n_c} (Y_{i,c} - \hat{Y}_{i,c})^2}{n_c - (f + 1)}} \quad (7)$$

Where: where f is the number of variables used in the regression model equation.

$$\text{RMSEP} = \sqrt{\frac{\sum_{i=1}^{n_p} (Y_{i,p} - \hat{Y}_{i,p})^2}{n_p}} \quad (8)$$

The SEP_c is the standard error of the prediction corrected by bias (Eq. (9) and Eq. (10)) and is equivalent to the standard deviation (SD) of the predicted residuals in validation dataset. The SEP_c and bias_p represent two independent components of the RMSEP.

$$\text{bias}_p = \frac{1}{n_p} \sum_{i=1}^{n_p} (Y_{i,p} - \hat{Y}_{i,p}) \quad (9)$$

$$\text{SEP}_c = \sqrt{\frac{\sum_{i=1}^{n_p} (Y_{i,p} - \hat{Y}_{i,p} - \text{bias}_p)^2}{n_p - 1}} \quad (10)$$

Table 4 – Descriptive statistics for SOM content in datasets used for calibration and validation. Average values for ten runs.

	Calibration					Validation				
	n	Min	Max	Mean	SD	n	Min	Max	Mean	SD
IS dataset	61	1.11	12.98	6.09	2.78	20	2.42	12.62	6.22	2.76
L dataset	61	1.04	12.98	6.08	2.74	20	2.35	12.59	6.24	2.86
CP dataset	61	1.11	13.24	6.12	2.75	20	2.15	11.82	6.11	2.82

Table 5 – SOM calibration results (for 61 samples). Presented values are averages for ten calibrations; the range of R^2_{CV} and RMSECV values is given in parenthesis.

Statistic	Setup IS	Setup L	Setup CP
R^2_{CV}	0.66 (0.62–0.70)	0.77 (0.74–0.78)	0.74 (0.68–0.77)
RMSECV (g 100 g ⁻¹)	1.91 (1.75–2.08)	1.56 (1.47–1.65)	1.69 (1.46–1.81)
f	5–20	7–20	11–20
Factors	3–6	5–6	5–6

RPD (Eq. (11)) is calculated to assess the predictive ability of the VIS-NIR-SWIR model.

$$RPD = \frac{\sqrt{\frac{\sum_{i=1}^{n_p} (Y_{ip} - \bar{Y}_p)^2}{n_p - 1}}}{RMSEP} \quad (11)$$

RPD thresholds suggested by Chang et al. (2001) and used to evaluate model performance in multiple studies (Gomez, Viscarra-Rossel, & McBratney, 2008; Gras, Barthès, Mahaut, & Trupin, 2014; Lu, Wang, Niu, Li, & Zhang, 2013) consider that predictive capacity of the model is good when RPD is higher than 2.0, reasonable when RPD is in the range 1.4–2.0; and poor when it is below 1.4.

3. Results and discussion

3.1. Comparison of soil reflectance spectra

Reflectance spectra obtained with the three setups (Figs. 11 and 12) are quite similar, which is not strange given that they were measured with the same spectroradiometer. This is in agreement with previous research (Ben-Dor et al., 2010; Ge et al., 2011; Knadel et al., 2013). However, published literature also contains indications that variations in instrumentation, protocols, environmental conditions and personnel may have negative consequences and affect comparability of the results (Ben-Dor et al., 2015; Brown, 2007; Ge et al., 2011).

Reflectance spectra present the shape characteristic for soils with major absorption features associated with the hydroscopic water and O–H group near 1400 nm and 1900 nm (Stoner & Baumgardner, 1981); and clay minerals near 1400 nm and 2200 nm (Hunt & Salisbury, 1970; Hunt, 1977; Viscarra-Rossel & Behrens, 2010). In spectral curves of some samples, these absorption features are small (Fig. 12d), while in others they are much more pronounced (Fig. 12e). Observed between-sample differences in the slope of the curve and overall level of reflectance are probably due to the differences in composition of analysed samples, i.e. heterogeneity present in the dataset (Ge et al., 2011), one of the aspect of this

heterogeneity being variation in the content of organic compounds (Ben-Dor et al., 1999).

In spite of similarity of reflectances from the three tested setups, visual appreciation reveals some differences (Fig. 11). The most noticeable is the noise in the IS spectra at wavelengths less than 400 nm and wavelengths greater than 2300 nm. There is a clear pattern in the levels of albedo intensity among the setups (Figs. 11 and 12): the highest values correspond to Setup CP, followed by Setup L and Setup IS.

Descriptive statistics of reflectances in selected bands are presented in Table 3. ANOVA demonstrates that differences in reflectance values among setups are not statistically significant at $p < 0.05$ level. The largest differences in albedo intensity are observed between IS and CP (RMSD 0.012); they range from 0.009 in 2201 nm wavelength to 0.014 in 850 nm and 870 nm spectral bands. CP-L and L-IS differences are smaller (RMSD 0.005 and 0.008, respectively). Compared to Setup IS, other configurations overestimate reflectances; the bias is 0.007 and 0.011 for Setup L and CP, respectively. Several previously published studies have already mentioned signal underestimation in measurements using integrating sphere (Merzlyak et al., 2002; Nostell, Roos, & Rönnow, 1999; Yáñez-Rausell et al., 2014) because there is a distance between the externally placed sample and the sphere inner cavity, causing part of the reflected light to fail to strike the integrating surface.

Reflectances registered with the three setups are highly variable; coefficients of variation (CV) above 16% for all the bands are probably explained by the heterogeneity of the dataset. Nevertheless, compared to other setups, CVs based on data from Setup CP are lower, demonstrating greater stability of the measurements, the fact observed by other researchers (Painter et al., 2007; Summers, Lewis, Ostendorf, & Chittleborough, 2011).

3.2. Distribution of SOM content

Measured reflectances were applied for modelling SOM content, a property considered a good indicator of soil post-fire recovery (Jiménez-González et al., 2016). Descriptive

statistics of SOM distribution in analysed data are presented in Fig. 13 and Table 4.

Soil samples are rich in SOM and present normal distribution with the mean close to $6 \text{ g } 100 \text{ g}^{-1}$, and the range between $\sim 1 \text{ g } 100 \text{ g}^{-1}$ and $\sim 13 \text{ g } 100 \text{ g}^{-1}$. These levels of organic content are typical for the study area (Pérez-Cabello, Echeverría, Ibarra, & de la Riva, 2009); they are higher than the average SOM for forest soils in European Land Use/Land Cover Area frame Statistical Survey (LUCAS) soil database (Stevens, Nocita, Tóth, Montanarella, & van Wesemael, 2013). It was a surprise to observe so high SOM values considering that soils affected by wildfires constitute half of the dataset, and, rather, we would have expected lower than usual content of organic material due to burning, as reported by Cécillon et al. (2009) studying similar ecosystems (Mediterranean pine forests). Unusually high content of organic matter is probably explained by the fact that burned soils were sampled six or more years after the burn, and accelerated vegetation recovery contributes to quick replenishing of organic material depleted by the fire (Jiménez-González et al., 2016; Vlassova & Pérez-Cabello, 2016).

ANOVA detected no statistically significant differences among data subsets used for predictive modelling.

3.3. SOM prediction

Table 5 summarises statistics estimating performance of the PLSR – Step-down Algorithm (SA-PLSR) calibration for SOM. Similar results were obtained in the 10 calibration runs. Examples of scatter plots (modelled versus predicted SOM values) corresponding to setups IS, L and CP, are presented in Fig. 14. The three setups provided data for SOM models capable of good (Setup IS, $R^2 = 0.66$) and accurate (Setups L and CP, $R^2_{CV} > 0.7$) predictions. Models based on Setup L demonstrate the highest R^2_{CV} (0.77) and the lowest RMSECV ($1.56 \text{ g } 100 \text{ g}^{-1}$). On the other hand, models using data from Setup IS present the lowest R^2_{CV} (0.66) and highest level of uncertainty (RMSECV = $1.91 \text{ g } 100 \text{ g}^{-1}$), probably because of the stray light in the space between the externally placed sample and the sphere inner cavity. It is possible that better results could be achieved with bigger (and much more expensive) integrating spheres in which the fraction of sphere surface occupied by the ports is smaller, ensuring better integration of the sample signal before it reaches the sphere's detector, although it should be also considered that the increase in the sphere diameter diminishes the energy flux on the sphere detector resulting in an increase in instrumental noise.

Compared to L, CP models showed comparable predictive capacity ($R^2_{CV} = 0.74$), but higher RMSECV ($1.69 \text{ g } 100 \text{ g}^{-1}$). This fact deserves closer attention because contact probes are the accessories widely used in soil VIS-NIR spectroscopy due to their versatility; they are second in popularity only to configurations featuring bare optic fibre (Ben-Dor et al., 2015). However, in our experiment, better results were obtained with setup featuring Illuminator Lamp, and not the contact probe.

Statistics estimating accuracy of validation models are summarised in Table 6. Coefficients of determination (R^2_v) are slightly above those achieved by the corresponding calibrations; closeness of calibration and validation estimates

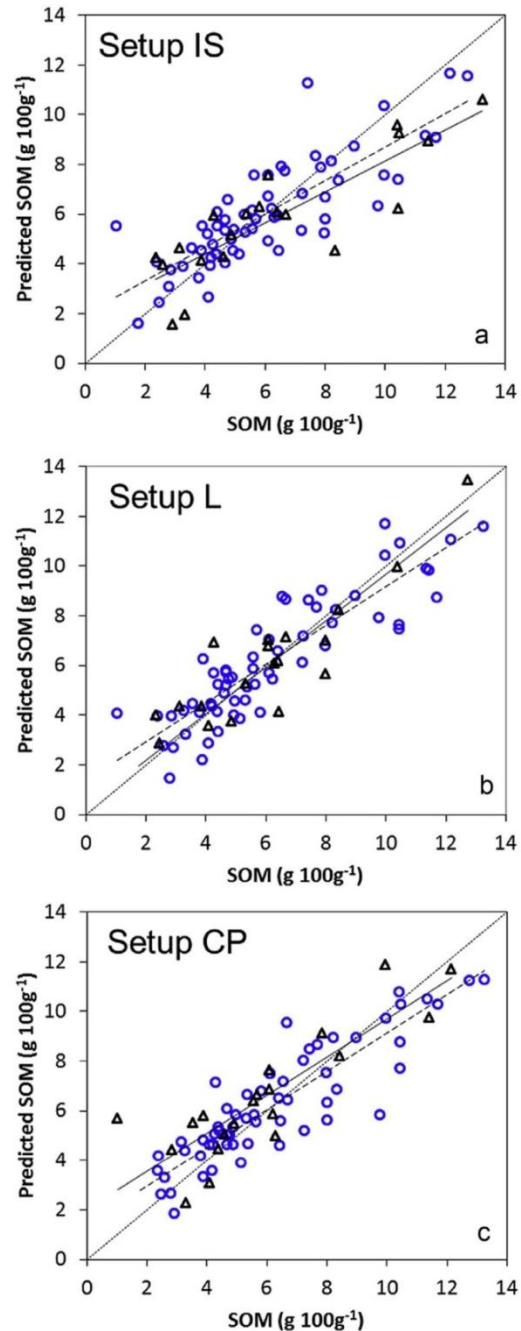


Fig. 14 – Examples of scatter plots of predicted versus observed SOM values for Setup IS (a), Setup L (b) and Setup CP (c). In each graphic data points corresponding to calibration are shown with circles; data points corresponding to validation are shown with triangles.

Table 6 – SOM validation results (for 20 samples). Presented values are averages ten validations; the range of obtained values is given in parenthesis.

Statistic	Setup IS		Setup L		Setup CP	
R^2_v	0.73	(0.64–0.83)	0.81	(0.78–0.86)	0.75	(0.69–0.81)
RMSEP ($\text{g } 100 \text{ g}^{-1}$)	1.48	(1.13–1.80)	1.28	(1.10–1.43)	1.41	(1.23–1.57)
SEP _c ($\text{g } 100 \text{ g}^{-1}$)	1.50	(1.16–1.78)	1.27	(1.11–1.45)	1.41	(1.22–1.54)
bias _{val} ($\text{g } 100 \text{ g}^{-1}$)	–0.34–0.47		–0.35–0.75		–0.63–0.65	
RPD	1.88	(1.60–2.21)	2.25	(2.13–2.55)	2.00	(1.81–2.25)

evidences good quality of models and leads to the conclusion that there is no overfitting. As in the case of calibration, models based on Setup L demonstrate the best predictive capacity, explaining around 80% of the variance (average $R^2_v = 0.81$; $0.78 \leq R^2_v \leq 0.86$; $2.13 \leq \text{RPD} \leq 2.55$) comparable to those obtained by Gras et al. (2014) and registering the lowest error among the three setups (average RMSEP = $1.28 \text{ g } 100 \text{ g}^{-1}$; $1.10 \text{ g } 100 \text{ g}^{-1} \leq \text{RMSEP} \leq 1.43 \text{ g } 100 \text{ g}^{-1}$). In terms of RPD the accuracy of L and CP models ($1.88 \leq \text{average RPD} \leq 2.25$) compared very well with results of other studies (Ge et al., 2011; Gubler, 2011; Knadel et al., 2013; Stevens et al., 2013; Vasques et al., 2008). According to (Brown, Bricklemeyer, & Miller, 2005; Terra et al., 2015; Viscarra-Rossel, McGlynn, & McBratney, 2006). Considerably greater between-runs variation of all the indicators related to IS model points to the reduced stability of IS model.

4. Conclusions

Comparison of soil reflectances obtained with the three laboratory setups, each one with a different spectroscopy accessory (integrating sphere, Illuminator lamp and contact probe) detected no statistically significant differences. The most stable measurements of fire-affected soils were obtained with the setup using Illuminator lamp (Setup L). Thus, the use of the Illuminator lamp or contact probe is preferable to that of the integrating sphere due to the noisier signal in some spectral regions and technical difficulties related to the measurement protocol.

Modelling based on a small number of previously defined spectral variables proved to be sufficient for obtaining SOM predictions of good quality. Acceptable accuracy levels with average R^2 above 0.65 were achieved in the SA-PLSR calibrations and validations of SOM content. Although reflectance levels obtained with the tested setups were quite close, between-setups differences in average R^2 of spectroscopic models were up to 11% for calibrations and 8% for validations. High predictive capacity of models based on the setup with Illuminator Lamp (Setup L) leads to a conclusion that VIS-NIR-SWIR spectroscopic configurations including this accessory can be used for monitoring post-fire evolution of soils, although it should be further examined with a larger number of samples and soil properties.

Acknowledgements

Authors appreciate the financial support provided to this research by Secretariat for Higher Education, Science, Technology and Innovation (SENESCYT), Ecuador, grant no. 211-2012.

REFERENCES

- Addinsoft S.A. (2014). XLSTAT software. New York, NY.
- ASD. (2008). Integrating sphere user manual, ASD document 600660. Boulder: ASD Inc.
- ASDA. (2012). FieldSpec[®]4 user manual, ASD document 6000979. Boulder: ASD Inc.
- ASDb. (2012). Illuminator[™] user manual, ASD document 600066. Boulder: ASD Inc.
- Badía-Villas, D., & del Moral, F. (2016). Soils of the arid areas the soils of Spain (pp. 145–161). Springer.
- Badía, D., & Martí, C. (2003). Plant ash and heat intensity effects on chemical and physical properties of two contrasting soils. *Arid Land Research and Management*, 17(1), 23–41.
- Baumgardner, M. F., Silva, L. F., Biehl, L. L., & Stoner, E. R. (1985). In B.N.C. (Ed.), *Reflectance properties of soils*. Academic Press.
- Beebe, K. R., Pell, R. J., & Seasholtz, M. B. (1998). *Chemometrics: A practical guide* (vol. 4). Wiley-Interscience.
- Bellon-Maurel, V., Fernandez-Ahumada, E., Palagos, B., Roger, J.-M., & McBratney, A. (2010). Critical review of chemometric indicators commonly used for assessing the quality of the prediction of soil attributes by NIR spectroscopy. *TrAC Trends in Analytical Chemistry*, 29(9), 1073–1081.
- Ben-Dor, E., Heller, D., & Chudnovsky, A. (2008). A novel method of classifying soil profiles in the field using optical means. *Soil Science Society of America Journal*, 72(4), 1113–1123.
- Ben-Dor, E., Irons, J. R., & Epema, G. F. (1999). Soil reflectance. *Manual of Remote Sensing, Remote Sensing for the Earth Sciences*, 1, 111.
- Ben-Dor, E., Ong, C., & Lau, I. C. (2015). Reflectance measurements of soils in the laboratory: Standards and protocols. *Geoderma*, 245, 112–124.
- Ben-Dor, E., Pimstein, A., & Notesco, G. (2010). Variation and stability of soil reflectance measurements with different ASD spectrometers under different conditions. In *Paper presented at the proceedings of the ASD and IEEE GRS; art, science and applications of reflectance spectroscopy symposium*. Boulder, CO, USA.
- Brown, D. J. (2007). Using a global VNIR soil-spectral library for local soil characterization and landscape modeling in a 2nd-order Uganda watershed. *Geoderma*, 140(4), 444–453.
- Brown, D. J., Bricklemeyer, R. S., & Miller, P. R. (2005). Validation requirements for diffuse reflectance soil characterization models with a case study of VNIR soil C prediction in Montana. *Geoderma*, 129(3), 251–267.
- Brown, D. J., Shepherd, K. D., Walsh, M. G., Mays, M. D., & Reinsch, T. G. (2006). Global soil characterization with VNIR diffuse reflectance spectroscopy. *Geoderma*, 132(3), 273–290.
- Brunet, D., Barthès, B. G., Chotte, J.-L., & Feller, C. (2007). Determination of carbon and nitrogen contents in Alfisols, Oxisols and Ultisols from Africa and Brazil using NIRS analysis: Effects of sample grinding and set heterogeneity. *Geoderma*, 139(1), 106–117.
- Cañasveras, J. C., Barrón, V., Del Campillo, M. C., Torrent, J., & Gómez, J. A. (2010). Estimation of aggregate stability indices in

- Mediterranean soils by diffuse reflectance spectroscopy. *Geoderma*, 158(1), 78–84.
- Castro-Esau, K., Sanchez-Azofeifa, G., & Rivard, B. (2006). Comparison of spectral indices obtained using multiple spectroradiometers. *Remote Sensing of Environment*, 103(3), 276–288.
- Cécillon, L., Cassagne, N., Czarnes, S., Gros, R., Venetier, M., & Brun, J.-J. (2009). Predicting soil quality indices with near infrared analysis in a wildfire chronosequence. *Science of The Total Environment*, 407(3), 1200–1205.
- Cerdà, A. (1999). Parent material and vegetation affect soil erosion in eastern Spain. *Soil Science Society of America Journal*, 63(2), 362–368.
- Cerdà, A., & Robichaud, P. (2009). *Fire effects on soil infiltration fire effects on soils and restoration strategies* (pp. 81–103). New Hampshire: Science Publishers.
- Chabrilat, S., Goetz, A. F. H., Olsen, H. W., & Krosley, L. (2001). Field and imaging spectrometry for identification and mapping of expansive soils. In *Imaging spectrometry* (pp. 87–109). Springer.
- Chang, C.-W., Laird, D. A., Mausbach, M. J., & Hurburgh, C. R. (2001). Near-infrared reflectance spectroscopy—principal components regression analyses of soil properties. *Soil Science Society of America Journal*, 65(2), 480–490.
- Cheng, J.-l., Shi, Z., & Zhu, Y.-w. (2007). Assessment and mapping of environmental quality in agricultural soils of Zhejiang Province, China. *Journal of Environmental Sciences*, 19(1), 50–54.
- Christy, A. A., & Kvalheim, O. M. (2007). Latent-variable analysis of multivariate data in infrared spectrometry. In *Near-infrared spectroscopy in food science and technology* (pp. 145–162).
- Condit, H. R. (1970). The spectral reflectance of American soils. In *Photogrammetric Engineering*.
- Cuadrat, J. M., & Vide, J. M. (2007). Spanish climatology. In *Past, Present and Future*.
- Curcio, D., Ciraolo, G., D'Asaro, F., & Minacapilli, M. (2013). Prediction of soil texture distributions using VNIR-SWIR reflectance spectroscopy. *Procedia Environmental Sciences*, 19(0), 494–503. <http://dx.doi.org/10.1016/j.proenv.2013.06.056>.
- DeBano, L. F. (2000). The role of fire and soil heating on water repellency in wildland environments: A review. *Journal of Hydrology*, 231, 195–206.
- Dematté, J. A. M. (2002). Characterization and discrimination of soils by their reflected electromagnetic energy. *Pesquisa Agropecuária Brasileira*, 37(10), 1445–1458.
- Dematté, J. A. M., Campos, R. C., Alves, M. C., Fiorio, P. R., & Nanni, M. R. (2004). Visible–NIR reflectance: A new approach on soil evaluation. *Geoderma*, 121(1–2), 95–112. <http://dx.doi.org/10.1016/j.geoderma.2003.09.012>.
- Dematté, J. A. M., & Terra, F. S. (2014). Spectral pedology: A new perspective on evaluation of soils along pedogenetic alterations. *Geoderma*, 217–218(0), 190–200. <http://dx.doi.org/10.1016/j.geoderma.2013.11.012>.
- Duckworth, J. H. (1998). Quantitative analysis. In *Applied spectroscopy: A compact reference for practitioners*, 93.
- Escadafal, R. (1989). *Caractérisation de la surface des sols arides par observations de terrain et par télédétection: Applications: Exemple de la région de Tataouine (Tunisie)*.
- Farifteh, J., Van der Meer, F., Van der Meijde, M., & Atzberger, C. (2008). Spectral characteristics of salt-affected soils: A laboratory experiment. *Geoderma*, 145(3), 196–206.
- Foley, W. J., McIlwee, A., Lawler, I., Aragones, L., Woolnough, A. P., & Berding, N. (1998). Ecological applications of near infrared reflectance spectroscopy—a tool for rapid, cost-effective prediction of the composition of plant and animal tissues and aspects of animal performance. *Oecologia*, 116(3), 293–305.
- Fyfe, S. K. (2004). *Hyperspectral studies of New South Wales seagrasses with particular emphasis on the detection of light stress in eelgrass Zostera capricorni*.
- Ge, Y., Morgan, C. L., Grunwald, S., Brown, D. J., & Sarkhot, D. V. (2011). Comparison of soil reflectance spectra and calibration models obtained using multiple spectrometers. *Geoderma*, 161(3), 202–211.
- Genot, V., Colinet, G., Bock, L., Vanvyve, D., Reusen, Y., & Dardenne, P. (2011). Near infrared reflectance spectroscopy for estimating soil characteristics valuable in the diagnosis of soil fertility. *Journal of Near Infrared Spectroscopy*, 19(2), 117.
- Gholizadeh, A., Borůvka, L., Saberioon, M. M., Kozák, J., Vašát, R., & Nemeček, K. (2015). Comparing different data preprocessing methods for monitoring soil heavy metals based on soil spectral features. *Soil and Water Research*, 10(4), 218–227.
- Gholizadeh, A., Borůvka, L., Vašát, R., Saberioon, M., Klement, A., Kratina, J., & Drábek, O. (2015). Estimation of potentially toxic elements contamination in anthropogenic soils on a brown coal mining dumpsite by reflectance spectroscopy: A case study. *PLoS One*, 10(2), e0117457.
- Giovannini, G., & Lucchesi, S. (1997). Modifications induced in soil physico-chemical parameters by experimental fires at different intensities. *Soil Science*, 162(7), 479–486.
- Goetz, A. F. H., Curtiss, B., & Shiley, D. A. (2009). Rapid gangue mineral concentration measurement over conveyors by NIR reflectance spectroscopy. *Minerals Engineering*, 22(5), 490–499. <http://dx.doi.org/10.1016/j.mineng.2008.12.013>.
- Gomez, C., Viscarra-Rossel, R. A., & McBratney, A. B. (2008). Soil organic carbon prediction by hyperspectral remote sensing and field vis-NIR spectroscopy: An Australian case study. *Geoderma*, 146(3–4), 403–411. <http://dx.doi.org/10.1016/j.geoderma.2008.06.011>.
- Gras, J.-P., Barthès, B. G., Mahaut, B., & Trupin, S. (2014). Best practices for obtaining and processing field visible and near infrared (VNIR) spectra of topsoils. *Geoderma*, 214–215(0), 126–134. <http://dx.doi.org/10.1016/j.geoderma.2013.09.021>.
- Gubler, A. (2011). *Quantitative estimations of soil properties by visible and near infrared spectroscopy—Applications for laboratory and field measurements* (Ph. D. Dissertation). Switzerland: Bern University.
- Guerrero, C., Wetterlind, J., Stenberg, B., Mouazen, A. M., Gabarrón-Galeote, M. A., Ruiz-Sinoga, J. D., et al. (2015). Do we really need large spectral libraries for local scale SOC assessment with NIR spectroscopy? *Soil and Tillage Research*, 155, 501–509.
- He, Y., Huang, M., García, A., Hernández, A., & Song, H. (2007). Prediction of soil macronutrients content using near-infrared spectroscopy. *Computers and Electronics in Agriculture*, 58(2), 144–153.
- Hill, J., Udelhoven, T., Vohland, M., & Stevens, A. (2010). The use of laboratory spectroscopy and optical remote sensing for estimating soil properties. In *Precision Crop Protection—the Challenge and Use of Heterogeneity* (pp. 67–85). Springer.
- Hunt, G. R. (1977). Spectral signatures of particulate minerals in the visible and near infrared. *Geophysics*, 42(3), 501–513.
- Hunt, G. R., & Salisbury, J. W. (1970). Visible and near-infrared spectra of minerals and rocks: I silicate minerals. *Modern Geology*, 1, 283–300.
- Jiménez-González, M. A., De la Rosa, J. M., Jiménez-Morillo, N. T., Almendros, G., González-Pérez, J. A., & Knicker, H. (2016). Post-fire recovery of soil organic matter in a Cambisol from typical Mediterranean forest in southwestern Spain. *Science of the Total Environment*. <http://dx.doi.org/10.1016/j.scitotenv.2016.02.134>.
- Kariuki, P. C., Van Der Meer, F., & Siderius, W. (2003). Classification of soils based on engineering indices and spectral data. *International Journal of Remote Sensing*, 24(12), 2567–2574.
- Knadel, M., Stenberg, B., Deng, F., Thomsen, A., & Greve, M. H. (2013). Comparing predictive abilities of three visible-near

- infrared spectrophotometers for soil organic carbon and clay determination. *Journal of Near Infrared Spectroscopy*, 21(1), 67–80.
- Kooistra, L., Wanders, J., Epema, G. F., Leuven, R. S. E. W., Wehrens, R., & Buydens, L. M. C. (2003). The potential of field spectroscopy for the assessment of sediment properties in river floodplains. *Analytica Chimica Acta*, 484(2), 189–200. [http://dx.doi.org/10.1016/S0003-2670\(03\)00331-3](http://dx.doi.org/10.1016/S0003-2670(03)00331-3).
- Kooistra, L., Wehrens, R., Leuven, R., & Buydens, L. M. C. (2001). Possibilities of visible–near-infrared spectroscopy for the assessment of soil contamination in river floodplains. *Analytica Chimica Acta*, 446(1), 97–105.
- Kuang, B., & Mouazen, A. M. (2013). Effect of spiking strategy and ratio on calibration of on-line visible and near infrared soil sensor for measurement in European farms. *Soil and Tillage Research*, 128, 125–136.
- Liu, W., Baret, F., Gu, X., Zhang, B., Tong, Q., & Zheng, L. (2003). Evaluation of methods for soil surface moisture estimation from reflectance data. *International Journal of Remote Sensing*, 24(10), 2069–2083.
- Lugassi, R., Ben-Dor, E., & Eshel, G. (2014). Reflectance spectroscopy of soils post-heating—Assessing thermal alterations in soil minerals. *Geoderma*, 213(0), 268–279. <http://dx.doi.org/10.1016/j.geoderma.2013.08.014>.
- Lu, P., Wang, L., Niu, Z., Li, L., & Zhang, W. (2013). Prediction of soil properties using laboratory VIS–NIR spectroscopy and hyperion imagery. *Journal of Geochemical Exploration*, 132, 26–33.
- Magidson, J. (2013). Correlated component regression: Re-thinking regression in the presence of near collinearity. In *New Perspectives in partial least Squares and related methods* (pp. 65–78). Springer.
- Martens, H., & Naes, T. (1989). Assessment, validation and choice of calibration method. In *Multivariate calibration* (pp. 237–266).
- Mataix Solera, J. (1999). *Alteraciones físicas, químicas y biológicas en suelos afectados por incendios forestales: Contribución a su conservación y regeneración* (Ph.D. Thesis). Alicante, Spain: Universidad de Alicante. Retrieved from <http://hdl.handle.net/10045/9988>.
- Melendez-Pastor, I., Navarro-Pedreño, J., Gómez, I., & Koch, M. (2008). Identifying optimal spectral bands to assess soil properties with VNIR radiometry in semi-arid soils. *Geoderma*, 147(3), 126–132.
- Merzlyak, M. N., Chivkunova, O. B., Melø, T. B., & Naqvi, K. R. (2002). Does a leaf absorb radiation in the near infrared (780–900 nm) region? A new approach to quantifying optical reflection, absorption and transmission of leaves. *Photosynthesis Research*, 72(3), 263–270.
- Miura, T., & Huete, A. R. (2009). Performance of three reflectance calibration methods for airborne hyperspectral spectrometer data. *Sensors*, 9(2), 794–813.
- Montorio, R., Pérez-Cabello, F., García-Martín, A., Palacios, V., de la Riva, J., Echeverría, M. T., et al. Lasanta, T. (2006). Methodology approach for analyzing relationships between fire severity levels and reflectance values. *Forest Ecology and Management*, 234, S108.
- Neary, D. G., Ryan, K. C., & DeBano, L. F. (2005). Wildland fire in ecosystems: Effects of fire on soils and water. In *General Technical Report RMRS-GTR-42* (vol. 4, p. 250). Ogden, UT: U.S. Department of Agriculture, Forest Service, Rocky Mountain Research Station.
- Nostell, P., Roos, A., & Rönnow, D. (1999). Single-beam integrating sphere spectrophotometer for reflectance and transmittance measurements versus angle of incidence in the solar wavelength range on diffuse and specular samples. *Review of Scientific Instruments*, 70(5), 2481–2494.
- Painter, T. H., Molotch, N. P., Cassidy, M., Flanner, M., & Steffen, K. (2007). Contact spectroscopy for determination of stratigraphy of snow optical grain size. *Journal of Glaciology*, 53(180), 121–127.
- Pérez-Cabello, F., Echeverría, M. T., Ibarra, P., & de la Riva, J. (2009). Effects of fire on vegetation, soil and hydrogeomorphological behavior in Mediterranean ecosystems. In *Earth Observation of Wildland Fires in Mediterranean Ecosystems* (pp. 111–128). Springer.
- Schaepman-Strub, G., Schaepman, M. E., Painter, T. H., Dangel, S., & Martonchik, J. V. (2006). Reflectance quantities in optical remote sensing—definitions and case studies. *Remote Sensing of Environment*, 103(1), 27–42. <http://dx.doi.org/10.1016/j.rse.2006.03.002>.
- Schaepman, M. E., & Dangel, S. (2000). Solid laboratory calibration of a nonimaging spectroradiometer. *Applied Optics*, 39(21), 3754–3764.
- Schmuck, G., San-Miguel-Ayanz, J., Camia, A., Durrant, T., Boca, R., Libertà, G., et al. (2012). Forest fires in Europe. In *Middle east and North Africa*.
- Schulze, D. G. (2002). An introduction to soil mineralogy. In *Soil Science Society of America Book Series* (pp. 1–36).
- Stenberg, B., Viscarra-Rossel, R. A., Mouazen, A. M., & Wetterlind, J. (2010). Chapter five-visible and near infrared spectroscopy in soil science. *Advances in Agronomy*, 107, 163–215.
- Stevens, A., Nocita, M., Tóth, G., Montanarella, L., & van Wesemael, B. (2013). Prediction of soil organic carbon at the European scale by visible and near infrared reflectance spectroscopy. *PLoS One*, 8(6), e66409.
- Stevens, A., van Wesemael, B., Bartholomeus, H., Rosillon, D., Tychon, B., & Ben-Dor, E. (2008). Laboratory, field and airborne spectroscopy for monitoring organic carbon content in agricultural soils. *Geoderma*, 144(1), 395–404.
- Stoner, E. R., & Baumgardner, M. (1981). Characteristic variations in reflectance of surface soils. *Soil Science Society of America Journal*, 45(6), 1161–1165.
- Summers, D., Lewis, M., Ostendorf, B., & Chittleborough, D. (2011). Visible near-infrared reflectance spectroscopy as a predictive indicator of soil properties. *Ecological Indicators*, 11(1), 123–131. <http://dx.doi.org/10.1016/j.ecolind.2009.05.001>.
- Tenenhaus, M. (1998). *La régression PLS: Théorie et pratique*. Paris: Editions Technip.
- Terra, F. S., Demattè, J. A. M., & Viscarra-Rossel, R. A. (2015). Spectral libraries for quantitative analyses of tropical Brazilian soils: Comparing vis–NIR and mid-IR reflectance data. *Geoderma*, 255, 81–93.
- Torrent, J., & Barrón, V. (2002). Diffuse reflectance spectroscopy of iron oxides. In *Encyclopedia of surface and colloid science* (pp. 1438–1446).
- Torrent, J., & Barrón, V. (2003). The visible diffuse reflectance spectrum in relation to the color and crystal properties of hematite. *Clays and Clay Minerals*, 51(3), 309–317.
- Torrent, J., & Barrón, V. (2008). Diffuse reflectance spectroscopy. *Methods of Soil Analysis*, 5, 367–387.
- Vasques, G. M., Grunwald, S. J. O. S., & Sickman, J. O. (2008). Comparison of multivariate methods for inferential modeling of soil carbon using visible/near-infrared spectra. *Geoderma*, 146(1), 14–25.
- Vergnoux, A., Dupuy, N., Guiliano, M., Vennetier, M., Théraulaz, F., & Doumenq, P. (2009). Fire impact on forest soils evaluated using near-infrared spectroscopy and multivariate calibration. *Talanta*, 80(1), 39–47. <http://dx.doi.org/10.1016/j.talanta.2009.06.028>.
- Vicente-Serrano, S. M., Pérez-Cabello, F., & Lasanta, T. (2011). Pinus halepensis regeneration after a wildfire in a semiarid environment: Assessment using multitemporal Landsat images. *International Journal of Wildland Fire*, 20(2), 195–208.

- Viscarra-Rossel, R. A., & Behrens, T. (2010). Using data mining to model and interpret soil diffuse reflectance spectra. *Geoderma*, 158(1), 46–54.
- Viscarra-Rossel, R. A., Behrens, T., Ben-Dor, E., Brown, D., Demattè, J., Shepherd, K., et al. Adamchuk, V. (2016). A global spectral library to characterize the world's soil. *Earth-Science Reviews*, 155, 198–230.
- Viscarra-Rossel, R. A., McGlynn, R. N., & McBratney, A. B. (2006). Determining the composition of mineral-organic mixes using UV–vis–NIR diffuse reflectance spectroscopy. *Geoderma*, 137(1–2), 70–82. <http://dx.doi.org/10.1016/j.geoderma.2006.07.004>.
- Viscarra-Rossel, R. A., Walvoort, D. J. J., McBratney, A. B., Janik, L. J., & Skjemstad, J. O. (2006). Visible, near infrared, mid infrared or combined diffuse reflectance spectroscopy for simultaneous assessment of various soil properties. *Geoderma*, 131(1–2), 59–75. <http://dx.doi.org/10.1016/j.geoderma.2005.03.007>.
- Vlassova, L., & Pérez-Cabello, F. (2016). Effects of post-fire wood management strategies on vegetation recovery and land surface temperature (LST) estimated from Landsat images. *International Journal of Applied Earth Observation and Geoinformation*, 44, 171–183.
- Waruru, B. K., Shepherd, K. D., Ndegwa, G. M., Kamoni, P. T., & Sila, A. M. (2014). Rapid estimation of soil engineering properties using diffuse reflectance near infrared spectroscopy. *Biosystems Engineering*, 121(0), 177–185. <http://dx.doi.org/10.1016/j.biosystemseng.2014.03.003>.
- Williams, P., Williams, P., & Norris, K. (1987). Interpretation of statistical evaluation of NIR analysis. Variables affecting near-infrared reflectance spectroscopic analysis. In P. Williams, & K. Norris (Eds.), *Near-infrared technology in the agricultural and food industries* (pp. 146–148).
- Wold, S., Sjöström, M., & Eriksson, L. (2001). PLS-regression: A basic tool of chemometrics. *Chemometrics and Intelligent Laboratory Systems*, 58(2), 109–130.
- Yañez-Rausell, L., Schaepman, M. E., Clevers, J. G. P. W., & Malenovsky, Z. (2014). Minimizing measurement uncertainties of coniferous needle-leaf optical properties, part I: Methodological review. *Selected Topics in Applied Earth Observations and Remote Sensing, IEEE Journal of*, 7(2), 399–405.

**6. Estimation of SOM content in areas of slash-and-burn agriculture
from VIS-NIR-SWIR spectra**

This chapter reproduces the text of the following article:

Title:

“Espectroscopía VIS-NIR aplicada para predicción del contenido de materia orgánica en los suelos bajo el sistema de cultivo roza-y-quema”

Authors:

Olga Rosero-Vlasova

Pedro Rosero Tufiño

Lidia Vlassova

Espectroscopia VIS-NIR aplicada para predicción del contenido de materia orgánica en los suelos bajo sistema de cultivo roza-y-quema

Olga Rosero Vlasova

Universidad de Zaragoza
oarosero@unizar.es

Pedro Rosero Tufiño

Universidad Técnica Estatal de Quevedo
prosero@uteq.edu.ec

Lidia Vlassova

Universidad Técnica Estatal de Quevedo
lvlassova@uteq.edu.ec

Resumen

El sistema de cultivo roza-y-quema tiene efectos negativos en la fertilidad del suelo a mediano-largo plazo, modificando sus propiedades físicas y químicas. Estos cambios implican cambios en propiedades espectrales, que pueden ser analizadas mediante espectro-radiometría de las regiones espectrales de visible e infrarrojo cercano (VIS-NIR). El estudio evalúa la viabilidad de aplicar espectro-radiometría para la predicción del contenido de materia orgánica (CMO) en suelos afectados por las quemas agrícolas. Las 18 muestras de suelo fueron recolectadas en 2015 en dos áreas de cultivo de maíz (*Zea mays*) en Los Ríos (6 años de quemas repetidas y una sola quema). El espectro-radiómetro ASD con rango espectral 350-2500nm fue utilizado en el laboratorio para obtener los espectros de las muestras previamente tamizadas y secadas al aire. Se detectaron las diferencias estadísticamente significativas entre curvas espectrales de las muestras de los dos grupos. La reflectividad de suelos repetidamente quemados fue 20% más alta para 65% de las muestras, siendo especialmente importante en VIS (>45%), probablemente debido al nivel más bajo de CMO. Los modelos de CMO obtenidos aplicando regresión de Mínimos Cuadrados Parciales (PLSR) mostraron alta capacidad predictiva ($R^2 > 0.8$). El estudio demuestra el gran potencial de espectro-radiometría para monitoreo de CMO en suelos bajo sistema roza-y-quema.

Palabras claves: espectro-radiometría VIS-NIR, materia orgánica, suelos, roza-y-quema, PLSR.

Abstract

Slash-and-burn agriculture have negative mid- and long-term effects on soil fertility, modifying its physical and chemical properties. These changes are accompanied with changes in spectral properties, which can be analysed using spectroradiometry in visible (VIS) and near-infrared (NIR) spectral regions. The study assesses the feasibility of applying spectroradiometry to predict organic matter content in soils (SOM) affected by agricultural burning. 18 soil samples were collected in 2015 in two areas of maize (*Zea mays*) cultivation in the province of Los Ríos (one with 6 burns and another with only one burn). ASD spectroradiometer (350-2500nm spectral range) was used in the laboratory to obtain spectra of sieved and air-dried samples. Statistically significant differences were detected between spectral curves of samples from two groups. The reflectivity of repeatedly burned soils was 20% higher for 65% of samples, being especially important in VIS (>45%), probably due to the lower SOM. PLSR models for SOM showed high predictive capacity ($R^2 > 0.8$). The study demonstrates high potential of spectroradiometry as a tool for monitoring status of soils in slash-and-burn

agriculture.

Keywords: VIS-NIR spectroradiometry, organic matter, soils, slash-and-burn, PLSR.

Introducción

En Ecuador el impacto de las actividades humanas sobre el medio ambiente resulta en pérdida de biodiversidad, tasas anuales de deforestación de hasta 3.5%, y disminución de calidad y erosión de suelos (Saltos & Vasquez, 2009), creando dificultades en el camino a conseguir la seguridad alimentaria de la población, derecho estipulado en el Art. 14 de la Constitución. Con el constante crecimiento demográfico y demanda de alimentos, es necesario aumentar y estabilizar su producción aplicando los modelos agrícolas sostenibles (De la Rosa, 2008).

La técnica de roza-y-quema es un sistema de cultivo tradicional en la agricultura tropical no-mecanizada (Hauser & Norgrove, 2013). En el litoral ecuatoriano es un método ampliamente utilizado por los pequeños agricultores, especialmente para los cultivos de ciclo corto, e.g., arroz y maíz (SINAGAP, 2012). La siembra se realiza en el suelo preparado quemando los residuos secos de la cosecha anterior (u otro tipo de vegetación pre-existente) con el mínimo de labranza (Cerri et al., 2007; Thomaz, 2009). La quema elimina las malezas, reduce riesgo de parásitos y enfermedades, siendo, además, un método de limpieza simple y económico (Jordan, 1989; Kato, Kato, Denich, & Vlek, 1999). La primera cosecha suele ser abundante por el incremento poco duradero de la fertilidad de suelos con la incorporación de calcio, magnesio y potasio provenientes de las cenizas (Nye & Greenland, 1961).

Este tipo de agricultura fue desarrollado por los indígenas durante siglos con la sostenibilidad asegurada por los largos ciclos de rotación. Sin embargo, la presión demográfica lleva a los períodos cada vez más cortos entre las quemadas (Lawrence, Radel, Tully, Schmook, & Schneider, 2010). El tiempo entre las quemadas resulta insuficiente para la recuperación de los suelos, mermándose cada vez más su fertilidad. Se ha demostrado que las quemadas de los restos orgánicos causan pérdidas significativas de los carbonos orgánicos y nutrientes por volatilización, así como procesos de erosión, escorrentía y lixiviación de suelos (Juo & Manu, 1996). Así, se pierde el delicado equilibrio entre los períodos de labranza y períodos de recuperación, característicos para los sistemas de roza-y-quema ancestrales.

A mediano y largo plazo las quemadas regulares tienen efectos negativos en los suelos. Se modifican las propiedades físicas y químicas, tales como textura y estabilidad estructural (Thomaz, 2017), acelerando los procesos de erosión, disminuye el contenido de la materia orgánica y nutrientes disponibles (Certini, 2005). Las propiedades biológicas del suelo también son afectadas observándose la disminución de la biomasa microbiana, macro y microfauna (Neary et al., 1999). El resultado cumulativo de estos cambios es la reducción de la fertilidad (Bento-Gonçalves et al., 2012, Certini, 2005, Mataix-Solera et al., 2011). La cuantificación y análisis de evolución de los cambios en el tiempo pueden ayudar en introducir los cambios conducentes al manejo sustentable (Uriarte, Schneider, & Rudel, 2010). Sin embargo, hasta donde conocemos, en Ecuador no existen estudios que determinen los períodos de cultivo y los de recuperación que asegurarían el equilibrio buscado para cada cultivo y tipo de suelo específicos.

Los cambios en las propiedades físicas y químicas de suelos implican cambios en sus propiedades espectrales, que pueden ser analizadas mediante espectro-radiometría de las regiones espectrales de visible (VIS), infrarrojo cercano (NIR) e infrarrojo de onda corta (SWIR), que comprenden las longitudes de onda de 400-700nm, 700-1300nm y 1300-2500nm, respectivamente (Lugassi, Ben-Dor, & Eshel, 2014; Rosero-Vlasova, Pérez-Cabello,

Llovería, & Vlassova, 2016). La técnica fue con éxito aplicada para detectar las propiedades del suelo relevantes para agricultura (Dematté, Campos, Alves, Fiorio, & Nanni, 2004; Stevens et al., 2008), fijándose algunos de ellos en problemas de contaminación (Cheng, Shi, & Zhu, 2007), salinidad (Farifteh, Van der Meer, Van der Meijde, & Atzberger, 2008), contenido de materia orgánica (He, Huang, García, Hernández, & Song, 2007), y nutrientes (Kuang & Mouazen, 2013). Esa nueva técnica ofrece una alternativa a los tradicionales métodos de análisis de suelos, que requieren de considerable inversión de tiempo y recursos (Ben-Dor, Irons, & Epema, 1999). Comparado con los métodos tradicionales espectro-radiometría de las regiones espectrales VIS-NIR-SWIR es (1) no-destrucciona, (2) flexible: las mediciones pueden ser realizadas tanto en el campo, como en el laboratorio; (3) varias propiedades pueden ser estimadas a partir de un mismo espectro (Viscarra Rossel, Walvoort, McBratney, Janik, & Skjemstad, 2006).

En este contexto, el propósito del estudio es evaluar la viabilidad de aplicar espectro-radiometría en condiciones controladas para la predicción del contenido de materia orgánica en suelos afectados por las quemadas agrícolas. La hipótesis operativa de esta investigación consiste en que la espectroradiometría VIS-NIR-SWIR es la herramienta suficientemente confiable para el monitoreo de la fertilidad de los suelos cultivados bajo el sistema de roza-y-quema.

Metodología

Área de estudio

Los Ríos es la provincia con la mayor superficie ocupada por el cultivo de maíz (*Zea mays*) en el Ecuador (140000 ha) siendo los cantones Ventanas y Mocache las áreas de mayor concentración. Se produce principalmente el maíz duro que se destina a la elaboración de balanceado que es esencial para la alimentación de pollos y cerdos. El maíz tiene una superficie cultivada de 21042.82 hectáreas y se localiza en todo el cantón ocupando el 37.17% de la superficie del cantón. Se cultiva en parcelas pequeñas de extensión entre 1ha y 5ha, muy pocas más de 5ha. El sistema de cultivo generalmente utilizado para este cultivo por los pequeños agricultores es el de roza-y-quema por ser el que involucra mínimos requerimientos financieros y tecnológicos.

El estudio se realizó en el sitio Bella Sombra del cantón Mocache, provincia de Los Ríos, Ecuador, en un área donde se cultiva maíz bajo el sistema roza-y-quema (Figura 1). La zona de topografía irregular cuyas elevaciones fluctúan entre 80msnm y 120msnm se caracteriza por un clima megatérmico húmedo (Pourrut, 1983) con la temperatura media anual de 24 °C y precipitación media anual de 1800-2000mm. Las estaciones secas (junio-diciembre) y la lluviosa (enero-mayo) están claramente diferenciadas. Según (Holdridge, 1987), la zona se clasifica como bosque tropical seco.

Muestreo de suelos

La Figura 2 presenta la vista general del área de estudio. Las 18 muestras de la capa superficial de suelo (0-2cm) fueron obtenidas en septiembre de 2015 en dos áreas dedicadas al cultivo de maíz bajo el sistema de roza-y-quema (área total de 5ha): (1) área sometida a quemadas periódicas durante los 6 años anteriores; y (2) área recientemente incorporada al cultivo donde se realizó una quema al eliminar los árboles de cacao para sembrar maíz y la siguiente, más reciente, después de la primera cosecha. Las muestras fueron obtenidas al siguiente día después de la quema.

Cada muestra fue dividida en dos partes: una parte se utilizó para los análisis convencionales de contenido de materia orgánica en el suelo efectuada en el laboratorio de Instituto de Investigaciones Agropecuarias INIAP, sede Quevedo; y la otra (~160g por muestra) se transportó al laboratorio de Espectroradiometría Ambiental de la Universidad de Zaragoza para las mediciones espectrales.

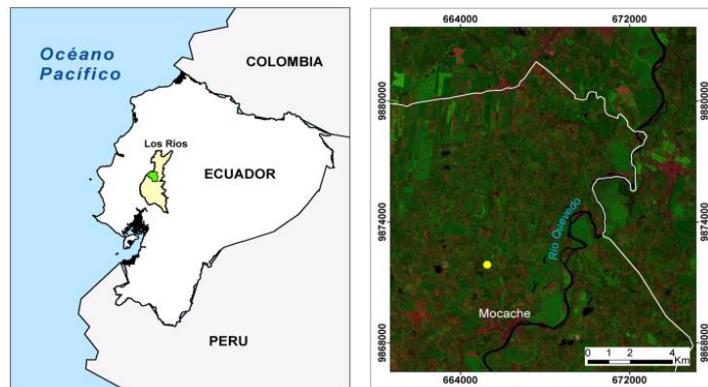


Figura 1

Localización del área de estudio: (A) Mapa de referencia. El polígono verde corresponde al Cantón Mocache, provincia de Los Ríos, Ecuador; (B) Imagen de Landsat-8 (Composición de bandas 7-5-3, año 2014). Límite del cantón Mocache se muestra como línea blanca. Punto amarillo indica el lugar de muestreo.

Fuente: Autores

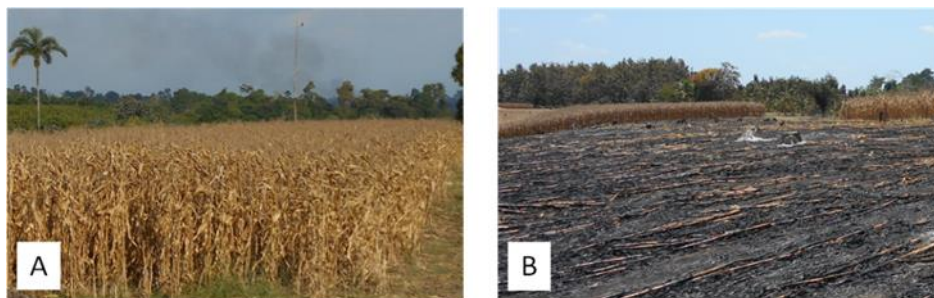


Figura 2

Vista general del área de estudio: (A) cultivo de maíz cosechado aún no quemado; (B) área después de la quema.

Fuente: Autores

Mediciones espectrales

Las mediciones espectrales se realizaron a las muestras recogidas en el campo que han sido anteriormente preparadas. El primer paso de la preparación fue separar la fracción fina (tamaño de partícula <2mm). Luego fueron colocadas en placas Petri de cristal (90 mm de diámetro) y presionadas para formar una capa de ~15mm de espesor. Posteriormente las muestras (~160g) de superficie homogénea fueron secadas en horno durante 24 horas a 105°.

Para obtener los espectros de suelos se utilizó un espectroradiómetro Analytical Spectral Device (ASD) FieldSpec®4, que está compuesto internamente por tres espectrómetros (detectores), cada uno dedicado al trabajo en un rango espectral específico. El instrumento registra la señal en el VIS-NIR (350-1000nm) y dos regiones en SWIR (1001-1800 nm y 1801-2500nm) con un intervalo de muestreo espectral de 1.4nm y 2nm, y una resolución espectral (Full Width at Half Maximum - FWHM) de 3nm y 10nm, respectivamente (ASDa, 2012). La señal recibida por el sensor es corregida por la señal eléctrica de base (corriente oscura) y re-muestreada a un intervalo de 1nm sobre toda la región de onda registrada por el software del dispositivo (Fyfe, 2004). Las medidas estimadas como factor de reflectancia son por lo general referidas simplemente como reflectancia. Este se define como la relación del flujo radiante reflejado por la superficie del objetivo con respecto a aquel reflejado

por una superficie estándar ideal bajo la misma geometría de observación (Shaepman-Strub, Schaepman, Painter, Dangel, Martonchik, 2006). Cuando las medidas son realizadas en condiciones de iluminación controladas, el espectroradiómetro registra un Factor de Reflectancia Bicónica (BCRF por sus siglas en inglés), ya que, en este caso, ambos, tanto la radiancia entrante como reflejada, pueden ser aproximadas a unos conos (Schaepman-Strub et al., 2006).

La superficie de referencia debe tener una reflectancia perfecta sobre todo el rango de longitud de onda y ser resistente a contaminantes del ambiente. El panel de referencia de Spectralon® calibrados hechos depolitetetrafluoroetileno (PTFE por sus siglas en inglés) proporcionado por el fabricante satisface todos los requerimientos y fue usado para convertir las medidas de radiancia en valores de reflectancia. Las mediciones fueron desarrolladas en un laboratorio oscuro bajo condiciones de iluminación controladas usando una configuración que incluyó el uso de la lámpara ASD IlluminatorLamp, accesorio de total compatibilidad con el espectroradiómetro, ya que está diseñado para trabajar sobre el mismo rango de longitud de onda que el equipo. La lámpara fue encendida previamente a las mediciones durante 15 minutos (ASDb, 2012).

Antes de empezar el escaneo de las muestras, el software ASD RS³ (ASDa, 2012) fue configurado para promediar 10 espectros por cada escaneo de muestra, 25 – blanco de referencia, y 10 – corriente oscura para reducir el ruido y mejorar la relación señal-al-ruido.

La *Figura 3* presenta una vista general de la configuración del experimento. Para una iluminación óptima de la muestra, se calculó previamente la geometría de observación, tomando en cuenta (i) la distancia entre la muestra y el sensor, (ii) la distancia entre la muestra y la fuente de iluminación, y (iii) el ángulo entre los dos. El cálculo del área detectada por el sensor se basó en la documentación del ASD Illuminator Lamp. Esto resultó en la siguiente configuración (*Figura 4*): (1) lámpara Illuminator Lamp (ángulo del haz de luz $\theta=12^\circ$) unida de manera vertical al trípode sobre la muestra de suelo ($H=42\text{cm}$) generando un lugar de iluminación sobre la superficie de la muestra de 8.82cm de diámetro (D); (2) pistol grip unido al otro trípode a una altura de $h=7.5\text{cm}$ ($\text{FOV}_{\text{Fibra_desnuda}} \beta=25^\circ$, diámetro del sitio escaneado $d=6.99\text{cm}$) y un ángulo $\alpha=45^\circ$ con respecto al eje vertical. En esta configuración los sensores registran la señal del sitio que cubre el área dentro de la Petri, y el procedimiento de medición no involucra la manipulación de la muestra. El espectro de la muestra es un promedio de 50 mediciones radiométricas.



Figura 3

Vista general de la instrumentación utilizada en las mediciones espectrales. Las imágenes de la derecha muestran (de arriba abajo): la lámpara ASD Illuminator Lamp, panel de referencia, y Pistol grip usado para fijar la fibra óptica.

Fuente: Autores

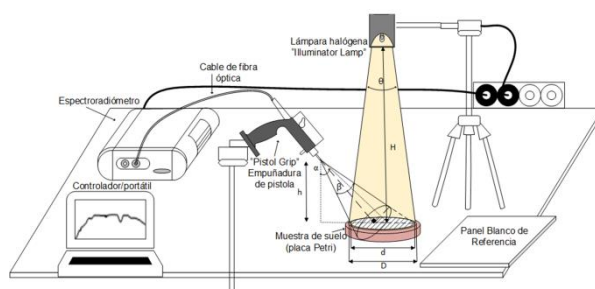


Figura 4

Diagrama de configuración y geometría de observación.

Fuente: Autores

Durante la sesión de trabajo, el cable de fibra óptica estaba regularmente dirigido al panel de referencia Spectralon con la misma geometría de observación. Debido a que las medidas fueron realizadas en el laboratorio bajo condiciones de iluminación controladas, no fue necesario realizar la calibración antes de cada escaneo de la muestra.

Análisis estadístico

El análisis de los espectros de reflectancia medidos se basó en longitudes de ondas con la mayor información de propiedades edáfica sugerida por Demattê y Terra (2014). La importancia de estas bandas para la detección de materia orgánica, minerales de arcilla, y óxidos de hierro y aluminio han sido ya publicados en investigaciones previas (Ben-Dor, Heller, Chudnovsky, 2008; Melendez-Pastor, Navarro-Pedreño, Gómez, Koch, 2008). Las bandas analizadas incluyen: 6 bandas en región espectral VIS (401nm, 440nm, 530nm, 550nm, 650nm, 700nm), 7 bandas en región espectral NIR (845nm, 850nm, 870nm, 901nm, 931nm, 951nm, 1051nm) and 8 bandas en región espectral SWIR (1302nm, 1401nm, 1903nm, 2201nm, 2263nm, 2300nm, 2352nm and 2430nm). No se aplicó ningún tipo de pre-procesamiento a los espectros originales, algo comúnmente utilizado para reducir la incertidumbre (Vasques, Grunwald, Sickman, 2008).

La significancia de las diferencias observadas entre los dos grupos de espectros de reflectancia, fue verificada por el análisis de varianza (one-way ANOVA). El análisis de varianza (one-way ANOVA) fue aplicado para probar la significancia de las diferencias observadas entre el grupo de espectros de reflectancia. Esta técnica usa la distribución F para averiguar si los promedios de dos o más grupos son diferentes. Se utiliza cuando variables continuas son usadas como predictores de una variable dependiente (por lo cual es llamada one-way ANOVA). La hipótesis nula dice que las muestras son tomadas de la misma población, esta es aceptada o rechazada basándose en el estadístico - F (la relación de la varianza calculada entre los promedios con respecto a la varianza dentro de la muestra). Para que el estadístico sea confiable, deben cumplirse algunas condiciones: (1) los errores son independientes y siguen una distribución normal; (2) las muestras son independientes y extraídas de poblaciones con varianzas iguales.

Finalmente, se aplicó Regresión de Mínimos Cuadrados Parciales (PLSR por sus siglas en inglés) (Tenenhaus, 1998; Wold, Sjöström, Eriksson, 2001) con el algoritmo de selección de predictores implementado en el software XLStat (Addinsoft S.A., 2014) para la calibración y validación del modelo predictivo para materia orgánica, una de las propiedades más relevantes para la valoración de la fertilidad y capacidad productiva del suelo.

PLSR es ampliamente utilizado en Espectroscopía VIS-NIR-SWIR de suelo (e.g. (Kooistra et al., 2003; Viscarra-Rossel, Walvoort, McBratney, Janik y Skjemstad, 2006) por su capacidad de resolver el problema de

multicolinealidad en modelos con la gran cantidad de predictores (Wold et al., 2001).

El método combina las características del análisis de componentes principales y regresión lineal múltiple. Los predictores se usan para calcular un conjunto de los vectores ortogonales llamados las variables latentes que explican la mayor parte de varianza en la variable dependiente (Martens & Naes, 1989). El número de las variables latentes (componentes) y el modelo final se definen a través de la validación cruzada, durante la cual se computa una serie de modelos de regresión, cada vez dejando fuera una de las muestras; el modelo luego se aplica para predecir el valor para la muestra omitida (Duckworth, 1998).

Los modelos obtenidos por la regresión PLSR a veces sufren de ajuste excesivo, por cuanto pueden incluir los predictores relevantes sólo para el conjunto de datos usados para calibración (ruido), mostrando disminución del poder predictivo, al analizar los datos adquiridos independientemente del conjunto original (Christy & Kvalheim, 2007). Para evitar el sobreajuste, el presente estudio aplica el algoritmo de selección de predictores, que excluye del modelo las variables independientes menos importantes. En el proceso iterativo de validación cruzada en cada ciclo se elimina el predictor con el menor (valor absoluto) coeficiente estandarizado.

La bondad de ajuste del modelo fue evaluado usando el Coeficiente de Determinación (R^2) que es el cociente de las varianzas de valores estimados (predichos) y valores observados de la variable dependiente. R^2 se calcula según la siguiente formula:

$$R^2 = \frac{\sum (\hat{Y}_i - \bar{Y})^2}{\sum (Y_i - \bar{Y})^2}$$

Dónde Y_i es el valor observado de CMO para la i -ésima muestra, \hat{Y}_i es el valor predicho de CMO para la i -ésima muestra, y \bar{Y} es el valor promedio para todas las muestras.

De acuerdo a Terra, Dematte y Viscarra-Rossel (2015), un valor de $R^2 > 0.75$ indica un modelo preciso para la predicción cuantitativa de propiedades del suelo, aquellos con valores para R^2 entre 0.50 and 0.75 revela un ajuste aceptable que puede ser mejorado y los modelos de calibración con R^2 menor de 0.50 son considerados poco fiables.

Resultados y Discusión

Análisis de laboratorio

La *Tabla 1* presenta los valores promedio de la textura y contenido de materia orgánica en las muestras estimadas por técnicas de laboratorio convencionales. Los resultados demuestran que en general, en el área de estudio, los suelos tienen alto contenido de materia orgánica ($\geq 6 \text{ g } 100 \text{ g}^{-1}$) y son franco-limosos con contenido de limo por encima de 50% y el de arena mayor de 30%.

Tabla 1

Textura y contenido de la materia orgánica de las muestras analizadas (valores promedios)

Grupo	Años bajo sistema Roza-y-Quema	Textura (%)			Materia orgánica (g 100 g ⁻¹)
		Arena	Limo	Arcilla	
Suelo 1	6	31.67	52.00	16.33	5.92
Suelo 2	1	39.33	51.67	9.00	7.00

Fuente: Autores

Análisis cualitativo de espectros de reflectancia

La Figura 5 muestra las curvas espectrales de reflectancia para los dos grupos de suelos. Presentan la forma típica para los suelos sin rasgos de absorción claros en la región del visible (VIS) y el infrarrojo cercano (NIR), donde las curvas se diferencian principalmente por el nivel de intensidad de reflectancia y la tendencia de la pendiente. Sin embargo, en SWIR resaltan los rasgos de absorción asociados con el agua higroscópica y grupo O-H en las longitudes de ondas de 1400nm y 1900nm (Stoner & Baumgardner, 1981); y con minerales de arcillas en las longitudes de ondas de 2200nm (Viscarra-Rossel & Behrens, 2010).

Las diferencias en la pendiente de las curvas y el nivel de reflectancia evidentes en todo el rango espectral analizado, probablemente se deben a las diferencias en la composición de las muestras, e.i. su heterogeneidad (Ge et al., 2011), siendo uno de los aspectos de esta heterogeneidad la variación en el contenido de los compuestos orgánicos (Ben-Dor et al., 1999). Estos resultados son consistentes con los resultados obtenidos por otros investigadores. Por ejemplo, Dematte et al. (2004) ha demostrado los niveles de reflectancia más bajos a lo largo de todo el espectro, debido al contenido más alto de materia orgánica en los suelos de los suelos de Brasil que analizaron, mientras que Henderson et al. (1992) explicaron esta disminución, en la intensidad de reflectancia por el hecho de mayor absorción de la energía por la materia orgánica.

Se aprecia claramente la diferencia en los niveles de reflectancia entre las curvas espectrales correspondientes a los dos grupos de suelos analizados, demostrando los suelos de las áreas con más ciclos de cultivo bajo el sistema de roza-y-quema las reflectancias más altas, especialmente en el rango de las longitudes de onda de 800nm-1350nm.

Además, en el espectro de los suelos del Grupo 1 se observa concavidad de la curva espectral en el rango de longitudes de onda 440-850nm, según estudios previos (Dematte et al., 2016) característico a los suelos con el alto contenido de materia orgánica; el rasgo ausente en el espectro de los suelos de Grupo 2 que han experimentado mayor impacto de las quemas agrícolas.

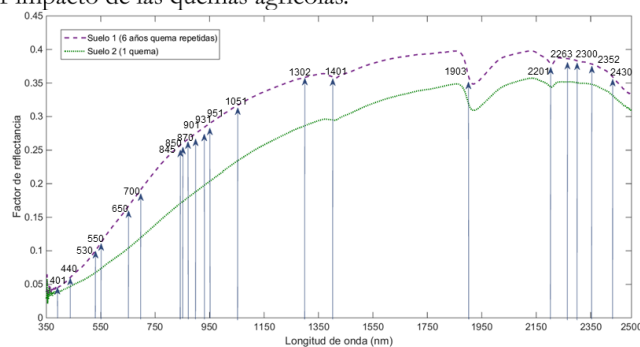


Figura 5

Curvas de reflectancia de los dos grupos de suelos analizados (espectro promedio en cada caso)

Fuente: Autores

Resultados de ANOVA

Se ha comprobado que los datos analizados cumplen las condiciones referentes a la normalidad de la distribución, igualdad de las varianzas e independencia de los datos muestreados, que garanticen la confiabilidad de los resultados del test.

Se detectaron las diferencias estadísticamente significativas entre las reflectancias en las bandas seleccionadas de los dos grupos ($p < 0.05$), siendo la reflectancia de suelos repetidamente quemados (Suelo 1) 20% más alta (promedio para todo el espectro) para 65% de las muestras. Las diferencias más importantes observadas en las regiones espectrales de VIS ($>45\%$) y NIR ($\sim 35\%$), probablemente se deben al contenido más bajo de materia orgánica en los suelos del primer grupo (Tabla 1).

Análisis usando PLSR

Los valores de contenido de materia orgánica (MO) y los datos de las respuestas espectrales en las longitudes de onda seleccionadas fueron usados para desarrollar los modelos predictivos utilizando el método de PLSR. El mejor poder predictivo fue demostrado por el modelo con 6-factores (componentes) y 19 predictores (Figura 6).

Las bandas de 650nm y 530nm fueron las que tienen coeficientes más altos, lo que significa que aportaron mayor información sobre MO para el modelo. Coincidiendo con los resultados de otros estudios, varias bandas de la región espectral de NIR y SWIR también mostraron altos coeficientes. El gran contenido informativo de reflectancias en estas longitudes de onda fue anteriormente comprobado por múltiples estudios (Knadel, Stenberg, Deng, Thomsen, & Greve, 2013; Demattê & da Silva Terra, 2014). Algunas de las bandas NIR-SWIR se asocian con la absorción por el agua (951nm y 1401nm) y presencia de las arcillas (2201nm y 2263nm). La importancia que tiene para el modelo la banda de 2201nm indica la probabilidad de alto contenido del mineral caolinita (Dematte et al., 2016).

El modelo también contiene los predictores con altos coeficientes (1903nm y 2201nm), que según los trabajos anteriores (Viscarra-Rossel & Behrens, 2010) se relacionan con el contenido de MO, que muestra los rasgos espectrales en esta región.

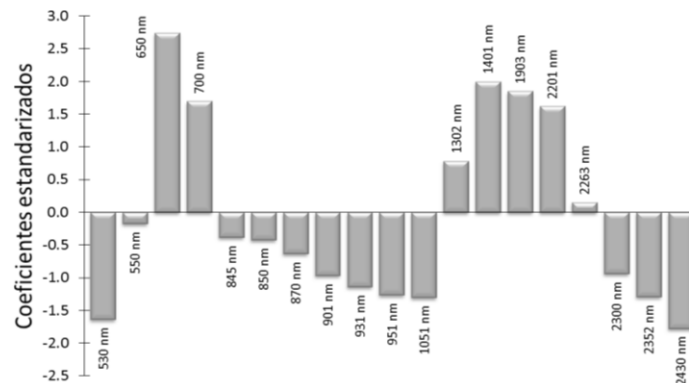


Figura 6

Gráfico de los coeficientes estandarizados de las variables predictoras

Fuente: Autores

El alto coeficiente de determinación del modelo de MO ($R^2=0.78$) obtenido aplicando regresión de mínimos cuadrados parciales (PLSR), es la evidencia de su gran poder predictivo y buen ajuste (Figura 7).

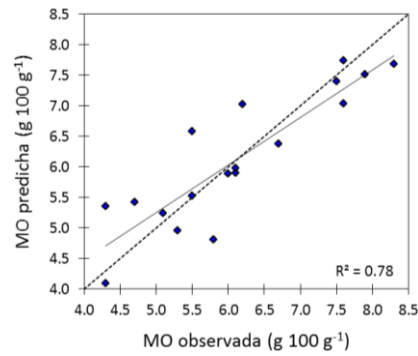


Figura 7

Gráfico de dispersión de la MO observada versus la MO predicha.

Fuente: Autores

Aunque se conoce que el contenido de materia orgánica es una de las propiedades que tiene una respuesta espectral directa y por eso puede modelarse con bastante éxito a partir de los datos de espectroscopia VIS-NIR-SWIR, el poder predictivo de los modelos estadísticos puede variar ampliamente dependiendo de los tipos de suelos y método estadístico empleado, comparándose los resultados obtenidos en este estudio con los mejores obtenidos por otros investigadores (Mouazen, Kuang, De Baerdemaeker, & Ramón, 2010; Udelhoven, Emmerling, & Jarmer, 2003).

Conclusiones

El estudio evaluó la capacidad de la espectroradiometría de suelos para detectar los cambios en los suelos utilizados en el sistema de cultivo de roza-y-quema. Se han detectado las diferencias estadísticamente significativas entre las curvas espectrales de suelos cultivados con este método durante los 6 años (grupo 1) y 1 año (grupo 2), asociándose los niveles de reflectancia más altos con los suelos del primer grupo. Las diferencias probablemente se explican por la disminución de la materia orgánica en los suelos que han soportado más ciclos de cultivo y mayor número de quemas agrícolas.

Los modelos de contenido de materia orgánica obtenidos aplicando regresión de mínimos cuadrados parciales (PLSR) presentaron el coeficiente de determinación superior a 0.75 demostrando alta precisión y capacidad predictiva. El estudio es una prueba del gran potencial de espectro-radiometría para monitoreo de cambios en los suelos cultivables con sistema roza-y-quema.

Agradecimientos

La realización de esta investigación ha sido posible gracias a la beca para realizar la investigación pre-doctoral concedida a Olga Rosero-Vlasova por SENESCYT-Ecuador.

Referencias

- ASDa. (2012). *Fieldspec Pro user's guide*. Boulder: ASD Inc.
- ASDb. (2012). *Illuminator™ user manual*. Boulder: ASD Inc.
- Addinsoft, X. (2014). *Data analysis and statistics with Microsoft Excel*. Paris, France.
- Ben-Dor, E., Irons, J. R., & Epema, G. F. (1999). Soil reflectance. In A. N. Rencz (Ed.), *Remote Sensing for the Earth Sciences* (Third ed.). New York: John Wiley & Sons. pp. 111-188.

*CHAPTER 6. Estimation of SOM content in areas of slash-and-burn agriculture from
VIS-NIR-SWIR spectra*

- Ben-Dor, E., Heller, D., & Chudnovsky, A. (2008). A novel method of classifying soil profiles in the field using optical means. *Soil Science Society of America Journal*, 72(4), pp.1113-1123.
- Bento-Gonçalves, A., Vieira, A., Úbeda, X., & Martin, D. (2012). Fire and soils: key concepts and recent advances. *Geoderma*, 191, pp.3-13.
- Cerri, C. E. P., Sparovek, G., Bernoux, M., Easterling, W. E., Melillo, J. M., & Cerri, C. C. (2007). Tropical agriculture and global warming: impacts and mitigation options. *Scientia Agricola*, 64(1), pp. 83-99.
- Certini, G. (2005). Effects of fire on properties of forest soils: a review. *Oecologia*, 143(1), pp.1-10.
- Comte, I., Davidson, R., Lucotte, M., de Carvalho, C. J. R., de Assis Oliveira, F., da Silva, B. P., & Rousseau, G. X. (2012). Physicochemical properties of soils in the Brazilian Amazon following fire-free land preparation and slash-and-burn practices. *Agriculture, Ecosystems & Environment*, 156, pp. 108-115. Recuperado de: <http://dx.doi.org/10.1016/j.agee.2012.05.004>.
- Cheng, J.-l., Shi, Z., & Zhu, Y.-w. (2007). *Assessment and mapping of environmental quality in agricultural soils of Zhejiang Province, China. Journal of Environmental Sciences*, 19(1), pp.50-54.
- Christy, A. A., & Kvalheim, O. M. (2007). *Latent-variable analysis of multivariate data in infrared spectrometry*. Near-infrared spectroscopy in food science and technology, pp.145-162.
- Demattê, J. A. M., Campos, R. C., Alves, M. C., Fiorio, P. R., & Nanni, M. R. (2004). Visible–NIR reflectance: a new approach on soil evaluation. *Geoderma*, 121(1–2), pp.95-112. Recuperado de: <http://dx.doi.org/10.1016/j.geoderma.2003.09.012>.
- Demattê, J. A. M., & da Silva Terra, F. (2014). Spectral pedology: A new perspective on evaluation of soils along pedogenetic alterations. *Geoderma*, pp.190-200. Recuperado de: <http://dx.doi.org/10.1016/j.geoderma.2013.11.012>.
- Demattê, J. A., Ramírez-López, L., Rizzo, R., Nanni, M. R., Fiorio, P. R., Fongaro, C. T., da S Barros, P. P. (2016). Remote sensing from ground to space platforms associated with terrain attributes as a hybrid strategy on the development of a pedological map. *Remote Sensing*, 8(10), p. 826.
- Duckworth, J. H. (1998). *Quantitative analysis Applied spectroscopy: A compact reference for practitioners*, p.93.
- Farifteh, J., Van der Meer, F., Van der Meijde, M., & Atzberger, C. (2008). Spectral characteristics of salt-affected soils: A laboratory experiment. *Geoderma*, 145(3), pp.196-206.
- Fyfe, S. K. (2004). *Hyperspectral Studies of New South Wales seagrasses with particular emphasis on the detection of light stress in eelgrass Zostera capricorni*.
- Ge, Y., Thomasson, J. A., & Sui, R. (2011). Remote sensing of soil properties in precision agriculture: A review. *Frontiers of Earth Science*, 5(3), pp.229-238.

*CHAPTER 6. Estimation of SOM content in areas of slash-and-burn agriculture from
VIS-NIR-SWIR spectra*

- Hauser, S., & Norgrove, L. (2013). Effects of slash-and-burn agriculture. In S. Levin (Ed.), *Encyclopedia of Biodiversity* (2 ed.). Waltham: Academic Press. pp. 551-562.
- He, Y., Huang, M., García, A., Hernández, A., & Song, H. (2007). Prediction of soil macronutrients content using near-infrared spectroscopy. *Computers and Electronics in Agriculture*, 58(2), pp.144-153.
- Holdridge, L. R. (1987). *Ecología basada en zonas de vida: Agroamérica*.
- Jordan, C. F. (1989). An Amazonian rain forest: the structure and function of a nutrient stressed ecosystem and the impact of slash-and-burn agriculture: *United Nations Educational, Scientific and Cultural Organization*.
- Kato, M. d. S. A., Kato, O. R., Denich, M., & Vlek, P. L. G. (1999). Fire-free alternatives to slash-and-burn for shifting cultivation in the eastern Amazon region: the role of fertilizers. *Field crops research*, 62(2), pp.225-237.
- Knadel, M., Stenberg, B., Deng, F., Thomsen, A., & Greve, M. H. (2013). Comparing predictive abilities of three visible-near infrared spectrophotometers for soil organic carbon and clay determination. *Journal of Near Infrared Spectroscopy*, 21(1), pp.67-80.
- Kooistra, L., Wanders, J., Epema, G. F., Leuven, R. S. E. W., Wehrens, R., & Buydens, L. M. C. (2003). The potential of field spectroscopy for the assessment of sediment properties in river floodplains. *Analytica Chimica Acta*, 484(2), pp.189-200. Recuperado de: [http://dx.doi.org/10.1016/S0003-2670\(03\)00331-3](http://dx.doi.org/10.1016/S0003-2670(03)00331-3).
- Kuang, B., & Mouazen, A. M. (2013). *Effect of spiking strategy and ratio on calibration of on-line visible and near infrared soil sensor for measurement in European farms. Soil and Tillage Research*, 128, pp.125-136.
- Lawrence, D., Radel, C., Tully, K., Schmook, B., & Schneider, L. (2010). Untangling a decline in tropical forest resilience: constraints on the sustainability of shifting cultivation across the globe. *Biotropica*, 42(1), pp.21-30.
- Lugassi, R., Ben-Dor, E., & Eshel, G. (2014). Reflectance spectroscopy of soils post-heating—Assessing thermal alterations in soil minerals. *Geoderma*, 213(0), pp.268-279. Recuperado de: <http://dx.doi.org/10.1016/j.geoderma.2013.08.014>.
- Martens, H., & Naes, T. (1989). *Assessment, validation and choice of calibration method*. Multivariate calibration, pp.237-266.
- Mataix-Solera, J., Cerdà, A., Arcenegui, V., Jordán, A., & Zavala, L. (2011). Fire effects on soil aggregation: a review. *Earth-Science Reviews*, 109(1), pp.44-60.
- Melendez-Pastor, I., Navarro-Pedreño, J., Gómez, I., & Koch, M. (2008). Identifying optimal spectral bands to assess soil properties with VNIR radiometry in semi-arid soils. *Geoderma*, 147(3), pp.126-132.

CHAPTER 6. Estimation of SOM content in areas of slash-and-burn agriculture from VIS-NIR-SWIR spectra

- Neary, D. G., Klopatek, C. C., DeBano, L. F., & Ffolliott, P. F. (1999). Fire effects on belowground sustainability: a review and synthesis. *Forest Ecology and Management*, 122(1), pp.51-71.
- Pourrut, P. (1983). *Los climas del Ecuador: fundamentos explicativos*. Ministerio de Agricultura y Ganadería: Quito, Ecuador.
- Rosero-Vlasova, O. A., Pérez-Cabello, F., Llovería, R. M., & Vlassova, L. (2016). Assessment of laboratory VIS-NIR-SWIR setups with different spectroscopy accessories for characterisation of soils from wildfire burns. *Biosystems Engineering* 152, pp.51-67.
- Schaepman-Strub, G., Schaepman, M. E., Painter, T. H., Dangel, S., & Martonchik, J. V. (2006). Reflectance quantities in optical remote sensing—definitions and case studies. *Remote Sensing of Environment*, 103(1), pp.27-42. Recuperado de: <http://dx.doi.org/10.1016/j.rse.2006.03.002>.
- SINAGAP. (2012). *Cantón Mocache. Sistemas productivos. Proyecto: generación de geoinformación para la gestión del territorio a nivel nacional escala 1: 25 000*. Quito: MAGAP, pp. 118.
- Stevens, A., van Wesemael, B., Bartholomeus, H., Rosillon, D., Tychon, B., & Ben-Dor, E. (2008). Laboratory, field and airborne spectroscopy for monitoring organic carbon content in agricultural soils. *Geoderma*, 144(1), pp. 395-404.
- Stoner, E. R., & Baumgardner, M. (1981). Characteristic variations in reflectance of surface soils. *Soil Science Society of America Journal*, 45(6), pp.1161-1165.
- Tenenhaus, M. (1998). *La régression PLS: théorie et pratique*. Editions Technip.
- Terra, F. S., Demattê, J. A., & Rossel, R. A. V. (2015). Spectral libraries for quantitative analyses of tropical Brazilian soils: Comparing vis-NIR and mid-IR reflectance data. *Geoderma*, 255, pp. 81-93.
- Thomaz, E. L. (2009). The influence of traditional steep land agricultural practices on runoff and soil loss. *Agriculture, Ecosystems & Environment*, 130(1), pp. 23-30.
- Thomaz, E. L. (2017). Fire changes the larger aggregate size classes in slash-and-burn agricultural systems. *Soil and Tillage Research*, 165, pp. 210-217. Recuperado de: <http://dx.doi.org/10.1016/j.still.2016.08.018>.
- Vasques, G. M., Grunwald, S., & Sickman, J. O. (2009). Modeling of soil organic carbon fractions using visible-near-infrared spectroscopy. *Soil Science Society of America Journal*, 73(1), pp.176-184.
- Viscarra Rossel, R., & Behrens, T. (2010). Using data mining to model and interpret soil diffuse reflectance spectra. *Geoderma*, 158(1), pp.46-54.
- Viscarra Rossel, R. A., Walvoort, D. J. J., McBratney, A. B., Janik, L. J., & Skjemstad, J. O. (2006). Visible, near infrared, mid infrared or combined diffuse reflectance spectroscopy for simultaneous assessment of various soil properties. *Geoderma*, 131(1-2), pp.59-75. Recuperado de: <http://dx.doi.org/10.1016/j.geoderma.2005.03.007>.

7. Testing algorithms applied in multivariate statistical modeling of SOM and texture fractions of fire-affected soils

This chapter reproduces the text of the following article:

Title:

Soil organic matter and texture estimation from visible-near infrared-shortwave infrared spectra in areas of land cover changes using correlated component regression.

Authors:

Olga A. Rosero Vlasova






Lidia Vlassova

Fernando Pérez-Cabello

Raquel Montorio

Estela Nadal-Romero

Soil organic matter and texture estimation from visible–near infrared–shortwave infrared spectra in areas of land cover changes using correlated component regression

Olga A. Rosero-Vlasova^{1,2}  | Lidia Vlassova³  | Fernando Pérez-Cabello^{1,2}  | Raquel Montorio^{1,2}  | Estela Nadal-Romero^{2,4} 

¹GEOFOREST Group, Environmental Sciences Institute (IUCA), University of Zaragoza, Pedro Cerbuna, 12, E-50009, Zaragoza, Spain

²Department of Geography and Land Management, University of Zaragoza, Pedro Cerbuna, 12, E-50009, Zaragoza, Spain

³Department of Environmental Sciences, Technical State University of Quevedo, EC-120509, Quevedo, Ecuador

⁴Geo-environmental Processes and Global Change, IPE-CSIC, Pyrenean Institute of Ecology, Avda. Montañana, 1005, E-50059, Zaragoza, Spain

Correspondence

Olga A. Rosero-Vlasova, Department of Geography and Land Management, Faculty of Arts, University of Zaragoza, Pedro Cerbuna, 12, E-50009, Zaragoza, Spain.
Email: oarosero@unizar.es

Funding information

Secretaría de Educación Superior, Ciencia, Tecnología e Innovación, Grant/Award Number: 211-2012; Universidad de Zaragoza and Santander Universidades, Grant/Award Number: Ayudas Movilidad Latinoamericanos-Estudios de Doctorado. UNIZAR - Santander Universidades|2017-2018; Marie Curie Intra-European Fellowship project "MED-AFFOR-EST", Grant/Award Number: PIEF-GA-2013-624974; Ministerio de Economía y Competitividad, Gobierno de España, Grant/Award Number: RYC-2013-14371

Abstract

Land use changes due to natural and human-related factors, which include wildfires and crop abandonment, are among the most important drivers of soil degradation and demand regular monitoring. Proximal soil sensing in visible–near infrared–shortwave infrared spectral regions could offer a solution. However, to become operational, optimal combination of data and technique has to be defined. Thus, the purpose of this study was (a) to predict the soil organic matter (SOM) content and soil texture in areas of wildfire burns and crop abandonment in Aragón Province, Northern Spain, from their laboratory reflectance spectra using novel correlated components regression with a step-down variable selection algorithm (CCR-SD) and (b) to compare the CCR-SD and the partial least squares regression (PLSR) methods. The results obtained by the tested methods were similar. CCR-SD models showed high predictive capacity with coefficients of determination (R^2) in the range of 0.80–0.86 and 0.70–0.87 for calibration and validation data sets, respectively, and the highest R^2 value was attained in the SOM estimation. Moreover, the CCR-SD models stand out for the superior accuracy–parsimony relationship: the number of predictors varied from 16 (silt models) to 49 (SOM models). On average, the CCR-SD calibrations needed less than a half of the predictors employed in PLSR models. This research confirmed that CCR-SD can be used for monitoring SOM content and texture of soils from visible–near infrared–shortwave infrared spectra in the study area and, probably, in other areas of land use/land cover change and that CCR-SD can create highly parsimonious models that achieve results comparable with the commonly used PLSR method.

KEYWORDS

correlated components regression, land cover change, soil organic matter, soil texture, VIS–NIR–SWIR spectroscopy

1 | INTRODUCTION

Deterioration of soil conditions closely related to land use and land cover (LULC) changes is a threat to human well-being (Lal & Stewart, 2010; Pimentel, 2006). The scope and environmental effects of LULC

changes caused by natural and human factors vary in space and time (García-Ruiz, 2010; Lu, Li, Valladares, & Batistella, 2004). In Mediterranean ecosystems, regular wildfires, which can trigger soil erosion (Cerdà & Robichaud, 2009), have contributed to landscape formation for several centuries (Pausas, Llovet, Rodrigo, & Vallejo, 2009),

whereas the spread of cropland abandonment in the region is an example of a more recent LULC phenomenon linked to the soil conditions (Nadal-Romero, Cammeraat, Pérez-Cardiel, & Lasanta, 2016).

The urgent need for action to reduce soil degradation is recognized in several sustainable development goals (SDGs) formulated in the United Nations 2030 Agenda for Sustainable Development (United Nations, 2015). The SDG 15.3 is specifically dedicated to land degradation and mentions the restoration of degraded land and soil and the achievement of a land degradation-neutral world. To evaluate the movement towards SDGs, it is necessary to establish, register, and compare relevant soil characteristics (Montanarella & Panagos, 2018). Moreover, in spite of the seriousness of the problem, our knowledge on soil degradation and the scope and effects of mitigation strategies are incomplete (Assessment, 2005). Thus, monitoring the soil status on a regular basis is imperative (Tóth, Hermann, da Silva, & Montanarella, 2018), especially in areas of natural and anthropogenic disturbances, such as Mediterranean (Merino, Moreno, Navarro, & Gallardo, 2016). Examples of successful systems for monitoring soil variables (including soil organic content (SOC) and texture) at a regional level exist in Europe (soil monitoring network in Slovakia; Kobza, 2015) and Australia (New South Wales Monitoring, Evaluation, and Reporting Programme; Chapman et al., 2011).

The soil status can be evaluated through a set of soil attributes/indicators. According to a published review (Bünemann et al., 2018), a minimum set of soil attributes/indicators should include chemical, physical and biological indicators. A large number of studies reviewed by Bünemann et al. (2018) include soil organic matter (SOM) and texture among the most important indicators of soil quality. SOM, which is one of the main sources of soil carbon and plant nutrients, determines soil fertility and plays an important role in both water cycle (infiltration and runoff) and quality (Tóth et al., 2018). On the other hand, land productivity is directly impacted by soil erosion (Troeh & Thompson, 2005), with texture being one of the basic indicators of soil erodibility (Goldman, Bursztynsky, & Jackson, 1986) and other hydraulic properties (Tóth et al., 2018).

Conventional methods for the estimation of soil properties require important investments of time and effort, which motivate the search for alternatives. Spectral sensing methods, such as visible (VIS)-near infrared (NIR)-shortwave infrared (SWIR) spectroscopy, may be one of the time and cost-effective solutions (Dematté et al., 2016). Based on results of previous research, which demonstrated that soil characteristics correlate with their spectral signatures (Dematté & da Silva Terra, 2014; Stevens, Nocita, Tóth, Montanarella, & van Wesemael, 2013), this technique uses electromagnetic spectra in VIS, NIR, and SWIR spectral regions to estimate soil properties. Because soil spectra are obtained by sensors located near (<2 m) the soil surface, this method is sometimes referred to as proximal sensing.

Spectroradiometers produce more accurate results than satellite and airborne instruments because of the high-resolution spectra (contain >2,000 of narrow [up to 1 nm] bands) obtained in controlled environmental conditions (Ben-Dor & Dematté, 2016). Soil VIS-NIR-SWIR spectra have been successfully applied to estimate soil carbon, SOM, and texture (Conforti, Matteucci, & Buttafuoco, 2018; Lugassi, Ben-Dor, & Eshel, 2014; Mouazen, Karoui, De

Baerdemaeker, & Ramon, 2005). High-resolution spectra of soil surface samples obtained under laboratory conditions serve as a standard in spectral unmixing of remote sensing images acquired by sensors on airborne and satellite platforms and are used for digital mapping of soils and other environmental variables (Ben-Dor & Dematté, 2016; Dematté et al., 2016).

Because soils are mixtures of organic and inorganic particles with highly variable proportions of each substance and particle size, their spectra present overlaps of spectral features corresponding to specific soil constituents (Ben-Dor & Dematté, 2016). Soil variables are not directly calculated from the spectra; instead, they are related to a set of known reference samples representative of the soil variation in the study area through the development of multivariate statistical models. Models calibrated for a certain area are not usually transferable to another area (Grunwald, Thompson, & Boettinger, 2011).

Extracting information from a large number of highly correlated spectral bands is a challenging task. There is a wide range of statistical tools available for multivariate modelling of soil properties. Ongoing research is continuously evaluating new tools at the same time striving to clarify the viability of application of VIS-NIR-SWIR soil spectroscopy in specific scenarios (e.g., Gholizadeh, Saberioon, Carmon, Boruvka, & Ben-Dor, 2018; Ogen, Neumann, Chabrilat, Goldshleger, & Ben-Dor, 2018; Ostovari et al., 2018; Terra, Dematté, & Viscarra Rossel, 2018; Viscarra Rossel & Brus, 2018).

Methods based on linear models, especially partial least squares regression (PLSR), are among the most popular (Mouazen, Kuang, De Baerdemaeker, & Ramon, 2010; Vasques, Dematté, Viscarra Rossel, Ramírez-López, & Terra, 2014; Viscarra Rossel, McGlynn, & McBratney, 2006), although latest comparative studies report on successful applications of data mining techniques and tools, such as artificial neural networks (Mouazen et al., 2010), support vector machines (Viscarra Rossel & Behrens, 2010), and memory-based learning (Gholizadeh, Borůvka, Saberioon, & Vašát, 2016).

The frequent choice of PLSR is explained by its capacity to produce well-fit models from data sets containing a small number of observations characterised by a great number of correlated predictors. Robustness of the models is mainly achieved through reduction of data dimensionality using a set of orthogonal vectors (components) (Wold, Sjöström, & Eriksson, 2001). Still, PLSR models sometimes demonstrate unrealistically high fit due to inclusion of noise variables relevant only for calibration dataset, which is known as overfitting (Babyak, 2004; Esbensen, Guyot, Westad, & Houmoller, 2002).

A recently introduced method of correlated components regression (CCR) is trying to avoid overfitting problem in a different way. It prevents model over fit through application of the regularisation process, which involves identification of suppressors and elimination of less relevant predictors (Magidson, 2013). Because of development, CCR has been successfully applied to very diverse research areas, such as socio-demography (Alkerwi, Vernier, Sauvageot, Crichton, & Elias, 2015), medicine (Ruiz-Rodado et al., 2014), and logistics research (Garver & Williams, 2018). However, CCR was not used in soil spectroscopic modelling until now, even though the characteristics of CCR are very attractive.

In this context, the study seeks to contribute to the search and assessment of the methods more adequate for modelling soil properties from spectral data in specific scenarios and answer the following research questions: (a) is it possible to predict SOM content and texture fractions of soils from wildfire burns and cropland abandonment in Mediterranean environment from VIS-NIR-SWIR spectra using CCR? and (b) what are the advantages of using CCR in simultaneous modelling SOM and soil texture compared to two versions of PLSR? This allows formulating the corresponding research hypotheses: (a) CCR is an adequate tool for monitoring SOM and texture of soils in areas of LULC changes, and (b) CCR offers several advantages in simultaneous modelling soil texture and SOM compared with PLSR.

2 | METHODOLOGY

2.1 | Study area and soil sampling

The study area of approximately 310 km² (Figure 1) is located in the Aragón region, Northern Spain (42°10'-42°37'N, 0°16'-1°17'W), and contains sites affected by (a) wildfire burns and (b) cropland abandonment. The area of uneven topography (elevations between 450 and 1,300 m) is characterised by a Mediterranean climate with a mean annual temperature of approximately 10°C and a precipitation range of 600–800 mm (Cuadrat & Martín-Vide, 2007).

The mosaic of vegetation covers in the study area is composed of plant communities dominated by *Quercus* gr. *Cerrioides* (Willk and

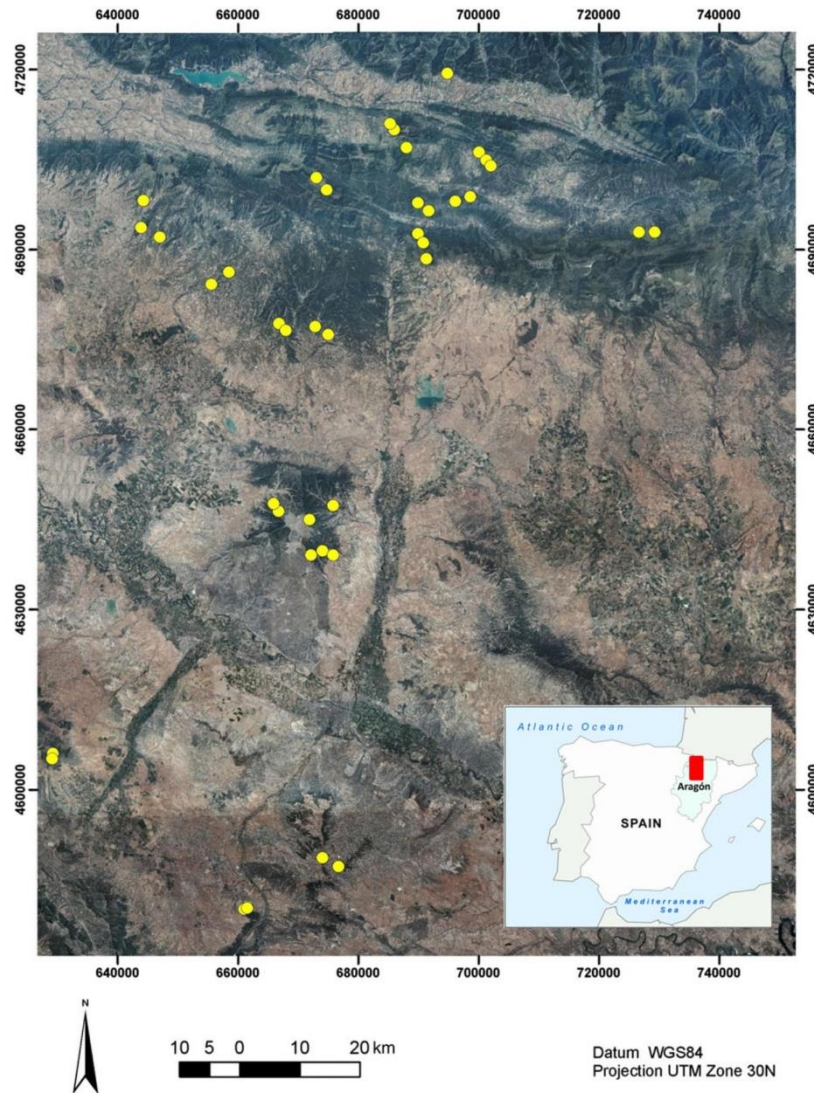


FIGURE 1 Location of the study area and sampling sites [Colour figure can be viewed at wileyonlinelibrary.com]

Costa) and *Quercus ilex* L. and pine forests of *Pinus sylvestris* L., *Pinus nigra* (Arnold), *Pinus halepensis* L., and *Pinus pinaster* (Aiton) interspersed with shrublands dominated by *Buxus sempervirens* L. and *Genista scorpius* L. (Ruiz de la Torre, 1990). In areas affected by wildfires, typical soils that formed on calcaric materials have coarse and medium textures and are classified as Cambisols, and there are some patches of Regosols and Leptosols (Badía-Villas & del Moral, 2016). On the other hand, in areas previously used for agriculture, thin soils with silt loam texture are classified as Leptic Calcaric Regosols (FAO, 2015).

A total of 113 soil samples were collected from the surface soil layer (0–10 cm) during the 2013 and 2014 field campaigns. Approximately two thirds of the samples (82) were from wildfire burns that occurred during 1975–2009. The sample site locations were determined by the spatial pattern of the burned areas throughout that period. Wildfire perimeters were identified using databases of the Aragón Government (Service for Management of Wildfires and Coordination, Head Office for Forest Management), as well as mapping products produced in the context of the research project “Forest fires and predictive models of ecologic vulnerability to fire: restoration management activities and application of climate change scenarios” GA-LC-042/2011 (Caixa-DGA). Within the wildfire boundaries, the precise location of the samples is a function of accessibility factors, plant-community variability in the context of Aragón and wildfire size. In the absence of prefire soil data, a paired-sample approach (Novara, La Mantia, Barbera, & Gristina, 2012) was applied; at each of the 41 selected sites, a pair of samples was obtained—one sample of the burned soil and a reference sample of the same/similar unburned soil. The unburned soils are located in areas near the outer perimeter of the burned lands that have not been affected by fire, which are representative of large areas with similar physical conditions. The SOM content in these samples was estimated with UV–VIS spectrophotometry. The soil texture, ie, the relative proportion of sand, silt, and clay (%) in the dry and sieved (<2 mm) samples, was determined using the standard particle size-distribution analysis (USDA, 1996).

Samples of soils affected by cropland abandonment (31) were collected in the Araguás catchment, where cultivation of terraced fields stopped in the 1950s. Subsequent afforestation with *P. nigra* and *P. sylvestris* occurred a decade later, although some areas underwent a process of natural secondary succession with *Genista scorpius* and *Buxus sempervirens*. Sampling was carried out at sites with five different landcovers typical for the area (bare soil, permanent pasturelands, secondary succession, afforestation with *P. sylvestris* and *P. nigra*) selected based on the analysis of aerial photography, topographic maps, and field survey information. The samples were obtained from five 5 m × 5 m plots with a similar topography established at each site. After collecting five surface (0–10 cm) samples from locations at each

of the plot diagonals, they were combined into one sample. For these samples, the loss on ignition method was used to determine SOM; soil texture fractions were determined using a particle analyser (Micromeritics, SediGraph 5100, Nocrross, USA). Descriptive statistics characterizing the collected samples are presented in Table 1.

Additional details on the study area, as well as the sampling procedure, are available in the studies of Rosero-Vlasova, Pérez-Cabello, Montorio Llovería, & Vlassova (2016; (wildfire burns) and Nadal-Romero et al. (2016; abandoned croplands).

2.2 | Soil spectra

For spectral measurements, the fine soil fraction (particle size <2 mm) of each sample was placed in a Petri dish (90 mm in diameter) and dried in an oven at 105°C for 24 hr.

Soil spectral curves were obtained using an analytical spectral device (ASD) FieldSpec@4spectroradiometer (Analytical Spectral Devices Inc., Boulder, CO, USA) under controlled laboratory conditions, with a setup that included an ASD illuminator lamp (Analytical Spectral Devices Inc., Boulder, CO, USA) and a pistol grip (Rosero-Vlasova et al., 2016). Figure 2 shows the general view and details of observations geometry. The soil sample area detected by the optic fibre cable (sensor) is determined by the following geometry: an illuminator lamp (field of view [FOV]: $\theta = 12^\circ$) is attached to the tripod in a central position at a height of $H = 42$ cm generating a lighted spot 8.82 cm in diameter (D). The setup also includes a pistol grip attached to another tripod at a height of $h = 7.5$ cm ($FOV_{\text{Bare Fibre}} \beta = 25^\circ$, diameter SPOT $d = 6.99$ cm) and an angle $\alpha = 25^\circ$ relative to the vertical axis (Figure 2a). The spectral response of the white reference panel was obtained with the same viewing geometry (Figure 2b).

Radiances measured in the VIS–NIR (350–1000 nm) and two SWIR regions (1,001–1,800 and 1,801–2,500 nm; Castro-Esau, Sanchez-Azofeifa, & Rivard, 2006) were corrected for the baseline electrical signal (dark current) and converted into reflectance values using a calibrated white Spectralon panel as a reference. The ASD illuminator halogen lamp was employed as a light source. Previous research (Rosero-Vlasova et al., 2016) has demonstrated that this experimental setup ensures an optimal observation environment resulting in low-noise spectra.

Radiometric jumps, evident at the wavelengths situated at the joins between the detectors (at 1,000 and 1,800 nm), were corrected using a procedure suggested in the study of Danner, Locherer, Hank, & Richter (2015), which compensates the difference between the reflectance using the values of the first detector (VIS range) as a baseline. The following formulas were applied:

TABLE 1 Descriptive statistics for soil organic matter content (g 100 g⁻¹) and clay, silt, and sand (%) in collected soil samples

Soil properties	n	Min	Max	Median	Mean	SD
SOM (g 100 g ⁻¹)	113	1.04	23.40	5.80	6.59	3.68
Clay (%)	113	9.21	48.04	27.28	27.14	8.09
Silt (%)	113	22.18	66.19	41.48	40.23	10.26
Sand (%)	113	5.41	66.37	32.16	32.64	14.57

Note. n: number of samples; Min: minimum; Max: maximum; SD: standard deviation; SOM: solid organic matter.

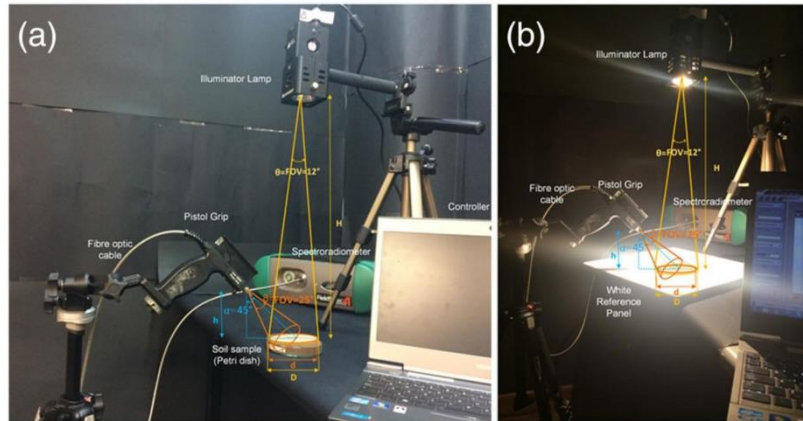


FIGURE 2 Experimental setup: (a) general view and (b) view during spectral measurements (optimization process) [Colour figure can be viewed at wileyonlinelibrary.com]

$$\text{Corr_val}_{1000} = R_{\lambda=1001} - (2 \cdot R_{\lambda=1000} - R_{\lambda=999}), \quad (1)$$

$$\text{Corr_val}_{1800} = R_{\lambda=1801} - (2 \cdot R_{\lambda=1800} - R_{\lambda=1799}), \quad (2)$$

where R_{λ} is the reflectance at λ wavelength and Corr_val_{1000} and Corr_val_{1800} are correction values at the spectral splitting points, which are added to the original values and, depending on their algebraic sign, either increase or decrease reflectances in all further wavelengths.

Moreover, the noisy bands at the extremes of the spectra (<400 and >2470 nm) were removed, leaving 2,071 bands for statistical modelling.

2.3 | Statistical modelling

Modelling of SOM content and texture fractions is based on 70 preselected spectral bands (11 bands in VIS, 18 bands in NIR, and 48 bands in SWIR spectral regions). The importance of this set of wavelengths for soil property detection was previously reported in multiple studies (Ben-Dor, Heller, & Chudnovsky, 2008; Dematté et al., 2016; Dematté & da Silva Terra, 2014; Melendez-Pastor, Navarro-Pedreño, Gómez, & Koch, 2008; Rosero-Vlasova, Borini Alves, Vlassova, Perez-Cabello, & Montorio Llovería, 2017).

The presence of outliers in scaled and centred data sets was assessed with principal components analysis. Three data points lying outside the 95% confidence level Hotelling's T^2 ellipse in the score plot representing the loadings of the two first principal components (Figure 3) were excluded as outliers, leaving 110 soil spectra for analysis. These were randomly divided into calibration (~65%) and validation (~35%) sets, containing 80 and 30 samples, respectively. To ensure robust results, this procedure was repeated three times to obtain three sample sets of calibration and validation data (S1, S2, and S3). Descriptive statistics of the data used in model building are presented in Table 2 and Figure 4. Because each data set contains more than 30 samples, the Kolmogorov-Smirnov test with Lilliefors significance

correction was applied to test the SOM, silt, clay, and sand distributions for normality; one-way ANOVA was run to detect significant differences between the distributions of the tested variables in S1, S2, and S3. All the tests were performed using IBM SPSS Statistics version 20.0.0 (2011) software (<https://www.ibm.com/products/spss-statistics>).

Statistical models were developed using (a) a routinely applied (Dematté et al., 2016) full-spectrum PLSR (PLSR-full; Wold et al., 2001) implemented in The Unscrambler X software (2016; CAMO Software AS, Norway, 2016), version 10.4 (<https://www.camo.com/unscrambler>); (b) PLSR with predictors selected by Martens uncertainty test (Martens & Martens, 2000) available in The Unscrambler X software (2016) version 10.4 (PLSR-MUT), and (c) a novel technique of CCR with a step-down variable selection algorithm (CCR-SD; Magidson, 2010; Magidson, 2013) implemented as an XLSTAT Pearson Edition (2014; Addinsoft S.A., New York, NY, USA, 2014), version 2014.5.03 (<http://www.xlstat.com>) complement for the Microsoft Office Excel (2010) software. For each sample, all the soil properties of interest in our study (SOM, clay, silt, and sand) were predicted simultaneously.

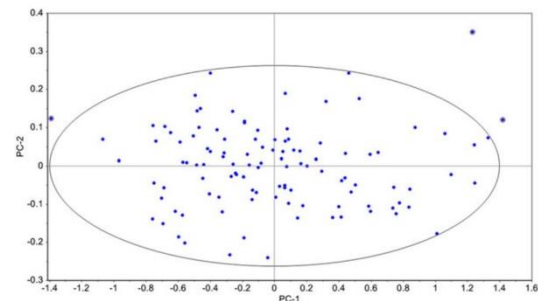


FIGURE 3 Score plot from principal components analysis showing PC1 versus PC2: Hotelling's T^2 ellipse (95% confidence level) for outlier detection [Colour figure can be viewed at wileyonlinelibrary.com]

TABLE 2 Descriptive statistics for soil organic matter content (g 100 g⁻¹), clay, silt, and sand (%) in three calibration and prediction sample sets (S1, S2, and S3)

Soil properties	Sample set	CALIBRATION							VALIDATION								
		n	Min	Max	Mean	SD	Q25	Q75	Skewness (Pearson)	n	Min	Max	Mean	SD	Q25	Q75	Skewness (Pearson)
SOM (g 100 g ⁻¹)	S1	80	1.04	20.74	6.28	3.45	4.08	6.69	1.79	30	2.59	23.40	7.46	4.30	4.86	9.72	1.78
	S2	80	1.04	20.74	6.53	3.49	4.34	8.00	1.55	30	2.46	23.40	6.81	4.33	4.20	7.99	2.17
	S3	80	1.04	23.40	6.35	3.52	4.25	7.73	2.35	30	1.77	19.02	7.27	4.19	4.52	10.32	0.93
Clay (%)	S1	80	9.82	48.04	27.33	8.32	29.63	42.28	0.22	30	9.21	43.77	26.72	7.86	32.45	47.57	-0.08
	S2	80	9.21	48.04	26.59	8.38	31.70	47.77	0.21	30	11.18	46.78	28.69	7.49	35.15	46.27	-0.12
	S3	80	9.21	48.04	27.34	8.39	32.36	47.21	0.15	30	11.18	43.00	26.70	7.66	32.45	47.47	0.10
Silt (%)	S1	80	22.46	66.19	40.44	10.30	19.86	29.77	0.40	30	23.66	55.89	40.21	10.30	22.90	30.53	-0.16
	S2	80	22.46	66.19	40.15	10.70	21.25	30.48	0.31	30	24.68	57.91	40.99	9.08	23.80	31.83	0.34
	S3	80	23.28	66.19	40.36	10.20	21.75	31.74	0.31	30	22.46	61.39	40.43	10.57	22.87	30.71	0.10
Sand (%)	S1	80	5.41	64.22	32.23	14.66	31.43	45.37	0.20	30	10.80	66.37	33.11	14.85	20.75	44.25	0.34
	S2	80	5.41	66.37	33.27	15.25	20.64	44.58	0.14	30	8.80	62.58	30.33	12.92	19.68	39.08	0.46
	S3	80	8.69	66.37	32.32	14.68	20.45	42.11	0.30	30	5.41	62.58	32.87	14.81	20.12	44.25	0.07

Note. S1: sample set 1; S2: sample set 2; S3: sample set 3; n: number of samples; Min: minimum; Max: maximum; Q25: lower quartile; Q75: upper quartile; SD: standard deviation; SOM: solid organic matter.

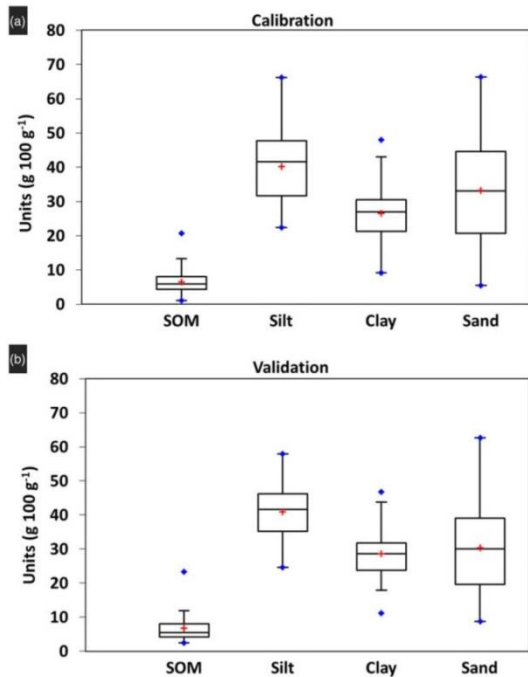


FIGURE 4 Box-whisker plots showing the soil organic matter (SOM), clay, silt, and sand distribution in S2 for the (a) calibration set and (b) validation set. The bottom and top of the box represent the 25th and 75th percentiles. The cross inside the box indicates the mean value. The band near the middle of the box is the median. The whiskers represent the 5th and 95th percentiles. The solid dots correspond to maximum and minimum values [Colour figure can be viewed at wileyonlinelibrary.com]

Both CCR and PLSR are capable of dealing with a large number of highly correlated predictors (in this study, the correlation coefficients R^2 are in the range of 0.639–0.999). Multicollinearity of spectral data

is approached by means of regularisation (the enforcement of model sparsity), consisting in dimension reduction.

PLSR proceeds by calculating a set of orthogonal components (latent variables) that explain most of the variance in predictors and responses (Wold, 2001). Determination of the optimum number of components and selection of the final model is performed through the leave-one-out cross-validation: the model is developed leaving out one of the samples, which is later substituted into the model to evaluate the adjustment; the process is repeated for each sample, and the final model is that showing the best fit.

Because exclusion of the less important (noisy) predictors may improve model accuracy, in the second tested method, PLSR models used only most important variables selected by the Martens uncertainty test (PLSR-MUT), which estimates uncertainty of regression coefficients obtained in leave-one-out cross validation (Martens & Martens, 2000).

On the other hand, in CCR-SD, data dimension is reduced through (a) calculation of correlated components and (b) elimination of less relevant predictors from the model with step-down variable selection algorithm, resulting in sparser models (Magidson, 2013).

CCR utilises $K < P$ correlated components, with each S_k component being an exact linear combination of g predictors ($g = 1, 2, \dots, P$). Predictions for Y in the first (primary) component (\hat{Y}) directly affect the outcome and are obtained from the simple ordinary least squares (OLS) regression of Y on S_1 . Similarly, the second component S_2 is calculated by the simple OLS regression of Y on S_1 and S_2 . The calculation of the remaining components follows the same process. Once the models for all the components are obtained, the final model (Equation 3) is computed using the expression:

$$\hat{Y} = \alpha^{(K)} + \sum_{g=1}^P \beta_g X_g, \quad (3)$$

where α and β are regression coefficients.

Thus, the components are not orthogonal; the second and subsequent components are correlated to the first component and represent the influence of 'suppressor' variables (Magidson & Wassmann,

2010). The inclusion of suppressor variables removes the noise of some irrelevant variables included in the first component, improving the model quality.

At the same time, the method controls overfitting through a reduction in the number of predictors, leaving out the less important predictors. Thus, CCR was combined with a step-down variable selection algorithm, which excludes the least important predictors (Bennett, 2013; Magidson, 2010). This is achieved through M-fold cross-validation. Each round (10 rounds in this study) consists of a series of operations. First, the data are randomly divided into M groups (folds) of equal size (5 groups of $80/5 = 16$ samples each in our study). Next, samples from four groups are used to build the model, while the samples from the fifth group are used for model validation. The process is run for each group (M times). In the next round, the process is repeated with newly randomised M groups. Thus, the quality of the final model is assessed on the out-of-sample fit, ensuring replication of the calibration results on real-life data, which has been a long-time concern related to published models (Nuzzo, 2014). Model assessment based on new out-of-sample cases means that modelling with CCR does not pose requirements to satisfy sampling assumptions, which are the basis of traditional hypothesis testing (Curl, Thompson, & Aspinall, 2015).

2.4 | Model performance assessment

Model performance was evaluated using the coefficient of determination R^2 (Equation 4), which measures how successful the calibration fit is in explaining the variation in the data, root mean square error of calibration (Equation 5) and root mean square error of cross-validation (Equation 6), which assess the model accuracy.

$$R^2 = 1 - \frac{\sum_{i=1}^n (Y_i - \hat{Y}_i)^2}{\sum_{i=1}^n (Y_i - \bar{Y})^2}, \quad (4)$$

$$RMSEC = \sqrt{\frac{\sum_{i=1}^{n_c} (Y_{i,c} - \hat{Y}_{i,c})^2}{n_c - (f + 1)}}, \quad (5)$$

$$RMSECV = \sqrt{\frac{\sum_{i=1}^{n_c} (Y_{i,c} - \hat{Y}_{i,c})^2}{n_c - 1}}, \quad (6)$$

where n is the number of samples, subscript c and p refer to calibration and validation datasets; Y_i is the measured value for sample i , \hat{Y}_i is the predicted value for sample i , \bar{Y} is the mean value, and f is the number of variables used in the regression equation. The predictive ability of the models was also evaluated with the root mean square error of prediction (RMSEP; Equation 7), with bias of validation ($bias_{val}$) and standard error of prediction (SEP_c) being independent components of RMSEP (Rosero-Vlasova et al., 2016; Stevens et al., 2013); and the ratio of performance to interquartile (RPIQ) range (Bellon-Maurel & McBratney, 2011), which was calculated according to Equation 8.

$$RMSEP = \sqrt{\frac{\sum_{i=1}^{n_p} (Y_{i,p} - \hat{Y}_{i,p})^2}{n_p}}, \quad (7)$$

$$RPIQ = \frac{Q_3 - Q_1}{RMSEP}, \quad (8)$$

RPIQ is based on inter-quartile distances ($IQ = Q_3 - Q_1$), where Q_1 represents the lowest 25% of the samples and Q_3 is the value below which 75% of the samples can be found. RPIQ is the ratio of IQ to the $RMSEP$ and adequately represents populations with skewed distributions and a large number of low values, such as the soil sample sets in this study. Finally, the Akaike information criterion (AIC), computed following Equation 9, was applied to determine the model with the best accuracy-parsimony relationship (Akaike, 1973; Viscarra Rossel & Behrens, 2010).

$$AIC = n \ln RMSEP + 2f, \quad (9)$$

where n is the number of samples and f is the number of predictors. The smaller the AIC criterion is, the better the model.

3 | RESULTS AND DISCUSSION

3.1 | SOM content and texture fractions

Table 2 and Figure 4 present descriptive statistics for the SOM and soil texture fractions (clay, silt, and sand) of the used data sets. ANOVA detected no statistically significant differences among S1, S2, and S3 ($p < 0.05$).

The SOM content ranges between ~ 1 –100 g and ~ 20 –100 g, and the mean is ~ 6 –100 g, demonstrating levels characteristic of the study area (Pérez-Cabello, Echeverría, Ibarra, & Riva, 2009). These values are higher than the average values registered in global (Brown, Shepherd, Walsh, Mays, & Reinsch, 2006) and European (Stevens et al., 2013) soil databases, which is rather surprising given that approximately one third of the samples is from the burned areas. However, the unusually high SOM content in samples of burned soils may be due to vigorous vegetation development in the burned areas, which may have contributed to accelerated recovery of organic material destroyed by the fire (Jiménez-González et al., 2016; Vlassova & Pérez-Cabello, 2016).

The soil texture fraction values are highly variable, especially for sand (Table 2 and Figure 5): The values change from approximately 5% to close to 65%, which is not strange considering the landscape heterogeneity in the study area. However, samples from different land covers in the cropland abandonment areas show similar textures dominated by silt, confirming the findings by Laudicina et al. (2012), who observed that land use change did not affect soil texture. Thus, the variability in the soil texture of the analysed set is caused by the contribution of soils from wildfire burns. In general, the clay content in sampled soils is higher (mean 27%), and the sand proportion is lower (mean 33%) than the average for European soils in the LUCAS database (Stevens et al., 2013).

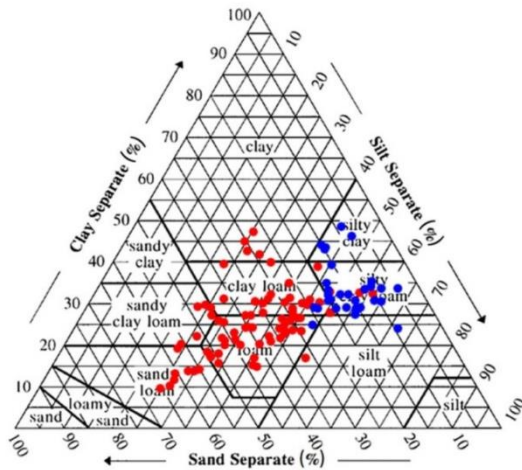


FIGURE 5 A soil texture triangle (USDA, 2010) showing the soil textures as determined by the proportion of sand, silt, and clay. The red points represent soil samples from areas affected by wildfires, and the blue points represent soil samples from areas of crop abandonment [Colour figure can be viewed at wileyonlinelibrary.com]

3.2 | Soil spectra

Spectral curves of the analysed soils are presented in Figure 6a, b (wildfire burns) and Figure 6c, d (abandoned croplands). Their form is typical for soil reflectance spectra: a gradual increase

through the VIS wave range, an almost flat segment in NIR, and slightly lower reflectance values in SWIR (Ben-Dor, Irons, & Epema, 1999). The small number of absorbance features can be ascribed to the presence of water (1,400 and 1,900 nm) and clay minerals (2200 nm; Brown, 2007; Brunet, Barthès, Chotte, & Feller, 2007).

The soil spectra differ mainly in reflectance intensity, confirming the results of previous research (Bellon-Maurel, Fernandez-Ahumada, Palagos, Roger, & McBratney, 2010; Chabrilat, Ben-Dor, Viscarra-Rossel, & Demattè, 2013; Demattè, Campos, Alves, Fiorio, & Nanni, 2004; Stenberg, Viscarra Rossel, Mouazen, & Wetterlind, 2010). Thus, the maximum reflectance values of soils from wildfire burns range from 0.25 to 0.65, whereas the maximum reflectance values of soil samples from cropland abandonment areas are considerably smaller (0.38–0.55). This finding can be explained by differences in organic matter and texture: high SOM contents and smaller particle size result in spectral curves with lower reflectance (Ben-Dor et al., 2009; Conforti, Froio, Matteucci, & Buttafuoco, 2015; Viscarra Rossel, Walvoort, McBratney, Janik, & Skjemstad, 2006). The high variability in the soil spectra from wildfire burns is caused by the inclusion of undisturbed forest soil samples with organic matter content higher than that of any of the soils from crop abandonment, as well as burned soils, whose organic matter was completely destroyed by fire (Figure 6b).

Shape is another key for the differentiation of soils through visual inspection. Thus, the shape of the bare soil spectrum in Figure 6d is quite different from the rest of the spectra: convex in the 500–600 nm wave range and almost horizontal in the NIR and part of the SWIR spectral regions, which is typical for weathered soils (Demattè, 2002).

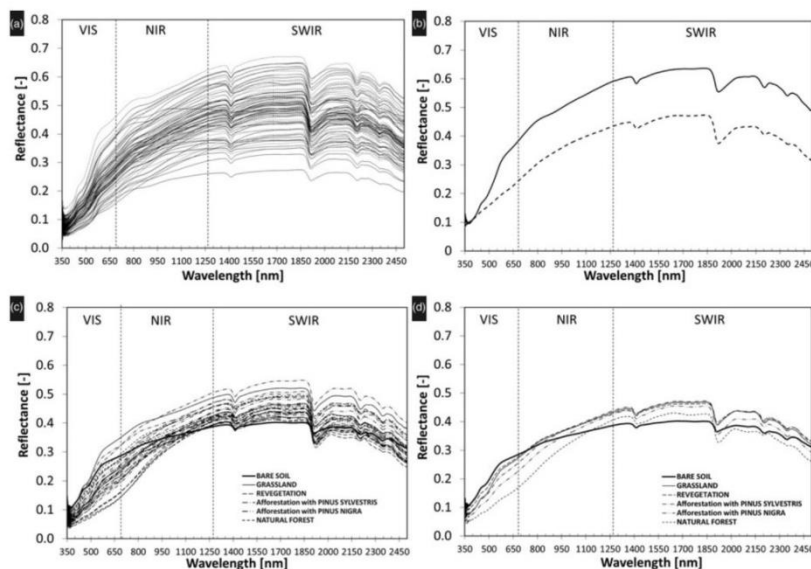


FIGURE 6 Spectra of soils from wildfire burns: (a) all the spectra and (b) spectra of the burned (dotted line) and unburned (dashed line) soil samples. Spectra of soils from agricultural abandonment areas: (c) all the spectra and (d) average spectra of soils from areas with different land use types after crop abandonment

3.3 | Statistical modelling

The results of simultaneous statistical modelling of SOM, clay, silt, and sand from reflectance spectra using the two versions of PLSR (PLSR-full and PLSR-MUT) and CCR-SD methods are presented in Table 3 (model calibration) and Table 4 (model validation).

The values correspond to three data sets (S1, S2, and S3), resulting from different random partitions of available samples in the calibration (80 samples) and validation (30 samples) groups. In each case, the final model was obtained after 100 iterations/rounds.

The optimal number of components is similar for all the models: 9–10 for PLSR-full and 8–10 for other methods (PLSR-MUT and CCR-SD); fewer components used in PLSR-MUT and CCR-SD models for SOM. The number of predictors is more variable. Because standard PLS regression (PLSR-full) does not discard any predictor, these models include the full range of available bands (2,071). In case of PLSR-MUT and CCR-SD models resulting from procedures eliminating less relevant predictors, the number of predictors varies

a lot depending on the predicted property and sample dataset. In PLSR-MUT models the number of predictors varies from one dataset to another, but it is the same for all the modelled properties (171, 39, and 197 for S1, S2, and S3, respectively), while in CCR-SD the number of predictors depends not only on the data set but also on the modelled property (e.g., there are 49, 28, 19, and 22 predictors in S1 models for SOM, clay, silt, and sand, respectively). It is worth to note, that variable selection in PLSR is realised after running the full spectrum model necessary to estimate importance of the variables, whereas in CCR-SD method, estimation of variable relevance and development of the final model are performed simultaneously.

In general, the number of predictors in CCR-SD models is greater for SOM (49, 61, 58 for S1, S2, and S3, respectively) because organic compounds exhibit spectral activity along the whole spectrum, although proportion of specific organic constituents in SOM varies a lot depending, among other factors, on overall SOM concentration and geological heterogeneity of the area (Stenberg et al., 2010). The number of predictors is decreasing in CCR-SD models

TABLE 3 Calibration and cross-validation results of soil organic matter, clay, silt, and sand modelling (80 samples) obtained with CCR-SD, PLSR-full, and PLSR-MUT

Soil Properties	Sample set	Statistic	Factors	f	R^2_c	RMSEC (g 100 g ⁻¹)	R^2_{cv}	RMSECV (g 100 g ⁻¹)
SOM	S1	CCR-SD	8	49	0.86	2.11	0.77	1.30
		PLSR-full	10	2,071	0.81	1.49	0.73	1.82
		PLSR-MUT	9	171	0.82	1.46	0.76	1.70
	S2	CCR-SD	8	61	0.86	2.75	0.78	1.31
		PLSR-full	9	2,071	0.81	1.51	0.72	1.86
		PLSR-MUT	8	39	0.79	1.60	0.73	1.82
	S3	CCR-SD	8	58	0.85	2.62	0.77	1.35
		PLSR-full	10	2,071	0.85	1.37	0.78	1.65
		PLSR-MUT	9	197	0.82	1.46	0.75	1.77
CLAY	S1	CCR-SD	10	28	0.80	4.68	0.67	3.76
		PLSR-full	10	2,071	0.73	4.32	0.58	5.41
		PLSR-MUT	9	171	0.64	4.96	0.51	5.86
	S2	CCR-SD	10	21	0.83	4.02	0.60	3.45
		PLSR-full	9	2,071	0.64	5.01	0.46	6.22
		PLSR-MUT	8	39	0.61	5.18	0.49	6.04
	S3	CCR-SD	10	29	0.83	4.32	0.67	3.44
		PLSR-full	10	2,071	0.69	4.63	0.54	5.76
		PLSR-MUT	9	197	0.67	4.81	0.53	5.79
SILT	S1	CCR-SD	10	19	0.86	4.39	0.75	3.83
		PLSR-full	10	2,071	0.83	4.23	0.73	5.42
		PLSR-MUT	9	171	0.80	4.52	0.73	5.36
	S2	CCR-SD	10	16	0.84	4.78	0.70	4.27
		PLSR-full	9	2,071	0.81	4.67	0.64	6.43
		PLSR-MUT	8	39	0.62	6.58	0.40	8.32
	S3	CCR-SD	10	58	0.86	7.40	0.72	3.82
		PLSR-full	10	2,071	0.78	4.66	0.62	6.32
		PLSR-MUT	9	197	0.75	5.10	0.52	6.32
SAND	S1	CCR-SD	10	22	0.84	6.90	0.71	5.86
		PLSR-full	10	2,071	0.86	5.46	0.76	7.23
		PLSR-MUT	9	171	0.78	6.87	0.70	8.11
	S2	CCR-SD	8	32	0.75	9.89	0.61	7.63
		PLSR-full	9	2,071	0.81	6.68	0.63	9.32
		PLSR-MUT	8	39	0.65	9.00	0.47	11.20
	S3	CCR-SD	10	70	0.79	19.81	0.61	6.69
		PLSR-full	10	2,071	0.81	6.40	0.65	8.78
		PLSR-MUT	9	197	0.79	6.64	0.67	8.52

Note. CCR-SD: correlated components regression with a step-down variable selection algorithm; PLSR-full: full-spectrum partial least squares regression; PLSR-MUT: partial least squares regression Martens uncertainty test; R^2_c : coefficient of determination for calibration; R^2_{cv} : coefficient of determination for cross-validation; RMSEC: root mean square error of calibration; RMSECV: root mean square error of cross-validation; S1: sample set 1; S2: sample set 2; S3: sample set 3; f : number of variables used in the regression equation. The presented values are averages for 100 rounds.

TABLE 4 Validation results for soil organic matter, clay, silt, and sand modelling (30 samples) obtained with CCR-SD, PLSR-full, and PLSR-MUT

Soil Properties	Sample set	Statistic	R^2_V	RMSEP (g 100 g ⁻¹)	SEP _c (g 100 g ⁻¹)	bias _{val} (g 100 g ⁻¹)	RPIQ	AIC
SOM	S1	CCR-SD	0.87	1.55	1.53	0.36	3.14	111.13
		PLSR-full	0.88	1.59	1.58	-0.33	3.06	4155.91
		PLSR-MUT	0.77	2.04	2.07	0.08	2.38	363.39
	S2	CCR-SD	0.86	1.61	1.64	0.07	2.36	136.30
		PLSR-full	0.82	1.81	1.83	-0.10	2.10	4159.80
		PLSR-MUT	0.76	2.08	2.11	0.03	1.82	99.97
	S3	CCR-SD	0.89	1.89	1.52	1.14	3.08	135.03
		PLSR-full	0.89	1.96	1.55	-1.24	2.96	4162.19
		PLSR-MUT	0.86	2.05	1.75	-1.12	2.93	415.54
CLAY	S1	CCR-SD	0.54	5.98	6.01	-0.95	1.28	109.66
		PLSR-full	0.53	6.91	6.68	2.14	1.10	4199.99
		PLSR-MUT	0.28	7.05	7.15	0.44	1.08	400.59
	S2	CCR-SD	0.71	4.71	4.76	0.52	1.71	88.47
		PLSR-full	0.59	5.18	5.21	-0.75	1.55	4191.34
		PLSR-MUT	0.56	5.34	5.21	-1.49	1.50	128.26
	S3	CCR-SD	0.73	4.47	4.47	0.83	1.75	102.94
		PLSR-full	0.55	5.80	5.69	-1.54	1.35	4194.74
		PLSR-MUT	0.57	6.14	5.82	-2.21	1.28	448.44
SILT	S1	CCR-SD	0.70	7.08	6.68	2.65	2.14	96.73
		PLSR-full	0.74	6.30	5.63	-3.02	2.40	4197.22
		PLSR-MUT	0.65	8.48	7.81	-3.60	1.78	406.13
	S2	CCR-SD	0.72	5.23	5.10	-1.48	2.13	81.63
		PLSR-full	0.80	4.29	4.09	1.51	2.59	4185.69
		PLSR-MUT	0.58	5.87	5.93	0.65	1.90	131.10
	S3	CCR-SD	0.68	6.80	6.60	2.01	2.21	173.49
		PLSR-full	0.80	5.12	5.21	0.09	2.93	4190.99
		PLSR-MUT	0.64	7.09	7.02	-1.62	2.12	452.76
SAND	S1	CCR-SD	0.69	8.76	8.61	-2.25	2.68	109.10
		PLSR-full	0.66	9.37	9.49	0.84	2.51	4209.13
		PLSR-MUT	0.59	11.62	11.38	3.12	2.02	415.58
	S2	CCR-SD	0.71	7.04	7.13	0.66	2.75	122.55
		PLSR-full	0.80	5.92	5.97	-0.75	3.28	4195.35
		PLSR-MUT	0.74	6.59	6.65	0.85	2.94	134.57
	S3	CCR-SD	0.69	9.18	8.75	-3.20	2.63	206.50
		PLSR-full	0.79	7.09	7.06	1.45	3.40	4200.76
		PLSR-MUT	0.71	9.31	8.62	3.84	2.59	460.93

Note. AIC: Akaike information criterion; bias_{val}: bias of validation; CCR-SD: correlated components regression with a step-down variable selection algorithm; PLSR-full: full-spectrum partial least squares regression; PLSR-MUT: partial least squares regression Martens uncertainty test; R^2_V : coefficient of determination for validation; RMSEP: root mean square error of prediction; RPIQ: ratio of performance to interquartile range; SEP_c: standard error of prediction; S1: sample set 1; S2: sample set 2; S3: sample set 3.

for silt and sand, although in these models it varies more from one analysed subset to another. The number of variables in clay models developed using the same method varies the least (21, 28, and 29 predictors for S1, S2, and S3, respectively), which is not strange, because it is the only texture fraction directly associated with minerals having detectable spectral features in VIS-NIR-SWIR (Escribano, Schmid, Chabrilat, Rodríguez-Caballero, & García, 2017), often referred to as clay minerals (for example, kaolinite, and illite).

Examples of the scatter plots for S2 (modelled versus predicted values) are presented in Figure 7. Among modelled properties, SOM calibrations showed the highest predictive capability accounting on average for 86% (CCR-SD) and 82% (PLSR-full and PLSR-MUT) of the variance in the calibration and 87% (PLSR-full and CCR-SD) and 79% (PLSR-MUT) in the validation data sets. The CCR-SD and PLSR-full models for SOM developed in this study are more accurate (R^2 0.05–0.07 higher and the average RPIQ above 3) than the SOM models we built previously for soil samples from wildfire burns from the same area using PLSR with the step-down variable selection algorithm (Rosero-Vlasova, Vlassova, Pérez-

Cabello, Montorio, & Nadal-Romero, 2018), which is probably due to the different modelling algorithm and larger calibration data set used in this study. The superior RPIQ of the SOM models (~3 or above) developed with CCR-SD and PLSR-full is another indicator of their high quality. Similar results were previously reported by researchers working on applications of VIS-NIR-SWIR spectroscopy for soil characterisation in other areas of LULC change (Ge, Thomasson, & Sui, 2011; Knadel, Stenberg, Deng, Thomsen, & Greve, 2013).

The CCR-SD models estimating texture fractions also showed good fit, with coefficients of determination in the ranges of 0.84–0.86 (calibration) and 0.68–0.72 (validation) for the silt models and 0.80 (calibration) and 0.70 (validation) for the clay and sand predictions. The coefficients of determination of PLSR silt models were lower and varied considerably among datasets (0.62–0.80). Sand was the only property where CCR-SD models ($R^2_C = 0.79$; $R^2_V = 0.70$) were outperformed by those developed with PLSR-full ($R^2_C = 0.83$; $R^2_V = 0.75$). The most important difference between methods was observed in clay models, where good fit of CCR-SD models contrasted with considerably lower performance of PLSR

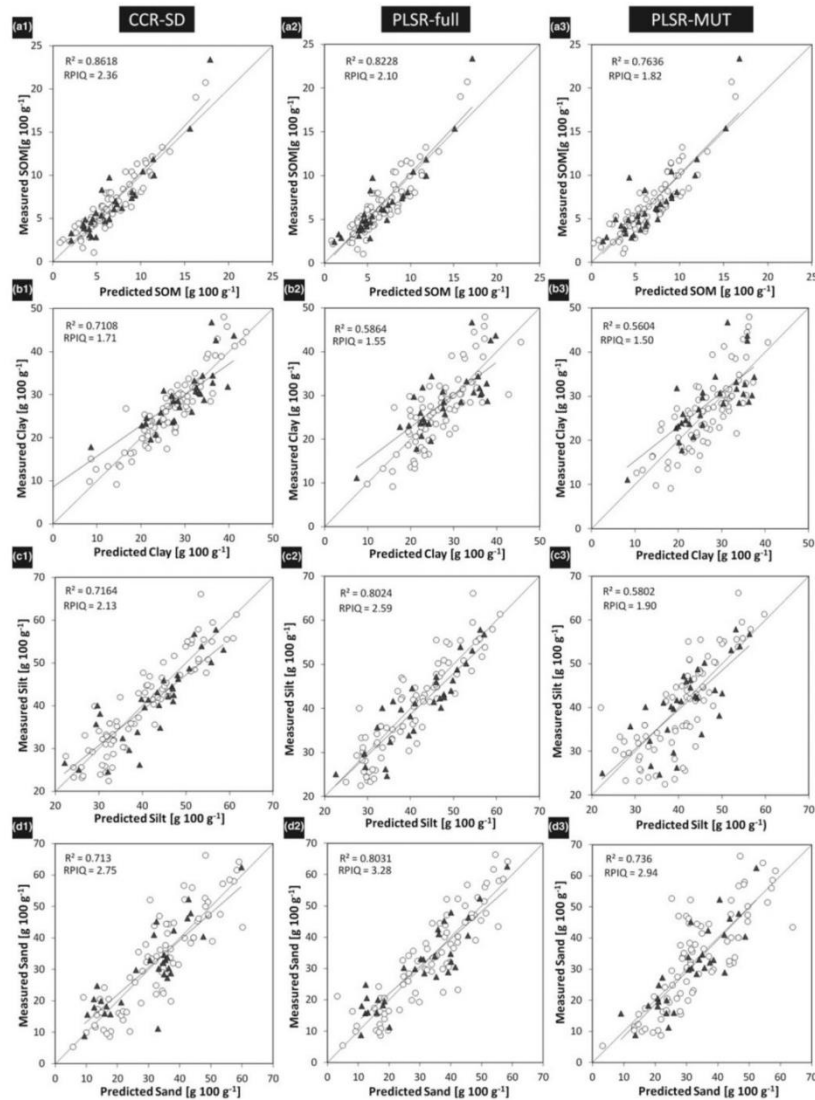


FIGURE 7 Scatter plot examples of predicted versus observed values of soil organic matter (SOM; a), clay (b), silt (c), and sand (d) for S2 for correlated components regression with a step-down variable selection algorithm (CCR-SD), full-spectrum partial least squares regression (PLSR-full), and partial least squares regression Martens uncertainty test (PLSR-MUT) models. In each plot, the data points corresponding to calibration are shown as circles, and the data points corresponding to validation are shown as triangles

calibrations ($R^2_C = 0.69$; $R^2_V = 0.56$ for PLSR-full and $R^2_C = 0.64$; $R^2_V = 0.47$ for PLSR-MUT vss $R^2_C = 0.82$; $R^2_V = 0.66$ for CCR-SD). A better fit of SOM models was previously observed by other researchers (Dematté et al., 2016; Viscarra Rossel, Walvoort, et al., 2006). However, it was rather unexpected that CCR-SD models for clay, silt and sand showed similar performance, albeit not as good as that of the SOM models. Usually clay is another successfully modelled property, but satisfactory fit for silt calibrations is rarely obtained (Pinheiro, Ceddia, Clingensmith, Grunwald, & Vasques, 2017; Stenberg et al., 2010).

On the whole, validation results were similar for all the methods. They compare well to the best achievements in modelling of the same soil characteristics reported in previous research (Conforti et al., 2018; Dematté et al., 2016; Mouazen et al., 2010; Rosero-Vlasova et al., 2017). However, the important difference lies in the structure of the models created by different algorithms evident in the number of predictors in models developed using the three compared methods. The same high quality of PLSR-full models using as predictors 2,071 bands present in the measured reflectance spectra was achieved by CCR-SD using a

greatly reduced number of bands/predictors (49, 21, 16, and 22 for SOM, clay, silt, and sand, respectively). Compared with the PLSR-MUT models, which also implements variable selection mechanism, the CCR-SD produced better results for all the modelled properties and data sets, except slightly better fit at validation of PLSR sand models for of S2 and S3 data sets (Table 4). The accuracy-parsimony relationship estimated by the AIC shows considerable superiority of all the CCR-SD models in this aspect (average AIC = 122.80, Table 4); the lowest (best) AIC values correspond to the CCR-SD models for clay (AIC = 100.35). Average AIC

values for PLSR-full and PLSR-MUT models are 4,186.93 and 327.19, respectively.

Figure 8 presents the coefficients for the CCR-SD model predictors and shows the relative importance of specific bands the studied soil properties. Thus, for analysed soil samples spectral regions closely related to SOM in these models (Figure 8a) include the 500–550, 1000–1050, 1500–1550, 1800–1910, 2200–2250, and 2310–2350 nm wave ranges and can be attributed to the presence of water and organic molecules with C–O, C=O, and N–H bonds (Bellon-Maurel et al., 2010). Although the absorption

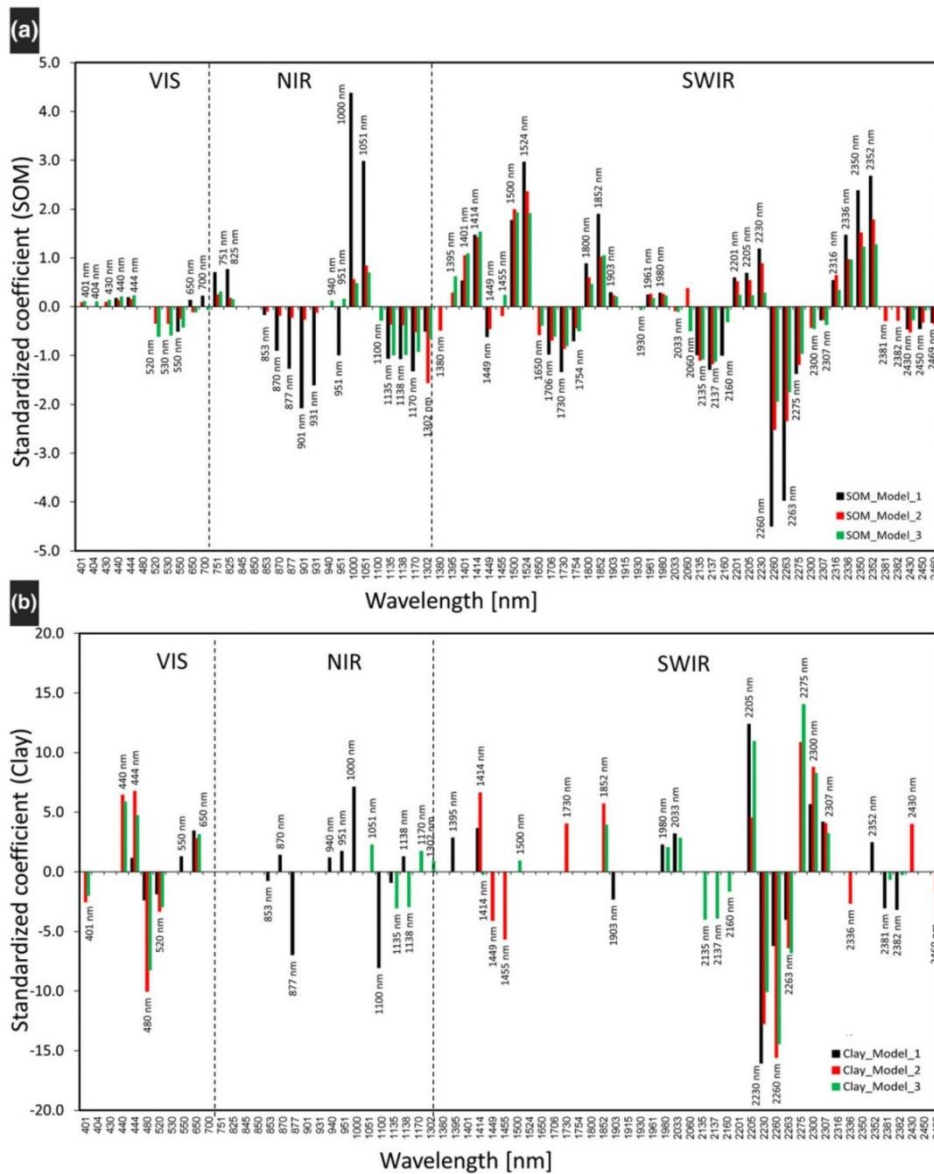


FIGURE 8 Band coefficients in the predictive models for S1, S2, and S3 for (a) soil organic matter (SOM) and (b) clay (c) silt and (d) sand [Colour figure can be viewed at wileyonlinelibrary.com]

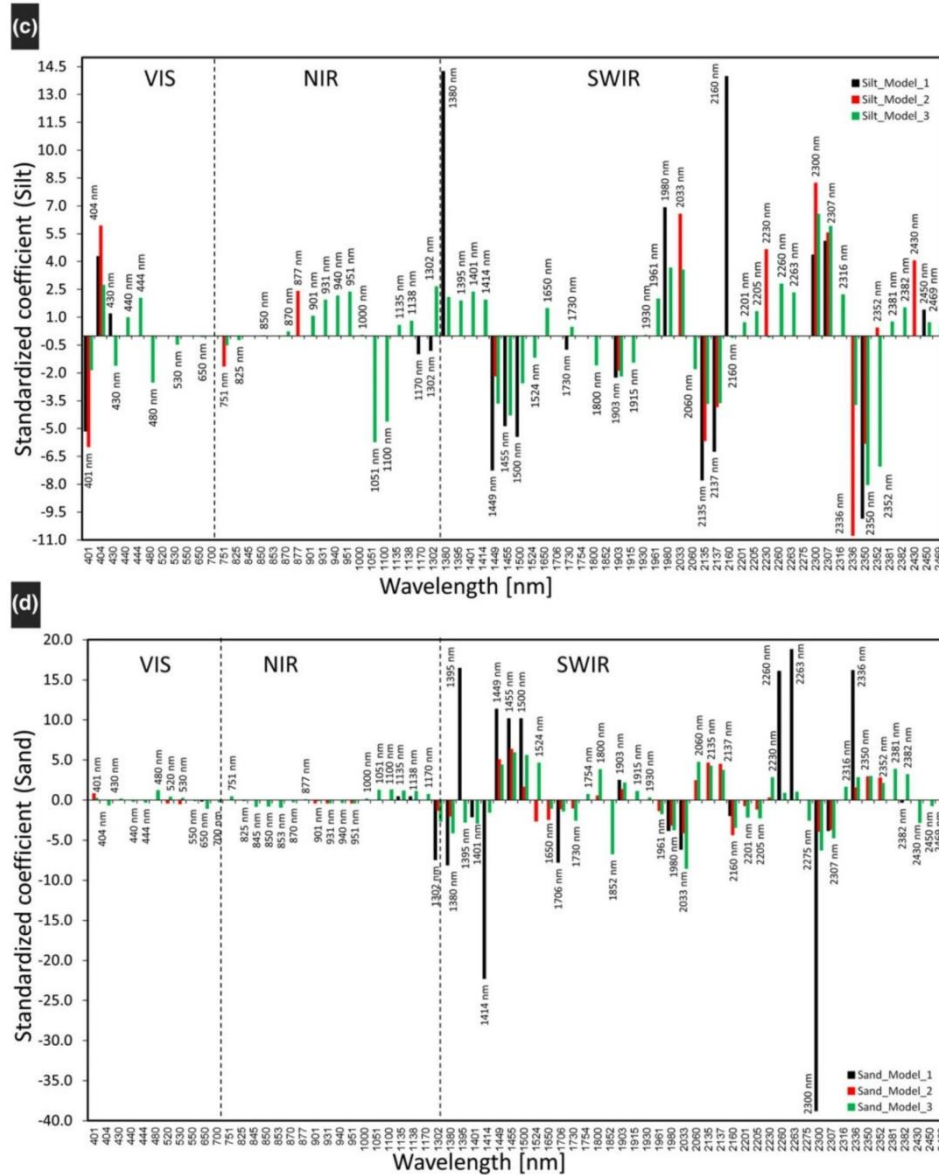


FIGURE 8 Continued.

features characteristic of clay minerals in these soils are masked by the high content of organic matter, the highest coefficients in the clay model (Figure 8b) correspond to bands related to clay minerals, such as kaolinite (1,395, 1,414, and 2,208 nm) and illite (2,206, 2,300–2,340 nm; Bellon-Maurel et al., 2010; Ben-Dor & Banin, 1995; Brunet et al., 2007). The presence of a considerable quantity of illite in soils from the studied areas of cropland abandonment (Nadal-Romero, Regüés, Martí-Bono, & Serrano-Muela, 2007) supports these findings. In most cases, bands from these intervals are also selected as important predictors in PLSR models.

4 | CONCLUSIONS

The study confirmed the viability of using CCR-SD algorithm in modelling of organic matter content and texture fractions of soils from VIS–NIR–SWIR spectra for monitoring soil quality in areas recovering from natural (wildfires) and anthropic (agricultural cultivation) disturbances. A novel CCR-SD algorithm created models with good predictive capacities that simultaneously estimated SOM, clay, silt, and sand (R^2 in the range of 0.80–0.86 for the calibration data set and 0.70–0.87 for the validation dataset), with the highest coefficient of determination being achieved by the SOM predictions.

The reliability of the CCR-SD models resulted similar to the PLSR models with full (PLSR-full) and reduced (PLSR-MUT) number of predictors. However, the CCR-SD models achieved good fit using a smaller number of available predictors. One of the advantages of CCR-SD application is the possibility of running calibrations in a familiar interface of the EXCEL (Microsoft) software package. Further research is planned to test the methodology on a wider database of soils from erosion-risk environments, such as areas of slash-and-burn agriculture.

Up-to-date information supporting activities protecting soil from degradation will allow the control of short- and long-term consequences of management decisions. The methodological results obtained in this work may provide an interesting operational tool to analyse soil properties and support sustainable management programmes in forest areas with degradation risks, thematic area explicitly mentioned in SDG 15: "Sustainably manage forests, combat desertification, halt and reverse land degradation, halt biodiversity loss" (2030 Agenda for Sustainable Development).

ACKNOWLEDGEMENTS

Authors appreciate the financial support provided to the first author of this article by Secretaría de Educación Superior, Ciencia, Tecnología e Innovación (SENESCYT), Ecuador, grant no. 211-2012 in the initial stage of the research, following the funding received in the framework of the "Ayudas Movilidad Latinoamericanos-Estudios de doctorado. UNIZAR - Santander Universidades | 2017-2018" of Bank Universidad de Zaragoza - Santander Universidades. Soil samples from abandoned croplands were collected during the Marie Curie Intra-European Fellowship project "MED-AFFOREST" (PIEF-GA-2013-624974), and Estela Nadal-Romero was the recipient of a "Ramón y Cajal" postdoctoral contract (RYC-2013-14371, Ministerio de Economía y Competitividad, Gobierno de España).

ORCID

Olga A. Rosero-Vlasova  <https://orcid.org/0000-0002-3104-0115>

Lidia Vlassova  <https://orcid.org/0000-0001-5025-5691>

Fernando Pérez-Cabello  <https://orcid.org/0000-0003-4831-4060>

Raquel Montorio  <https://orcid.org/0000-0001-7403-1764>

Estela Nadal-Romero  <https://orcid.org/0000-0002-4651-7828>

REFERENCES

Akaike, H. (1973). Maximum likelihood identification of Gaussian autoregressive moving average models. *Biometrika*, 60(2), 255–265. <https://doi.org/10.1093/biomet/60.2.255>

Alkerwi, A., Vernier, C., Sauvageot, N., Crichton, G. E., & Elias, M. F. (2015). Demographic and socioeconomic disparity in nutrition: Application of a novel correlated component regression approach. *BMJ Open*, 5(5), e006814. <https://doi.org/10.1136/bmjopen-2014-006814>

Assessment, M. E. (2005). Ecosystems and human well-being: Biodiversity: Synthesis. In J. Sarukhán, & A. Whyte (Eds.), *A report of the millennium ecosystem assessment*. Washington DC, USA: Island Press. Retrieved from <https://www.millenniumassessment.org/documents/document.356.aspx.pdf>

Babiyak, M. A. (2004). What you see may not be what you get: A brief, nontechnical introduction to overfitting in regression-type models. *Psychosomatic Medicine*, 66(3), 411–421. Retrieved from https://journals.lww.com/psychosomaticmedicine/Fulltext/2004/05000/What_You_See_May_Not_Be_What_You_Get_A_Brief.21.aspx

Badia-Villas, D., & del Moral, F. (2016). *Soils of the arid areas the soils of Spain* (pp. 145–161). Cham, Switzerland: Springer International Publishing. https://doi.org/10.1007/978-3-319-20541-0_4

Bellon-Maurel, V., Fernandez-Ahumada, E., Palagos, B., Roger, J. M., & McBratney, A. (2010). Critical review of chemometric indicators commonly used for assessing the quality of the prediction of soil attributes by NIR spectroscopy. *TrAC Trends in Analytical Chemistry*, 29, 1073–1081. <https://doi.org/10.1016/j.trac.2010.05.006>

Bellon-Maurel, V., & McBratney, A. (2011). Near-infrared (NIR) and mid-infrared (MIR) spectroscopic techniques for assessing the amount of carbon stock in soils—Critical review and research perspectives. *Soil Biology and Biochemistry*, 43(7), 1398–1410. <https://doi.org/10.1016/j.soilbio.2011.02.019>

Ben-Dor, E., & Banin, A. (1995). Near-infrared analysis as a rapid method to simultaneously evaluate several soil properties. *Soil Science Society of America Journal*, 59(2), 364–372. <https://doi.org/10.2136/sssaj1995.03615995005900020014x>

Ben-Dor, E., Chabrillat, S., Demattè, J. A. M., Taylor, G. R., Hill, J., Whiting, M. L., & Sommer, S. (2009). Using imaging spectroscopy to study soil properties. *Remote Sensing of Environment*, 113, Supplement 1(0), S38–S55. <https://doi.org/10.1016/j.rse.2008.09.019>

Ben-Dor, E., & Demattè, J. (2016). Chapter 25-Remote sensing of soil in the optical domains. In P. S. Thenkabail (Ed.), *Remote sensing handbook vol. II: Land resources monitoring, modeling, and mapping with remote sensing* (pp. 733–787). Boca Raton, FL, USA: CRC Press (Taylor & Francis Group).

Ben-Dor, E., Heller, D., & Chudnovsky, A. (2008). A novel method of classifying soil profiles in the field using optical means. *Soil Science Society of America Journal*, 72(4), 1113–1123. <https://doi.org/10.2136/sssaj2006.0059>

Ben-Dor, E., Irons, J. R., & Epema, G. F. (1999). Chapter 3—Soil reflectance. In A. N. Rencz, & R. A. Ryerson (Eds.), *Manual of remote sensing, remote sensing for the earth sciences (3rd ed.)* (vol. 3) (pp. 111–188). New York, NY, USA: John Wiley & Sons.

Bennett, G. (2013). *Regression modelling with many correlated predictors and few cases*. York, United Kingdom: Presentation in ASSESS Event. Retrieved from <http://www.spssusers.co.uk/Events/2013/Bennett2013.pdf>

Brown, D. J. (2007). Using a global VNIR soil-spectral library for local soil characterization and landscape modeling in a 2nd-order Uganda watershed. *Geoderma*, 140(4), 444–453. <https://doi.org/10.1016/j.geoderma.2007.04.021>

Brown, D. J., Shepherd, K. D., Walsh, M. G., Mays, M. D., & Reinsch, T. G. (2006). Global soil characterization with VNIR diffuse reflectance spectroscopy. *Geoderma*, 132(3), 273–290. <https://doi.org/10.1016/j.geoderma.2005.04.025>

Brunet, D., Barthès, B. G., Chotte, J.-L., & Feller, C. (2007). Determination of carbon and nitrogen contents in Alfisols, Oxisols and Ultisols from Africa and Brazil using NIRS analysis: Effects of sample grinding and set heterogeneity. *Geoderma*, 139(1–2), 106–117. <https://doi.org/10.1016/j.geoderma.2007.01.007>

Bünemann, E. K., Bongiorno, G., Bai, Z., Creamer, R. E., De Deyn, G., de Goede, R., ... Mäder, P. (2018). Soil quality—A critical review. *Soil Biology and Biochemistry*, 120, 105–125. <https://doi.org/10.1016/j.soilbio.2018.01.030>

Castro-Esau, K., Sanchez-Azofeifa, G., & Rivard, B. (2006). Comparison of spectral indices obtained using multiple spectroradiometers. *Remote Sensing of Environment*, 103(3), 276–288. <https://doi.org/10.1016/j.rse.2005.01.019>

Cerdà, A. (Ed.), & Robichaud, P. (Ed.). (2009). *Fire effects on soil infiltration. Fire effects on soils and restoration strategies* (pp. 81–103). Boca Raton, FL, USA: CRC Press (Taylor & Francis Group). <https://doi.org/10.1201/9781439843338>

- Chabrilat, S., Ben-Dor, E., Viscarra-Rossel, R. A. V., & Dematté, J. A. M. (2013). Quantitative soil spectroscopy. *Applied and Environmental Soil Science*, 2013(ID 616578), 1–3. <https://doi.org/10.1155/2013/616578>
- Chapman, G., Gray, J., Murphy, B., Atkinson, G., Leys, J., Muller, R., ... McInnes-Clarke, S. (2011). *Assessing the condition of soils in NSW. State of the Catchments 2010: Soil condition–technical report series*. Sydney: Office of Environment and Heritage. Retrieved from <https://www.environment.nsw.gov.au/-/media/OEH/Corporate-Site/Documents/Land-and-soil/assessing-condition-soils-nsw.pdf>
- Conforti, M., Froio, R., Matteucci, G., & Buttafuoco, G. (2015). Visible and near infrared spectroscopy for predicting texture in forest soil: An application in southern Italy. *iForest - Biogeosciences and Forestry*, 8(3), 339–347. <https://doi.org/10.3832/ifor1221-007>
- Conforti, M., Matteucci, G., & Buttafuoco, G. (2018). Using laboratory Vis-NIR spectroscopy for monitoring some forest soil properties. *Journal of Soils and Sediments*, 18(3), 1009–1019. <https://doi.org/10.1007/s11368-017-1766-5>
- Cuadrat, J. M. (Ed.), & Martín-Vide, J. M. (Ed.). (2007). *Spanish climatology: Past, present and future*. Zaragoza, Ar, Spain: University of Zaragoza Press.
- Curl, A., Thompson, C. W., & Aspinall, P. (2015). The effectiveness of 'shared space' residential street interventions on self-reported activity levels and quality of life for older people. *Landscape and Urban Planning*, 139, 117–125. <https://doi.org/10.1016/j.landurbplan.2015.02.019>
- Danner, M., Locherer, M., Hank, T., & Richter, K. (2015). Spectral sampling with the ASD FIELDSPEC 4. In EnMap (Ed.), *EnMAP Field Guides Technical Report* (p. 20). Potsdam, Germany: EnMAP Consortium-GFZ Data Services. <https://doi.org/10.2312/enmap.2015.008>
- Dematté, J. A., Morgan, C. L. S., Chabrilat, S., Rizzo, R., Franceschini, M., Terra, F. D., ... Wetterlind, J. (2016). Chapter 24—Spectral sensing from ground to space in soil science: State of the art, applications, potential and perspectives. In P. S. Thenkabail (Ed.), *Remote sensing handbook vol. II: Land resources monitoring, modeling, and mapping with remote sensing* (pp. 661–732). Boca Raton, FL, USA: CRC press (Taylor & Francis Group).
- Dematté, J. A. M. (2002). Characterization and discrimination of soils by their reflected electromagnetic energy. *Pesquisa Agropecuária Brasileira*, 37(10), 1445–1458. <https://doi.org/10.1590/S0100-204X2002001000013>
- Dematté, J. A. M., Campos, R. C., Alves, M. C., Fiorio, P. R., & Nanni, M. R. (2004). Visible–NIR reflectance: A new approach on soil evaluation. *Geoderma*, 121(1–2), 95–112. <https://doi.org/10.1016/j.geoderma.2003.09.012>
- Dematté, J. A. M., & da Silva Terra, F. (2014). Spectral pedology: A new perspective on evaluation of soils along pedogenetic alterations. *Geoderma*, 217–218(0), 190–200. <https://doi.org/10.1016/j.geoderma.2013.11.012>
- Esbensen, K. H. (Ed.), Guyot, D. (Ed.), Westad, F. (Ed.), & Houmoller, L. P. (Ed.). (2002). *Multivariate data analysis-in practice: An introduction to multivariate data analysis and experimental design. Multivariate data analysis*, (5th ed.) (pp 600). Oslo, Norway: CAMO Process AS.
- Escribano, P., Schmid, T., Chabrilat, S., Rodríguez-Caballero, E., & García, M. (2017). Optical remote sensing for soil mapping and monitoring. In P. Pereira, E. Brevik, M. Muñoz-Rojas, & B. A. Miller (Eds.), *Soil mapping and process modeling for sustainable land use management* (pp. 87–125). Amsterdam, Boston, Heidelberg, London, New York: Elsevier Inc. <https://doi.org/10.1016/B978-0-12-805200-6.00004-9>
- FAO (2015). *World reference base for soil resources*. Retrieved from Rome, Italy: <http://www.fao.org/3/i3794en/i3794en.pdf>
- García-Ruiz, J. M. (2010). The effects of land uses on soil erosion in Spain: A Review. *Catena*, 81(1), 1–11. <https://doi.org/10.1016/j.catena.2010.01.001>
- Garver, M. S., & Williams, Z. (2018). Improving the validity of theory testing in logistics research using correlated components regression. *International Journal of Logistics Research and Applications*, 21(4), 363–377. <https://doi.org/10.1080/13675567.2017.1401054>
- Ge, Y., Thomasson, J. A., & Sui, R. (2011). Remote sensing of soil properties in precision agriculture: A review. *Frontiers of Earth Science*, 5(3), 229–238. <https://doi.org/10.1007/s11707-011-0175-0>
- Gholizadeh, A., Borůvka, L., Saberioon, M., & Vašát, R. (2016). A memory-based learning approach as compared to other data mining algorithms for the prediction of soil texture using diffuse reflectance spectra. *Remote Sensing*, 8(4), 341. <https://doi.org/10.3390/rs8040341>
- Gholizadeh, A., Saberioon, M., Carmon, N., Boruvka, L., & Ben-Dor, E. (2018). Examining the performance of PARACUDA-II data-mining engine versus selected techniques to model soil carbon from reflectance spectra. *Remote Sensing*, 10(8), 1172. <https://doi.org/10.3390/rs10081172>
- Goldman, S. J., Bursztynsky, T. A., & Jackson, K. (1986). *Erosion and sediment control handbook*. New York, USA: McGraw-Hill.
- Grunwald, S., Thompson, J., & Boettinger, J. (2011). Digital soil mapping and modeling at continental scales: Finding solutions for global issues. *Soil Science Society of America Journal*, 75(4), 1201–1213. <https://doi.org/10.2136/sssaj2011.0025>
- Jiménez-González, M. A., De la Rosa, J. M., Jiménez-Morillo, N. T., Alendros, G., González-Pérez, J. A., & Knicker, H. (2016). Post-fire recovery of soil organic matter in a Cambisol from typical Mediterranean forest in Southwestern Spain. *Science of the Total Environment*, 572, 1414–1421. <https://doi.org/10.1016/j.scitotenv.2016.02.134>
- Knadell, M., Stenberg, B., Deng, F., Thomsen, A., & Greve, M. H. (2013). Comparing predictive abilities of three visible-near infrared spectrophotometers for soil organic carbon and clay determination. *Journal of Near Infrared Spectroscopy*, 21(1), 67–80. <https://doi.org/10.1255/jnirs.1035>
- Kobza, J. (2015). Permanent soil monitoring system as a basic tool for protection of soils and sustainable land use in Slovakia. *IOP Conference Series: Earth and Environmental Science*, 25(1), 1–10. <https://doi.org/10.1088/1755-1315/25/1/012011>
- Lal, R. (Ed.), & Stewart, B. A. (Ed.). (2010). *Food security and soil quality*. Boca Raton, FL, USA: CRC Press (Taylor & Francis Group), <https://doi.org/10.1201/EBK1439800577>.
- Laudicina, V. A., De Pasquale, C., Conte, P., Badalucco, L., Alonzo, G., & Palazzolo, E. (2012). Effects of afforestation with four unmixed plant species on the soil–water interactions in a semiarid Mediterranean region (Sicily, Italy). *Journal of Soils and Sediments*, 12(8), 1222–1230. <https://doi.org/10.1007/s11368-012-0522-0>
- Lu, D., Li, G., Valladares, G. S., & Batistella, M. (2004). Mapping soil erosion risk in Rondônia, Brazilian Amazonia: using RUSLE, remote sensing and GIS. *Land Degradation & Development*, 15(5), 499–512. <https://doi.org/10.1002/ldr.634>
- Lugassi, R., Ben-Dor, E., & Eshel, G. (2014). Reflectance spectroscopy of soils post-heating—Assessing thermal alterations in soil minerals. *Geoderma*, 213(0), 268–279. <https://doi.org/10.1016/j.geoderma.2013.08.014>
- Magidson, J. (2010). Correlated component regression: A prediction/classification methodology for possibly many features. *Proceedings of the American Statistical Association*. pp.4372–4386.
- Magidson, J. (2013). Correlated component regression: Re-thinking regression in the presence of near collinearity. In H. Abdi, W. W. Chin, V. E. Vinzi, G. Russolillo, & L. Trinchera (Eds.), *New perspectives in partial least squares and related methods* (pp. 65–78). New York, NY, USA: Springer International Publishing. https://doi.org/10.1007/978-1-4614-8283-3_3
- Magidson, J., & Wassmann, K. (2010). The role of proxy genes in predictive models: an application to early detection of prostate cancer. *Proceedings of the American Statistical Association, Biometrics section*. pp.2739–2753.
- Martens, H., & Martens, M. (2000). Modified Jack-knife estimation of parameter uncertainty in bilinear modelling by partial least squares regression (PLSR). *Food Quality and Preference*, 11(1–2), 5–16. [https://doi.org/10.1016/S0950-3293\(99\)00039-7](https://doi.org/10.1016/S0950-3293(99)00039-7)
- Melendez-Pastor, I., Navarro-Pedreño, J., Gómez, I., & Koch, M. (2008). Identifying optimal spectral bands to assess soil properties with VNIR

- radiometry in semi-arid soils. *Geoderma*, 147(3), 126–132. <https://doi.org/10.1016/j.geoderma.2008.08.004>
- Merino, A., Moreno, G., Navarro, F. B., & Gallardo, J. F. (2016). Future issues. In J. F. Gallardo (Ed.), *The soils of Spain* (pp. 189–195). Cham, Switzerland: Springer International Publishing. https://doi.org/10.1007/978-3-319-20541-0_6
- Montanarella, L., & Panagos, P. (2018). Soil data needs for sustainable agriculture. In H. Ginzky, E. Dooley, I. Heuser, E. Kasimbazi, T. Markus, & T. Qin (Eds.), *International Yearbook of Soil Law and Policy 2017. (IYSLP, Vol 2017)* (pp. 151–166). Cham, Switzerland: Springer International Publishing. https://doi.org/10.1007/978-3-319-68885-5_9
- Mouazen, A. M., Karoui, R., De Baerdemaeker, J., & Ramon, H. (2005). Classification of soil texture classes by using soil visual near infrared spectroscopy and factorial discriminant analysis techniques. *Journal of Near Infrared Spectroscopy*, 13(4), 231–240. <https://doi.org/10.1255/jnirs.541>
- Mouazen, A. M., Kuang, B., De Baerdemaeker, J., & Ramon, H. (2010). Comparison among principal component, partial least squares and back propagation neural network analyses for accuracy of measurement of selected soil properties with visible and near infrared spectroscopy. *Geoderma*, 158(1), 23–31. <https://doi.org/10.1016/j.geoderma.2010.03.001>
- Nadal-Romero, E., Cammeraat, E., Pérez-Cardiel, E., & Lasanta, T. (2016). Effects of secondary succession and afforestation practices on soil properties after cropland abandonment in humid Mediterranean mountain areas. *Agriculture, Ecosystems & Environment*, 228, 91–100. <https://doi.org/10.1016/j.agee.2016.05.003>
- Nadal-Romero, E., Regüés, D., Martí-Bono, C., & Serrano-Muela, P. (2007). Badland dynamics in the Central Pyrenees: Temporal and spatial patterns of weathering processes. *Earth Surface Processes and Landforms*, 32(6), 888–904. <https://doi.org/10.1002/esp.1458>
- Novara, A., La Mantia, T., Barbera, V., & Gristina, L. (2012). Paired-site approach for studying soil organic carbon dynamics in a Mediterranean semiarid environment. *Catena*, 89(1), 1–7. <https://doi.org/10.1016/j.catena.2011.09.008>
- Nuzzo, R. (2014). Scientific method: Statistical errors. *Nature*, 506(7487), 150–152. <https://doi.org/10.1038/506150a>
- Ogen, Y., Neumann, C., Chabrilat, S., Goldshleger, N., & Ben-Dor, E. (2018). Evaluating the detection limit of organic matter using point and imaging spectroscopy. *Geoderma*, 321, 100–109. <https://doi.org/10.1016/j.geoderma.2018.02.011>
- Ostovari, Y., Ghorbani-Dashtaki, S., Bahrami, H.-A., Abbasi, M., Dematté, J. A. M., Arthur, E., & Panagos, P. (2018). Towards prediction of soil erodibility, SOM and CaCO₃ using laboratory Vis-NIR spectra: A case study in a semi-arid region of Iran. *Geoderma*, 314, 102–112. <https://doi.org/10.1016/j.geoderma.2017.11.014>
- Pausas, J. G., Llovet, J., Rodrigo, A., & Vallejo, R. (2009). Are wildfires a disaster in the Mediterranean basin?—A review. *International Journal of Wildland Fire*, 17(6), 713–723. <https://doi.org/10.1071/WF07151>
- Pérez-Cabello, F., Echeverría, M., Ibarra, P., & Riva, J. (2009). Effects of fire on vegetation, soil and hydrogeomorphological behavior in Mediterranean ecosystems. In E. Chuvieco (Ed.), *Earth observation of wildland fires in Mediterranean ecosystems* (pp. 111–128). Berlin, Heidelberg: Springer International Publishing. https://doi.org/10.1007/978-3-642-01754-4_9
- Pimentel, D. (2006). Soil erosion: A food and environmental threat. *Environment, Development and Sustainability*, 8(1), 119–137. <https://doi.org/10.1007/s10668-005-1262-8>
- Pinheiro, É. F., Ceddia, M. B., Clingensmith, C. M., Grunwald, S., & Vasques, G. M. (2017). Prediction of soil physical and chemical properties by visible and near-infrared diffuse reflectance spectroscopy in the Central Amazon. *Remote Sensing*, 9(4), 293. <https://doi.org/10.3390/rs9040293>
- Rosero-Vlasova, O., Borini Alves, D., Vlassova, L., Perez-Cabello, F., & Montorio Lloveria, R. (2017). Modeling soil organic matter (SOM) from satellite data using VISNIR-SWIR spectroscopy and PLS regression with step-down variable selection algorithm: Case study of Campos Amazonicos National Park savanna enclave, Brazil. Paper Presented at the SPIE Remote Sensing Conference. USA: The International Society for Optics and Photonics. <https://doi.org/10.1117/12.2278701>
- Rosero-Vlasova, O., Pérez-Cabello, F., Montorio Lloveria, R., & Vlassova, L. (2016). Assessment of laboratory VIS-NIR-SWIR setups with different spectroscopy accessories for characterisation of soils from wildfire burns. *Biosystems Engineering*, 152, 51–67. <https://doi.org/10.1016/j.biosystemseng.2016.06.011>
- Rosero-Vlasova, O. A., Vlassova, L., Pérez-Cabello, F., Montorio, R., & Nadal-Romero, E. (2018). Modeling soil organic matter and texture from satellite data in areas affected by wildfires and cropland abandonment in Aragón, Northern Spain. *Journal of Applied Remote Sensing*, 12(4), 042803. <https://doi.org/10.1117/1.JRS.12.042803>
- Ruiz de la Torre, J. (1990). Distribución y características de las masas forestales españolas. *Ecología* (Nº. 1), (pp. 11–13). Retrieved from <https://dialnet.unirioja.es>
- Ruiz-Rodado, V., Marcos Luque-Baena, R., te Vrucchte, D., Probert, F., Lachmann, R. H., Hendriksz, C. J., ... Grootveld, M. (2014). 1H NMR-linked urinary metabolic profiling of niemann-pick class C1 (NPC1) disease: Identification of potential new biomarkers using correlated component regression (CCR) and genetic algorithm (GA) analysis strategies. *Current Metabolomics*, 2(2), 88–121. <https://doi.org/10.2174/2213235X02666141112215616>
- Stenberg, B., Viscarra Rossel, R. A., Mouazen, A. M., & Wetterlind, J. (2010). Chapter five-visible and near infrared spectroscopy in soil science. *Advances in Agronomy*, 107, 163–215. [https://doi.org/10.1016/S0065-2113\(10\)07005-7](https://doi.org/10.1016/S0065-2113(10)07005-7)
- Stevens, A., Nocita, M., Tóth, G., Montanarella, L., & van Wesemael, B. (2013). Prediction of soil organic carbon at the European scale by visible and near infrared reflectance spectroscopy. *PLoS One*, 8(6), e66409. <https://doi.org/10.1371/journal.pone.0066409>
- Terra, F. S., Dematté, J. A. M., & Viscarra Rossel, R. A. (2018). Proximal spectral sensing in pedological assessments: Vis-NIR spectra for soil classification based on weathering and pedogenesis. *Geoderma*, 318, 123–136. <https://doi.org/10.1016/j.geoderma.2017.10.053>
- Tóth, G., Hermann, T., da Silva, M. R., & Montanarella, L. (2018). Monitoring soil for sustainable development and land degradation neutrality. *Environmental Monitoring and Assessment*, 190(2), 57. <https://doi.org/10.1007/s10661-017-6415-3>
- Troeh, F. R., & Thompson, L. M. (2005). Chapter 20—Soil erosion and its control. In *Soils and soil fertility* (6th ed.). Ames, Iowa, USA: Blackwell (John Wiley & Sons).
- United Nations (2015). *Transforming our world: The 2030 agenda for sustainable development. Resolution adopted by the General Assembly, (A/RES/70/1)*. United Nations Headquarters, New York, NY, USA: Press release. Retrieved from <https://sustainabledevelopment.un.org/content/documents/21252030%20Agenda%20for%20Sustainable%20Development%20web.pdf>
- USDA. (1996). Soil survey manual. Retrieved from Washington, USA: https://www.nrcs.usda.gov/Internet/FSE_DOCUMENTS/nrcsepr1335011.pdf
- Vasques, G. M., Dematté, J. A. M., Viscarra Rossel, R. A., Ramírez-López, L., & Terra, F. S. (2014). Soil classification using visible/near-infrared diffuse reflectance spectra from multiple depths. *Geoderma*, 223–225(0), 73–78. <https://doi.org/10.1016/j.geoderma.2014.01.019>
- Viscarra Rossel, R., & Behrens, T. (2010). Using data mining to model and interpret soil diffuse reflectance spectra. *Geoderma*, 158(1), 46–54. <https://doi.org/10.1016/j.geoderma.2009.12.025>
- Viscarra Rossel, R., & Brus, D. J. (2018). The cost-efficiency and reliability of two methods for soil organic C accounting. *Land Degradation & Development*, 29(3), 506–552. <https://doi.org/10.1002/ldr.2887>
- Viscarra Rossel, R., Walvoort, D., McBratney, A., Janik, L. J., & Skjemstad, J. (2006). Visible, near infrared, mid infrared or combined diffuse reflectance spectroscopy for simultaneous assessment of various soil properties. *Geoderma*, 131(1–2), 59–75. <https://doi.org/10.1016/j.geoderma.2005.03.007>
- Viscarra Rossel, R. A., McGlynn, R. N., & McBratney, A. B. (2006). Determining the composition of mineral-organic mixes using UV-Vis-NIR

- diffuse reflectance spectroscopy. *Geoderma*, 137(1–2), 70–82. <https://doi.org/10.1016/j.geoderma.2006.07.004>
- Vlassova, L., & Pérez-Cabello, F. (2016). Effects of post-fire wood management strategies on vegetation recovery and land surface temperature (LST) estimated from Landsat images. *International Journal of Applied Earth Observation and Geoinformation*, 44, 171–183. <https://doi.org/10.1016/j.jag.2015.08.011>
- Wold, S., Sjöström, M., & Eriksson, L. (2001). PLS-regression: A basic tool of chemometrics. *Chemometrics and Intelligent Laboratory Systems*, 58(2), 109–130. [https://doi.org/10.1016/S0169-7439\(01\)00155-1](https://doi.org/10.1016/S0169-7439(01)00155-1)

How to cite this article: Rosero-Vlasova OA, Vlassova L, Pérez-Cabello F, Montorio R, Nadal-Romero E. Soil organic matter and texture estimation from visible-near infrared-shortwave infrared spectra in areas of land cover changes using correlated component regression. *Land Degrad Dev*. 2019;30:544–560. <https://doi.org/10.1002/ldr.3250>

8. Modeling soil organic matter and texture from satellite data.

8.1. Case study of Aragón, Northern Spain

This section in the chapter reproduces the text of the following article:

Title:

Modeling soil organic matter and texture from satellite data in areas affected by wildfires and cropland abandonment in Aragón, Northern Spain

Authors:

Olga A. Rosero-Vlasova

Lidia Vlassova

Fernando Pérez-Cabello

Raquel Montorio

Estela Nadal-Romero

Journal of Applied Remote Sensing

RemoteSensing.SPIEDigitalLibrary.org

Modeling soil organic matter and texture from satellite data in areas affected by wildfires and cropland abandonment in Aragón, Northern Spain

Olga A. Rosero-Vlasova,^{a,*} Lidia Vlassova,^b Fernando Pérez-Cabello,^a
Raquel Montorio,^a and Estela Nadal-Romero^a

^aUniversity of Zaragoza, Department of Geography and Land Management, Zaragoza, Spain

^bTechnical State University of Quevedo, Department of Environmental Sciences, Quevedo, Ecuador

Abstract. Land use/land cover (LULC) changes create the need for regular monitoring of soil properties. Modern technology and data sources offer possibilities to perform it. In this context, the objective of the study is to explore the possibility of predicting soil organic matter (SOM) content and texture from the spectral information of the three last generation satellites [Landsat-8, Sentinel-2, and the Environmental Mapping and Analysis Program (EnMAP)]. Soil samples (113) were collected in areas affected by wildfires and cropland abandonment in Aragón, Northern Spain. Reflectance spectra of soils were obtained in controlled laboratory conditions using the analytical spectral device Fieldspec4 spectroradiometer (spectral range 350 to 2500 nm). Reflectances simulated for Landsat-8, Sentinel-2, and EnMAP bands were used as predictors in multivariate models developed using partial least squares regression (PLSR) and step-down variable selection algorithm (SD). Modeling of all soil variables was performed simultaneously. The EnMAP models employed few predictors (10 to 58 of 244) and demonstrated good fit ($R_{\text{cal}}^2 > 0.8$ and $R_{\text{val}}^2 \sim 0.8$), especially for SOM (R_{cal}^2 and $R_{\text{val}}^2 = 0.9$; RMSEP ~ 1.6). Landsat models showed the least reliable estimates (R_{cal}^2 0.54 to 0.77 and R_{val}^2 0.42 to 0.80), whereas Sentinel-2 models showed R_{cal}^2 of 0.70 to 0.81 and R_{val}^2 between 0.67 (clay) and 0.79 (SOM). The results confirm high potential of spectral data from multispectral and hyperspectral satellites for soil monitoring. Application of PLSR combined with SD results in sparser and better-fit models. SOM and soil texture can be estimated with an acceptable accuracy from EnMAP and Sentinel-2 data enabling soil status monitoring in areas of wildfire burns and cropland abandonment. © 2018 Society of Photo-Optical Instrumentation Engineers (SPIE) [DOI: 10.1117/1.JRS.12.042803]

Keywords: soil properties; VIR-NIR-SWIR spectroscopy; Landsat-8; Sentinel-2; EnMAP; partial least squares regression; step-down variable selection algorithm.

Paper 180264SS received Apr. 12, 2018; accepted for publication Jun. 8, 2018; published online Aug. 2, 2018.

1 Introduction

Land use/land cover changes (hereafter LULC) affect soil properties and may contribute to soil erosion. In Mediterranean landscapes, LULC changes are caused by natural and human-related drivers. Among the most important natural factors are the wildfires, which have long been a natural process for landscape development in this area.^{1,2} However, at present the number and intensity of wildfires are experiencing continuous increase.³ Frequent high intense fires modify physical and chemical characteristics of soils, triggering erosion and soil losses.⁴ On the other hand, one of the most important human-related drivers of LULC changes is the phenomenon of cropland abandonment.⁵ Management activities undertaken to prevent soil erosion

*Address all correspondence to: Olga A. Rosero-Vlasova, E-mail: oarosero@unizar.es

in abandoned areas often include afforestation, although sometimes it may result in unforeseen hydrological impacts.^{6,7} Thus, to assess the effects of LULC change and to understand the most effective components of land management systems, it is necessary to have an accurate picture of soil status, which can be evaluated through soil organic matter (SOM) content and texture. Both properties play a key role in belowground carbon storage, availability, and retention of nutrients⁸ and closely related to soil erodibility.⁹

One of the tools gaining popularity for regular estimation of several soil variables, including organic matter and texture, is proximal soil sensing, also known as soil spectroscopy.^{10,11} It offers a cost-effective alternative to traditional laboratory methods of soil analysis. Spectral signatures obtained with spectroradiometers can be used together with data obtained by satellite remote sensing for soil mapping and analysis.^{12–14} Reviews,^{14,15,16} including recently published,^{13,17} offer a thorough inspection and state-of-the-art assessment of advances in this field. Examples include mapping of expansive soils in Colorado, USA, from advanced visible/infrared imaging spectrometer (AVIRIS) and HyMap hyperspectral images;² mineral composition of soils in a volcanic area of the Chilean–Bolivian Altiplano from Hyperion, advanced land imager and ASTER images;¹⁸ maps of soil properties (iron, SOM, and texture) in Santa Monica Mountains, California;¹⁹ as well as recent experience with mapping of soil properties from Sentinel-2 and Landsat in South-Western Burkina Faso.²⁰

Decades of research have also revealed major challenges. A great difference may exist between a soil spectrum registered in a carefully configured and performed laboratory experiment and that obtained with the multi- or even hyperspectral satellite/airborne sensor because it contains information not only about soil, but also about the mixture of elements naturally present on the land surface, such as photosynthetic and nonphotosynthetic vegetation, rock outcrops, dust, and water, to name a few. Moreover, satellite images need preprocessing (radiometric, geometric, and atmospheric corrections) not necessary for the laboratory spectra.²¹ Different spectral unmixing techniques²² have been tested to differentiate soils and quantify their properties from the real-life images. For example, Palacios-Orueta et al.¹⁹ applied a two-step hierarchical analysis when mapping soil properties in coastal valleys in California from AVIRIS data; first, using singular-value decomposition to discriminate the soils between two valleys, and then training vectors for each area to estimate and map their organic matter and iron oxides content. In contrast, García-Haro et al.²³ achieved delineation of spectrally homogeneous soil zones using variable multiple end member spectral mixture analysis (VMESMA). Once the areas and spectral signatures are defined, statistical modeling of soil variables is usually performed using partial least squares regression (PLSR) and stepwise multiple linear regression, although application of data mining algorithms is becoming more popular.¹³ The accuracy of the models is quite variable, with coefficient of determination R^2 ranging between 0.1 and 0.7 for Landsat and 0.05 to 0.9 for hyperspectral sensors (e.g., Hyperion, AHS, AVIRIS, CASI, and DAIS);¹³ the best results demonstrated modeling soil texture and SOM content. It had been also demonstrated that combined use of different sensors/satellites and ancillary data (terrain metrics and other landscape characteristics) may significantly improve the results.^{13,16,17,24}

Coexistence and availability of compatible data from multiple satellites, such as Landsat-8, Sentinel-2A/B (orbiting the Earth since February 2013, and June 2015/March 2017, respectively), and the launch of satellites expected to provide data of even higher resolution in near future the Environmental Mapping and Analysis Program [(EnMAP) scheduled for 2020] open possibilities for land surface monitoring and sustainable management.

In this context, the objective of this study is to explore the potential of the three last generation satellites (Landsat-8, Sentinel-2, and EnMAP) to estimate SOM content and texture in soils from areas of the wildfire burns and cropland abandonment.

2 Study Area and Data

Study area extends over 300 km² located in Aragón, Northern Spain (Fig. 1) at elevations ranging from 450 to 1300 m above the sea level. Its vegetation is typical for Mediterranean with forests of *Quercus gr. cerrioides* (Willk and Costa) and *Quercus ilex* L.; and several pine species, such as *Pinus sylvestris* L. (PS), *Pinus nigra* (PN) (Arnold), *Pinus halepensis* L., and *Pinus*

Rosero-Vlasova et al.: Modeling soil organic matter and texture from satellite data in areas...

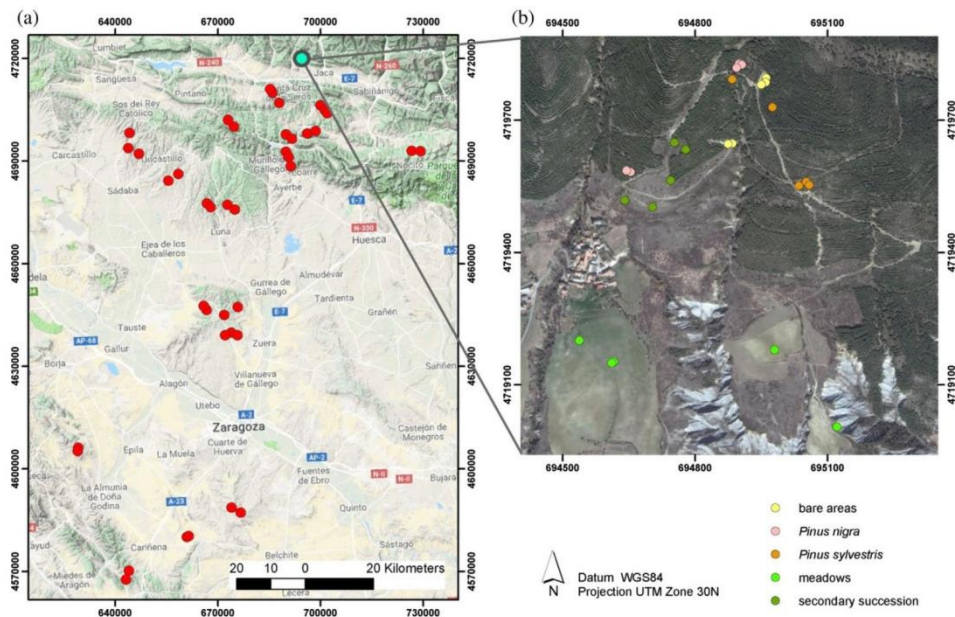


Fig. 1 Map of the study area: (a) General view. Red points indicate sampling sites in areas affected by wildfire burns (two samples collected at each site); (b) enlarged area showing the Araguás catchment with sampling sites in the areas of cropland abandonment (one sample per site).

pinaster (Aiton). Complex vegetation mosaic includes shrublands consisting mainly of *Buxus sempervirens* L. and *Genista scorpius* L.²⁵ Soil cover is heterogeneous with patches of cambisols, regosols, and leptosols.²⁶ Highly variable Mediterranean climate of the area is characterized by 10°C to 12°C average annual temperature and precipitation of around 560 mm with maxima in spring and autumn and minimum in summer.²⁷

Studied soil samples were collected in areas of wildfire burns in spring of 2013 and in September 2014 in areas cropland abandonment (Fig. 1). Samples from the wildfire burns constitute pairs of burnt and corresponding unburnt soil from the same sampling site. Samples from abandoned croplands were gathered in a small catchment (Araguás catchment), where terraced fields abandoned in 1950s present different vegetation covers due to different postabandonment

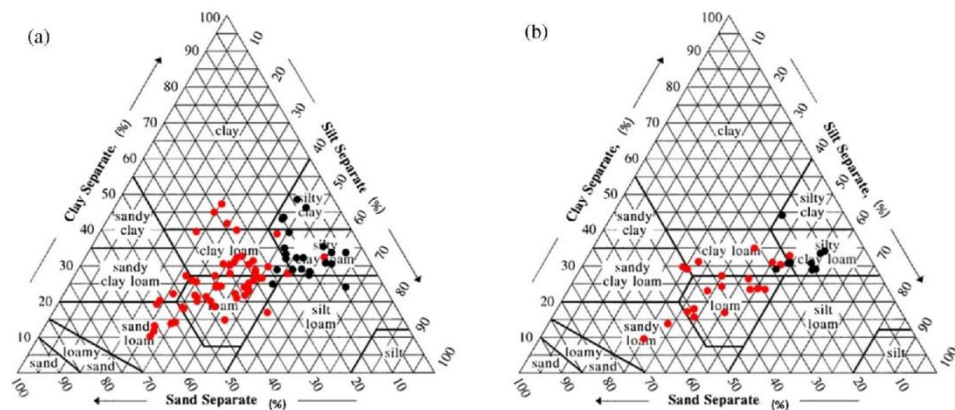


Fig. 2 Soil textures as determined by the proportion of sand, silt, and clay in soil texture triangle (USDA, 2010): (a) calibration dataset and (b) validation dataset. Red points indicate soil samples from wildfire burns; black points indicate soil samples from areas of cropland abandonment.

evolution paths: natural secondary succession, afforestation with PN and PS, permanent pastureland and bareland. More details on the study area, as well as on sampling procedure, are available in Refs. 11 (wildfire burns) and 28 (abandoned croplands).

In general, soil samples present characteristics typical for the study area. The average SOM content is around $6 \text{ g } 100 \text{ g}^{-1}$ with the range between $\sim 1 \text{ g } 100 \text{ g}^{-1}$ in bare areas and $\sim 20 \text{ g } 100 \text{ g}^{-1}$ under the undisturbed forests.²⁹ These levels are higher than the world and European averages.^{30,31} In terms of texture, the averages for clay and sand content are 27% and 33%, respectively. Thus, according to the USDA (United States Department of Agriculture) soil texture triangle, most soils from the wildfire burns can be classified as loam and clay loam, and those from the areas of cropland abandonment as silty loam (Fig. 2).

3 Methodology

3.1 Spectral Measurements

Sample preparation for spectral measurement consisted in placing of dry and sieved soils (<2 mm) in glass Petri dishes 90 mm in diameter. Analytical Spectral Device (ASD) FieldSpec4 spectroradiometer that is used to obtain soil spectra employs three sensors registering radiances in the spectral regions of 350- to 1000-nm (VIS-NIR), 1001- to 1800-nm (SWIR1), and 1801- to 2500-nm (SWIR2) wavelengths. The spectra consist of 2101 narrow bands with full width at half maximum of 3 nm in VIS-NIR and 10 nm in SWIR, respectively. Calibrated white Spectralon[®] panel acts as a reference necessary for the transformation of radiances into reflectance spectra. The setup, which uses ASD Illuminator halogen lamp as a light source (Fig. 3), ensures generation of stable low noise spectra and demonstrated reliability in our previous research.¹¹

3.2 Preparation of Reflectance Spectra for Multivariate Modeling

Bands from measured soil spectra and simulated reflectance values were used as predictors in statistical models for SOM, silt, clay, and sand. Models based on original laboratory-measured soil spectra considered 70 bands with the highest information content on SOM and other soil properties.³² The selected wavebands are located in VIS,¹¹ NIR,¹⁸ and SWIR³³ spectral regions. Because of high stability of obtained spectra, no spectral preprocessing was performed. Three outliers detected with principal components analysis (PCA) were excluded from the dataset. After this, a total of 110 samples used in multivariate modeling were splitted into calibration (80 samples) and validation (30 samples) sets, which constitute $\sim 65\%$ and $\sim 35\%$ of the total number of the samples.



Fig. 3 Laboratory setup used for spectral measurements.

Rosero-Vlasova et al.: Modeling soil organic matter and texture from satellite data in areas...

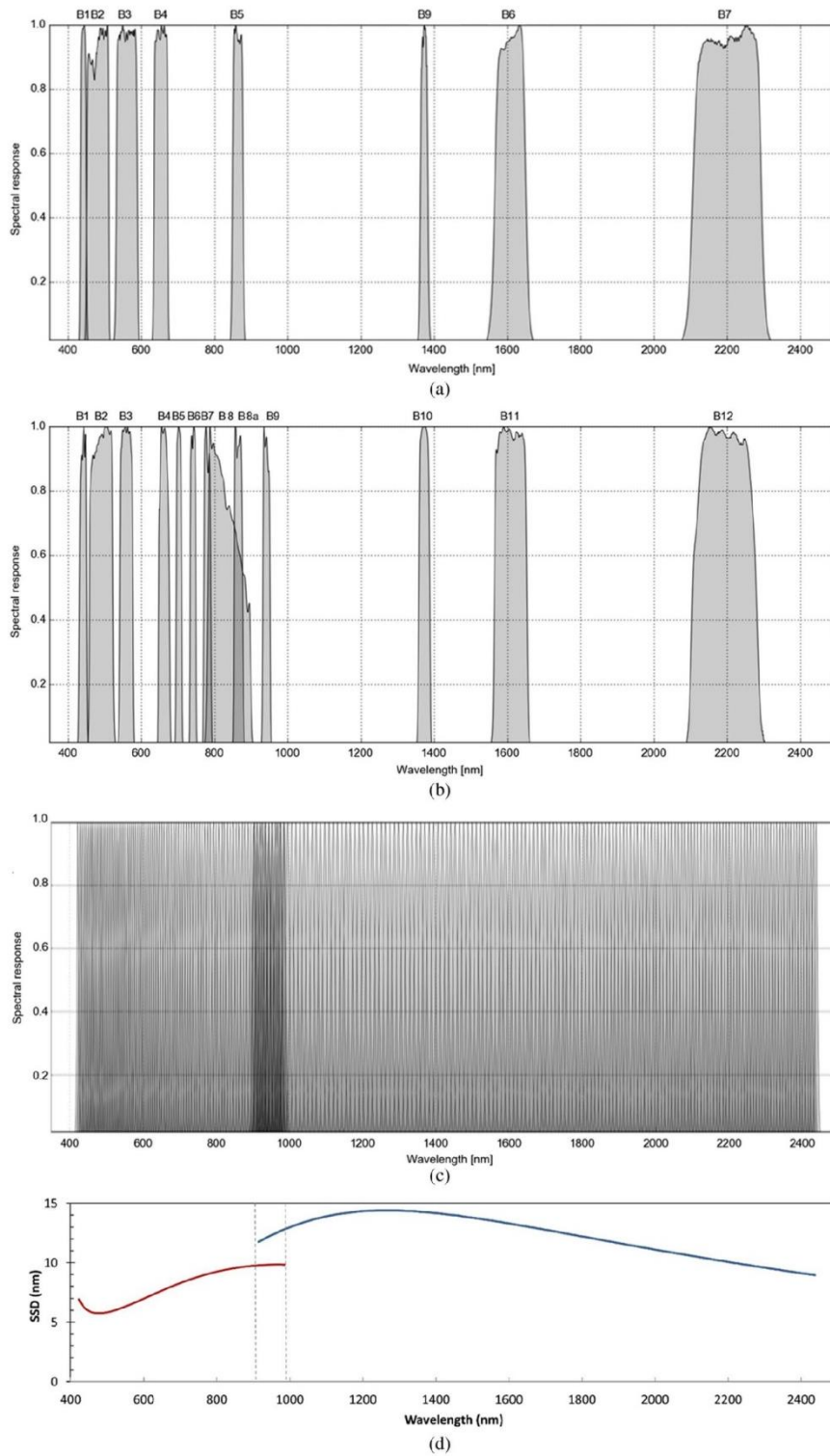


Fig. 4 Spectral response functions for (a) Landsat-8 OLI,³⁴ (b) Sentinel-2 MSI,³⁶ (c) EnMAP bands, and (d) EnMAP spectral sampling distance as a function of wavelength.³⁷

3.3 Simulation of Satellite Spectral Bands

High-resolution spectra generated using ASD were resampled to simulate reflectance values for the optical bands of one hyperspectral (EnMAP) and two multispectral (Landsat-8 and Sentinel-2) satellites.

Landsat-8 is the recent addition to the series of NASA's missions, which has been orbiting the Earth for almost 50 years. Its optical sensor Operational Land Imager (OLI) registers signal in nine spectral ranges: VIS—bands 1 to 4 and 8 (panchromatic); NIR—band 5 and SWIR—bands 6, 7, and 9, providing images of 30-m spatial resolution. Resampling of ASD spectra to OLI bands was performed using the corresponding spectral response functions available from NASA.³⁴

We also simulated bands of another Sentinel-2 satellite built and put on orbit by the European Space Agency (ESA). It is equipped with the multispectral instrument (MSI) sensor, which acquires data in 13 VIS-SWIR bands at 10- to 60-m spatial resolution and has a 5-day revisit period (versus 16 days for Landsat).³⁵ Spectral response functions of MSI bands used for resampling were downloaded from the ESA.³⁶

Finally, we simulated reflectances for the hyperspectral imager instrument of the EnMAP satellite created in the frame of the German satellite program. The satellite will obtain data in the 244 narrow bands (420- to 2450-nm wavelengths) sampled at 6.5 nm in VIS-NIR and at 10-nm intervals in SWIR at a spatial resolution of 30 m [Figs. 4(c) and 4(d)].³⁷ Spectral response functions were obtained from the freely available EnMAP toolbox.³⁸ All the processing related to resampling was performed using the ENVI 4.7 (The Environment for Visualizing Images) software.³⁹

Reference values of SOM ($\text{g } 100 \text{ g}^{-1}$) and texture fractions (%) were determined by analytical methods traditionally used in soil analysis. UV-visible spectrophotometry and the loss on ignition method were applied for SOM estimation in samples from wildfire burns and areas of cropland abandonment, respectively. Standard particle size distribution analysis method⁴⁰ was employed to estimate texture fractions in the samples from the wildfire burns, whereas particle analyzer (Micromeritics, SediGraph 5100, Nocross) was used for soils from the areas of cropland abandonment. Normal distribution of SOM, silt, clay, and sand values in both subsets was confirmed with Shapiro-Wilk test.

3.4 Statistical Modeling

Modeling of SOM, clay, silt, and sand was performed simultaneously using PLSR.^{41,42} Due to its capacity to deal with a great number of predictors, PLSR is routinely applied in soil VIS-NIR-SWIR spectroscopy.^{43,44} It is recognized that PLSR is prone to overfitting, i.e., including in models predictors relevant only to the calibration dataset.⁴⁵ One of the ways to control overfitting is to reduce the number of predictors, leaving out less important, which results in sparser models.⁴⁶ Thus, PLSR was combined with the step-down variable selection algorithm (PLSR-SD). The step-down variable selection algorithm reduces the number of variables without the loss of information through elimination of the less important variables, i.e., those with the lowest (absolute value) coefficient, during cross validation.⁴⁷ For each model, this iterative process was configured to run 10 rounds of fivefold cross validation.

Models fit was evaluated with the following statistics: coefficient of determination of calibration (R_{cal}^2), coefficient of determination of validation (R_{val}^2), and root mean square error (RMSE).

4 Results and Discussion

4.1 Soil Spectra

Reflectance spectra of the samples (Fig. 5) present a shape typical for soils: continuous positive tendency along the visible wave range, close to flat spectrum line in NIR, and gradual reflectance decrease in SWIR.^{48,49} As usual for soil spectra, absorbance features are few and are related to the presence of water (1400 and 1900 nm), iron oxides (510, 650, and 940 nm), clay minerals

Rosero-Vlasova et al.: Modeling soil organic matter and texture from satellite data in areas...

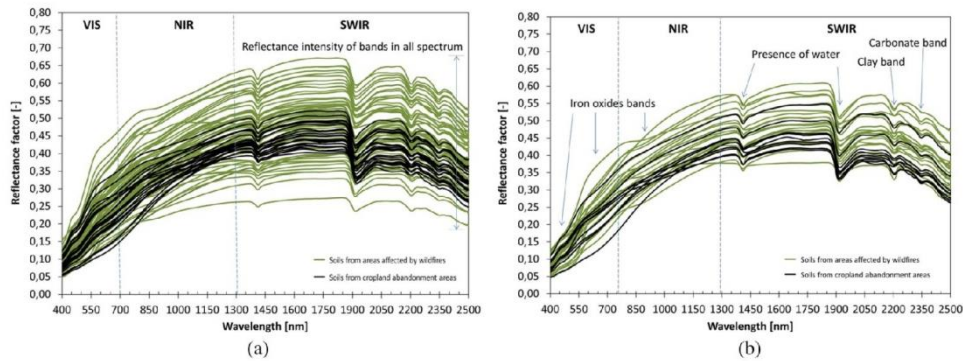


Fig. 5 Reflectance spectra for: (a) calibration set and (b) validation set. Spectra of soils from wildfire burns are shown in green; spectra of soils from areas of cropland abandonment are shown in black.

(2200 nm), and carbonate bands (2330 nm).^{2,50} These features are more pronounced in some spectra compared with the others, probably due to the heterogeneity of the dataset.¹⁵

Visual appreciation of Fig. 5 confirms that spectra can be differentiated by reflectance intensity.^{10,12,33,51} It is evident that the range of reflectance maximums is greater for the soils from wildfire burns than for the soils from the areas of cropland abandonment (0.25 to 0.65 versus 0.38 to 0.55), one of the reasons being variability in the SOM content and differences in texture: increase in SOM and reduction of soil particle size produce lower reflectance spectra.⁵²⁻⁵⁴ The fact that the samples from the wildfire burns include undisturbed highly fertile soils and burned soils with very low organic matter explains higher variability of their spectra compared with the spectra of soils from cropland abandonment areas (Fig. 5).

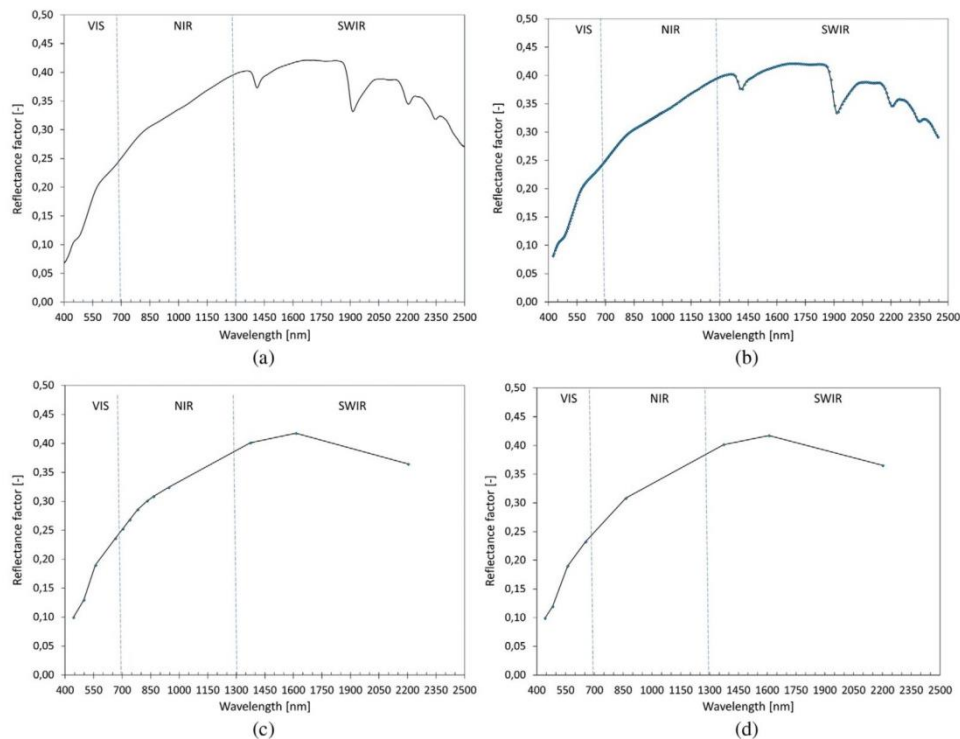


Fig. 6 Reflectance spectra of varying resolution for one of the soil samples: (a) original radiometric scan (2101 bands), (b) spectrum resampled to EnMAP bands (244), (c) spectrum resampled to Sentinel-2 bands,¹³ and (d) spectrum resampled to Landsat-8 optical bands.⁸

The effect of sensor spectral resolution on the spectrum can be visually appreciated in Fig. 6, whereas the shape and detail of EnMAP spectrum are very similar to the original spectrum, none of the absorption features can be seen in the broadband spectra of Sentinel-2 and Landsat-8, respectively.

4.2 Prediction of Soil Properties

Table 1 summarizes statistics estimating performance of the PLSR-SD models for SOM, silt, clay, and sand, whereas Fig. 7 shows scatter plots (modeled versus predicted values) illustrating the models fit. The results demonstrate that there is a relationship between the number of available predictors (reflectance bands) and the predictive capacity of the model: higher spectral resolution (greater number of narrower bands) of spectroradiometer and EnMAP bands explains higher predictive capacity of their models. The R^2 of models based on hyperspectral (ASD and EnMAP) and broadband data is around 0.07 to 0.15 for Sentinel-2 and 0.10 to 0.30 for Landsat-8, respectively.

The best results were achieved by the EnMAP and ASD models for SOM: $R_{cal}^2 = 0.89$ and $R_{val}^2 = 0.86$ for EnMAP, and $R_{cal}^2 = 0.88$ and $R_{val}^2 = 0.85$ for ASD. The performance of the ASD, EnMAP, and Sentinel-2 models predicting texture fractions was also quite good

Table 1 Statistics assessing performance of predictive model. R_{cal}^2 is the coefficient of determination for calibration dataset; R_{val}^2 is the coefficient of determination for validation dataset; the highest coefficient values are in bold; RMSEC, root mean square of calibration; and RMSEP, root mean square error of prediction.

	Components	Predictors	R_{cal}^2	RMSEC	R_{val}^2	RMSEP
SOM (g 100 g ⁻¹)						
ASD	10	10	0.882	1.286	0.847	1.685
EnMAP	10	58	0.892	2.221	0.861	1.614
Sentinel-2	10	11	0.814	1.625	0.773	2.044
Landsat-8	8	8	0.778	1.736	0.801	1.900
Silt (%)						
ASD	10	39	0.860	5.636	0.754	4.813
EnMAP	10	10	0.808	5.021	0.775	4.568
Sentinel-2	10	10	0.768	5.510	0.786	4.336
Landsat-8	6	6	0.543	7.527	0.424	7.020
Clay (%)						
ASD	10	42	0.834	4.992	0.733	4.516
EnMAP	10	38	0.806	5.086	0.761	4.870
Sentinel-2	10	13	0.707	4.961	0.673	4.955
Landsat-8	8	8	0.632	5.363	0.621	5.155
Sand (%)						
ASD	10	50	0.831	10.357	0.804	5.973
EnMAP	10	36	0.844	8.131	0.822	6.878
Sentinel-2	10	10	0.760	7.997	0.759	6.893
Landsat-8	8	8	0.568	10.566	0.500	9.797

Rosero-Vlasova et al.: Modeling soil organic matter and texture from satellite data in areas...

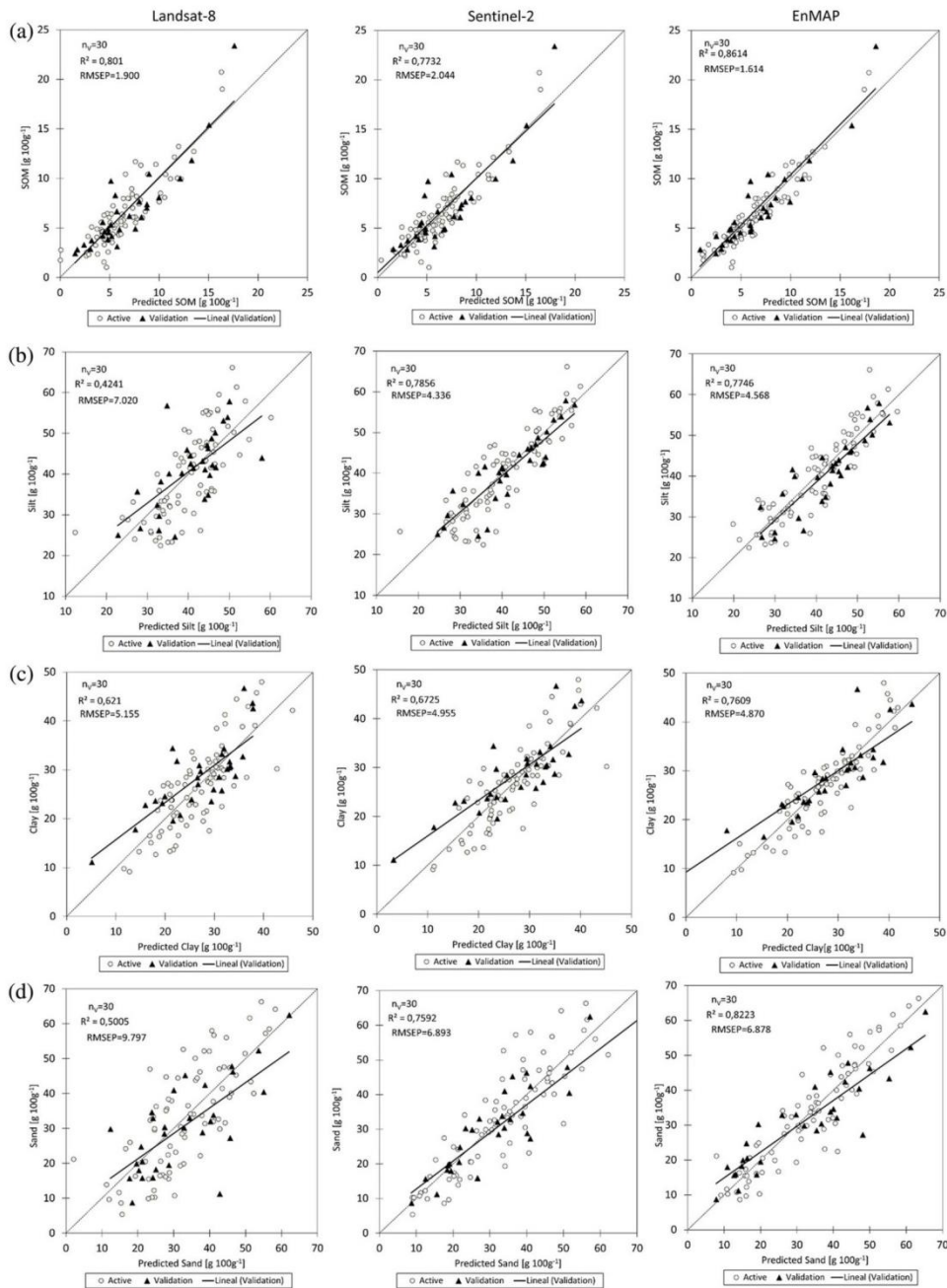


Fig. 7 Scatter plots of predicted versus observed values of (a) SOM, (b) silt, (c) clay, and (d) sand for models based on data simulated for Landsat-8, Sentinel-2, and EnMAP satellites. In each graphic, data points corresponding to calibration are shown with circles; data points corresponding to validation are shown with triangles.

(coefficients of determination for calibration and validation > 0.70). Models based on Landsat-8 bands were not so accurate: they could explain between 54% (silt) and 78% (SOM) of variance at calibration, and between 42% (silt) and 0.80% (SOM) at validation stages, whereas Sentinel-2 models showed R^2 in the ranges of 0.71 to 0.81 and 0.67 to 79 at calibration and validation, respectively. These results are in agreement with the earlier efforts in statistical modeling of SOM and soil texture.^{53,55,56} They also coincide with the information available for soils in other areas of LULC changes.^{15,57}

Rosero-Vlasova et al.: Modeling soil organic matter and texture from satellite data in areas...

Application of the step-down variable selection algorithm is especially important for the models based on bands of hyperspectral sensors, i.e., spectroradiometer and EnMAP. Variable selection allowed development of high-quality models (R^2 close or above 0.8) for all the modeled properties (SOM, silt, clay, and sand). The models using reflectances from ASD and EnMAP stand out because they are capable of obtaining accurate prediction while employing a few numbers of available predictors. Best ASD models use 10, 39, 42, and 50 bands, whereas EnMAP employ 58, 38, 10, and 36 reflectance bands out of more than 2000 to estimate SOM, clay, silt, and sand, respectively (Table 1).

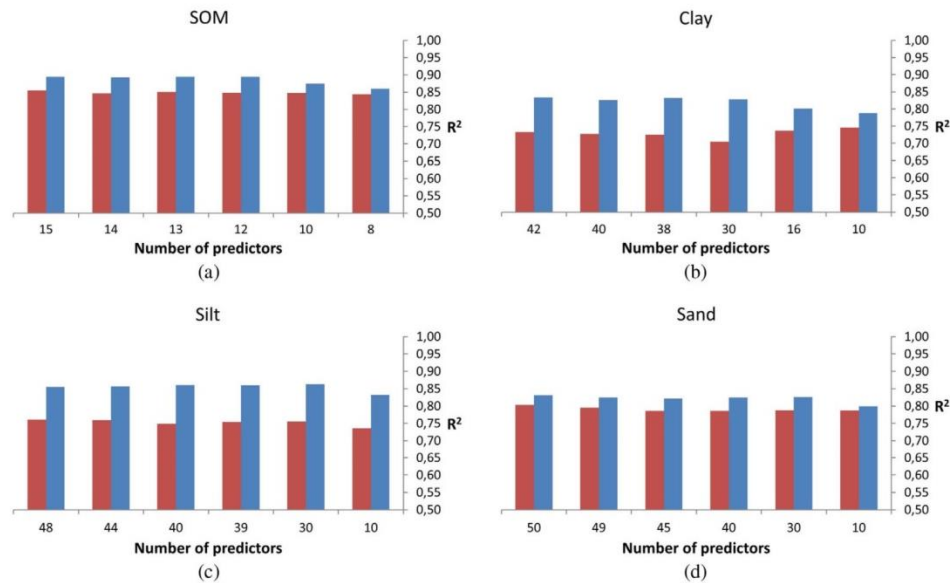


Fig. 8 Coefficients of determination R^2 for calibration (in blue) and validation (in red) of models based on original ASD bands: (a) SOM, (b) clay, (c) silt, and (d) sand. Horizontal axis shows the number of predictors.

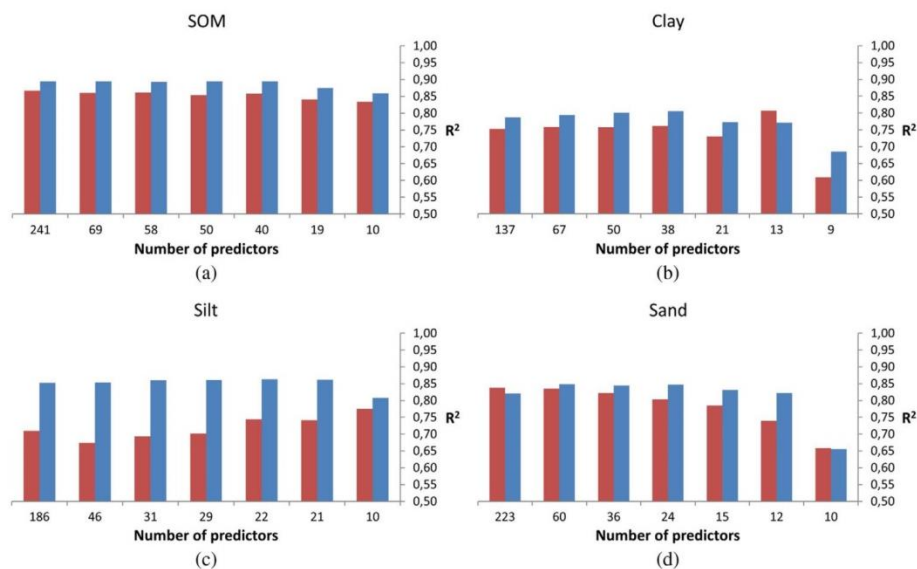


Fig. 9 Coefficients of determination R^2 for calibration (in blue) and validation (in red) of models based on simulated EnMAP bands: (a) SOM, (b) clay, (c) silt, and (d) sand. Horizontal axis shows the number of predictors.

To test the capabilities of the SD algorithm, we ran it several times on the same reflectance bands each time limiting the maximum number of predictors included in the final model to 70, 60, 50, 40, 30, and 10. The results of this test shown in Fig. 8 (spectroradiometer bands) and Fig. 9 (simulated EnMAP bands) reveal that even when limited to no more than 10 predictors, the algorithm was capable to create models whose quality was comparable with models based on the initially available number of bands. Moreover, SOM, clay, and sand models demonstrated almost the same or a little higher R^2 both for calibration (R_{cal}^2) and validation (R_{val}^2), which means that the values are not inflated by overfitting.⁴⁵

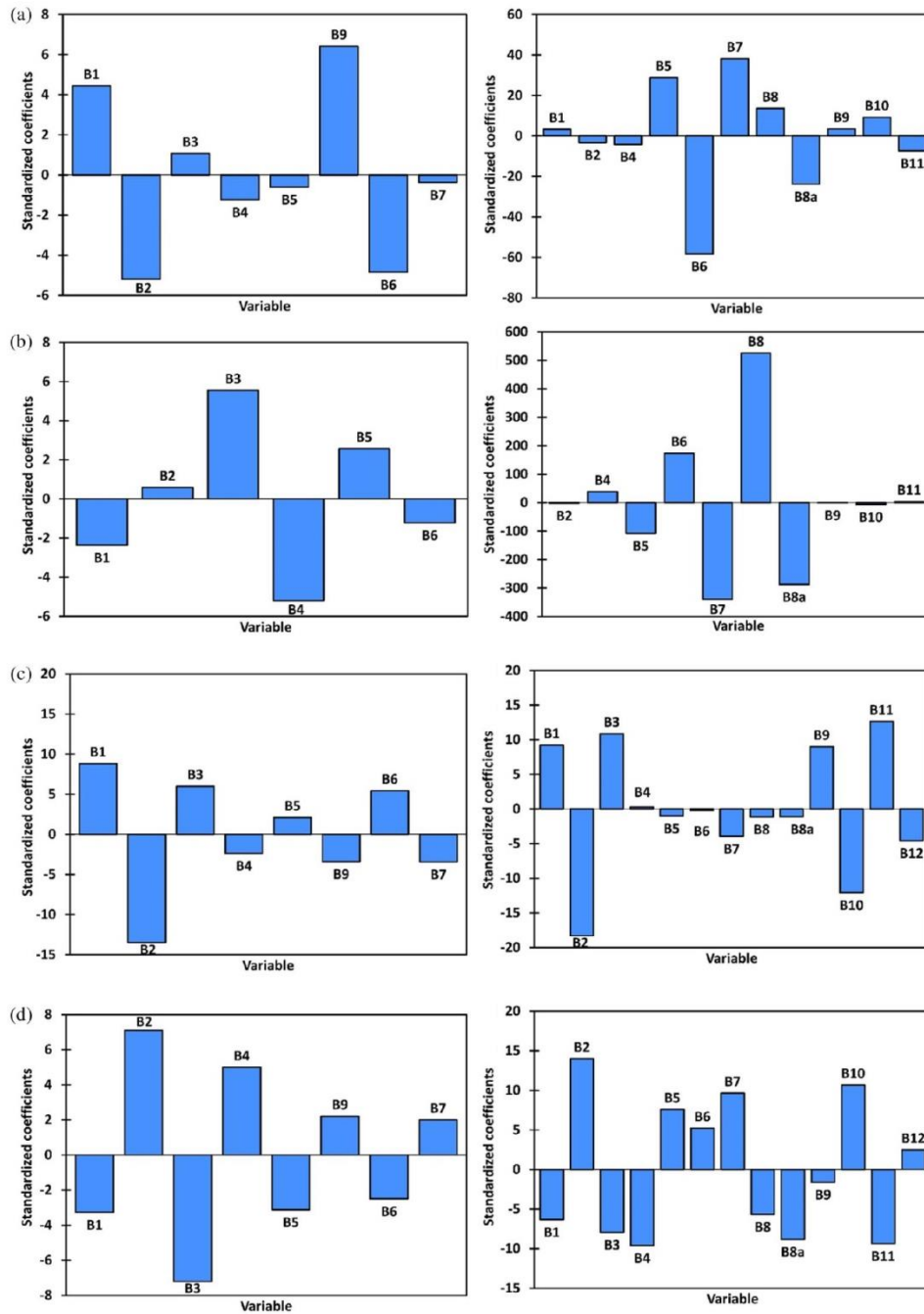


Fig. 10 Standardized coefficients of predictors in (left) Landsat-8 and (right) Sentinel-2 models for: (a) SOM, (b) silt, (c) clay, and (d) sand.

As soils represent a complex heterogeneous mixture of particles of a different form, size, and chemical composition, relating spectral bands and ranges to specific properties is not a simple task. Their importance can be assessed by analyzing coefficients of predictors included in the model (Fig. 10). SOM and sand models based on Landsat-8 data present the highest coefficients for the bands in visible and SWIR spectral regions, whereas predictions based on Sentinel reflectances contain the highest coefficients for the Vegetation Red Edge bands (B5, B6, and B7) not available for Landsat. As for the hyperspectral models (ASD and EnMAP), the results point to the wavelengths located in the 500 to 1000-nm and 2150- to 2300-nm ranges as the most relevant. These results are supported by numerous earlier published researches: it has been long recognized, that organic compounds are spectrally active through all the visible range;^{48,49} the importance of SWIR bands according to the recent review¹⁷ being related to the presence of nitrogen and carbon groups. The highest coefficients in the Sentinel-2 silt model also correspond to the vegetation red edge bands; the highest coefficients in the EnMAP silt models correspond to the wavelengths around 2080 and 2098 nm in the SWIR region. As for the clay predictions, the bands in blue and green visible, and SWIR bands appear as most relevant for all the sensors, except EnMAP, which gives more importance (bigger coefficients in absolute values) for the wavelengths >1830 nm. Importance of these wavelengths has been already reported in other studies.^{17,50} Further research on image data is necessary to assess the possibility of applying the spectral potential on the operational level.

5 Conclusions

The results confirm high potential of operational multispectral satellites (Landsat-8 and Sentinel-2) and even so of the EnMAP satellite data for detection and quantification of SOM, silt, clay, and sand in areas of LC changes due to the wildfires and cropland abandonment. The spectra of the analyzed soils are nonspecific, but due to the higher proportion of sand particles, reflectances of soils from the wildfire burns are in general higher compared with soils from the areas of cropland abandonment.

PLSR models were successful simultaneously predicting modeled soil properties with coefficients of determination around 0.80 for calibration and validation datasets. Predictions of the SOM content (R^2 around 0.90) are the most accurate. Combination of the PLSR and the step-down variable selection algorithm result in considerable model improvement, especially for hyperspectral data, producing sparser, and better-fit models.

Further research will be centered at the analysis of contribution of specific spectral ranges and wavelengths to soil reflectances.

Acknowledgments

This article was based on the presentation realized in the frame of the SPIE-Remote Sensing Conference (Remote Sensing for Agriculture, Ecosystems, and Hydrology session) held on 11–14 September 2017, in Warsaw, Poland. Authors appreciate the financial support provided to the first author of this article by Secretariat for Higher Education, Science, Technology, and Innovation (SENESCYT), Ecuador, grant no. 211–2012 in the initial stage of the research, following the funding received in the framework of the “Mobility Program for Latin Americans 2017/2018” of Bank Santander and University of Zaragoza. Soil samples from abandoned croplands were collected during the Marie Curie Intra-European Fellowship project “MED-AFFOREST” (PIEF-GA-2013-624974) and Estela Nadal-Romero was the recipient of a “Ramón y Cajal” postdoctoral contract (RYC-2013-14371, Spanish Ministry of Economy and Competitiveness). We are also grateful to Dr. Karl Segl and Dr. Theres Kuester for support with the graphics of EnMAP spectral response.

References

1. J. Hardesty, R. Myers, and W. Fulks, “Fire, ecosystems, and people: a preliminary assessment of fire as a global conservation issue,” *George Wright Forum* **22**, 78–87 (2005).
2. S. Chabrilat et al., “Field and imaging spectrometry for identification and mapping of expansive soils,” in *Imaging Spectrometry: Basic Principles and Prospective Applications*,

Rosero-Vlasova et al.: Modeling soil organic matter and texture from satellite data in areas...

- F. D. D. V. Meer and S. M. D. Jong, Eds., pp. 87–109, Springer, Dordrecht, The Netherlands (2001).
3. J. Goldammer, “Historical biogeography of fire: tropical and subtropical,” in *Fire in the Environment: The Ecological Atmospheric, and Climatic Importance of Vegetation Fires*, pp. 297–314, Wiley, New York (1993).
 4. G. Certini, “Effects of fire on properties of forest soils: a review,” *Oecologia* **143**(1), 1–10 (2005).
 5. J. M. García-Ruiz et al., “Erosion in mediterranean landscapes: changes and future challenges,” *Geomorphology* **198**, 20–36 (2013).
 6. E. Chirino et al., “Effects of 30-year-old Aleppo pine plantations on runoff, soil erosion, and plant diversity in a semi-arid landscape in south eastern Spain,” *Catena* **65**(1), 19–29 (2006).
 7. P. Porto, D. E. Walling, and G. Callegari, “Investigating the effects of afforestation on soil erosion and sediment mobilisation in two small catchments in Southern Italy,” *Catena* **79**(3), 181–188 (2009).
 8. E. D. C. C. Telles et al., “Influence of soil texture on carbon dynamics and storage potential in tropical forest soils of Amazonia,” *Global Biogeochem. Cycles* **17**(2), 1040 (2003).
 9. S. J. Goldman, T. A. Bursztynsky, and K. Jackson, *Erosion and Sediment Control Handbook*, McGraw-Hill, New York (1986).
 10. J. A. M. Demattê et al., “Visible-NIR reflectance: a new approach on soil evaluation,” *Geoderma* **121**(1–2), 95–112 (2004).
 11. O. Rosero-Vlasova et al., “Assessment of laboratory VIS-NIR-SWIR setups with different spectroscopy accessories for characterisation of soils from wildfire burns,” *Biosyst. Eng.* **152**, 51–67 (2016).
 12. S. Chabrilat et al., “Quantitative soil spectroscopy,” *Appl. Environ. Soil Sci.* **2013**, 1–3 (2013).
 13. J. A. Demattê et al., “Spectral sensing from ground to space in soil science: state of the art, applications, potential and perspectives,” in *Remote Sensing Handbook Vol. II: Land Resources Monitoring, Modeling, and Mapping with Remote Sensing*, P. S. Thenkabail, Ed., pp. 661–732, CRC Press, Taylor & Francis Group, Boca Raton, Florida (2016).
 14. P. Escribano et al., “Optical remote sensing for soil mapping and monitoring,” in *Soil Mapping and Process Modeling for Sustainable Land Use Management*, P. Pereira et al., Eds., pp. 87–125, Elsevier, Netherlands, United Kingdom (2017).
 15. Y. Ge, J. A. Thomasson, and R. Sui, “Remote sensing of soil properties in precision agriculture: a review,” *Front. Earth Sci.* **5**(3), 229–238 (2011).
 16. V. Mulder et al., “The use of remote sensing in soil and terrain mapping—a review,” *Geoderma* **162**(1–2), 1–19 (2011).
 17. E. Ben-Dor and J. Demattê, “Remote sensing of soil in the optical domains,” in *Land Resources Monitoring, Modeling, and Mapping with Remote Sensing*, P. S. Thenkabail, Ed., pp. 733–787, CRC Press, Boca Raton, Florida (2016).
 18. B. E. Hubbard and J. K. Crowley, “Mineral mapping on the Chilean–Bolivian Altiplano using co-orbital ALI, ASTER and hyperion imagery: data dimensionality issues and solutions,” *Remote Sens. Environ.* **99**(1–2), 173–186 (2005).
 19. A. Palacios-Orueta et al., “Remote sensing of soils in the Santa Monica Mountains: II. Hierarchical foreground and background analysis,” *Remote Sens. Environ.* **68**(2), 138–151 (1999).
 20. G. Forkuor et al., “Landsat-8 vs. Sentinel-2: examining the added value of sentinel-2’s red-edge bands to land-use and land-cover mapping in Burkina Faso,” *GISci. Remote Sens.* **55**(3), 331–354 (2018).
 21. E. Chuvieco and A. Huete, *Fundamentals of Satellite Remote Sensing*, CRC Press, Boca Raton, Florida (2010).
 22. B. Somers et al., “Endmember variability in spectral mixture analysis: a review,” *Remote Sens. Environ.* **115**(7), 1603–1616 (2011).
 23. F. García-Haro, S. Sommer, and T. Kemper, “A new tool for variable multiple endmember spectral mixture analysis (VMESMA),” *Int. J. Remote Sens.* **26**(10), 2135–2162 (2005).

24. G. Forkuor et al., “High resolution mapping of soil properties using remote sensing variables in South-Western Burkina Faso: a comparison of machine learning and multiple linear regression models,” *PLoS One* **12**(1), e0170478 (2017).
25. J. Ruiz de la Torre, “Distribución y características de las masas forestales españolas,” in *Revista Montes*, N^o. 86, Vol. **1**, 38–53 (2006).
26. D. Badía-Villas and F. del Moral, “Soils of the Arid areas,” in *The Soils of Spain*, J. F. Gallardo, Ed., pp. 145–161, Springer, Springer Cham, Heidelberg, New York, Dordrecht, London (2016).
27. J. M. Cuadrat and J. M. Vide, “Spanish climatology,” Past, Present and Future (2007).
28. E. Nadal-Romero et al., “Effects of secondary succession and afforestation practices on soil properties after cropland abandonment in humid Mediterranean mountain areas,” *Agric. Ecosyst. Environ.* **228**, 91–100 (2016).
29. F. Perez-Cabello et al., “Effects of fire on vegetation, soil and hydrogeomorphological behavior in mediterranean ecosystems,” in *Earth Observation of Wildland Fires in Mediterranean Ecosystems*, E. Chuvieco, Ed., pp. 111–128, Springer, Berlin, Heidelberg (2009).
30. D. J. Brown et al., “Global soil characterization with VNIR diffuse reflectance spectroscopy,” *Geoderma* **132**(3), 273–290 (2006).
31. A. Stevens et al., “Prediction of soil organic carbon at the European scale by visible and near infrared reflectance spectroscopy,” *PloS One* **8**(6), e66409 (2013).
32. J. A. M. Demattê and F. da Silva Terra, “Spectral pedology: a new perspective on evaluation of soils along pedogenetic alterations,” *Geoderma* **217–218**, 190–200 (2014).
33. R. Viscarra Rossel and T. Behrens, “Using data mining to model and interpret soil diffuse reflectance spectra,” *Geoderma* **158**(1), 46–54 (2010).
34. <https://landsat.gsfc.nasa.gov>.
35. M. Drusch et al., “Sentinel-2: ESA’s optical high-resolution mission for GMES operational services,” *Remote Sens. Environ.* **120**, 25–36 (2012).
36. <https://earth.esa.int/web/sentinel/>.
37. K. Segl et al., “EeteS—The EnMAP end-to-end simulation tool,” *IEEE J. Sel. Top. Appl. Earth Obs. Remote Sens.* **5**(2), 522–530 (2012).
38. <http://www.EnMAP.org>.
39. E. U. S. Guide, “ENVI on-line software user’s manual,” ITT Visual Information Solutions (2008).
40. Soil Survey, “Soil survey staff soil survey manual,” Washington, DC (1993).
41. M. Tenenhaus, *La Régression PLS: Théorie et Pratique*, Editions Technip, Paris, France (1998).
42. S. Wold, M. Sjöström, and L. Eriksson, “PLS-regression: a basic tool of chemometrics,” *Chemom. Intell. Lab. Syst.* **58**(2), 109–130 (2001).
43. L. Kooistra et al., “The potential of field spectroscopy for the assessment of sediment properties in river floodplains,” *Anal. Chim. Acta* **484**(2), 189–200 (2003).
44. R. A. Viscarra Rossel et al., “Visible, near infrared, mid infrared or combined diffuse reflectance spectroscopy for simultaneous assessment of various soil properties,” *Geoderma* **131**(1–2), 59–75 (2006).
45. M. A. Babyak, “What you see may not be what you get: a brief, nontechnical introduction to overfitting in regression-type models,” *Psychosom. Med.* **66**(3), 411–421 (2004).
46. H. Chun and S. Keles, “Sparse partial least squares regression for simultaneous dimension reduction and variable selection,” *J. R. Stat. Soc.: Ser. B (Stat. Methodol.)* **72**(1), 3–25 (2010).
47. G. Bennett, “Regression modelling with many correlated predictors and few cases,” in *Presentation in ASSESS Event*, United Kingdom (2013).
48. E. Ben-Dor, J. R. Irons, and G. F. Epema, “Soil reflectance,” in *Remote Sensing for the Earth Sciences*, A. N. Rencz, Ed., pp. 111–188, John Wiley & Sons, New York (1999).
49. E. R. Stoner and M. Baumgardner, “Characteristic variations in reflectance of surface soils,” *Soil Sci. Soc. Am. J.* **45**(6), 1161–1165 (1981).
50. G. R. Hunt and J. W. Salisbury, “Visible and near infrared spectra of minerals and rocks. II. Carbonates,” *Mod. Geol.* **2**, 23–30 (1971).

Rosero-Vlasova et al.: Modeling soil organic matter and texture from satellite data in areas...

51. B. Stenberg et al., "Chapter five-visible and near infrared spectroscopy in soil science," *Adv. Agron.* **107**, 163–215 (2010).
52. E. Ben-Dor et al., "Using imaging spectroscopy to study soil properties," *Remote Sens. Environ.* **113**(Suppl. 1), S38–S55 (2009).
53. M. Conforti et al., "Visible and near infrared spectroscopy for predicting texture in forest soil: an application in southern Italy," *iForest—Biogeosci. For.* **8**(3), 339–347 (2015).
54. R. A. Viscarra Rossel, R. N. McGlynn, and A. B. McBratney, "Determining the composition of mineral-organic mixes using UV-vis–NIR diffuse reflectance spectroscopy," *Geoderma* **137**(1–2), 70–82 (2006).
55. V. Bellon-Maurel and A. McBratney, "Near-infrared (NIR) and mid-infrared (MIR) spectroscopic techniques for assessing the amount of carbon stock in soils-critical review and research perspectives," *Soil Biol. Biochem.* **43**(7), 1398–1410 (2011).
56. A. M. Mouazen et al., "Comparison among principal component, partial least squares and back propagation neural network analyses for accuracy of measurement of selected soil properties with visible and near infrared spectroscopy," *Geoderma* **158**(1), 23–31 (2010).
57. M. Knadel et al., "Comparing predictive abilities of three visible-near infrared spectrophotometers for soil organic carbon and clay determination," *J. Near Infrared Spectrosc.* **21**(1), 67–80 (2013).

Olga A. Rosero-Vlasova is a PhD student from Ecuador at the Department of Geography and Land Management, University of Zaragoza, Spain. She received her engineering degree in electronics from National Polytechnic School, Ecuador, in 2009 and obtained her master's degree in environmental technology from the University of Huelva, Spain, in 2012. Her research interests include monitoring of ecosystems affected by wildfires, slash-and-burn agriculture and cropland abandonment, especially proximal and remote sensing of soils in these areas.

Lidia Vlassova lives and works in Quevedo, Ecuador. She obtained her MA degree in geography from Moscow State University, Russia (1981), her MA degree from the University of Cincinnati, USA (2002), and her PhD from the University of Zaragoza, Spain (2016), and is now a faculty member of Department of Environmental Sciences, Technical State University of Quevedo. Her research focuses on environmental applications of thermal remote sensing.

Fernando Pérez-Cabello is a professor at the Department of Geography and Land Management of University of Zaragoza. He got his PhD and MS degrees in geography from the University of Zaragoza, Spain, 2001 and 1997, respectively. Results of his research focusing on application of GIS and remote sensing in multitemporal analysis of areas affected by wildfire burns and have been made public during multiple scientific events and publications.

Raquel Montorio received her PhD in geography and her MS degree in GIS and remote sensing from the University of Zaragoza, Spain, in 2014 and 2005, respectively. In 2010, she started working as assistant professor at Department of Geography and Land Management of University of Zaragoza. Her research focuses on management of forest areas, primarily on the postfire forest dynamics. In her research, she uses a combination of field spectrometry and remote sensing methods along with statistical modeling.

Estela Nadal-Romero got her degree in geography from the University of Zaragoza, Spain, 1999–2003. In 2008, she presented her PhD on weathering and erosion processes in badland areas. She has been awarded postdoctoral contracts by the Katholieke Universiteit Leuven (Belgium), University of Amsterdam (The Netherlands), and University of Zaragoza (Spain). Her research is devoted to the integration of knowledge derived from the geomorphological, hydrological, climatological, soil science, and ecological disciplines for the study of Mediterranean mountain areas.

8.2. Case study of Campos Amazônicos National Park savanna enclave, Brazil

This section in the chapter reproduces the text of the following article:

Title:

Modeling soil organic matter (SOM) from satellite data using VISNIRSWIR spectroscopy and PLS regression with step-down variable selection algorithm: case study of Campos Amazônicos National Park.

Authors:

O. Rosero-Vlasova

D. Borini Alves

L. Vlassova

F. Pérez-Cabello

R. Montorio Llovería

PROCEEDINGS OF SPIE

SPIEDigitalLibrary.org/conference-proceedings-of-spie

Modeling soil organic matter (SOM) from satellite data using VIS-NIR-SWIR spectroscopy and PLS regression with step-down variable selection algorithm: case study of Campos Amazonicos National Park savanna enclave, Brazil.

Rosero-Vlasova O.^{1*}, Borini Alves D.¹, Vlassova L.², Perez-Cabello F.¹, Montorio Lloveria R.¹

¹University of Zaragoza, Pedro Cerbuna 12, 50006 Zaragoza, Spain, oarosero@unizar.es

²Technical State University of Quevedo, Ecuador

ABSTRACT

Deforestation in Amazon basin due, among other factors, to frequent wildfires demands continuous post-fire monitoring of soil and vegetation. Thus, the study posed two objectives: (1) evaluate the capacity of Visible – Near InfraRed – ShortWave InfraRed (VIS-NIR-SWIR) spectroscopy to estimate soil organic matter (SOM) in fire-affected soils, and (2) assess the feasibility of SOM mapping from satellite images. For this purpose, 30 soil samples (surface layer) were collected in 2016 in areas of grass and riparian vegetation of Campos Amazonicos National Park, Brazil, repeatedly affected by wildfires. Standard laboratory procedures were applied to determine SOM. Reflectance spectra of soils were obtained in controlled laboratory conditions using Fieldspec4 spectroradiometer (spectral range 350nm–2500nm). Measured spectra were resampled to simulate reflectances for Landsat-8, Sentinel-2 and EnMap spectral bands, used as predictors in SOM models developed using Partial Least Squares regression and step-down variable selection algorithm (PLSR-SD). The best fit was achieved with models based on reflectances simulated for EnMap bands ($R^2=0.93$; $R^2_{cv}=0.82$ and $NMSE=0.07$; $NMSE_{cv}=0.19$). The model uses only 8 out of 244 predictors (bands) chosen by the step-down variable selection algorithm. The least reliable estimates ($R^2=0.55$ and $R^2_{cv}=0.40$ and $NMSE=0.43$; $NMSE_{cv}=0.60$) resulted from Landsat model, while Sentinel-2 model showed $R^2=0.68$ and $R^2_{cv}=0.63$; $NMSE=0.31$ and $NMSE_{cv}=0.38$. The results confirm high potential of VIS-NIR-SWIR spectroscopy for SOM estimation. Application of step-down produces sparser and better-fit models. Finally, SOM can be estimated with an acceptable accuracy ($NMSE\sim 0.35$) from EnMap and Sentinel-2 data enabling mapping and analysis of impacts of repeated wildfires on soils in the study area.

KEYWORDS: Soil Organic Matter (SOM), VIS-NIR-SWIR spectroscopy, Landsat, Sentinel-2, EnMap, PLSR, step-down variable selection algorithm (SD)

1. INTRODUCTION

Tropical savannas locally known as Cerrado occupy more than 2 million km² and are among the most important biomes in Brazil [1]. These areas are prone to wildfires, which have long been a natural process for their development [2]. However, at present, due to human activities and climate change, the number and intensity of wildfires are experiencing continuous increase [3]. Frequent high intense fire influence modifies physical and chemical characteristics of soils, triggering erosion and soil losses [4]. Thus, monitoring of changes in soil properties after fire is of great importance since it provides information for decisions related to choice of landscape management practices.

One of the tools gaining popularity for regular estimation of key soil variables, such as organic matter and texture, is proximal sensing, also known as soil spectroscopy [5, 6]. It offers a cost-effective alternative to traditional laboratory methods of soil analysis. Spectral signatures obtained with spectroradiometers can be integrated with data obtained by satellite remote sensing and used for soil mapping and analysis [7, 8]. Coexistence and availability of compatible data from multiple satellites, such as Landsat-8, Sentinel-2A/B (orbiting the Earth since February, 2013 and June,

* Corresponding author.

E-mail address: oarosero@unizar.es (O.A. Rosero-Vlasova)

Remote Sensing for Agriculture, Ecosystems, and Hydrology XIX, edited by Christopher M. U. Neale, Antonino Maltese, Proc. of SPIE Vol. 10421, 104210V © 2017 SPIE · CCC code: 0277-786X/17/\$18 · doi: 10.1117/12.2278701

Proc. of SPIE Vol. 10421 104210V-1

2015/March, 2017, respectively), and the launch of satellites expected to provide data of even higher resolution in near future (EnMap scheduled for 2019) opens new possibilities for land surface monitoring and sustainable management.

In this context, the study posed two objectives: (1) to evaluate the capacity of Visible – Near InfraRed – ShortWave InfraRed (VIS-NIR-SWIR) spectroscopy to estimate Soil Organic Matter (SOM) content in fire-affected soils for their further discrimination, and (2) to assess the feasibility of SOM mapping from images of the three last generation satellites (Landsat-8, Sentinel-2 and EnMap).

2. STUDY AREA AND DATA

Study area is located in Campos Amazonicos Savanna Enclave (CASE), Brazil, a continuous area of savanna vegetation in a region dominated by rainforest (Figure 1a) [9]. It spreads over 4342 km² and is considered one of the biggest savanna enclaves in Amazon [10]. Currently, 47% of the CASE belong to the limits of the Campos Amazonicos National Park (CANP). Vegetation is not restricted to savanna-type; it varies from grasslands to forests [11]. Detailed distribution of vegetation can be appreciated in Figure 1b, showing Landsat Vegetation Continuous Field tree cover layer for 2015. Grasslands, shrubby grasslands and shrubby savanna predominate in the interfluvial areas, while forested areas are mainly located in the proximity of the streams (riparian vegetation).

The climate is characterized by mean annual temperatures in the range of 24°C-28°C, and average annual rainfall up to 2000mm. There are two seasons, wet (November-March) and dry (May-September); April and October usually correspond to the transition between the two seasons [12]. Typical soils are neosols marked by the presence of plinthite in the B horizon [10, 13].

Field campaign which included collection of soil samples was realized in September 2016 in parts of CASE within CANP, which are characterized by different wildfire [14]. Soil samples were obtained from surface layer (0-10cm) in areas of shrubby grassland (15 samples) and riparian (15 samples) vegetation. Sampled locations are shown in Figure 1c.

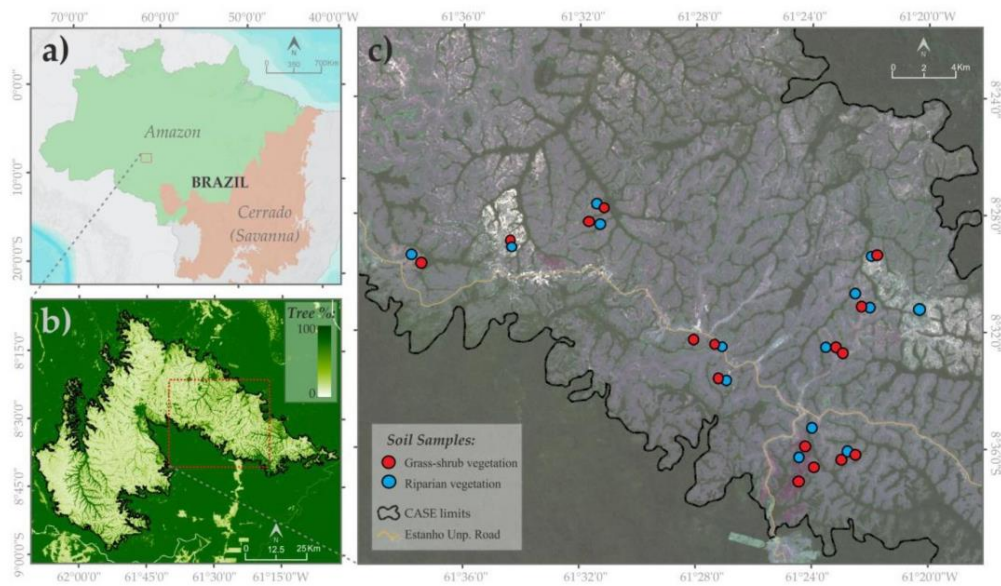


Figure 1. Map of the study area: a) the CASE in the middle of Brazilian Amazon biome; b) tree cover (% per pixel); c) location of soil sampling sites.

3. METHODOLOGY

Reference SOM values were determined using wet combustion, which is the standard laboratory procedure. Spectral measurements were performed on air-dried sieved (particle size <2mm) samples placed in Petri dishes (90 mm in diameter, ~15mm high). Reflectance spectra of soils were obtained in controlled laboratory conditions using Fieldspec4 spectro-radiometer (spectral range 350nm–2500nm). We used ASD Illuminator halogen lamp as a light source. Observation geometry was determined considering (i) distance between the target and the sensor, (ii) distance between the target and the source of illumination, and (iii) the angle between the two. This setup (Figure 2) demonstrated reliability in our previous research [6].



Figure 2. Laboratory setup used for spectral measurements.

Measured high resolution spectra were resampled to simulate reflectance values for Landsat-8, Sentinel-2 and EnMap optical spectral bands (8, 13 and 244 bands, respectively) in VIS, NIR and SWIR spectral regions. Since obtained spectra demonstrated high stability, no spectral pre-processing was performed.

Bands from measured soil spectra and simulated reflectance values were used as predictors in SOM models. Models based on original laboratory-measured soil spectra considered 21 bands, which according to previous research have the highest information content on SOM and other soil properties [15]. Two outliers detected by initial Principal Components Analysis were excluded from the set of predictors resulting in 28 analyzed soil samples.

Modeling was performed using Partial Least Squares regression [16, 17]. Due to its capacity to deal with a great number of predictors PLSR is routinely applied in soil VIS-NIR spectroscopy (e.g. [18, 19]). In this study it was combined with the step-down variable selection algorithm (PLSR-SD). The step-down variable selection algorithm reduces the number of variables without the loss of information through elimination of the less important variables during the process of cross-validation [20]. The procedure was run with 10 rounds of 7-fold cross-validation.

Model performance was assessed using the determination coefficient of the model (R^2), the determination coefficient of cross-validation (R^2_{CV}) and the Normed Root-Mean-Square Error (NMSE).

4. RESULTS AND DISCUSSION

Reflectance spectra of samples (Figure 3) present the shape with very few absorption features, which is typical for soils [21]. There is a lot of similarity, but there are also observable differences between particular curves: the absorption features, e.g. near 1400nm and 1900nm (due to presence of water and O-H group) [22], are small in some spectra and more pronounced in the others, probably due to the heterogeneity of the dataset [23], one of the reasons of this heterogeneity being differences in SOM content [24].

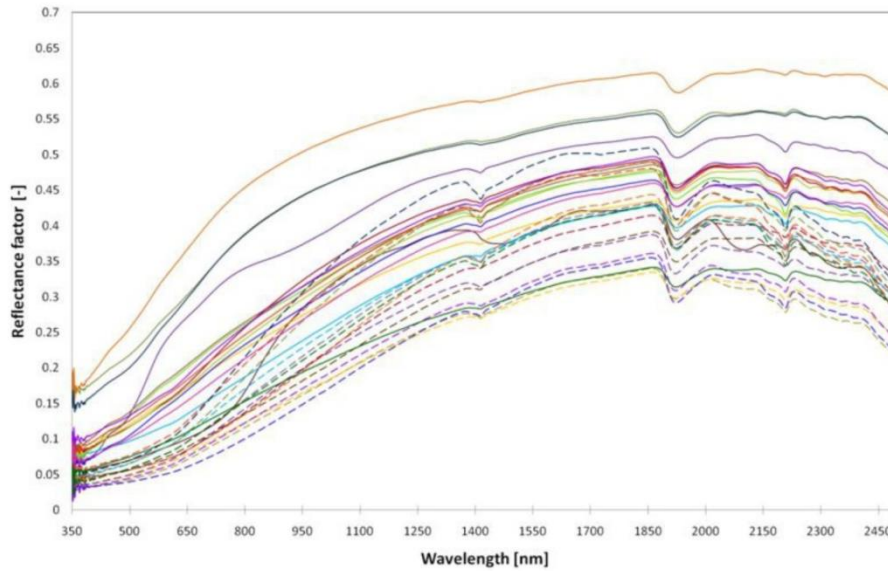


Figure 3. Reflectance spectra of soil samples.

Table 1 summarizes statistics estimating performance of the PLSR-SD models for SOM, while Figure 4 shows scatter plots (modeled versus predicted SOM values) illustrating fit of SOM models based on reflectances from bands simulated for three satellites (Landsat-8, Sentinel-2 and EnMap) and original bands from measured spectra (21 selected bands). The results demonstrate that there is the relationship between the number of available predictors (reflectance bands) and the predictive capacity of the model: higher spectral resolution (greater number of narrower bands) corresponds to higher predictive capacity of the SOM model.

Table 1. Statistics assessing quality of SOM models.

		PLSR_SD	NMSE	f	Factors
21 bands	R^2	0.909	0.088	7	7
	R^2_{CV}	0.830	0.168		
EnMap	R^2	0.929	0.068	8	7
	R^2_{CV}	0.816	0.189		
Sentinel-2	R^2	0.682	0.306	10	1
	R^2_{CV}	0.617	0.375		
Landsat-8	R^2	0.549	0.435	2	2
	R^2_{CV}	0.401	0.601		

Thus, the best model based on 21 original bands with 7 predictors chosen by the SD algorithm produced SOM values very close to the reference ($R^2_{cal}=0.909\%$; $R^2_{cv}=0.83\%$ and Normed Mean Square Error $NMSE_{cal}=0.09$; $NMSE_{cv}=0.18$ for calibration and cross-validation, respectively). Very similar results were achieved with models based on reflectances simulated for EnMap bands ($R^2=0.93$; $R^2_{cv}=0.82$ and $NMSE=0.07$; $NMSE_{cv}=0.19$). This quality was achieved by the model with only 8 out of 244 predictors (bands) chosen by the step-down variable selection algorithm. The least reliable estimates ($R^2=0.55$ and $R^2_{cv}=0.40$ and $NMSE=0.43$; $NMSE=0.60$) resulted from Landsat-8 model (bands 6 and 8 as predictors), while Sentinel-2 model (10 predictors) showed $R^2=0.68$ and $R^2_{cv}=0.63$; $NMSE=0.31$ and $NMSE_{cv}=0.38$.

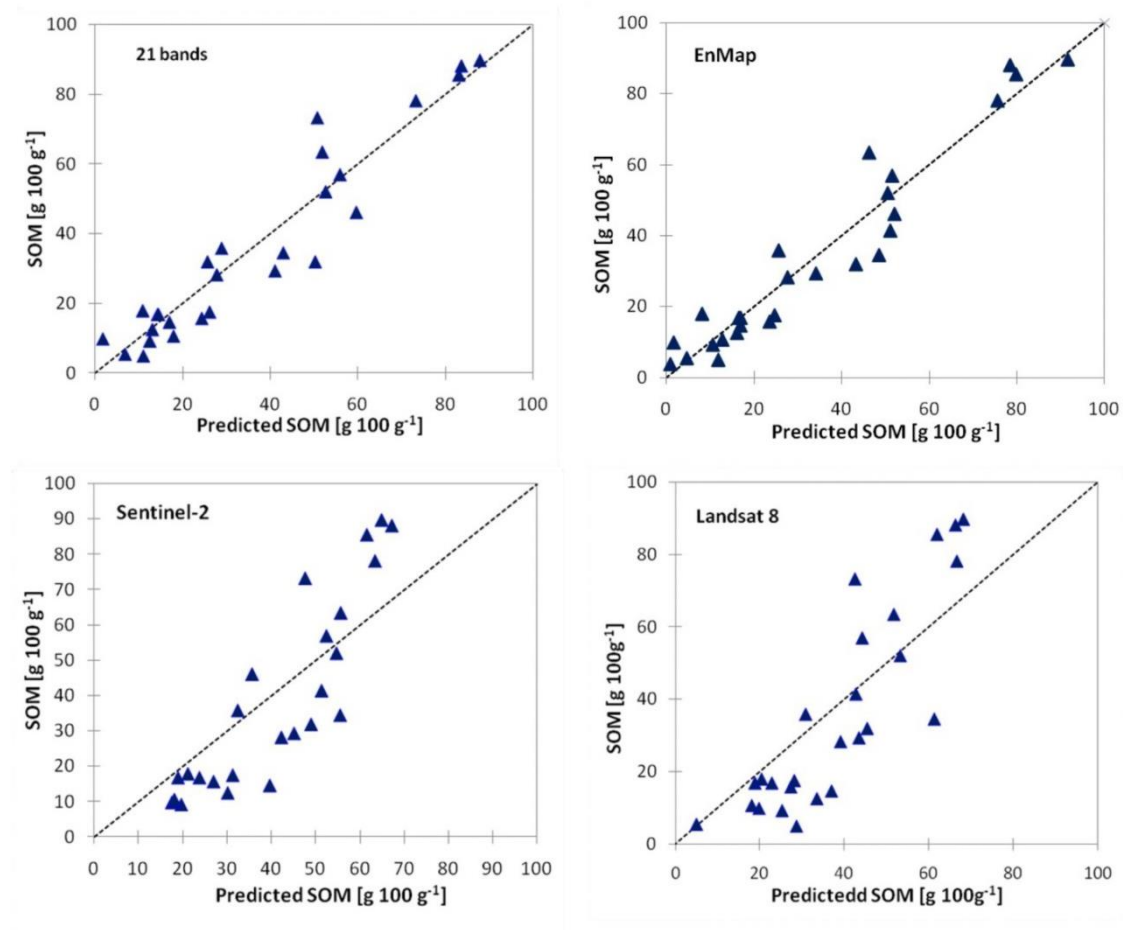


Figure 4. Scatter plots of predicted versus observed SOM values for models based on data from (a) original bands measured by spectroradiometer; bands simulated for the following satellites (b) EnMap, (c) Sentinel-2, and (d) Landsat-8.

CONCLUSIONS

The results confirm high potential of VIS-NIR-SWIR spectroscopy as a flexible and cost-effective alternative for determining SOM content in soil samples in laboratory conditions. Application of step-down variable selection algorithm resulted in considerable model improvement producing sparser and better-fit models. We conclude that SOM can be

estimated with an acceptable accuracy (NMSE=0.35) from EnMap hyperspectral and Sentinel-2 multispectral satellite images providing the basis for mapping and analysis of impacts of repeated wildfires on soils in the study area.

ACKNOWLEDGEMENTS

Authors appreciate financial support provided to the first author of this article by Secretariat for Higher Education, Science, Technology and Innovation (SENESCYT), Ecuador, grant no. 211-2012. We also thank the CAPES Foundation (Brazil) for the grant (process number 9540-13-0) given to Daniel Borini Alves. We are also grateful to Bruno Contursi Cambraia and all the team of the Campos Amazônicos National Park for help in data collection and for encouragement of research development.

REFERENCES

- [1] Cavalcanti, R. B., Joly, C. A. "Biodiversity and conservation priorities in the Cerrado region," The cerrados of Brazil: ecology and natural history of a neotropical savanna, Columbia University Press, New York, USA, 351-367 (2002).
- [2] Hardesty, J., Myers, R., and Fulks, W., "Fire, ecosystems, and people: a preliminary assessment of fire as a global conservation issue." *Fire Management*, 22 (4), 78-87 (2005).
- [3] Goldammer, J., "Historical biogeography of fire: tropical and subtropical," *Fire in the environment: the ecological atmospheric, and climatic importance of vegetation fires*. Wiley, New York, 297-314 (1993).
- [4] Certini, G., "Effects of fire on properties of forest soils: a review," *Oecologia*, 143(1), 1-10 (2005).
- [5] Demattê, J. A. M., Campos, R. C., Alves, M. C. *et al.*, "Visible-NIR reflectance: a new approach on soil evaluation," *Geoderma*, 121(1-2), 95-112 (2004).
- [6] Rosero-Vlasova, O. A., Pérez-Cabello, F., Llovería, R. M. *et al.*, "Assessment of laboratory VIS-NIR-SWIR setups with different spectroscopy accessories for characterisation of soils from wildfire burns," *Biosystems Engineering*, (2016).
- [7] Chabrilat, S., Ben-Dor, E., Rossel, R. A. V. *et al.*, "Quantitative soil spectroscopy," *Applied and Environmental Soil Science*, (2013).
- [8] Demattê, J., Morgan, C., Chabrilat, S. *et al.*, "Spectral sensing from ground to space in soil science: State of the art, applications, potential and perspectives," *Land Resources Monitoring, Modeling, and Mapping with Remote Sensing*, CRC Press, Boca Raton, USA, 661-732 (2015).
- [9] Ratter, J. A., Bridgewater, S., and Ribeiro, J. F., "Analysis of the floristic composition of the Brazilian cerrado vegetation III: comparison of the woody vegetation of 376 areas," *Edinburgh journal of botany*, 60(1), 57-109 (2003).
- [10] ICMBio, Chico Mendes Institute for Biodiversity Conservation, [Management plan of Campos Amazônicos National Park], ICMBIO/MMA, Brasília, Brazil, (2016).
- [11] Oliveira-Filho, A. T., and Ratter, J. A., "Vegetation physiognomies and woody flora of the cerrado biome," *The cerrados of Brazil: ecology and natural history of a neotropical savanna*, Columbia University Press, New York, USA, 91-120 (2002).
- [12] Marengo, J. A., Nobre, C. A., Tomasella, J. *et al.*, "The drought of Amazonia in 2005," *Journal of Climate*, 21(3), 495-516 (2008).
- [13] Motta, P. E., Curi, N., and Franzmeier, D. P., "Relation of soils and geomorphic surfaces in the Brazilian Cerrado," *The cerrados of Brazil: ecology and natural history of a neotropical savanna*, Columbia University Press, New York, USA, 13-32 (2002).
- [14] Alves, D. B., and Pérez-Cabello, F., "Multiple remote sensing data sources to assess spatio-temporal patterns of fire incidence over Campos Amazônicos Savanna Vegetation Enclave (Brazilian Amazon)," *Science of The Total Environment*, 601, 142-158 (2017).
- [15] Demattê, J. A. M., and Da Silva Terra, F., "Spectral pedology: A new perspective on evaluation of soils along pedogenetic alterations," *Geoderma*, 217-218(0), 190-200 (2014).
- [16] Tenenhaus, M., [La régression PLS: théorie et pratique] Editions Technip, Paris, France, (1998).
- [17] Wold, S., Sjöström, M., and Eriksson, L., "PLS-regression: a basic tool of chemometrics," *Chemometrics and intelligent laboratory systems*, 58(2), 109-130 (2001).
- [18] Kooistra, L., Wanders, J., Epema, G. F. *et al.*, "The potential of field spectroscopy for the assessment of sediment properties in river floodplains," *Analytica Chimica Acta*, 484(2), 189-200 (2003).

CHAPTER 8. Modeling soil organic matter and texture from satellite data

- [19] Viscarra Rossel, R. A., McGlynn, R. N., and McBratney, A. B., "Determining the composition of mineral-organic mixes using UV-vis-NIR diffuse reflectance spectroscopy," *Geoderma*, 137(1-2), 70-82 (2006).
- [20] Magidson, J., "Correlated component regression: Re-thinking regression in the presence of near collinearity," *New perspectives in partial least squares and related methods*, Springer, New York, USA, 65-78 (2013).
- [21] Stoner, E. R., and Baumgardner, M., "Characteristic variations in reflectance of surface soils," *Soil Science Society of America Journal*, 45(6), 1161-1165 (1981).
- [22] Hunt, G. R., and Salisbury, J. W., "Visible and near infrared spectra of minerals and rocks. II. Carbonates," *Modern Geology*, 2, 23-30 (1971).
- [23] Ge, Y., Thomasson, J. A., and Sui, R., "Remote sensing of soil properties in precision agriculture: A review," *Frontiers of Earth Science*, 5(3), 229-238 (2011).
- [24] Ben-Dor, E., Irons, J. R., and Epema, G. F., [Soil reflectance], John Wiley & Sons, New York, USA, (1999).

9. Conclusions and future research

This study deals with application of soil spectroscopy in VIS-NIR-SWIR (400-2500nm) spectral regions for estimation of organic matter (SOM) content and texture (percent of sand, silt and clay) of soils which suffered from anthropogenic disturbances (controlled agricultural burning and cropland abandonment) and wildfires. It uses soil samples collected at different locations: areas affected by wildfires in Campos Amazônicos National Park in Brazil, areas of agricultural burns in Mocache district on Ecuadorian coast, and burns and abandoned croplands in Aragón (Spain), the latter being the data source. The main findings of this research are presented below.

During last decades in a great number of publications present proximal soil sensing as a relatively low cost technology for estimation of soil properties in controlled laboratory conditions using different commercially available accessories. However, at present there is no consensus on which experimental setup, the accessories and the protocol are the most suitable for each particular situation. In this context, the study compared laboratory setups with different spectroscopic accessories applied for soil spectral measurements: (1) integrating sphere in the setup IS; (2) ASD illuminating sphere and pistol grip in the setup L; and (3) contact probe in the setup CP. The results demonstrated that:

- The highest reflectance values correspond to the setup CP and the lowest to the setup IS.
- Spectral curves obtained with setup CP are characterized by greater stability and show lower coefficients of variation compared to other setups.
- Soil spectra obtained with setup IS show considerable noise at wavelengths less than 400 nm and wavelengths greater than 2300 nm.
- Application of soil spectra in development of predictive models with standard method of partial least squares regression (PLSR) yielded the best results produced with the L setup. The differences between estimations realized with the models based on data obtained with different laboratory setups were up to 11% for calibration models and 8% for validation models.

Because of good results obtained with setup L, it was considered to be the optimum configuration for spectral measurements of soils from the areas of study.

The determination of the most appropriate statistical method for modeling of soil organic matter content and texture was approached through comparison of the following methods: (i) partial least squares regression using the full range of available reflectances as predictors (PLSR-full); (ii) partial least squares regression using as predictors the bands selected by Martens uncertainty test (PLSR-MUT); as well as a novel statistical method of (c) correlated components regression with step-down variable selection algorithm (CCR-SD). In general terms, all statistical approaches were capable of generating good quality models ($R^2 > 0.7$), especially in case of organic matter ($R^2 > 0.8$). Models created using CCR-SD demonstrated the best predictive capacity estimating organic matter content, clay, silt and sand at calibration and validation stages (R^2 in the range of 0.80-0.86 and 0.70-0.87, respectively). Besides good fit, CCR-SD models stand out for their parsimony, i.e. they are capable of achieving parameters/soil properties with the same or better precision as other methods employing fewer predictors.

Analysis of soil properties estimations allowed the identification of certain patterns in their spectral behavior. For soils analyzed in this study, the spectral regions particularly important for SOM predictions include 500–550, 750-830, 850-930, 1000–1050, 1500–1550, 1800–1910, 2200–2230, 2260-2280 and 2310–2360 nm, with reflectance levels affected mainly by the presence of water and C-O, C=O, and N-H links in organic molecules. On the other hand, although absorption features related to clay minerals appeared masked by the spectral influence of the relatively high organic matter content in the analyzed soil samples, the highest coefficients in clay models correspond to the bands related to kaolinite (1395, 1414 and 2205 nm) and illite (1414, 2205 and 2300-2340 nm).

Finally, laboratory analysis of VIS-NIR-SWIR spectra confirmed high potential of three last generation satellites (Landsat-8, Sentinel-2 and EnMAP) in estimation of organic matter content and texture of analyzed soils. It was observed that apart from location of the satellite reflectance bands within the electromagnetic spectrum, the predictive capacity of the model is related to the number of available predictors. Hence, greater number of bands in EnMAP images is one of the factors explaining higher predictive capacity of corresponding models. The results of this research demonstrate that SOM and sand models based on Landsat-8 data present the highest coefficients for the bands in visible and SWIR spectral regions; whereas predictions based on Sentinel-2

reflectances contain the highest coefficients for the Vegetation Red Edge bands (B5, B6, and B7).

Considering the results of the present research further advances in development of statistical models estimating soil properties is deemed of great importance. The arising research lines could include incorporation of reflectance normalization with ISS (Internal soil standard) suggested by Pimstein et al. (2011) and Ben-Dor et al. (2015) in the soil spectral measurements procedure; mapping of soil properties from hyperspectral images; and wider integration of soil spectroscopy in work on other research topics in the frame of evaluation of consequences of forest fires other land cover/land use change processes.

10. Conclusiones y trabajos futuros

La presente tesis doctoral se ha centrado en la aplicación de técnicas de espectroscopia de suelos, regiones VIS-NIR-SWIR (400-2500nm), para la estimación del contenido de materia orgánica (CMO) y textura (porcentajes de arenas, limos y arcillas) en suelos que han sufrido alteraciones de origen antropogénico (quemadas agrícolas, abandono de la superficie cultivable) o incendios forestales. Se han utilizado muestras de suelos procedentes de diferentes localizaciones: áreas afectadas por incendios forestales en el Parque Nacional de Campos Amazónicos en Brasil, áreas de quemadas agrícolas en el cantón Mocache en la costa del Ecuador, áreas correspondientes a zonas quemadas y de abandono de cultivos en Aragón (España), siendo esta última la zona principal en cuanto a suministro de muestras. Los principales hallazgos de este trabajo de investigación se exponen en los siguientes párrafos.

En las últimas décadas, se han publicado numerosos trabajos en los que la espectroscopia de suelos se presenta como una técnica de relativo bajo coste, para realizar estimaciones de propiedades edáficas en condiciones controladas de laboratorio, mediante el uso de diferentes accesorios disponibles en el mercado. Sin embargo, no hay consenso sobre la configuración experimental, los accesorios más adecuados y el protocolo de mediciones óptimo para cada situación particular. En este contexto, se compararon diferentes configuraciones y accesorios de espectroscopia: (1) esfera integradora en la configuración –IS-; (2) lámpara halógena de ASD y empuñadura de tipo pistola para la fibra óptica en la configuración experimental –L-; y (3) sonda de contacto en la configuración experimental –CP-. Los resultados demostraron que:

- Los valores más altos corresponden a la configuración con CP y los más bajos a la configuración IS.
- Las curvas espectrales obtenidas con la configuración CP se caracterizan por una mayor estabilidad, mostrando los coeficientes de variación más bajos
- Los espectros obtenidos con la configuración IS muestran un considerable ruido en longitudes de onda inferiores a 400nm y longitudes de onda superiores a 2300nm.
- La aplicación de los espectros con una finalidad predictiva mediante el método estándar de regresión parcial por mínimos cuadrados (PLSR) arrojó los mejores resultados con la configuración L. Las diferencias entre estimaciones realizados

por modelos que usaron los datos de diferentes configuraciones fueron ~11% para los modelos de calibración y del ~8% para los modelos de validación.

Dados los buenos resultados de la Lámpara halógena (L), esta fue la configuración considerada como óptima para la adquisición de los espectros VIS-NIR-SWIR de los suelos en las áreas de estudio.

En relación con la identificación del método estadístico más adecuado para la modelación del contenido de la materia orgánica y textura se compararon los siguientes métodos: (i) regresión parcial por mínimos cuadrados usando todas las bandas de reflectancia disponibles como predictores (PLSR-full), (ii) regresión parcial por mínimos cuadrados usando como predictores las bandas seleccionadas con la prueba de incertidumbre de Martens (PLSR-MUT), así como un método de modelamiento estadístico novedoso de (iii) regresión de las componentes correlacionadas y el algoritmo iterativo para la selección de los predictores (CCR-SD). En términos generales, todos los enfoques estadísticos fueron capaces de generar modelos de buena calidad ($R^2 > 0.7$), especialmente en el caso de la materia orgánica ($R^2 > 0.8$). Los modelos creados con CCR-SD demostraron la mejor capacidad predictiva al estimar CMO, arcilla, limo y arena en las etapas de calibración y validación (R^2 en el rango de 0.80–0.86 y 0.70–0.87, respectivamente). Además de buen ajuste, los modelos CCR-SD se destacan por su parsimonia, es decir, crean modelos capaces de estimar los parámetros/propiedades de suelo con igual o mejor precisión que otros métodos empleando un número menor de predictores.

El análisis de las estimaciones de las propiedades edáficas permitió identificar algunos patrones en su comportamiento espectral. Para los suelos analizados en este trabajo, las regiones espectrales particularmente importantes para predicciones de CMO incluyen 500–550, 750–830, 850–930, 1000–1050, 1500–1550, 1800–1910, 2200–2230, 2260–2280 y 2310–2360 nm con niveles de reflectividad afectados principalmente por la presencia de agua y los enlaces C-O, C=O, y N-H en las moléculas orgánicas. Por otro lado, aunque los rasgos de absorción característicos para los minerales de arcilla resultan enmascarados por la influencia espectral del relativamente alto contenido de materia orgánica en las muestras analizadas, los coeficientes más altos en los modelos de arcilla corresponden a las bandas relacionadas con caolinita (1395, 1414, and 2205 nm) e illita (1414, 2205, 2300–2340 nm).

Finalmente, el análisis en laboratorio de los espectros (VIS-NIR-SWIR) confirma el alto potencial de tres satélites de última generación (Landsat-8, Sentinel-2 y EnMAP) en la estimación del contenido de materia orgánica y la textura de los suelos analizados. Se comprobó que, además de la ubicación de las bandas de reflectividad dentro del espectro electromagnético, la capacidad predictiva de los modelos está relacionada con la cantidad de predictores disponibles. En este sentido, el elevado número de bandas en las imágenes de EnMAP, se relaciona con una mayor capacidad predictiva en los modelos correspondientes. Los resultados de la investigación demuestran, que los modelos de CMO y de arena basados en los datos de Landsat-8 presentan los coeficientes más altos para las bandas en las regiones espectrales del visible y SWIR, mientras que las predicciones basadas en Sentinel-2 contienen los coeficientes más altos para las bandas de *Vegetation Red Edge* (B5, B6, y B7).

A partir de los resultados de esta tesis se considera necesario seguir avanzando en el desarrollo de modelos de calibración de las propiedades edáficas. Estos avances podrían ir en la línea de integrar estándares de reflectividad del suelo (*ISS -InternalSoil Standard*) como sugieren Pimstein et al. (2011) y Ben-Dor et al. (2015); explorar el desarrollo de productos cartográficos sobre propiedades edáficas a partir de imágenes hiperespectrales; y amplificar la integración de la espectroscopia de suelos en trabajos sobre nuevos objetivos temáticos en el marco de las consecuencias de los incendios forestales y los cambios de usos del suelo.

References

- Akaike, H. (1973). Maximum likelihood identification of Gaussian autoregressive moving average models. *Biometrika*, 60(2), 255–265. <https://doi.org/10.1093/biomet/60.2.255>
- ASD. (2008). *Integrating sphere user manual, ASD Document 600660*. Boulder: ASD Inc.
- ASD. (2012a). *Fieldspec Pro user's guide*. Boulder: ASD Inc.
- ASD. (2012b). *Illuminator™ user manual, ASD document 600066*. Boulder: ASD Inc.
- Babyak, M. A. (2004). What you see may not be what you get: a brief, nontechnical introduction to overfitting in regression-type models. *Psychosomatic medicine*, 66(3), 411-421. Retrieved from: https://journals.lww.com/psychosomaticmedicine/Fulltext/2004/05000/What_You_See_May_Not_Be_What_You_Get__A_Brief,.21.aspx
- Badía-Villas, D., & del Moral, F. (2016). Soils of the Arid Areas *The Soils of Spain* (pp. 145-161). Cham, Switzerland: Springer International Publishing. https://doi.org/10.1007/978-3-319-20541-0_4
- Badía, D., Valero, R., Gracia, A., Martí, C., & Molina, F. (2007). Ten-year growth of woody species planted in reclaimed mined banks with different slopes. *Arid Land Research and Management*, 21(1), 67-79. <https://doi.org/10.1080/15324980601094022>
- Baumgardner, M. F., Silva, L. F., Biehl, L. L., & Stoner, E. R. (1986). Reflectance properties of soils. *Advances in agronomy*, 38, 1-44. [https://doi.org/10.1016/S0065-2113\(08\)60672-0](https://doi.org/10.1016/S0065-2113(08)60672-0)
- Bellon-Maurel, V., Fernandez-Ahumada, E., Palagos, B., Roger, J.-M., & McBratney, A. (2010). Critical review of chemometric indicators commonly used for assessing the quality of the prediction of soil attributes by NIR spectroscopy. *TrAC Trends in Analytical Chemistry*, 29(9), 1073-1081. <https://doi.org/10.1016/j.trac.2010.05.006>
- Bellon-Maurel, V., & McBratney, A. (2011). Near-infrared (NIR) and mid-infrared (MIR) spectroscopic techniques for assessing the amount of carbon stock in soils—Critical review and research perspectives. *Soil Biology and Biochemistry*, 43(7), 1398-1410. <https://doi.org/10.1016/j.soilbio.2011.02.019>

- Ben-Dor, E., Chabrillat, S., & Demattê, J., Lyon, J. (2019). Characterization of soil properties using reflectance spectroscopy. In P. S. Thenkabail, J. G. Lyon & A. Huete (Eds.), *Fundamentals, sensor systems, spectral libraries, and data mining for vegetation* (pp. 187-247). Boca Raton, FL, USA: CRC Press (Taylor & Francis Group).
- Ben-Dor, E., & Demattê, J. (2016). Chapter 25-Remote sensing of soil in the optical domains. In P. S. Thenkabail (Ed.), *Remote sensing handbook vol. II: Land resources monitoring, modeling, and mapping with remote sensing* (pp. 733–787). Boca Raton, FL, USA: CRC Press (Taylor & Francis Group).
- Ben-Dor, E., Goldshleger, N., Benyamini, Y., Agassi, M., & Blumberg, D. (2003). The spectral reflectance properties of soil structural crusts in the 1.2-to 2.5- μm spectral region. *Soil Science Society of America Journal*, 67(1), 289-299. <http://dx.doi.org/10.2136/sssaj2003.2890>
- Ben-Dor, E., Inbar, Y., & Chen, Y. (1997). The reflectance spectra of organic matter in the visible near-infrared and short wave infrared region (400–2500 nm) during a controlled decomposition process. *Remote Sensing of Environment*, 61(1), 1-15. [https://doi.org/10.1016/S0034-4257\(96\)00120-4](https://doi.org/10.1016/S0034-4257(96)00120-4)
- Ben-Dor, E., Irons, J. R., & Epema, G. F. (1999). Chapter 3—Soil reflectance. In A. N. Rencz, & R. A. Ryerson (Eds.), *Manual of remote sensing, remote sensing for the earth sciences (3rd ed.) (vol. 3)* (pp. 111–188). New York, NY, USA: John Wiley & Sons.
- Ben-Dor, E., Ong, C., & Lau, I. C. (2015). Reflectance measurements of soils in the laboratory: Standards and protocols. *Geoderma*, 245–246, 112-124. doi: <http://dx.doi.org/10.1016/j.geoderma.2015.01.002>
- Bennett, G. (2013). *Regression modelling with many correlated predictors and few cases*. York, United Kingdom: Presentation in ASSESS Event. Retrieved from <http://www.spssusers.co.uk/Events/2013/Bennett2013.pdf>.
- Bishop, J. L., Pieters, C. M., & Edwards, J. O. (1994). Infrared spectroscopic analyses on the nature of water in montmorillonite. *Clays and Clay Minerals*, 42(6), 702-716. <https://doi.org/10.1346/CCMN.1994.0420606>
- Blake, G. R., Steinhardt, G. C., Pombal, X. P., Muñoz, J. C. N., Cortizas, A. M., Arnold, R. W., . . . Spaargaren, O. (2008). Plinthosols. In W. Chesworth (Ed.), *Encyclopedia of Soil Science* (pp. 579-580). Dordrecht: Springer Netherlands.

- Bünemann, E. K., Bongiorno, G., Bai, Z., Creamer, R. E., De Deyn, G., de Goede, R., . . . Mäder, P. (2018). Soil quality—A critical review. *Soil Biology and Biochemistry*, *120*, 105-125. <https://doi.org/10.1016/j.soilbio.2018.01.030>
- Cerdà, A., & Robichaud, P. (2009). Fire effects on soil infiltration *Fire effects on soils and restoration strategies* (pp. 81-103). New Hampshire: Science Publishers.
- Certini, G. (2005). Effects of fire on properties of forest soils: a review. *Oecologia*, *143*(1), 1-10. <https://doi.org/10.1007/s00442-004-1788-8>
- Chabrillat, S., Goetz, A. F., Krosley, L., & Olsen, H. W. (2002). Use of hyperspectral images in the identification and mapping of expansive clay soils and the role of spatial resolution. *Remote Sensing of Environment*, *82*(2-3), 431-445. [https://doi.org/10.1016/S0034-4257\(02\)00060-3](https://doi.org/10.1016/S0034-4257(02)00060-3)
- Chun, H., & Keleş, S. (2010). Sparse partial least squares regression for simultaneous dimension reduction and variable selection. *Journal of the Royal Statistical Society: Series B (Statistical Methodology)*, *72*(1), 3-25. <https://doi.org/10.1111/j.1467-9868.2009.00723.x>
- Comte, I., Davidson, R., Lucotte, M., de Carvalho, C. J. R., de Assis Oliveira, F., da Silva, B. P., & Rousseau, G. X. (2012). Physicochemical properties of soils in the Brazilian Amazon following fire-free land preparation and slash-and-burn practices. *Agriculture, ecosystems & environment*, *156*, 108-115. doi: <http://dx.doi.org/10.1016/j.agee.2012.05.004>
- Condit, H. R. (1970). The spectral reflectance of American soils. *Photogrammetric Engineering*, *36*, 955-966.
- Cuadrat, J. M. (Ed.), & Martín-Vide, J. M. (Ed.). (2007). *Spanish climatology: Past, present and future*. Zaragoza, Ar, Spain: University of Zaragoza Press.
- Curcio, D., Ciralo, G., D'Asaro, F., & Minacapilli, M. (2013). Prediction of Soil Texture Distributions Using VNIR-SWIR Reflectance Spectroscopy. *Procedia Environmental Sciences*, *19*(0), 494-503. doi: <http://dx.doi.org/10.1016/j.proenv.2013.06.056>
- Curl, A., Thompson, C. W., & Aspinall, P. (2015). The effectiveness of 'shared space' residential street interventions on self-reported activity levels and quality of life for older people. *Landscape and Urban Planning*, *139*, 117-125. <https://doi.org/10.1016/j.landurbplan.2015.02.019>

- Danner, M., Locherer, M., Hank, T., & Richter, K. (2015). Spectral sampling with the ASD FIELDSPEC 4. In EnMap (Ed.), *EnMAP Field Guides Technical Report* (p. 20). Potsdam, Germany: EnMAP Consortium-GFZ Data Services. <https://doi.org/10.2312/enmap.2015.008>
- DeBano, L. F., & Neary, D. G. (2005). Part A—the soil resource: its importance, characteristics, and general responses to fire. *Wildland Fire in Ecosystems: Effects of Fire on Soil and Water. Gen. Tech. Rep. RMRS-GTR-42-vol, 4*, 21-28.
- Demattê, J. A., L.S. Morgan, C., Chabrillat, S., Rizzo, R., Franceschini, M., Terra, F. d., . . . Wetterlind, J. (2016). Spectral sensing from ground to space in soil science: State of the art, applications, potential and perspectives. In P. S. Thenkabail (Ed.), *Remote Sensing Handbook Vol. II: Land Resources Monitoring, Modeling, and Mapping with Remote Sensing* (pp. 661-732). Boca Raton, FL.: CRC press (Taylor & Francis Group).
- Demattê, J. A. M. (2002). Characterization and discrimination of soils by their reflected electromagnetic energy. *Pesquisa Agropecuária Brasileira*, 37(10), 1445-1458. <https://doi.org/10.1590/S0100-204X2002001000013>
- Demattê, J. A., Campos, R. C., Alves, M. C., Fiorio, P. R., & Nanni, M. R. (2004). Visible–NIR reflectance: a new approach on soil evaluation. *Geoderma*, 121(1-2), 95-112. <https://doi.org/10.1016/j.geoderma.2003.09.012>
- Demattê, J. A. M., Bellinaso, H., Romero, D. J., & Fongaro, C. T. (2014). Morphological Interpretation of Reflectance Spectrum (MIRS) using libraries looking towards soil classification. *Scientia Agricola*, 71(6), 509-520. <http://dx.doi.org/10.1590/0103-9016-2013-0365>
- Duckworth, J. H. (1998). Quantitative analysis *Applied spectroscopy: A compact reference for practitioners*, (93-159).
- Elachi, C., & Van-Zyl, J. J. (2006). *Introduction to the physics and techniques of remote sensing* (Vol. 28): John Wiley & Sons.
- Esbensen, K. H. (Ed.), Guyot, D. (Ed.), Westad, F. (Ed.), & Houmoller, L. P. (Ed.). (2002). Multivariate data analysis-in practice: An introduction to multivariate data analysis and experimental design. *Multivariate data analysis*, (5th ed.) (pp 600). Oslo, Norway: CAMO Process AS.

- Escadafal, R. (1989). *Caractérisation de la surface des sols arides par observations de terrain et par télédétection: applications: exemple de la région de Tataouine (Tunisie)*: ORSTOM.
- Escribano, P., Schmid, T., Chabrilat, S., Rodríguez-Caballero, E., & García, M. (2017). Optical remote sensing for soil mapping and monitoring. In P. Pereira, E. Brevik, M. Muñoz-Rojas, & B. A. Miller (Eds.), *Soil mapping and process modeling for sustainable land use management* (pp. 87–125). Amsterdam, Boston, Heidelberg, London, New York: Elsevier Inc. <https://doi.org/10.1016/B978-0-12-805200-6.00004-9>
- FAO (2015). *World reference base for soil resources*. Retrieved from Rome, Italy: <http://www.fao.org/3/i3794en/I3794en.pdf>
- Fyfe, S. K. (2004). *Hyperspectral Studies of New South Wales seagrasses with particular emphasis on the detection of light stress in eelgrass *Zostera capricorni**. Retrieved from: <https://ro.uow.edu.au/cgi/viewcontent.cgi?referer=https://scholar.google.es/&httpsredir=1&article=1472&context=theses>
- Ge, Y., Thomasson, J. A., & Sui, R. (2011). Remote sensing of soil properties in precision agriculture: A review. *Frontiers of Earth Science*, 5(3), 229-238. <https://doi.org/10.1007/s11707-011-0175-0>
- Geladi, P., MacDougall, D., & Martens, H. (1985). Linearization and scatter-correction for near-infrared reflectance spectra of meat. *Applied spectroscopy*, 39(3), 491-500.
- Gholizadeh, A., Borůvka, L., Saberioon, M., & Vašát, R. (2016). A Memory-Based Learning Approach as Compared to Other Data Mining Algorithms for the Prediction of Soil Texture Using Diffuse Reflectance Spectra. *Remote Sensing*, 8(4), 341. <https://doi.org/10.3390/rs8040341>
- Gholizadeh, A., Saberioon, M., Carmon, N., Boruvka, L., & Ben-Dor, E. (2018). Examining the Performance of PARACUDA-II Data-Mining Engine versus Selected Techniques to Model Soil Carbon from Reflectance Spectra. *Remote Sensing*, 10(8), 1172. <https://doi.org/10.3390/rs10081172>
- Goldman, S. J., Bursztynsky, T. A., & Jackson, K. (1986). *Erosion and sediment control handbook*. New York, USA: McGraw-Hill.

- Gomez, C., Viscarra-Rossel, R. A., & McBratney, A. B. (2008). Soil organic carbon prediction by hyperspectral remote sensing and field vis-NIR spectroscopy: An Australian case study. *Geoderma*, 146(3–4), 403-411. doi: <http://dx.doi.org/10.1016/j.geoderma.2008.06.011>
- Gras, J. P., Barthès, B. G., Mahaut, B., & Trupin, S. (2014). Best practices for obtaining and processing field visible and near infrared (VNIR) spectra of topsoils. *Geoderma*, 214–215(0), 126-134. doi: <http://dx.doi.org/10.1016/j.geoderma.2013.09.021>
- Grunwald, S., Vasques, G. M., & Rivero, R. G. (2015). Fusion of soil and remote sensing data to model soil properties *Advances in agronomy* (Vol. 131, pp. 1-109): Elsevier.
- Guerrero, C., Viscarra-Rossel, R., & Mouazen, A. M. (2010). Special issue ‘Diffuse reflectance spectroscopy in soil science and land resource assessment’. *Geoderma*, 158(1–2), 1-2. doi: <http://dx.doi.org/10.1016/j.geoderma.2010.05.008>
- Hauser, S., & Norgrove, L. (2013). Slash-and-burn agriculture, effects of. *Encyclopedia of biodiversity, Volume 6*, (Ed. 2), 551-562.
- Hill, J., Udelhoven, T., Vohland, M., & Stevens, A. (2010). The use of laboratory spectroscopy and optical remote sensing for estimating soil properties. In E.-C. Oerke, R. Gerhards, G. Menz & R. A. Sikora (Eds.), *Precision Crop Protection-the Challenge and Use of Heterogeneity* (pp. 67-85): Springer. https://doi.org/10.1007/978-90-481-9277-9_5
- Hong, Y., Chen, S., Liu, Y., Zhang, Y., Yu, L., Chen, Y., . . . Liu, Y. (2019). Combination of fractional order derivative and memory-based learning algorithm to improve the estimation accuracy of soil organic matter by visible and near-infrared spectroscopy. *CATENA*, 174, 104-116. <https://doi.org/10.1016/j.catena.2018.10.051>
- Hunt, G. R. (1977). Spectral signatures of particulate minerals in the visible and near infrared. *Geophysics*, 42(3), 501-513.
- Hunt, G. R., & Salisbury, J. W. (1971). Visible and near infrared spectra of minerals and rocks. II. Carbonates. *Modern Geology*, 2, 23-30.

- Ingram, J., & Fernandes, E. (2001). Managing carbon sequestration in soils: concepts and terminology. *Agriculture, Ecosystems & Environment*, 87(1), 111-117. [https://doi.org/10.1016/S0167-8809\(01\)00145-1](https://doi.org/10.1016/S0167-8809(01)00145-1)
- Jensen, J. R. (2009). *Remote sensing of the environment: An earth resource perspective 2/e*: Pearson Education India.
- Jordán, J. B. (1989). *La economía campesina: crisis, reactivación y desarrollo* (No. 19). Ilica.
- Kato, M. D. S., Kato, O. R., Denich, M., & Vlek, P. L. (1999). Fire-free alternatives to slash-and-burn for shifting cultivation in the eastern Amazon region: the role of fertilizers. *Field crops research*, 62(2-3), 225-237. [https://doi.org/10.1016/S0378-4290\(99\)00021-0](https://doi.org/10.1016/S0378-4290(99)00021-0)
- Koricheva, J., Gurevitch, J., & Mengersen, K. (2013). *Handbook of meta-analysis in ecology and evolution*: Princeton University Press.
- Kuang, B., & Mouazen, A. M. (2013). Effect of spiking strategy and ratio on calibration of on-line visible and near infrared soil sensor for measurement in European farms. *Soil and Tillage Research*, 128, 125-136. <https://doi.org/10.1016/j.still.2012.11.006>
- Lal, R. (2004). Soil carbon sequestration impacts on global climate change and food security. *Science*, 304(5677), 1623-1627.
- Lal, R. (Ed.), & Stewart, B. A. (Ed.). (2010). *Food security and soil quality*. Boca Raton, FL, USA: CRC Press (Taylor & Francis Group), <https://doi.org/10.1201/EBK1439800577>.
- Lasanta, T., Nadal-Romero, E., & Arnáez, J. (2015). Managing abandoned farmland to control the impact of re-vegetation on the environment. The state of the art in Europe. *Environmental Science & Policy*, 52, 99-109. <https://doi.org/10.1016/j.envsci.2015.05.012>
- Lawrence, D., Radel, C., Tully, K., Schmook, B., & Schneider, L. (2010). Untangling a decline in tropical forest resilience: constraints on the sustainability of shifting cultivation across the globe. *Biotropica*, 42(1), 21-30.
- Lentile, L. B., Holden, Z. A., Smith, A. M., Falkowski, M. J., Hudak, A. T., Morgan, P., . . . Benson, N. C. (2006). Remote sensing techniques to assess active fire characteristics and post-fire effects. *International Journal of Wildland Fire*, 15(3), 319-345. <https://doi.org/10.1071/WF05097>

- Lillesand, T., Kiefer, R. W., & Chipman, J. (2014). *Remote sensing and image interpretation*: John Wiley & Sons.
- Liu, W., Baret, F., Gu, X., Zhang, B., Tong, Q., & Zheng, L. (2003). Evaluation of methods for soil surface moisture estimation from reflectance data. *International Journal of Remote Sensing*, 24(10), 2069-2083. <https://doi.org/10.1080/01431160210163155>
- Louis, B., Saby, N., Orton, T., Lacarce, E., Boulonne, L., Jolivet, C., . . . Arrouays, D. (2014). Statistical sampling design impact on predictive quality of harmonization functions between soil monitoring networks. *Geoderma*, 213, 133-143. <https://doi.org/10.1016/j.geoderma.2013.07.018>
- Mackensen, J., Hölscher, D., Klinge, R., & Fölster, H. (1996). Nutrient transfer to the atmosphere by burning of debris in eastern Amazonia. *Forest Ecology and Management*, 86(1-3), 121-128.
- Magidson, J. (2010). Correlated component regression: A prediction/classification methodology for possibly many features. *Proceedings of the American Statistical Association*. pp.4372-4386.
- Magidson, J. (2013). Correlated component regression: Re-thinking regression in the presence of near collinearity. In H. Abdi, W. W. Chin, V. E. Vinzi, G. Russolillo, & L. Trinchera (Eds.), *New perspectives in partial least squares and related methods* (pp. 65–78). New York, NY, USA: Springer International Publishing. https://doi.org/10.1007/978-1-4614-8283-3_3
- Magidson, J., & Wassmann, K. (2010). The role of proxy genes in predictive models: an application to early detection of prostate cancer. *Proceedings of the American Statistical Association, Biometrics section*. pp.2739-2753.
- Marengo, J. A., Nobre, C. A., Tomasella, J., Oyama, M. D., Sampaio de Oliveira, G., De Oliveira, R., . . . Brown, I. F. (2008). The drought of Amazonia in 2005. *Journal of Climate*, 21(3), 495-516. <https://doi.org/10.1175/2007JCLI1600.1>
- Martens, H., & Martens, M. (2000). Modified Jack-knife estimation of parameter uncertainty in bilinear modelling by partial least squares regression (PLSR). *Food quality and preference*, 11(1-2), 5-16. [https://doi.org/10.1016/S0950-3293\(99\)00039-7](https://doi.org/10.1016/S0950-3293(99)00039-7)

- Mataix-Solera, J., Cerdà, A., Arcenegui, V., Jordán, A., & Zavala, L. M. (2011). Fire effects on soil aggregation: a review. *Earth-Science Reviews*, *109*(1-2), 44-60. <https://doi.org/10.1016/j.earscirev.2011.08.002>
- Matthias, A., Fimbres, A., Sano, E., Post, D., Accioly, L., Batchily, A., & Ferreira, L. (2000). Surface roughness effects on soil albedo. *Soil Science Society of America Journal*, *64*(3), 1035-1041. <http://dx.doi.org/10.2136/sssaj2000.6431035x>
- Melendez-Pastor, I., Navarro-Pedreño, J., Gómez, I., & Koch, M. (2008). Identifying optimal spectral bands to assess soil properties with VNIR radiometry in semi-arid soils. *Geoderma*, *147*(3), 126-132. <https://doi.org/10.1016/j.geoderma.2008.08.004>
- Merino, A., Moreno, G., Navarro, F. B., & Gallardo, J. F. (2016). Future issues. In J. F. Gallardo (Ed.), *The soils of Spain* (pp. 189–195). Cham, Switzerland: Springer International Publishing. https://doi.org/10.1007/978-3-319-20541-0_6
- Minasny, B., & McBratney, A. (2013). Why you don't need to use RPD. *Pedometron*, *33*, 14-15. Retrieved from: <http://www.pedometrics.org/Pedometron/Pedometron33.pdf#page=14>
- Minasny, B., & McBratney, A. B. (2016). Digital soil mapping: A brief history and some lessons. *Geoderma*, *264*, 301-311. doi: <https://doi.org/10.1016/j.geoderma.2015.07.017>
- Miura, T., & Huete, A. R. (2009). Performance of three reflectance calibration methods for airborne hyperspectral spectrometer data. *Sensors*, *9*(2), 794-813. <https://doi.org/10.3390/s90200794>
- Montanarella, L., & Panagos, P. (2018). Soil data needs for sustainable agriculture. In H. Ginzky, E. Dooley, I. Heuser, E. Kasimbazi, T. Markus, & T. Qin (Eds.), *International Yearbook of Soil Law and Policy 2017*. (IYSLP, Vol 2017) (pp. 151–166). Cham, Switzerland: Springer International Publishing. https://doi.org/10.1007/978-3-319-68885-5_9
- Mouazen, A. M., Kuang, B., De-Baerdemaeker, J., & Ramon, H. (2010). Comparison among principal component, partial least squares and back propagation neural network analyses for accuracy of measurement of selected soil properties with visible and near infrared spectroscopy. *Geoderma*, *158*(1), 23-31. <https://doi.org/10.1016/j.geoderma.2010.03.001>

- Nadal-Romero, E., Cammeraat, E., Pérez-Cardiel, E., & Lasanta, T. (2016). Effects of secondary succession and afforestation practices on soil properties after cropland abandonment in humid Mediterranean mountain areas. *Agriculture, Ecosystems & Environment*, 228, 91-100. <https://doi.org/10.1016/j.agee.2016.05.003>
- Nations, U. (2015). Transforming our world: the 2030 Agenda for Sustainable Development [Press release]. Retrieved from <https://sustainabledevelopment.un.org/topics/sustainabledevelopmentgoals>
- Nortcliff, S., Hulpke, H., Bannick, C., Terytze, K., Knoop, G., Bredemeier, M., . . . Dworshak, U. (2006). Soil, Definition, Function, and Utilization of Soil. Retrieved from: https://www.researchgate.net/profile/H_Schulte-Bisping/publication/227557214_Soil_Definition_Function_and_Utilization_of_Soil/links/5a33c30faca2727144b77e3b/Soil-Definition-Function-and-Utilization-of-Soil.pdf
- Nuzzo, R. (2014). Scientific method: statistical errors. *Nature News*, 506(7487), 150–152. <https://doi.org/10.1038/506150a>
- Ogen, Y., Neumann, C., Chabrilat, S., Goldshleger, N., & Ben-Dor, E. (2018). Evaluating the detection limit of organic matter using point and imaging spectroscopy. *Geoderma*, 321, 100-109. doi: <https://doi.org/10.1016/j.geoderma.2018.02.011>
- Oliveira-Filho, A. T., & Ratter, J. A. (2002). Vegetation physiognomies and woody flora of the cerrado biome. *The cerrados of Brazil: ecology and natural history of a neotropical savanna*, 91-120.
- Ostovari, Y., Ghorbani-Dashtaki, S., Bahrami, H.-A., Abbasi, M., Dematte, J. A. M., Arthur, E., & Panagos, P. (2018). Towards prediction of soil erodibility, SOM and CaCO₃ using laboratory Vis-NIR spectra: A case study in a semi-arid region of Iran. *Geoderma*, 314, 102-112. doi: <https://doi.org/10.1016/j.geoderma.2017.11.014>
- Palacios-Orueta, A., Pinzon, J. E., Ustin, S. L., & Roberts, D. A. (1999). Remote sensing of soils in the Santa Monica Mountains: II. Hierarchical foreground and background analysis. *Remote Sensing of Environment*, 68(2), 138-151. [https://doi.org/10.1016/S0034-4257\(98\)00106-0](https://doi.org/10.1016/S0034-4257(98)00106-0)

- Palacios-Orueta, A., & Ustin, S. L. (1998). Remote Sensing of Soil Properties in the Santa Monica Mountains I. Spectral Analysis. *Remote Sensing of Environment*, 65(2), 170-183. doi: [http://dx.doi.org/10.1016/S0034-4257\(98\)00024-8](http://dx.doi.org/10.1016/S0034-4257(98)00024-8)
- Pausas, J. G. (2004). Changes in fire and climate in the eastern Iberian Peninsula (Mediterranean basin). *Climatic change*, 63(3), 337-350. <https://doi.org/10.1023/B:CLIM.0000018508.94901.9c>
- Pérez-Cabello, F., Echeverría, M., Ibarra, P., & Riva, J. (2009). Effects of Fire on Vegetation, Soil and Hydrogeomorphological Behavior in Mediterranean Ecosystems. In E. Chuvieco (Ed.), *Earth Observation of Wildland Fires in Mediterranean Ecosystems* (pp. 111-128): Springer Berlin Heidelberg. https://doi.org/10.1007/978-3-642-01754-4_9
- Pigott, T. (2012). *Advances in meta-analysis*: Springer Science & Business Media.
- Pimentel, D. (2006). Soil erosion: a food and environmental threat. *Environment, development and sustainability*, 8(1), 119-137. <https://doi.org/10.1007/s10668-005-1262-8>
- Sánchez, P. A., Ahamed, S., Carré, F., Hartemink, A. E., Hempel, J., Huising, J., . . . de Lourdes Mendonça-Santos, M. (2009). Digital soil map of the world. *Science*, 325(5941), 680-681. <http://dx.doi.org/10.1126/science.1175084>
- Savitzky, A., & Golay, M. J. (1964). Smoothing and differentiation of data by simplified least squares procedures. *Analytical chemistry*, 36(8), 1627-1639. <https://doi.org/10.1021/ac60214a047>
- Schaepman-Strub, G., Schaepman, M. E., Painter, T. H., Dangel, S., & Martonchik, J. V. (2006). Reflectance quantities in optical remote sensing—definitions and case studies. *Remote Sensing of Environment*, 103(1), 27-42. doi: <http://dx.doi.org/10.1016/j.rse.2006.03.002>
- Schaepman, M. E., & Dangel, S. (2000). Solid laboratory calibration of a nonimaging spectroradiometer. *Applied Optics*, 39(21), 3754-3764. <https://doi.org/10.1364/AO.39.003754>
- Schulze, D. G. (2002). An introduction to soil mineralogy. In J. B. Dixon & D. G. Schulze (Eds.), *Soil mineralogy with environmental applications* (pp. 1-36). Madison: Soil Science Society of America.
- Sommer, R., Vlek, P. L., de Abreu Sá, T. D., Vielhauer, K., Coelho, R. d. F. R., & Fölster, H. (2004). Nutrient balance of shifting cultivation by burning or

- mulching in the Eastern Amazon—evidence for subsoil nutrient accumulation. *Nutrient Cycling in Agroecosystems*, 68(3), 257-271. <https://doi.org/10.1023/B:FRES.0000019470.93637.54>
- Sørensen, A. S., Demler, E., & Lukin, M. D. (2005). Fractional quantum Hall states of atoms in optical lattices. *Physical review letters*, 94(8), 086803. <https://doi.org/10.1103/PhysRevLett.94.086803>
- Sponsel, L. E. (2013). Human impact on biodiversity, overview. In S.A. Levin (Ed.), *Encyclopedia of Biodiversity*, (pp. 137-152). Waltham, NY: Academic Press.
- Soriano-Disla, J. M., Janik, L. J., Viscarra Rossel, R. A., Macdonald, L. M., & McLaughlin, M. J. (2014). The performance of visible, near-, and mid-infrared reflectance spectroscopy for prediction of soil physical, chemical, and biological properties. *Applied Spectroscopy Reviews*, 49(2), 139-186. <https://doi.org/10.1080/05704928.2013.811081>
- Stenberg, B., & Viscarra-Rossel, R. (2010). Diffuse reflectance spectroscopy for high-resolution soil sensing *Proximal Soil Sensing* (pp. 29-47): Springer. https://doi.org/10.1007/978-90-481-8859-8_3
- Stenberg, B., Viscarra-Rossel, R. A., Mouazen, A. M., & Wetterlind, J. (2010). Chapter five-visible and near infrared spectroscopy in soil science. *Advances in agronomy*, 107, 163-215. [https://doi.org/10.1016/S0065-2113\(10\)07005-7](https://doi.org/10.1016/S0065-2113(10)07005-7)
- Stevens, A., Nocita, M., Tóth, G., Montanarella, L., & van Wesemael, B. (2013). Prediction of soil organic carbon at the European scale by visible and near infrared reflectance spectroscopy. *PloS one*, 8(6), e66409. <https://doi.org/10.1371/journal.pone.0066409>
- Stevens, A., van Wesemael, B., Bartholomeus, H., Rosillon, D., Tychon, B., & Bendor, E. (2008). Laboratory, field and airborne spectroscopy for monitoring organic carbon content in agricultural soils. *Geoderma*, 144(1), 395-404. <https://doi.org/10.1016/j.geoderma.2007.12.009>
- Stoner, E. R., & Baumgardner, M. (1981). Characteristic variations in reflectance of surface soils. *Soil Science Society of America Journal*, 45(6), 1161-1165. <http://dx.doi.org/10.2136/sssaj1981.03615995004500060031x>
- Terra, F. S., Demattê, J. A. M., & Viscarra Rossel, R. A. (2018). Proximal spectral sensing in pedological assessments: vis–NIR spectra for soil classification based

- on weathering and pedogenesis. *Geoderma*, 318, 123-136. doi: <https://doi.org/10.1016/j.geoderma.2017.10.053>
- Tobias, R. D. (1995). *An introduction to partial least squares regression*. Paper presented at the Proceedings of the twentieth annual SAS users group international conference. Retrieved from: <https://horticulture.triforce.cals.wisc.edu/wp-content/uploads/sites/20/2013/09/Tobias-1995.pdf>
- Torrent, J., & Barrón, V. (2002). Diffuse reflectance spectroscopy of iron oxides. *Encyclopedia of surface and Colloid Science*, 1438-1446. Retrieved from: https://www.researchgate.net/profile/Vidal_Barron/publication/264869284_Diffuse_Reflectance_Spectroscopy_of_Iron_Oxides/links/53f74c400cf24a9236ceb07f/Diffuse-Reflectance-Spectroscopy-of-Iron-Oxides.pdf
- Torrent, J., & Barrón, V. (2008). Diffuse reflectance spectroscopy. In A. L. Ulery & L. R. Drees (Eds.), *Methods of soil analysis* (Vol. 5, pp. 367-387): Soil Science Society of America.
- Tóth, G., Hermann, T., da Silva, M. R., & Montanarella, L. (2018). Monitoring soil for sustainable development and land degradation neutrality. *Environmental Monitoring and Assessment*, 190(2), 57. doi: 10.1007/s10661-017-6415-3
- Troeh, F. R., & Thompson, L. M. (2005). *Soils and soil fertility* (Vol. 489): Blackwell Ames.
- Tsakiridis, N. L., Theocharis, J. B., Ben-Dor, E., & Zalidis, G. C. (2019). Using interpretable fuzzy rule-based models for the estimation of soil organic carbon from VNIR/SWIR spectra and soil texture. *Chemometrics and Intelligent Laboratory Systems*. <https://doi.org/10.1016/j.chemolab.2019.03.011>
- Úbeda, X., & Outeiro, L. (2009). Physical and chemical effects of fire on soil. *Fire effects on soils and restoration strategies*, 5.
- Udelhoven, T., Emmerling, C., & Jarmer, T. (2003). Quantitative analysis of soil chemical properties with diffuse reflectance spectrometry and partial least-square regression: A feasibility study. *Plant and soil*, 251(2), 319-329. <https://doi.org/10.1023/A:1023008322682>
- United Nations (2015). Transforming our world: The 2030 agenda for sustainable development. Resolution adopted by the General Assembly, (A/RES/70/1). United Nations Headquarters, New York, NY, USA: Press release.

- Van-der-Meer, F. (1995). Spectral reflectance of carbonate mineral mixtures and bidirectional reflectance theory: Quantitative analysis techniques for application in remote sensing. *Remote Sensing Reviews*, 13(1-2), 67-94. <https://doi.org/10.1080/02757259509532297>
- Vasques, G. M., Demattê, J. A. M., Viscarra Rossel, R. A., Ramírez-López, L., & Terra, F. S. (2014). Soil classification using visible/near-infrared diffuse reflectance spectra from multiple depths. *Geoderma*, 223–225(0), 73-78. doi: <http://dx.doi.org/10.1016/j.geoderma.2014.01.019>
- Vicente-Serrano, S. M., Pérez-Cabello, F., & Lasanta, T. (2011). Pinus halepensis regeneration after a wildfire in a semiarid environment: assessment using multitemporal Landsat images. *International Journal of Wildland Fire*, 20(2), 195-208. doi: <http://dx.doi.org/10.1071/WF08203>
- Viscarra-Rossel, R., Adamchuk, V., Sudduth, K., McKenzie, N., & Lobsey, C. (2011). Proximal soil sensing: an effective approach for soil measurements in space and time *Advances in agronomy* (Vol. 113, pp. 243-291): Elsevier. <https://doi.org/10.1016/B978-0-12-386473-4.00005-1>
- Viscarra-Rossel, R., & Behrens, T. (2010). Using data mining to model and interpret soil diffuse reflectance spectra. *Geoderma*, 158(1), 46-54. <https://doi.org/10.1016/j.geoderma.2009.12.025>
- Viscarra-Rossel, R., & Brus, D. J. (2018). *The cost-efficiency and reliability of two methods for soil organic C accounting*. <https://doi.org/10.1002/ldr.2887>
- Viscarra-Rossel, R., & Chen, C. (2011). Digitally mapping the information content of visible–near infrared spectra of surficial Australian soils. *Remote Sensing of Environment*, 115(6), 1443-1455. <https://doi.org/10.1016/j.rse.2011.02.004>
- Viscarra-Rossel, R. A., Behrens, T., Ben-Dor, E., Brown, D. J., Demattê, J. A. M., Shepherd, K. D., . . . Ji, W. (2016). A global spectral library to characterize the world's soil. *Earth-Science Reviews*, 155, 198-230. doi: <https://doi.org/10.1016/j.earscirev.2016.01.012>
- Viscarra-Rossel, R. A., McGlynn, R. N., & McBratney, A. B. (2006). Determining the composition of mineral-organic mixes using UV–vis–NIR diffuse reflectance spectroscopy. *Geoderma*, 137(1–2), 70-82. doi: <http://dx.doi.org/10.1016/j.geoderma.2006.07.004>

- Viscarra Rossel, R. A., Walvoort, D. J. J., McBratney, A. B., Janik, L. J., & Skjemstad, J. O. (2006). Visible, near infrared, mid infrared or combined diffuse reflectance spectroscopy for simultaneous assessment of various soil properties. *Geoderma*, *131*(1–2), 59-75. doi: <http://dx.doi.org/10.1016/j.geoderma.2005.03.007>
- Wold, S., Sjöström, M., & Eriksson, L. (2001). PLS-regression: a basic tool of chemometrics. *Chemometrics and Intelligent Laboratory Systems*, *58*(2), 109-130.

Appendix A

Contribution of PhD student to the published research articles

1. **Rosero-Vlasova, O. A.**, Pérez-Cabello, F., Llovería, R. M., & Vlassova, L. (2016). Assessment of laboratory VIS-NIR-SWIR setups with different spectroscopy accessories for characterisation of soils from wildfire burns. *Biosystems Engineering*, 152, 51-67. <https://doi.org/10.1016/j.biosystemseng.2016.06.011>

As the first author of this article, Olga Alexandra Rosero Vlasova contributed to all the stages of the research, from planning and data processing to analysis of the results and writing the draft. The coauthors contributed in reviewing the results.

Impact Factor	Impact Factor (5 year)	JCR® Category	Rank in Category	Quartile in Category
2.983	3.112	AGRICULTURAL MULTIDISCIPLINARY	7 of 56	Q1
		AGRICULTURAL ENGINEERING	4 of 13	Q2

Data from the 2018 edition of [Journal Citation Reports](#)

2. **Rosero-Vlasova, O.**, Rosero Tufiño, P., & Vlassova, L. (2017). Capítulo I: Gestión Ambiental - Espectroscopia VIS-NIR aplicada para predicción del contenido de materia orgánica en los suelos bajo sistema de cultivo roza-y-quema. In P. Domínguez, J. Morán, O. Rea, I. Parra, & L. Corzo (Eds.), *Memoria Científica del III Congreso Internacional de Ingeniería, Ambiental, Forestal y Ecoturismo* (pp. 16-28). Guayaquil, Ecuador: Editorial CIDE Centro de Investigación y Desarrollo Ecuador. Retrieved from: https://docs.wixstatic.com/ugd/54b18d_130e402800d74b4aa0fb8a45301d1cb8.pdf

As the first author of this article, Olga Alexandra Rosero Vlasova contributed to all the stages of the research, from planning and data collection to analysis of the results and writing the draft. The coauthors contributed in reviewing the results.

3. **Rosero-Vlasova, O. A.**, Vlassova, L., Pérez-Cabello, F., Montorio, R., & Nadal-Romero, E. (2019). Soil organic matter and texture estimation from visible-near infrared-shortwave infrared spectra in areas of land cover changes using correlated component regression. *Land Degradation & Development*, 30(5), 544-560. <https://doi.org/10.1002/ldr.3250>

As the first author of this article, Olga Alexandra Rosero Vlasova contributed to all the stages of the research, from planning and data processing to analysis of the results and writing the draft. Dr.Fernando Pérez Cabello and Dra. Raquel Montorio Llovería listed as coauthors are directors of this PhD research.

Impact Factor	Impact Factor (5 year)	JCR® Category	Rank in Category	Quartile in Category
4.275	4.866	SOIL SCIENCE	5 of 35	Q1
		ENVIRONMENTAL SCIENCES	54 of 250	Q1

Data from the 2018 edition of [Journal Citation Reports](#)

4. **Rosero-Vlasova, O. A.**, Vlassova, L., Pérez-Cabello, F., Montorio, R., & Nadal-Romero, E. (2018). Modeling soil organic matter and texture from satellite data in areas affected by wildfires and cropland abandonment in Aragón, Northern Spain. *Journal of Applied Remote Sensing*, 12(4), 042803. <https://doi.org/10.1117/1.JRS.12.042803>

As the first author of this article, Olga Alexandra Rosero Vlasova contributed to all the stages of the research, from planning and data processing to analysis of the results and writing the draft. The coauthors contributed in reviewing the results.

Impact Factor	Impact Factor (5 year)	JCR® Category	Rank in Category	Quartile in Category
1.344	1.391	REMOTE SENSING	26 of 30	Q4
		ENVIRONMENTAL SCIENCES	198 of 250	Q4
		IMAGING SCIENCE & PHOTOGRAPHIC TECHNOLOGY	22 of 28	Q4

Data from the 2018 edition of [Journal Citation Reports](#)

- 5. Rosero-Vlasova, O.,** Alves, D. B., Vlassova, L., Pérez-Cabello, F., & Llovería, R. M. (2017, November). Modeling soil organic matter (SOM) from satellite data using VIS-NIR-SWIR spectroscopy and PLS regression with step-down variable selection algorithm: case study of Campos Amazônicos National Park savanna enclave, Brazil. *Remote Sensing for Agriculture, Ecosystems, and Hydrology XIX* (Vol. 10421, p. 104210V). International Society for Optics and Photonics. <https://doi.org/10.1117/12.2278701>

As the first author of this article, Olga Alexandra Rosero Vlasova contributed to all the stages of the research, from planning and data processing to analysis of the results and writing the draft. The coauthors contributed in reviewing the results.

Proceedings paper (SPIE.)	Web of Science categories	Research areas
Conference on Remote Sensing for Agriculture, Ecosystems, and Hydrology (Warsaw, POLAND)	REMOTE SENSING	REMOTE SENSING

Data source:

https://apps.webofknowledge.com/full_record.do?product=WOS&search_mode=GeneralSearch&qid=9&SID=F5KTRKNFUZgIG2Yko18&page=1&doc=1